UNIVERSIDADE DE LISBOA

FACULDADE DE CIÊNCIAS
DEPARTAMENTO DE QUÍMICA E BIOQUÍMICA

COPPER, SAMARIUM AND HOLMIUM COMPLEXES WITH TETRAAZAMACROCYCLES POTENCIALLY INTERESTING FOR NUCLEAR MEDICINE

SARA MARTINS VASCO DE LACERDA

DOUTORAMENTO EM QUÍMICA
(QUIMICA INORGANICA)

2009

UNIVERSIDADE DE LISBOA

FACULDADE DE CIÊNCIAS
DEPARTAMENTO DE QUÍMICA E BIOQUÍMICA

COPPER, SAMARIUM AND HOLMIUM COMPLEXES WITH TETRAAZAMACROCYCLES POTENCIALLY INTERESTING FOR NUCLEAR MEDICINE

SARA MARTINS VASCO DE LACERDA

DOUTORAMENTO EM QUÍMICA
(QUIMICA INORGANICA)

SUPERVISOR
ISABEL REGO DOS SANTOS (PhD)
INSTITUTO TECNOLÓGICO E NUCLEAR, SACAVÉM, PORTUGAL

2009

The work presented in this thesis has been performed at the Radiopharmaceutical Sciences Group of the Instituto Tecnológico e Nuclear (ITN), under the supervision of Doctor Isabel Rego dos Santos. The studies with $^{64/67}$Cu have been performed at the Forchungzentrum-Dresden, Rossendorf, Germany. The solution studies have been performed at the ITQB, Oeiras, Portugal, at the Inorganic Chemistry Department of the Karlova University, Prague, Czech Republic and at the Centre de Biophysique Moléculaire, Orléans, France. This work has been partially supported by the Fundação para a Ciência e a Tecnologia (SFRH/BD/19168/2004).

Acknowledgements

First of all, I would like to give my sincerest thanks to my supervisor, Dr. Isabel Rego dos Santos, for affording me the opportunity to integrate and grow scientifically at the Radiopharmaceutical Sciences Group from the Instituto Tecnológico e Nuclear (ITN). Thank you for guidance and patience. Also, for setting up a great model on how to work hard to achieve our goals.

My heartfelt thanks to Dr. Maria Paula Campello for providing her unconditional support, guidance, encouragement and humor that helped me in the successful completion of my doctoral projects.

I am very thankful to Dra. Lurdes Gano for performing the *in vivo* experiments and Dra. Fernanda Marques for the help in the radiochemical studies.

Thanks to all members of the Radiopharmaceutical Sciences Group for your kind support and friendly atmosphere during my work.

I would also like to thank Dra. Isabel Cordeiro dos Santos (SS/ITN) for the X-ray crystalographic measurements and Dr. Joaquim Marçalo (IOC/ITN) for the mass spectrometry analysis and their help in the discussion of those results. I also thank the ITN Research Portuguese Reactor Group for their help in carrying out the production of ^{153}Sm and ^{166}Ho.

To Dra. Rita Delgado I thank the opportunity to work in the Coordination and Supramolecular Chemistry group of the Instituto Tecnologia Química e Bioquímica (ITQB), and the help on the scientific discussions. I also would like to thank the CSC group and namely to Dra. Sílvia Carvalho/ITQB for the EPR measurements.

I thank Profs. Dr. Ivan Lukeš and Prof. Dr. Petr Hermann for the opportunity to work in the Group of Coordination and Bioinorganic Chemistry, Department of Inorganic Chemistry, at Universita Karlova (UK) in Prague. Thank you for all the support in my stays in Prague and all the scientific discussions. I would also like to express my gratitude to the group, namely to Dr. Vojtěch Kubíček, Dr. Jan Kotek, Dr. Miloslav Polášek, Dr. Petra Fousková, Mgr.Tomáš Vitha, Mgr. Jana Havlíčková and Ms. Martina Malíková for their help and support on the experimental work.

I would also like to thank Dr. Hans-Jürgen Pietzsch the opportunity to integrate the Institut für Radiopharmazie, Forschungszentrum Dresden-Rossendorf in Dresden. Thank you for all the support in my stays in Dresden and all the scientific discussions. I would also like to express my gratitude to the group, namely to Dr. Stefanie Juran, Dr. Martin Walther and Dr. Eik Schiller for their help and support on the experimental work.

I also thank Dr. Petra Fousková and Dr. Vojtěch Kubíček that, under the supervision of Dr. Eva Toth, have performed some solution studies presented in this thesis at the Centre de Biophysique Moléculaire, CNRS, Orleans, France.

I thank Dr. Helena Garcia who has accepted to be the responsible for my thesis in the Faculdade de Ciências da Universidade de Lisboa.

It was also very important to me to find good friends during my stays in Prague and in Dresden. Ania, Oskar, Bartek, Eik, Stefania, Ulrich, Natalia, Sofia and to all Barrackudas, thank you all for the good moments and to feel at home away from home.

Aos meus amigos queria agradecer o vosso apoio, optimismo, por estarem presentes nas comemorações e nos momentos mais difíceis.

Finalmente, queria agradecer o constante e incondicional apoio da minha família, Pai, Mãe, André, Lisa, Pedro, Rodrigo, Joana, Avó, Rita e Miguel. Obrigada por acrediterem e estarem sempre presentes.

I also thank all those who could not find a separate name but have helped directly and/or indirectly.

Last but not least, I would like to thank the Fundação para a Ciência e a Tecnologia for the financial support via the grant SFRH/BD/19168/2004. Also, some of the work performed in this thesis has been partially supported by the ITN/ITQB project (POCTI/CBO/35859/99), the bilacteral project GRICES Portugal (ITN)/ Czech Republic (UK) (GRICES/AS ČR 2006) and COST Action D38.

“O sucesso é ir de fracasso em fracasso sem perder entusiasmo.”
Winston Churchill

“No fundo das montanhas está guardado um tesouro para aquele que nunca o procurar.”

Abstract

The main goal of the work presented in this thesis was to introduce new tetraazamacrocycles and to study the possibility of using these chelators to stabilize copper and lanthanides for, in a later stage, to label biologically relevant molecules and/or to target bone. In this context, were synthesized four cyclen-derivatives, namely do1SH, do3aSH, bz2ac and *trans*-do2a2p. The characterization of these compounds has been done by mass spectrometry, multinuclear NMR spectroscopy and, in some cases, by X-ray diffraction analysis. Potentiometric studies, NMR titrations and UV-vis spectroscopy have been performed to calculate their protonation constants and the stability constants with Cu(II) (do1SH, bz2ac) and with lanthanides (do3aSH, *trans*-do2a2p). The stability constants of these tetraazamacrocycles have also been determined for other biologically relevant metals, such as Zn^{2+}, Ca^{2+}, Cd^{2+} and Pb^{2+}. Solution and/or solid state structural studies of Cu^{2+}/Zn^{2+}-do1SH, Cu^{2+}-bz2ac, Cu^{2+}/Ln^{3+}-do3aSH and Ln^{3+}-do2a2p have been performed to assess the nature of the inner sphere of the respective complexes.

Reactions of do3aSH and bz2ac with $^{64/67}$Cu showed that bz2ac form stable radiocomplexes, but the number and nature of the pendant arms does not make it suitable for conjugation to biomolecules.

Reactions of do3aSH, *trans*-do2a2p and do3ap^{R} (R= $P(O)(OH)_2$, $P(O)(OH)(CH_2)_2COOOH$ or $P(O)(OH)CH_2C_6H_4$-*p*NH_2) with ^{153}Sm and ^{166}Ho were also studied. Complex ^{153}Sm-do3aSH is very stable *in vitro* and *in vivo* and its biological profile compares well with those of ^{153}Sm-do3a/dota. These results and the non-involvement of the thiol on the coordination sphere of Sm^{3+}, revealed that do3aSH is suitable for conjugation to biomolecules *via* the thiol group, without compromising the stability of the ^{153}Sm-conjugates. Complexes ^{153}Sm/^{166}Ho-do2a2p are stable *in vitro* and *in vivo* presenting moderate bone uptake. Their biological behaviour compared with that of ^{153}Sm/^{166}Ho-do3ap^{R}, ^{153}Sm/^{166}Ho-dota, ^{153}Sm/^{166}Ho-do3pa and ^{153}Sm/^{166}Ho-dotp show clearly the effect of the number, position and nature of pendant arms on bone uptake.

Resumo

A Medicina Nuclear utiliza radiofármacos para diagnóstico e/ou terapia de certas patologias, sendo o seu principal objectivo a realização de diagnósticos cada vez mais precoces e precisos e terapias cada vez mais direccionadas. O sucesso desta área depende da sensibilidade e resolução do equipamento utilizado, das técnicas de tratamento de imagem, mas depende também significantemente da possibilidade de se conceberem e sintetizarem radiofármacos cada vez mais sensiveis e especificos para certos orgãos alvo. O trabalho apresentado nesta tese centrou-se essencialmente no estudo de complexos de cobre, samário e hólmio estabilizados por ligandos do tipo tetraazamacrociclo contendo grupos funcionais para ligação a biomoléculas e/ou com afinidade para o osso.

Realizaram-se alguns estudos com [14]aneN-tetraazamacrociclos mas as dificuldades encontradas na síntese, bem como o facto de complexos radioactivos formados com esta família de compostos serem pouco estáveis *in vivo*, levou-nos a centrar a atenção em [12]aneN-tetraazamacrociclos.

Foram então sintetizados três novos ligandos: 1-etanotiol-tetraazaciclododecano (do1SH), ácido 1-etanotiol-[1,4,7,10-tetraazaciclododecano-4,7,10-triil] triacético (do3aSH) e ácido 2,2'-[4,10-bis(fosfonometil)-1,4,7,10-tetraazaciclododecano-1,7-diil] diacético (*trans*-do2a2p), e foi também estudado o composto ácido dioxo-1,4,7,10-tetraazabiciclo[1.10.1]hexadeca-1(11),13,15-trieno-4,7-diacético (bz2ac) já descrito na literatura.

O derivado cicleno mono-substituído com um grupo tiol, do1SH, foi isolado e caracterizado pelas técnicas habituais em química, tendo ainda sido caracterizado por cristalografia de raios-X o seu percursor do1Strit, em que trit é um grupo protector do tiol. Foram determinadas quatro constantes de protonação por potenciometria (25.0ºC, 0.10M KNO_3) e espectroscopia de RMN de ^{13}C. Foi possível estabelecer a ordem de protonação deste ligando, tendo-se verficado que a primeira protonação ocorria no grupo tiol e as restantes nas aminas do macrociclo. A avaliação das constantes de estabilidade com Cu^{2+}, Zn^{2+} e Cd^{2+}, mostrou que do1SH forma complexos de cobre mais estáveis do que o parente cicleno ($pM_{Cu\text{-}do1SH}$=14.24; $pM_{Cu\text{-}cicleno}$=10.02), mas é menos selectivo face a outros metais *d*-, tais como o zinco ($pM_{Zn\text{-}do1SH}$=11.77; $pM_{Zn\text{-}cicleno}$=5.68). Estudos de espectroscopia de ressonância paramagnética (EPR) e de UV-vis realizados com [Cu(do1SH)] e estudos de espectroscopia de RMN de ^{13}C realizados com [Zn(do1SH)] a diferentes valores de pH

mostraram que o composto do1SH formava complexos pentacoordenados com estes metais e que o enxôfre apenas coordena ao centro metálico a valores de pH superiores a 8.

Para o composto bz2ac foram determinadas quatro das seis constantes de protonação por potenciometria (25.0ºC, 0.10M KNO_3) e espectroscopia de de RMN de ^1H. As constantes de estabilidade deste tetraazamacrociclo com Cu^{2+}, Zn^{2+}, Ni^{2+}, Cd^{2+} e Pd^{2+} foram também determinadas por potenciometria. A presença do anel benzénico, que confere maior rigidez ao macrociclo, levou à formação de complexos mais estáveis com cobre do que o cicleno ($pM_{Cu\text{-}bz2ac}$=11.73; $pM_{Cu\text{-}cicleno}$=10.02), mas com uma selectividade inferior relativamente a outros metais *d*-, como por exemplo o zinco ($pM_{Zn\text{-}do1SH}$=8.00; $pM_{Zn\text{-}cicleno}$=5.68). Estudos de espectroscopia de ressonância paramagnética (EPR) e de UV-vis realizados com [Cu(bz2ac)] a diferentes valores de pH mostraram que o grupo amida coordena ao Cu^{2+} a pH>10.
A reacção de bz2ac com $CuCl_2$ em etanol, seguida de recristalização de uma mistura etanol/metanol levou à obtenção de monocristais. Os estudos de difracçao de raios-X de cristal único confirmaram a formação do complexo [Cu(bz2ac-OEt)Cl]. Este complexo monomérico é neutro e o cobre encontra-se pentacoordenado, por dois átomos de azoto das aminas, dois átomos de oxigénio (um de um grupo amida e outro de um grupo carboxilato) e por um átomo de cloro. O segundo grupo carboxilato do macrociclo não se coordenou ao metal pois sofreu uma esterificação *in situ*, originando um ester etílico. A geometria de coordenação em torno do cobre era do tipo pirâmide quadrangular distorcida. Reacções com $^{64/67}Cu$ mostraram que bz2ac formava rapidamente radiocomplexos estáveis. A conjugação de um aminoácido protegido a um dos braços carboxilato levou á formação de um conjugado que ao raegir com $^{64/67}Cu$ não conduziu a uma espécie bem definida e estável.

O composto do3aSH, que contém um grupo tiol e três grupos carboxilato, foi caracterizado por várias técnicas incluindo espectrometria de massa e espectroscopia de RMN multinuclear. A atribuição inequívoca das ressonâncias encontradas foi conseguida recorrendo a estudos de RMN a 2 dimensões. Foram determinadas seis das oito constantes de protonação por potenciometria (25.0ºC, 0.10mM KCl) e espectroscopia de RMN de ^1H e ^{13}C. A ordem de protonação foi estabelecida com base nesta última técnica e mostrou que as duas primeiras protonações ocorriam em aminas do macrociclo, a terceira no grupo tiol e as restantes três nos grupos carboxilato. Apesar de não ter sido determinada a estabilidade termodinâmica deste

novo composto com cobre, a elevada estabilidade do parente do3a ($pM_{Cu\text{-}do3a}$=16.84) levou-nos a estudar este composto com cobre inactivo e radioactivo. Os estudos mostraram a formação de duas espécies quer ao nível macroscópico quer ao radioactivo. A análise destas espécies por espectrometria de massa permitiu concluir que eram idênticas e que muito provavelmente correspondiam ao dímero [(Cu-do3aS)$_2$].

O composto do3aSH foi também estudado com lantanídeos. Foram determinadas as constantes de estabilidade de do3aSH com Sm^{3+}, Ho^{3+} e Ce^{3+} por potenciometria (25.0ºC, 0.10mM KCl) e especroscopia de UV-vis. A constante de estabilidade com samário e hólmio é ligeiramente inferior aos valores encontrados com dota (Sm: pM_{do3aSH}=9.22, pM_{dota}=10.75; Ho: pM_{do3aSH}=8.72, pM_{dota}=11.65). Estudos em solução e de relaxatividade do complexo Gd-do3aSH a diferentes valores de pH mostraram que o grupo tiol não está envolvido na coordenação aos iões lantanídeos estudados, mesmo quando desprotonado. Foram sintetisados os radiocomplexos ^{153}Sm/^{166}Ho-do3aSH e estudada a sua estabilidade *in vitro* em meio fisiológico e na presença de cisteína e glutationa. O complexo mais estável, ^{153}Sm-do3aSH, foi estudado *in vivo* em ratinhos fêmea CD-1 e o seu perfil biológico comparado com o perfil dos complexos ^{153}Sm-do3a e ^{153}Sm-dota, utilizados como referência. O bom perfil biológico de ^{153}Sm-do3aSH e o facto de o grupo tiol não estar envolvido na coordenação ao metal revelaram que o composto do3aSH tem potencial para ser explorado como agente quelante bifuncional.

O composto *trans*-do2a2p, contendo grupos fosfonato e carboxilato em posição *trans*, foi sintetisado e caracterizado pelas técnicas usuais incluindo por cristalografia de raios-X. Foram determinadas as constantes de protonação por potenciometria (25.0ºC, 0.1M NMe_4Cl) e espectroscopia de RMN de ^{31}P. As constantes de estabilidade com Y^{3+}, Sm^{3+}, Ho^{3+}, Ca^{2+} e outros elementos *d*- foram avaliadas. Os complexos formados com elementos *f*- são mais estáveis do que os formados com elementos *d*- ($pM_{Sm\text{-}do2a2p}$=16.87 e $pM_{Cu\text{-}do2a2p}$=15.36). Reacções de *trans*-do2a2p com $SmCl_3$ em água levaram à obtenção de monocristais. A análise de difracçao de raios-X permitiu identificar os complexos H[Sm(H_2do2a2p)].5H_2O.3HCl e H[Sm(H_2do2a2p)(H_2O)].8.5H_2O.2.5HCl. No anião [Sm(H_2do2a2p)]$^-$ os quatro átomos de azoto do macrociclo e quatro átomos de oxigénio - dois dos carboxilatos e um de cada fosfonato, coordenam-se ao metal, sendo a geometria de coordenação em torno do Sm do tipo antiprisma quadrangular distorcido (TSA). No anião [Sm(H_2do2a2p)(H_2O)]$^-$ o metal está coordenado aos quatro átomos de azoto, a quatro

átomos de oxigénio dos braços e ainda a uma molécula de água, apresentando uma geometria de coordenação do tipo antiprisma distorcido enchapelado (CTSA). A síntese dos radiocomplexos ^{153}Sm/^{166}Ho-do2a2p foi quantitativa e as espécies formadas são estáveis *in vitro* e apresentam ligação moderada à hidroxiapatite (matrix inorgânica do osso, que permite prever a ligação *in vivo* ao osso). A avaliação biológica destes complexos foi também feita em ratinhos CD-1 e o perfil obtido comparado com o do ^{153}Sm/^{166}Ho-dota e ^{153}Sm/^{166}Ho-dotp no mesmo modelo animal. O perfil biológico de ^{153}Sm/^{166}Ho-do2a2p é semelhante aos dos radiocomplexos com dota e dotp mas apresenta uma ligação ao osso mais baixa do que os complexos ^{153}Sm/^{166}Ho-dotp.

Foram ainda estudados os radiocomplexos ^{153}Sm/^{166}Ho-do3ap^{R} (R= $P(O)(OH)_2$, $P(O)(OH)(CH_2)_2COOOH$, $P(O)(OH)CH_2C_6H_4$-*p*NH_2). Estes compostos são derivados do ácido 1,4,7,10-tetraazaciclododecano-4,7,10-tris(carboximetil)-1-metilenofosfónico (do3ap). Verificou-se que a natureza do grupo fosfonato não afectava significamente o comportamento radioquímico e biológico das espécies formadas.

Key Words

Radiopharmaceuticals

Macrocyclic Ligands

Solution Studies

Copper, Samarium and Holmium Complexes

Radioactive Complexes

Palavras-Chave

Radiofármacos

Ligandos Macrocíclicos

Estudos em solução

Complexos de Cobre, Samário e Hólmio

Complexos Radioactivos

Table of Contents

Index of Figures

Index of Tables

Index of Schemes

Scope and Aim

The origin of Nuclear Medicine arises from many scientific discoveries, most notably the discovery of X-rays, in 1895, and the discovery of "*artificial radioactivity*" in 1934. The first great event for nuclear medicine occurred in 1946 when a patient with thyroid cancer was treated with radioactive iodine and a complete disappearance of the spread of the cancer was observed. This has been considered as the true beginning of Nuclear Medicine. However, wide-spread clinical use of Nuclear Medicine did not take place until the early 1950s.[1]

Per year, in developed countries (26% of world population), nuclear medicine diagnostics represent 1.9% of all diagnostics and the frequency of therapy with radioisotopes is about one tenth of this percentage. In Europe there are about 10 millions of nuclear medicine exams each year and the use of radiopharmaceuticals, compounds which contain a radioactive element in its composition, in diagnosis is growing at over 10% per year.[2]

Nuclear Medicine plays a significant role in a wide range of pathologies, namely inflammation, neurological disorders, cardiovascular diseases and cancer. From all these pathologies, cancer and cardiovascular disorders are the ones where the application of Nuclear Medicine is growing more significantly. The development and application of Nuclear Medicine strongly depend on the advances in radiopharmaceutical sciences, a multidisciplinary research area which needs the input of organic, inorganic and bioinorganic chemists, radiopharmacists, radiochemists and clinicians. The role of the chemists is to design and synthesize radiopharmaceuticals for diagnosis and/or therapy, namely metal-based radiopharmaceuticals. To achieve such goals is very important to study the coordination chemistry of metals having radioisotopes with physical properties interesting for diagnosis and/or therapy. The main goal of this research is to find compounds with adequate pharmacokinetics and for that those metals are normally anchored by chelators bearing or not a clinically relevant biomolecule. The final complexes must present:

- A high stability *in vivo*
- A fast blood clearance

[1] L.S. Graham, J.G. Kereiakes, C. Haris and M.B. Cohen, "Nuclear Medicine: From Becquerel to the present", *Nuclear Medicine*, **1989**, *9*, 1189-1202.
[2] "Radioisotopes in medicine", January **2008** in http://world-nuclear.org/info/inf55.html

- A specific interaction with the target-organ
- A fast elimination from the non-target organs

The aim of this work was to explore the chemistry, radiochemistry and, in some cases, the biological behaviour of macrocyclic metal complexes to evaluate their potential interest for Nuclear Medicine applications. The metals studied were copper and lanthanides as these elements have radioisotopes interesting for diagnostic and/or therapy ($^{64/67}$Cu, ^{153}Sm, ^{166}Ho). For the stabilization of these metals we have synthesized and characterized tetraazamacrocycles bearing different pendant arms.
In chapter 1 we present a general introduction on radiopharmaceuticals and nuclear imaging techniques as well as a brief overview of the copper and lanthanides coordination chemistry, relevant for Nuclear Medicine applications.
Chapter 2 describes the synthesizes and the characterization of several novel tetraazamcocycles bearing different pendant arms, as well as reactions of some of these compounds with inactive and radioactive Cu^{2+}. In chapter 3, the synthesis and the characterization of a new cyclen derivative bearing carboxylate and phosphonate pendant arms as well as reactions of this compound with lanthanides are described. The influence of the nature and number of phosphonate pendant arms on the macrocyclic framework on the biological behaviour of the respective radiolanthanide complexes is also discussed. In this chapter, we also report reactions of lanthanides with a cyclen-derivative bearing carboxylate and thiol pendant arms, synthesized and characterized in chapter 2. Finally, in chapter 4 all the experimental details are given.

1.
INTRODUCTION

1.1 Introduction

1.1.1. Nuclear Medicine and Radiopharmaceuticals

Nuclear Medicine is the branch of medicine that uses radiation to provide information about a specific organ or to treat diseases. In terms of imaging, this area supplies knowledge about the biochemical and physiological status of certain organs, being such information used by physicians to make a quick and accurate diagnosis of the patient. For therapy the physicians use particle-emitting radionuclides to deliver a cytotoxic radiation dose to selected target tissues [1,2].

In both cases, Nuclear Medicine requires the use of radiopharmaceuticals, which are drug formulations suitable for administration in humans which contain radionuclides in their composition. The radiopharmaceuticals can be small organic, inorganic or organometallic compounds with defined composition, or can also be large molecules, such as monoclonal antibodies, antibody fragments or peptides [1-3].

The radiopharmaceuticals can be divided in two categories: perfusion radiopharmaceuticals and targeted-specific radiopharameuticals. The biodistribution of the *perfusion radiopharmaceuticals* is determined mainly by their chemical and physical properties (figure 1.1a) and those whose ultimate distribution is determined by the nature of a bioactive molecule with a specific mechanism to interact with a targeted tissue are called *target-specific radiopharmaceuticals* (figure 1.1b) [4,5].

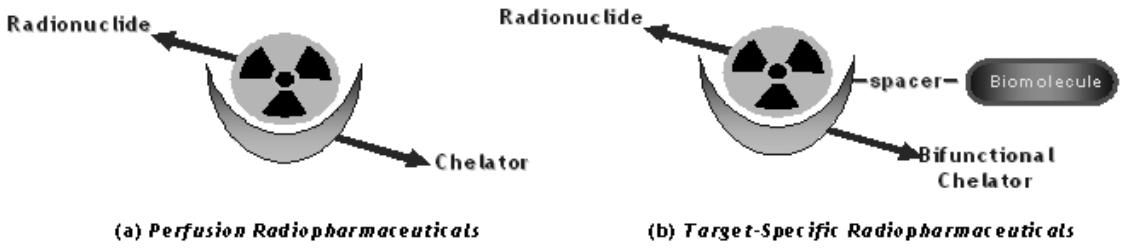

Figure 1.1: Schematic representation of a radiopharmaceutical: (**a**) *Perfusion* and (**b**) *Targeted-Specific*.

A radiopharmaceutical needs to be highly stable *in vivo*, namely against hydrolysis, redox reactions, transchelatation and transmetalation, so they should be thermodynamic and kinetically stable. The pharmacokinetics of a radiopharmaceutical depends on several parameters, being some of the most significant solubility, charge, lipophilicity, molecular weight and composition.

Depending on the physical properties of the radionuclide the perfusion or targeted-specific radiopharmaceuticals can be suitable either for diagnosis or therapy.

1.1.2. Radionuclides

A nuclide is an atomic nucleus identified by a unique combination of a given number of protons and neutrons. A nuclide of an atomic element ***X*** is represented by ${}^{A}_{Z}X_{N}$: where A = mass number, Z = atomic number and N = number of neutrons. The unstable nuclides are termed radionuclides, most of which are artificially produced in cyclotrons or reactors, with a few naturally occurring. Radionuclides are unstable due to the unsuitable composition of the nucleus, and they desintegrate emitting gamma ray(s) an/or subatomic particles – α, β^- or β^+ [6]. The time necessary for half of the original atoms to decay is known as the half-life ($T_{1/2}$) of the radionuclide.

The choice of a radionuclide for medical diagnosis or therapeutical applications depends on its decay process, energy of the particles or radiation emitted, half-life of the radionuclide, production mode, radionuclidic purity, specific activity, availability and price.

Table 1.1 shows examples of radionuclides that decay by α, β^-, β^+ or γ emission, electron capture, isomeric transition or a mixture of some of these processes [6,7].

Table 1.1: Decay modes and examples, adapted from [6,7].

Decay mode	Instability cause *	Example
α	Excess of **n** and **p**	${}^{235}_{92}U \rightarrow {}^{231}_{90}Th + {}^{4}_{2}He$ (or α)
β^-	Excess of **n**	${}^{32}_{15}P \rightarrow {}^{32}_{16}S + \hat{a}^- + \acute{\imath}$
β^+	Excess of **p**	${}^{18}_{9}F_{9} \rightarrow {}^{18}_{8}O_{10} + \beta^+ + \nu$
EC	Excess of **p**	${}^{67}_{31}Ga + e^- \rightarrow {}^{67}_{30}Zn + \nu$
IT	Excitated state	${}^{99m}_{43}Tc \rightarrow {}^{99}_{43}Tc + \gamma$

EC= Electron Capture; **IT=** Isomeric Transition; * **p**= proton; **n**= neutron; **ν**= neutrino.

The production of artificial radionuclides can be achieved by bombarding stable targets with particles, such as, neutrons, produced in nuclear reactors, or charged particles produced in cyclotrons. It is also possible to have indirect production routes like radionuclide generators. In this case a radionuclide (parent), produced in a

reactor or cyclotron, is immobilised in a chromatographic column allowing the elution of another radionuclide (daughter) with shorter half-life. The advantage of this process is to deliver very short-lived radionuclides (daughter) to hospitals or medical institutions that don't have cyclotron or reactor facilities [6,8].

1.1.3. Molecular Imaging and Targeted-Therapy

"Molecular Imaging" enables temporal and spatial imaging of biological or biochemical processes throughout an intact living subject. With this approach, it is possible to obtain more meaningful results than can be achieved by comparable *in vitro* methods. With the advance of molecular imaging techniques, properly tagged molecules can be visualized leading to insights on cell function, membrane binding sites, and the effectiveness of particular therapies [9].

For Molecular Imaging there are different techniques available, namely nuclear techniques – Single Photon Emission Computed Tomography (SPECT) and Positron Emission Tomography (PET), Magnetic Resonance (MRI), Computed Tomography (CT) and Ultrasound (US). Examples of images obtained with these techniques are shown in figure 1.2. SPECT and PET are highly sensitive and non-invasive when compared to the other techniques, requiring the use of radioactive probes in very low concentrations (10^{-12}–10^{-10}M) [1-3].

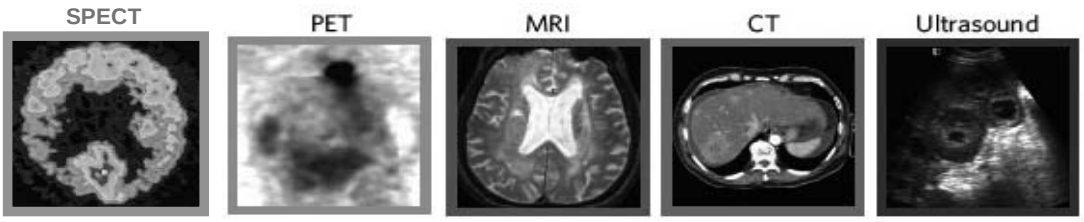

Figure 1.2: Examples of image obtained with SPECT, PET, MRI, CT and US imaging techniques, adapted from ref. [10]

Table 1.2: Molecular Imaging modalities, adapted from ref. [9b,10]

Imaging Modality*	Spatial Resolution	Sensitivity	Scan Time	Key Use
US	50 μm	Not well characterized	Secs to Min.	Morphological / Vascular Imaging
CT	50 μm	Not well characterized	Mins.	Morphological and Anatomical Imaging
MRI	10 – 100 μm	10^{-5}–10^{-3}M	Mins. to Hrs.	Morphological and Anatomical Imaging
PET	1 – 2 mm	10^{-12}–10^{-11}M	Mins. to Hrs.	Metabolic Imaging
SPECT	1 – 2 mm	10^{-11}–10^{-10}M	Mins. to Hrs.	Metabolic Imaging

*** US** = Ultrasound; **CT** = Computed Tomography; **MRI** = Magnetic Resonance Imaging; **PET** = Positron Emission Tomography; **SPECT** = Single Photon Emission Computed Tomography.

CT and MRI are primarily anatomical imaging techniques that provide superior resolution, while PET and SPECT are nuclear medicine imaging modalities that image physiological processes that are occurring within the living system. Of the latter two, PET has advantages with respect to sensitivity and resolution [11]. While each modality provides important information to the physician, dual modality imaging techniques like PET/CT (figure 1.3) or SPECT/CT integrate the high-resolution anatomical images with physiological information and enable the investigator to identify the physiological basis of disease and correlate it with the anatomical image [11,12].

Figure 1.3: Example of image obtained with PET-CT

From the nuclear imaging modalities, SPECT requires a radiopharmaceutical containing a nuclide that emits gamma (γ) radiation and a gamma camera for imaging the patient injected with the gamma emitting radiopharmaceutical. PET requires a radiopharmaceutical labelled with a positron-emitting radionuclide (β^+) and a PET camera [13]. Apart from the improvement in equipment and technology for nuclear molecular imaging, combination with others such as PET/CT or SPECT/CT, its success depends strongly on the availability of specific radiopharmaceuticals.

The search for more specific compounds for diagnosis and targeted-therapy is an intense and important research area. To design accurate "delivery systems" to a specific target tissue is mandatory to avoid possible secondary effects.

In table 1.3 are shown some of the radionuclides with medical interest. Some of their characteristics and production mode are also referred.

Table 1.3: Some radionuclides with established medical applications, adapted from ref. [6,8]

Element	Radionuclide	$T_{½}$	Decay type	Common Production Mode / Source *	Application †
Technetium	**^{99m}Tc**	6.0h	γ	$^{98}Mo(n,\gamma)\,^{99}Mo$ $^{99}Mo \xrightarrow[66\ h]{\beta^-} {}^{99m}Tc$	G	D
Rhenium	**^{186}Re**	89.2 h	β^-	$^{185}Re(n,\gamma)^{186}Re$	R	T
	^{188}Re	17 h	β^-	$^{186}W(2n,\gamma)^{188}W$ $^{188}W \xrightarrow[65\ d]{\beta^-} {}^{188}Re$	G	T
Iodine	**^{123}I**	13.2 h	γ	$^{121}Sb(\alpha,2n)^{123}I$	C	D
	^{125}I	59.4d	**EC**	$^{124}Xe(n,\gamma)\,^{125}Xe$ $^{125}Xe \xrightarrow[17\ h]{EC} {}^{125}I$	R	D
	^{131}I	8.02 d	β^- ; γ	$^{130}Te(n,\gamma)^{131}Te$ $^{131}Te \xrightarrow[25\ min]{\beta^-} {}^{131}I$	R	D/T
Fluor	**^{18}F**	109.8 min	β^+	$^{18}O(p,n)^{18}F$	C	D
Carbon	**^{11}C**	20.3 min	β^+	$^{14}N(p,\alpha)^{11}C$ or $^{10}B(d,n)^{11}C$	C	D
Yttrium	**^{86}Y**	14.7 h	β^+	$^{86}Sr(p,n)^{86}Y$	C	D
	^{90}Y	64.1 h	β^-	$^{89}Y(n,\gamma)^{90}Y$	R	T
Indium	**^{111}In**	2.80 d	γ	$^{111}Cd(p,n)^{111}In$	C	D
Gallium	**^{67}Ga**	3.26 d	**EC**	$^{68}Zn(p,2n)^{67}Ga$	C	D
	^{68}Ga	67.8 min	β^+	$^{68}Zn(p,n)^{68}Ga$	G	D
Copper	**^{64}Cu**	12.7 h	β^- ; β^+ ; γ	$^{64}Ni(n,p)^{64}Cu$	C	D / T
	^{67}Cu	61.8 h	β^- ; β^+; γ	$^{67}Zn(n,p)^{67}Cu$	C	T
Samarium	**^{153}Sm**	46.3 d	β^- ; γ	$^{152}Sm(n,\gamma)^{153}Sm$	R	T
Holmium	**^{166}Ho**	26.8 d	β^- ; γ	$^{165}Ho(n,\gamma)^{166}Ho$	R	T
Lutetium	**^{177}Lu**	6.73 d	β^- ; γ	$^{176}Lu(n,\gamma)^{177}Lu$	R	T

EC = Electronic Capture; * **R** = Reactor; **C** = Cyclotron; **G** = Generator; † **D** = Diagnosis; **T** = Therapy

1.2. Coordination Chemistry of Copper Relevant for Medical Applications

1.2.1. Introduction

Copper is a *d*-transition element essential in all higher plants and animals. It can be found in a variety of enzymes, such as cytochrome C oxidase and superoxide dismutase. In addition to its enzymatic roles, copper is also used *in vivo* for biological electron transport (in azurin and plastocyanin proteins). Endothelial cells contain a high concentration of copper salts, indicating it's involvement in angiogenesis [14,15]. In the bloodstream, copper is carried by plasma proteins, such as ceruloplasmin or serum albumin. Copper has been found to be causative in several diseases, such as Wilson's disease, Menke's disease, infantile and childhood copper toxicosis syndromes, aceruloplasminemia, Alzheimer, amyotrophic lateral sclerosis and prion diseases [16].

In aqueous solution, the chemistry of this first-row transition element is restricted to Cu(I) and Cu(II). The Cu(III) may also be formed under certain conditions, but it is a powerful oxidant and is not stable in biochemical systems.

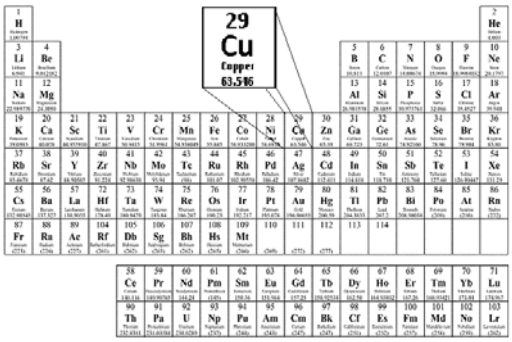

Cu(I) has a d^{10} configuration and the Cu(I) complexes remain stable in aqueous solution when in their composition there are soft donor chelators, such as phosphines, thioethers and isonitriles. The Cu(I) complexes generally have a tetrahedral coordination geometry, are colorless and diamagnetic. When formed based on less polarisable ligands (e.g., H_2O, ClO_4^-, SO_4^{2-}, etc.), the metal centre in such complexes disproportionates yielding Cu metal and Cu(II) [5,17,18].

Cu(II) has a d^9 configuration and forms mononuclear or polynuclear complexes which are generally coloured. The mononuclear complexes are paramagnetic, but the polynuclear ones are diamagnetic. The Cu(II) complexes present coordination numbers varying from 4 to 6, depending on the denticity of the chelator. The 4-coordinated Cu(II) complexes are normally square-planar, while the square-pyramid coordination geometry is often displayed by 5-coordinated Cu(II) complexes. In the

six-coordinated Cu(II) complexes the two apical donor atoms are normally weakly bonded to Cu(II), in a distorted octahedral arrangement, due to Jahn-Teller distortion. Cu(II) generally prefers nitrogen donors (amines, Schiff bases, pyridine, bipyridyl, etc.) and anionic ligands (e.g., halides, β-diketonates). The Cu(II) complexes are often kinetically labile with respect to ligand dissociation, due to its d^9 configuration [5,17,18].

The rich coordination chemistry of copper in combination with the possibility of producing different radionuclides of this element offer many opportunities for the development of diagnostic (^{60}Cu, ^{61}Cu, ^{62}Cu and ^{64}Cu) or therapeutic (^{64}Cu, ^{66}Cu and ^{67}Cu) radiotracers. Table 1.4 shows the different copper radionuclides.

Table 1.4: Copper radioisotopes and respective physical properties, adapted from refs. [17,19]

Isotope	Half-life	Imaging emission, energy (KeV)[a], abund.	Therapy emission, energy (KeV)[a], range (mm)[b]	Source [c]
^{60}Cu	20 min	PET β^+, 873, 93%		C
^{61}Cu	3.3 h	PET β^+, 527, 62%		C
^{62}Cu	9.7 min	PET β^+, 1315, 98%		G / C
^{64}Cu	12.7 h	PET β^+, 278, 19%	β^-, 190, 0.95	R / C
^{66}Cu	5.4 min		β^-, 1109, 5.6	R / C
^{67}Cu	62 h	SPECT γ, 91, 7%; 93, 16%; 185, 48%	β^-, 121, 0.61	R / C

[a] Average energy of the radiation; [b] Average range in tissues; [c] **C** = Cyclotron, **G** = Generator and **R** = Reactor

From all the radionuclides, ^{62}Cu may be the most suitable isotope for widespread diagnosis use, as is available as a ^{62}Zn/^{62}Cu generator. So this short-lived PET isotope is available even in locations remote from cyclotron-based radionuclide production facilities [20]. The ^{64}Cu isotope, due to its nuclear properties, is the most versatile of all copper radionuclides, being suitable for PET (β^+ emission) and for targeted radiotherapy (β^- emission). Moreover, this duality offers the possibility of using PET to quantify *in vivo* the regional distribution of radioactivity, a crucial issue in the assessment of radiation dosimetry when planning targeted radionuclide therapy. In

addition, the high specific activity achieved in the production of ^{64}Cu makes it more feasible to develop target-specific radiopharmaceuticals [19].

1.2.2. Coordination Chemistry

The importance of ligands in shaping the biological behaviour of metal-based drugs cannot be overestimated [21]. In general, for radiopharmaceutical applications the coordination chemistry of copper has been explored using acyclic or cyclic polidentate chelators. Usually these chelators are nitrogen and oxygen donors, due to the well recognised preference of copper(II) for these donor atoms. More recently, some chelators with sulphur donor atoms have also been synthesized and studied with Cu(II) [5, 11, 17-19, 23-27].

1.2.2.1. Polydentate Acyclic Ligands

Acyclic polyaminocarboxylates, such as DTPA (diethylenetriaminepentaacetic acid) and EDTA (ethylenediaminetetraacetic acid) (figure 1.4), have been investigated with copper radionuclides.

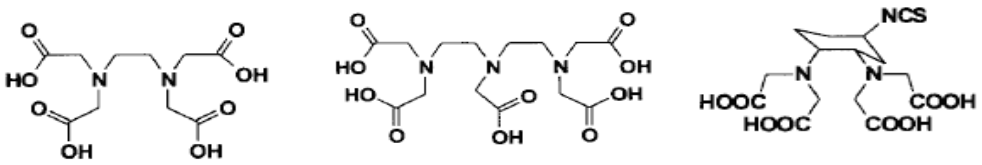

Figure 1.4: Structure of Acyclic Polyaminocarboxylate ligands

Despite the high stability constant of Cu-EDTA and Cu-DTPA (log $K_{Cu\text{-}EDTA}$ = 18.8 and log $K_{Cu\text{-}DTPA}$ = 21.4), copper-EDTA and DTPA-based conjugates have shown to loose copper rapidly *in vitro* to serum albumin. Hence, these ligands have been considered unsuitable for irreversible coupling of copper to carrier molecules. To reduce the lability of such derivatives, a cyclohexyl has been incorporated in the EDTA backbone, providing the "semi-rigid" chelator – N-(isothiocyanato) trans-1,2-diaminocyclohexane (CDTA-SCN, figure 1.4). However, such strategy did not improve significantly the stability of the corresponding copper complex [28].

Another class of acyclic ligands, which form stable, neutral, low molecular weight and almost planar complexes with copper(II), are bis(thiosemicarbazone) ligands (figure 1.5).

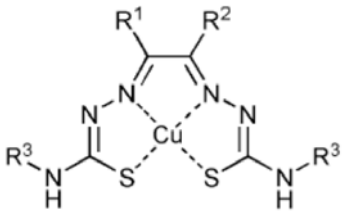

Figure 1.5: Structure of copper bis(thiosemicarbazone) complexes: $\mathbf{R^1}$=$\mathbf{R^2}$=$\mathbf{R^3}$=H **Cu(GTS) -** Glioxal bis(thiosemicarbazone); $\mathbf{R^1}$=$\mathbf{R^2}$=$\mathbf{R^3}$=CH_3 **Cu(ATSM)** - Diacetyl bis(N^4-methylthiosemicarbazone); $\mathbf{R^1}$=H, $\mathbf{R^2}$=$\mathbf{R^3}$=CH_3 **Cu(PTSM)** - Pyruvaldehyde bis(N^4-methylthiosemicarbazone) and $\mathbf{R^1}$=$\mathbf{R^2}$=CH_2CH_3, $\mathbf{R^3}$=H **Cu(ETS)** - Ethylglyoxal bis(thiosemicarbazone).

Bis(thiosemicarbazone) ligands provide an N_2S_2 chelate system for copper. Such donor atom set provides an hybrid system, as it stabilises Cu(II) and Cu(I). The Cu(II) complexes are inherently planar, as evidenced in figure 1.6a for [Cu(ATSM)].

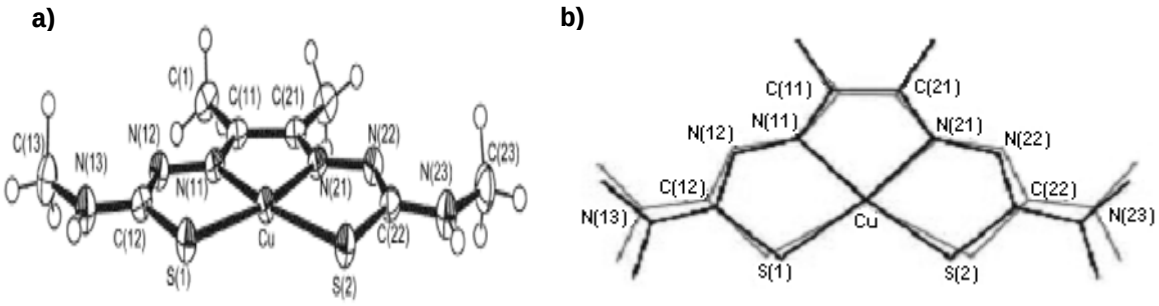

Figure 1.6: (**a**) Ortep view of [Cu-ATMS]; (**b**) Geometry changes (exaggerated for purposes of illustration) caused by the C(11)–C(21) bond stretching on expansion of the ligand cavity by pivoting at coordinated nitrogen atoms. Grey lines: without backbone alkylation; bold lines: with alkylation at C(11) and C(21); adapted from [29].

In [Cu-ATMS] the copper is stabilised by two amines and the two sulphur atoms from the backbone, displaying a square planar geometry. Alkylation at the backbone carbon atoms ($\mathbf{R^1}$ or $\mathbf{R^2}$, fig. 1.5) increases the backbone C–C bond length, allowing the metal to fit slightly better into the ligand cavity, affecting the complex stability and redox potential. Figure 1.6b schematically represents the differences in the structure due to the alkylation on C-C bounds. The grey lines represent a structure

without alkylation and the bold line an alkylation occurring at the C(11) or C(21). Alkylation of the terminal nitrogen atoms (**R**^{3}, fig. 1.5) interrupts intermolecular interactions, and the complexes can adopt idealised tetragonal planar geometries. Moreover, any slight distortions from planarity are due only to intermolecular interactions, especially pairs of N–H–N and N–H–S hydrogen bonds. These bonds give rise to supramolecular architectures involving cross-linked flat or helical ribbons of complexes, and may allow the complexes to interact with various biological molecules containing complementary hydrogen-bonding motifs (*e.g.* purines, pyrimidines and peptide bonds) [29].

Several bis(thiosemicarbazone) derivatives have shown different potential applications: the complex [Cu(ATSM)] is a successful hypoxia tracer, due to its selective retention in hypoxic tissues [30]. Complex [Cu(ETS)] has shown promising application as a PET radiopharmaceutical for evaluation of renal perfusion [31] and the complex [Cu(PTSM)] has interest as heart and tumor imaging agent [27].

1.2.2.2. Polydentate Cyclic Ligands

The polydentate cyclic chelators are interesting due to their ability to adopt preorganized conformations in the free form. Cyclen and generally all tetraazamacrocycles exhibit high basicity in the first two protonation steps and rather low basicity in the last two steps. Table 1.5 shows the protonation constants for some representative acyclic and cyclic ligands.

Table 1.5: Protonation constants of edta, dtpa, cyclen, cyclam, dota and teta

	EDTA[a]	DTPA[b]	cyclen[d]	cyclam[e]	dota[f]	teta[f]
$\log K_{H1}$	9.80	10.54	10.6	11.29	12.09	10.85
$\log K_{H2}$	6.12	8.56	9.6	10.19	9.69	10.13
$\log K_{H3}$	2.56*	4.30*	1.5	1.61	4.54*	4.11*
$\log K_{H4}$	1.96*	2.77*	0.5	1.91	4.36*	3.27*
$\log K_{H5}$	---	2.0*	---	---	1.9 [g,*]	2.17 [g,*]
$\log K_{H6}$	---	1.7[c]	---	---	1.7 [g,*]	---
$\log K_{H7}$	---	0.9[c]	---	---	---	---

[a] 25.0ºC, 0.2M $NaClO_4$, ref. [32]; [b] 25ºC, 0.1M KNO_3, ref. [33]; [c] 1.0M K/HCl, ref. [33], [d] 25ºC, 0.1M KCl, ref. [34], [e] 25.0ºC, 0.1M KCl, ref. [34]; [f] 25.0ºC, 0.1M NMe_4Cl, ref. [34]; [g] 25ºC, 0.1M NaCl, ref. [34]; * protonation at a COOH group.

As can be seen in table 1.5, the difference for cyclic ligands between logK_{H1} and logK_{H2} is significantly higher than the value calculated for a statistical separation of two protonation constants (usually about 0.6), reflecting electrostatic repulsion between the protonated sites. In order to minimize such repulsion, protonation occurs on *trans*-located nitrogen atoms. Such dramatic increase in the electrostatic repulsion energy of these cyclic ligands leads also to a logK_{H3} which is of about eight orders of magnitude lower than logK_{H2}. This behavior differs clearly from what is observed for open-chain tetraamines: in the noncyclic series, the difference between two consecutive amine protonation constants is approximately constant, since the flexibility of the chain minimizes the electrostatic repulsion between the positively charged nitrogen atoms [34].

The structures of free dota and teta are presented in figure 1.7. The conformations found show that dota is stabilised by multiple and cooperative intramolecular N–H···O and O–H···O hydrogen bonding interactions, while in teta only one acetate arm forms hydrogen bonds with one N–H group, through a bridged water.

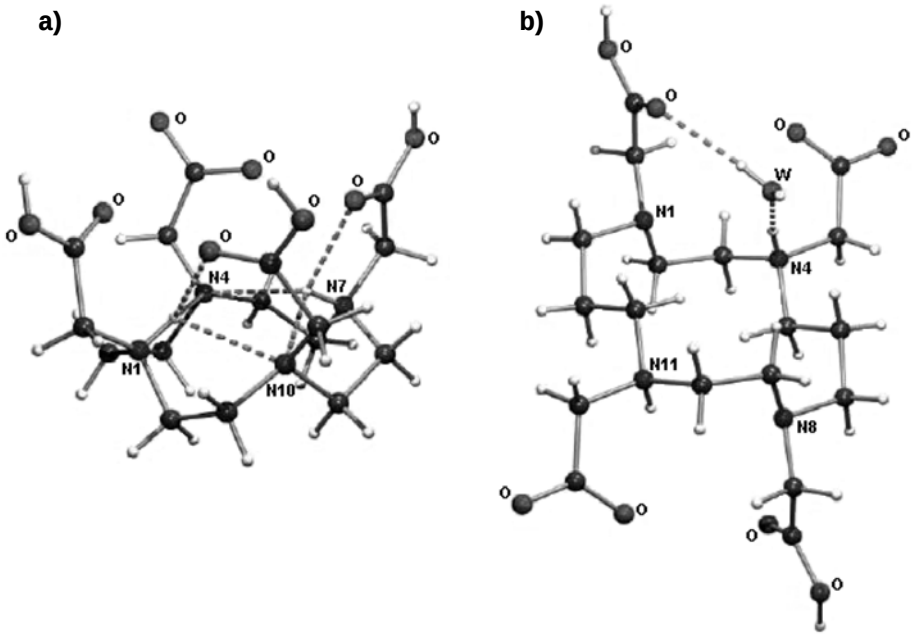

Figure 1.7: Structure of (a) $[H_6dota]^{2+}$ and (b) $[H_4teta(H_2O)]$, **w** = water molecule

Due to the preorganization, the cyclic ligands do not have to reorganize themselves around a metal ion during complexation, forming complexes thermodynamically more stable than with EDTA and DTPA and also leading to kinetically inert complexes [35].

Figure 1.8 shows some of the tetraazamacrocycles more explored with copper for radiopharmaceutical applications.

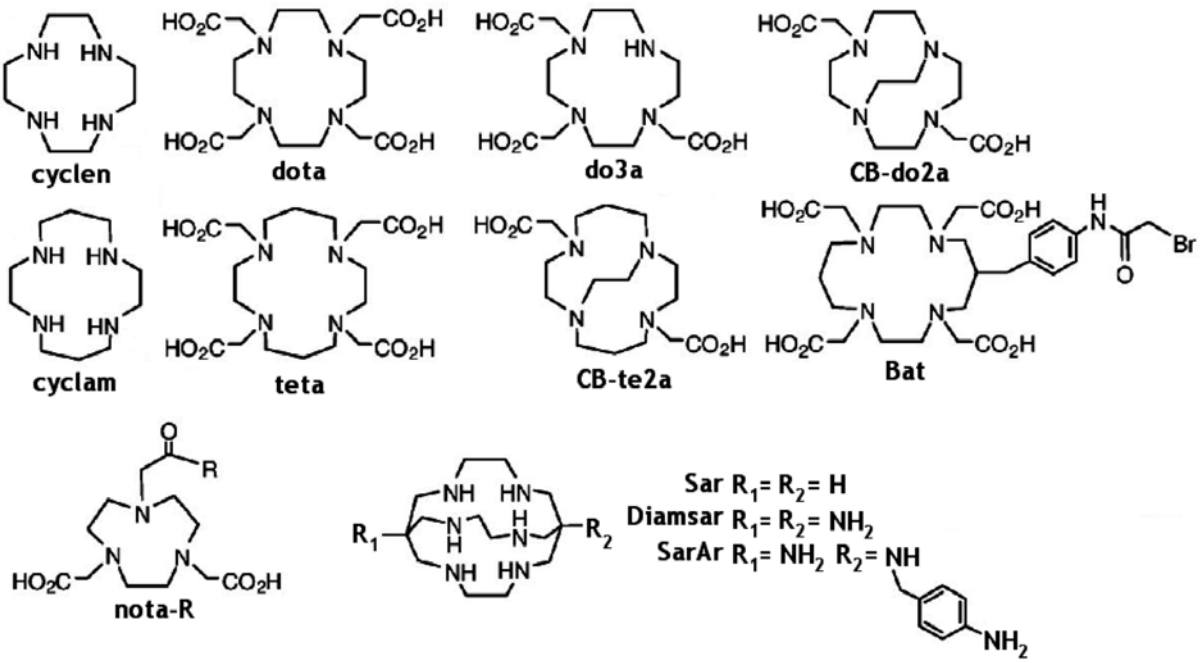

Figure 1.8: Structure of macrocyclic ligands: **cyclen =** 1,4,7,10-tetraazacyclodecane**; dota =** 1,4,7,10-tetraazacyclododecane-1,4,7,10-tetraacetic acid**; do3a =** 1,4,7,10-tetraazacyclododecane-1,4,7-triacetic acid**; CB-do2a =** 4,10-bis(carboxymethyl)-1,4,7,10-tetraazabicyclo[5.5.2]tetradecane**; cyclam =** 1,4,8,11-tetraazacyclotetradecane**; teta =** 1,4,8,11-tetraazacyclotetradecane-1,4,8,11-tetraacetic acid**; CB-te2a** = 2,2′-(1,4,8,11-tetraazabicyclo[6.6.2]hexadecane-4,11-diyl)diacetic acid**; Bat=** Bromoacetamidobenzyl-1,4,8,11-tetraazacyclotetradecane-1,4,8,11-tetraacetic acid**; nota-R =** 1,4,7-Triazacyclononane-1-"R substituted"-4,7-diacetic acid**; Sar =** 3,6,10,13,16,19-hexaazabicyclo(6,6,6)eicosane**; Diamsar =** 1,8-diamino-3,6,10,13,16,19-hexaazabicyclo(6,6,6)eicosane**; SarAr =** N1-(4-aminobenzyl)-3,6,10,13,16,19-hexaazabicyclo[6.6.6]icosane-1,8-diamine

High thermodynamic stability is an important parameter but only reflects the direction of the reaction, not the association/dissociation rate. The kinetic inertness of the complex (the rate of dissociation of the radionuclide from the complex) determines the *in vivo* solution stability of a radiopharmaceutical. While fast dissociation kinetics is characteristic of metal complexes of acyclic BFCAs, an accumulated body of literature has shown that metal complexes of macrocyclic chelators are kinetically more inert [6].

Table 1.6 shows the stability constants of copper complexes formed with some of the macrocyclcles represented in figure 1.8. The values for EDTA and DTPA, the more studied acyclic polydentate chelators, are also shown.

Table 1.6: Stability constants of Cu(II) complexes with different ligands and some relevant properties

Ligand	Log K_{CuL}	Ref.	$T_{1/2}$	Ref.	K_d (s^{-1})	Ref.	% $^{64/67}$Cu [2]	Ref.
EDTA	18.7	28	---	--	$7.8x10^{-2}$	34f	14	19
DTPA	21.4	28	---	--	$1.2x10^{-1}$	34f	23	19
tacn	15.52	36c	---	--	---	--	---	--
cyclen	24.8	36a	< 1min [1]	36d	$2.54x10^{-4}$	34g	---	--
cyclam	27.2	36a	< 3min [1]	36d	$5.52x10^{-4}$	34g	>99.5	19
nota	21.63	36b	---	--	---	--	---	--
dota	22.7	36a	< 3min [1]	36e	---	--	>99	19
teta	21.9	36a	4.5min [1]	36d	---	--	98	19
CB-te2a	27.1	28	155h [1]	36e	---	--	>99	36h
diamsar	> 26.3*	19	40h [1]	36e	---	--	>99.9	19

* Value too high to be determined. It is supposed to be higher than logK_{Hg}= 26.3. [1] 5M HCl, 90ºC; [2] Percentage of $^{64/67}$Cu-ligand complex after 24h in human serum.

Analysing table 1.6, we can say that the thermodynamic stability overall trend for Cu^{2+} complexes is as follows:

diamsar > CB-te2a ≈ cyclam > cyclen ≈ dota ≈ teta ≈ nota ≈ DTPA > EDTA > tacn

Several parameters can be used to assess the kinetic inertness of a complex. In table 1.6 are shown values reported in the literature for some of these parameters. One parameter is the dissociation constant of a metal complex (K_d), another is the stability of the metal complex in high acidic conditions ($T_{1/2}$), finally is also important to test the kinetic stability of a radiocomplex when incubated with excess of human serum (at 37ºC) (**% intact $^{64/67}$Cu-complex**, after 24h). From the analysis of all these parameters we can conclude that:

1- Complexes formed with macrocyclic ligands are more inert than the ones formed with open chain ligands, namely EDTA and DTPA.

2- Complexes anchored on unsubstituted macrocycles are comparable:
K_d(Cu-cyclen) ≈ K_d(Cu-cyclam).

3- Complexes anchored on substituted macrocycles present similar kinetic inertness. However, the complexes Cu-CB-teta and Cu-diamsar are really significantly inert.

In the Cu(II) complexes with 12-membered tetraazamacrocycles, the metal is normally five- or six-coordinated by the four nitrogens of the macrocyclic backbone and by a solvent molecule or donor atoms of the pendant arms. For cyclen or tetramethyl cyclen (Me_4[12]aneN_4), X-ray analysis, together with EPR and UV-vis studies, showed that the copper is 5-coordinated by the four nitrogens of the macrocyclic backbone and by a solvent molecule. The coordination geometry has been assigned as square-pyramidal (figure 1.9a) [37,38]. When the macrocycle has pendant arms with donor atoms suitable for copper, such as dota or do3a, two oxygen atoms from opposite pendant arms also coordinate to copper, being usually the metal stabilised in an octahedral coordination geometry (figure 1.9b and 1.9c) [19].

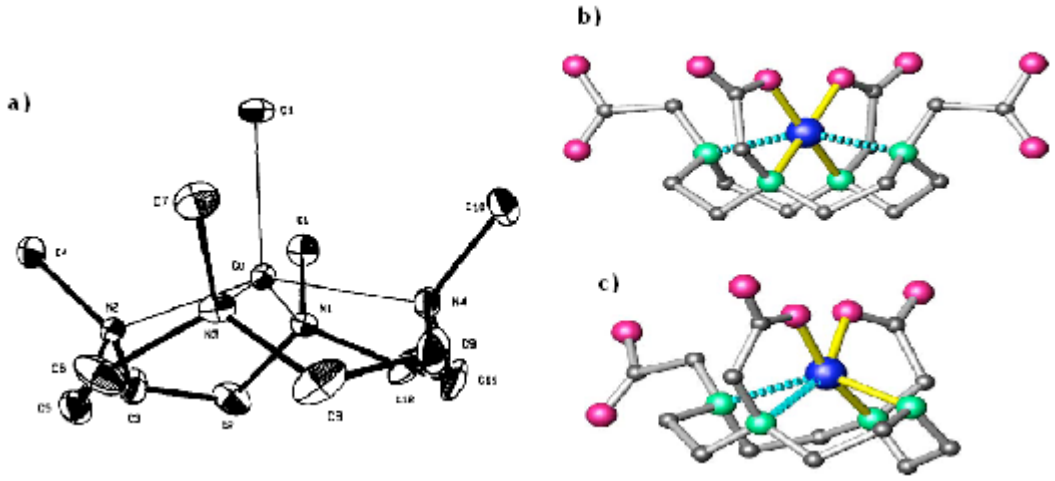

Figure 1.9: Structure of copper-12N_4 macrocyclic complexes: a) ORTEP of [Cu(Me_4[12]aneN_4)$H_2$0]$^{2+}$, from ref.[37]; b) [Cu-dota]$^{2-}$; c) [Cu-do3a]$^{-1}$. Colours: ● Copper, ● Oxygen, ● Carbon, ● or ● Nitrogen, ● Phosphorus, ● Chlorine; from ref. [19]

The 14-membered tetraazamacrocyclic (14N_4) such as, cyclam and teta, have also been used to stabilize $^{64/67}$Cu [19, 35]. Due to the cavity size of the cyclam and teta, the metal stays in the plane defined by the four nitrogen atoms. In both complexes the metal ion is six-coordinated by four nitrogen atoms of the 14N_4 tetraazamacrocycle and by two oxygen atoms from ClO_4^- or from the carboxylic pendant arms, as in the case of Cu-cyclam (figure 1.10a) and Cu-teta-ArNO_2 (figure 1.10b), respectively.

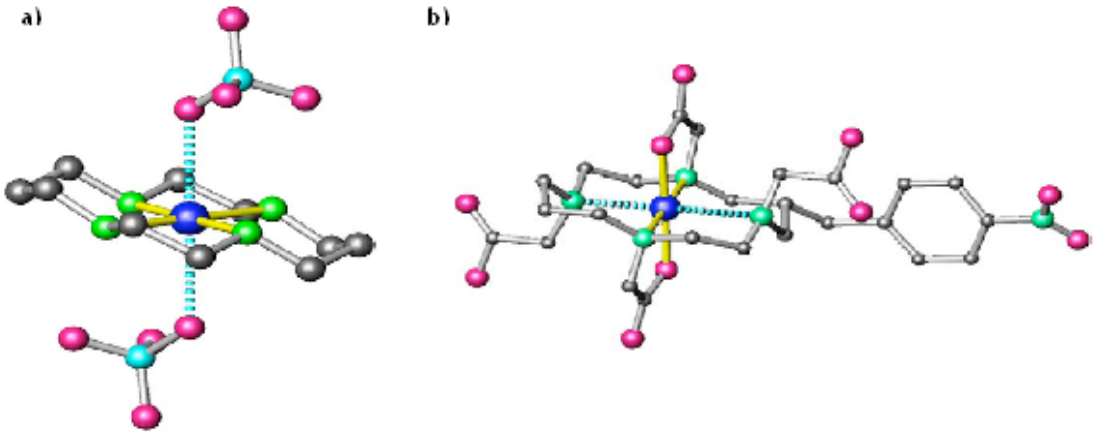

Figure 1.10: ORTEP views of copper-14N_4 macrocyclic complexes: a) $[Cu\text{-}cyclam]^{2+}.2ClO_4^-$; b) $[Cu\text{-}teta\text{-}ArNO_2]^{2-}$, for colours see legend of fig. 1.9, [19]

For the 1,4,7-triazacyclononane ($9N_3$, tacn), the complex formed is $[Cu(tacn)_2]^{2+}$. In this complex the copper is stabilised by six nitrogen atoms, three from each tacn unit, displaying a octahedral coordination geometry (figure 1.11) [39].

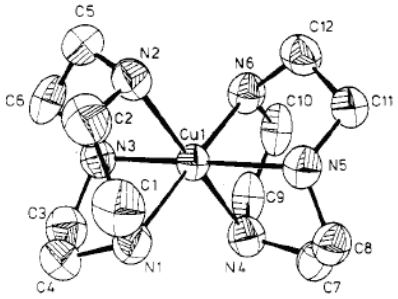

Figure 1.11: ORTEP view of $[Cu(tacn)_2]^{2+}$ [39]

For tacn derivatives, such as nota, two different complexes have been reported, namely $[Cu(nota)]^-$ and $[CuCl(H_2nota)]$. In these structures, the Cu(II) is six-coordinated by the three nitrogen atoms of the macrocycle backbone and either by three oxygen atoms of the pendant arm (figure 1.12a) or by two oxygen atoms of two arms and a chloride (figure 1.12b) [40,41]. In the first case, the anion $[Cu(nota)]^-$ displays a distorted-pseudo-prismatic geometry, and the complex may be divided into a hydrophobic part, consisting of the 1,4,7-triazacyclononane fragment, and a more hydrophilic counterpart comprising six oxygens of three coordinated carboxylate groups, that roughly lie on one plane [40]. In complex $[CuCl(H_2nota)]$, two of the three acetate groups are protonated, as shown in figure 1.12b. So, one of the

protonated arms is not coordinated to copper while the other protonated arm is only weakly coordinated trough the carbonyl group, occupying an axial site. The unprotonated acetate coordinates with a normal Cu-O bond. The chloride ion also occupies a position in the plane. The coordination around the metal in [CuCl(H_2nota)] is much more distorted than in $[Cu(nota)]^-$ [41].

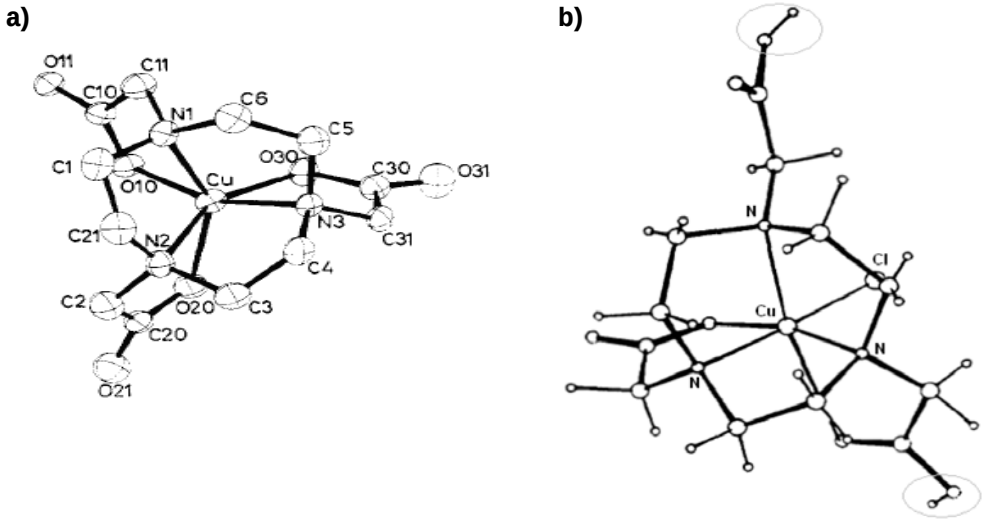

Figure 1.12: ORTEP view of **a)** [Cu-nota]$^-$, [40]; **b)** [CuCl(H_2nota)], adapted form ref. [41]

The ligand diamsar forms a hexadentate complex with copper coordinated to all six secondary nitrogen atoms, and the complex was formulated as $[Cu(II)\text{-diamsar-}2H)]^{4+}$, figure 1.13.

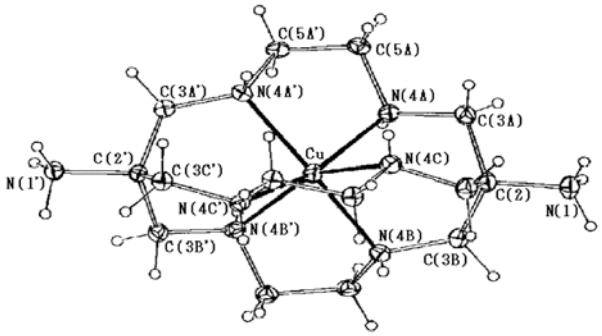

Figure 1.13: ORTEP structure of $[Cu(II)\text{-diamsar-}2H]^{4+}$ [42]

The Cu–N bond distances are different, being two bond distances slightly longer than the other four. The Jahn–Teller effect makes the $[Cu(II)\text{-diamsar-}2H]^{4+}$ to lose its D3 symmetry forming a somewhat distorted trigonal complex. The apical nitrogens are protonated, giving a complex with an overall tetra-positive charge [42].

Due to the copper coordination characteristics, the use of polidentate acyclic or cyclic chelators allows not only the fully stabilization of the metal but also its conjugation to different biomolecules.

1.2.3. Labelling of Biomolecules with Radioactive Copper

Different strategies can be used to label biomolecules with radioactive copper. The most popular consists in using a BFCA bearing a functional group which can react covalently with another group naturally present in the biomolecule or synthetically introduced. For example, in peptides naturally occurring functional groups include terminal, as well as side-chain, amino and carboxylic groups or thiol or *p*-hydroxyphenyl groups from cysteine and tyrosine, respectively. Conjugation groups in the BFCAs can also be of different nature, namely active esters, isothiocyanates, maleimides, hydrazides, and R-haloamides. Although in proteins the lysine side chain amino groups are the most commonly labelled, conjugation of dota to the thiol groups of cystein residues, through maleimides has also been reported [43-45]. Several biomolecules have been labelled with radioactive copper using as BFCA some of the tetraazamacrocycles shown in figures 1.8, and some examples will be given below.

Even if EDTA and DTPA are not the best ligand choice for stabilising Cu^{2+}, Nahrendorf *et al.* have recently reported the development of a new DTPA PET agent with optimized pharmacokinetics for *in vivo* imaging of macrophages in atherosclerotic plaques. This novel class of macrophage-targeted PET agents is based on long-circulating magnetic dextran-coated nanoparticles, which have been coupled to ^{64}Cu-DTPA and to a near-infrared fluorochrome for fluorescence imaging, yielding a trimodal reporter nanoparticle [^{64}Cu-TNP] (PET, MRI, and fluorescence (figure 1.14)). The authors found that ^{64}Cu-TNP directly detects macrophages in atherosclerotic plaques [46]. Advantages of this agent include improved sensitivity, quantification of PET signal and correlation with an established biomarker (CD68), whole-body vascular surveys, spatial localization of the probe by microscopy and clinical translatability of the agent given similarities to magnetic resonance imaging probes in clinical trials.

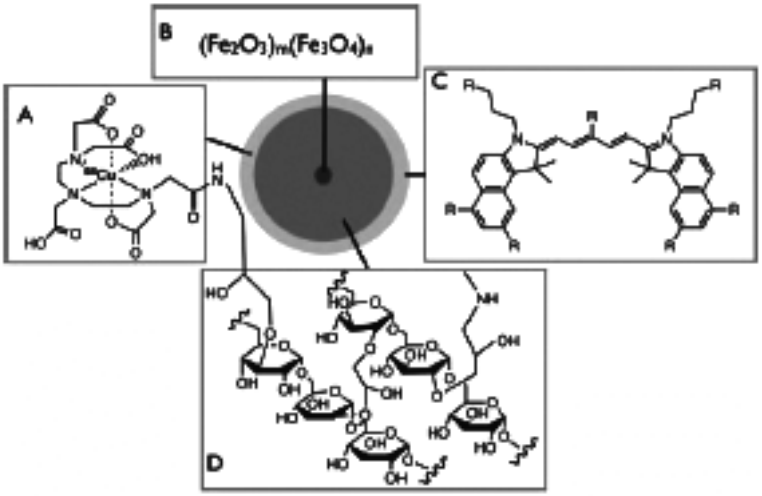

Figure 1.14: Schematic view of the tri-reporter ^{64}Cu-TNP: **A**) Derivatization with the chelator DTPA allows attachment of ^{64}Cu; **B**) Iron oxide core to provide contrast in MRI; **C**) Fluorochrome for fluorescence imaging; **D**) Crosslinked aminated polysaccharide coating which provides biocompatibility, determines blood half-life and provides linker for attachment of tracers and potentially affinity ligands [46]

Some bifunctional chelates based on bis(thiosemicarbazones) bearing pendant carboxylate arms on the backbone of the ligand (Figure 1.15a) have also been explored to stabilize $^{64/67}$Cu, and evaluated as potential new targeted PET imaging agents. However, the structure of the metal complexes has not unequivocally been established. Two novel ATSM derivatives (figures 1.15b), bearing amino acids (such as lysine or ornithine) or octreotide, were reported and copper stability measurements as well as radiolabelling studies with ^{64}Cu are in progress [47].

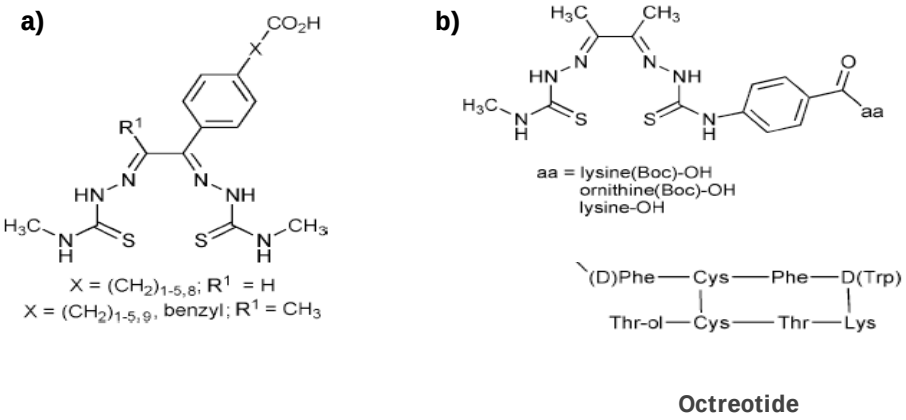

Figure 1.15: (a) Bis(thiosemicarbazone) ligands derivatised with carboxylate arms on the carbon backbone; **(b)** structure of dissymmetric bis(thiosemicarbazone) ligand bearing a single phenyl carboxylate group coupled to amino acids (aa), such as lysine or octreotide

Macrocyclic chelators as BFCAs have been reported for the first time in 1985, by Meares and co-workers. This research group has developed a teta derivative (BAT, figure 1.16) and reported its conjugation to monoclonal antibodies and further labelling with ^{67}Cu [48]. Some years later, DeNardo et al. have developed a new BFCA – a BAT derivative with 2-iminithiolane (2IT) as a linker to bind ^{67}Cu to the monoclonal antibody mAb Lym-1 (figure 1.16). The authors have tested this new conjugate in humans with non-Hodgkin's lymphoma as a potential radiopharmaceutical [49].

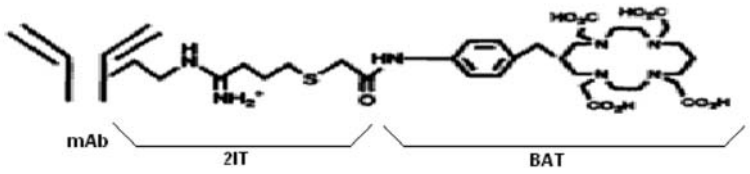

Figure 1.16: Structure of BAT-2IT-mAb

Since then, several dota and teta derivatives have been successfully used for the labeling of biomolecules with $^{64/67}$Cu, including antibodies and small peptides [50-70]. Some BFCA's based on other macrocyclic cavities have also been explored.

Teta derivatives labelled with $^{64/67}$Cu, such as the conjugate ^{64}Cu-teta-D-Phe^{1}-octreotide (teta-OC, figure 1.17) often have high liver uptake and long liver retention, being such biodistribution attributed to the transfer of $^{64/67}$Cu from the complex to ceruloplasim and/or to the liver superoxide dismutase [71,72].

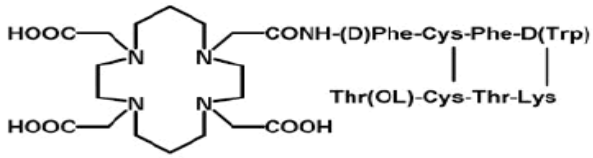

Figure 1.17: Structure of teta-OC

Aiming to overcome this drawback, Anderson *et al.* performed a series of chemical and biological studies of copper complexes with the reinforced cross-bridged tetraazamacrocyclic ligands CB-do2a and CB-te2a [65, 73, 72]. CB-te2a has been coupled to bombesin, octreotide and RGD analogues [65, 73, 74]. These conjugates were labelled with ^{64}Cu and evaluated *in vivo*. It was found that the ^{64}Cu-CB-te2a-bombesin conjugates had higher *in vivo* stability than their dota analogues, also

showing a significantly higher resistance to *in vivo trans*-chelatation when compared to the congener complex with the conventional teta macrocycle.

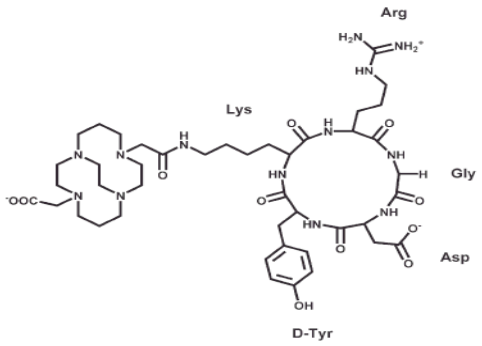

Figure 1.18: Structure of CB-te2a-c(RGDyK), from ref. [65]

Chen et al. have studied the conjugates ^{64}Cu-dota-RGD and ^{64}Cu-dota-PEG-RGD (figure 1.19). These authors have found that the complex ^{64}Cu-dota-RGD is suitable for PET imaging of $\alpha_v\beta_3$-integrins in breast cancer. The complex had a prolonged tumor retention but also a significant amount of liver and kidney retention [52]. To improve the *in vivo* biodistribution, the complex ^{64}Cu-dota-PEG-RGD, having polyethylene glycol (PEG) as a spacer between dota and the RGD, has been synthesized and evaluated (figure 1.19b) [75].

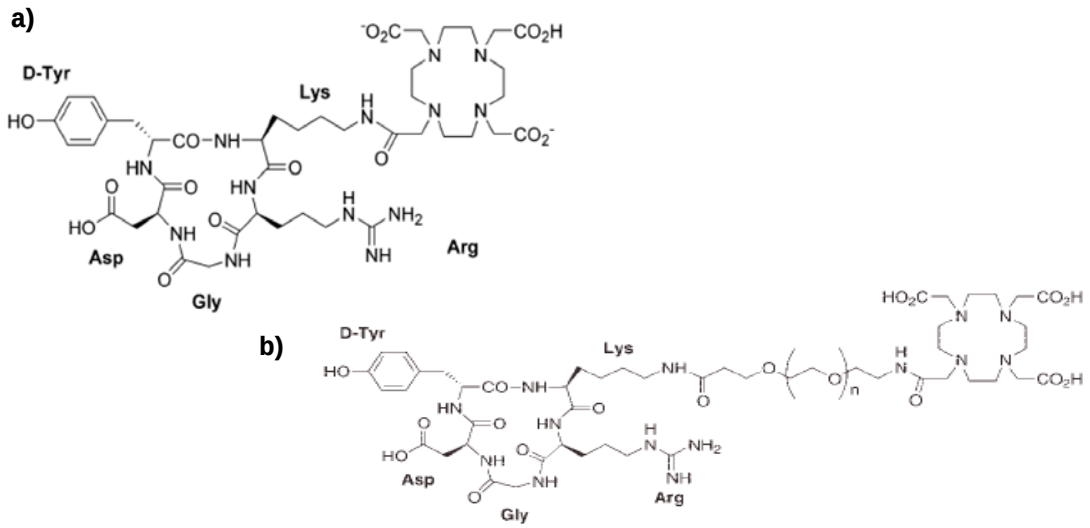

Figure 1.19: Schematic structure of (**a**) dota-RGD (ref. [52]) and (**b**)dota-PEG-RGD (ref. [75])

The pegylated RGD peptide demonstrated rapid blood clearance and the accumulation in the tumor was rapid and high at early time points, with some

activity washout seen over time. Compared with the analogue ^{64}Cu-dota-RGD (figure 1.19a), the tracer ^{64}Cu-dota-PEG-RGD showed improved *in vivo* kinetics as it had a significantly reduced liver uptake and the high renal accumulation, at early time points, cleared rapidly.

BFCA's based on the $9N_3$ macrocyclic cavity have also been explored, Prasanphanich and co-workers reported the use of ^{64}Cu-labeled nota and dota-bombesin conjugates for imaging gastrin-releasing peptide receptor positive tumors [76].

The authors claim a high ^{64}Cu-labeling efficiency and a high solution stability for the ^{64}Cu-nota conjugates. Figure 1.20 shows maximum-intensity microPET images with uptake and retention of the conjugate in tumor, and minimal accumulation of radioactivity in collateral tissues, making possible the PET imaging of prostate tumors of the lower abdomen with [^{64}Cu-nota-8-Aoc-BBN(7-14)NH_2]. Some accumulation and retention of radioactivity is observed in liver.

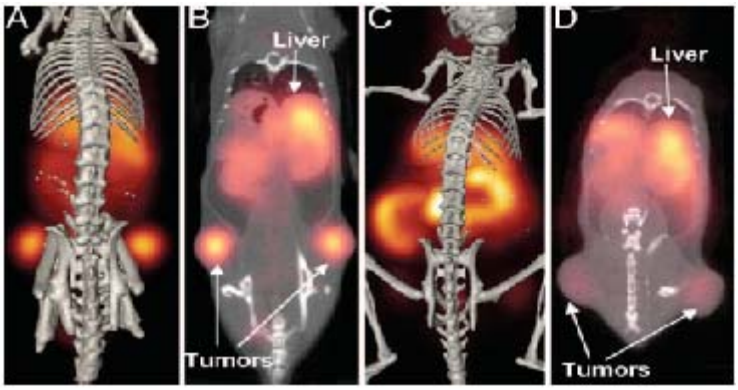

Figure 1.20: *In vivo* microPET/CT and microMRI images of a PC-3 tumor-bearing mouse 24h after tail vein injection of [^{64}Cu-nota-8-Aoc-BBN(7-14)NH_2] or [^{64}Cu-dota-8-Aoc-BBN(7-14)NH_2] (liver and bilateral, xenografted left and right flank tumors are denoted by white arrows). (***A***) Maximum intensity microPET tumor and microCT skeletal fusion coronal image for [^{64}Cu-nota-8-Aoc-BBN(7-14)NH_2]. (***B***) MicroPET coronal image slice showing specific tumor uptake of [^{64}Cu-nota-8-Aoc-BBN(7-14)NH_2]. (***C***) Maximum intensity microPET tumor and microCT skeletal fusion coronal image for [^{64}Cu-dota-8-Aoc-BBN(7-14)NH_2]. (***D***) MicroPET coronal image slice showing specific tumor uptake of [^{64}Cu-dota-8-Aoc-BBN(7-14)NH_2], [76]

In this study, they have demonstrated the effectiveness of using the nota chelator to produce kinetically inert BBN conjugates having very high affinity for GRPrs overexpressed on PC-3 prostate cancer cells. Results from both biodistribution and

microPET imaging studies indicate that the ^{64}Cu-labeled nota-bombesin conjugates have very little or no *in vivo* dissociation of ^{64}Cu from the radiotracer [76, 77].

Shively et al have recently reported a versatile dota-based bifunctional chelator, DO3A-VS (figure 1.21). This BFCA can stabilise a range of radiometals, including ^{64}Cu, and simultaneously be conjugated with negligible loss of immunoreactivity either to sulfhydryls (SH) in the hinge region of lightly reduced immunoglobulins or surface amino groups (NH_2) from lysines, of immunoglobulins. The authors have successfully labelled the conjugated DO3A-VS-M5A (M5A = humanized anti-CEA antibody) with ^{64}Cu. The results suggest that DO3A-VS may be conjugated to antibodies under several conditions offering alternatives to the conventional NHS-active ester derivatives of DOTA that are inherently unstable and therefore less predictable in batch-to-batch conjugations. In addition, the quality of the PET images, 24h after injection, indicates that ^{64}Cu-DO3A-VS-M5A should be evaluated for clinical use to image anti-carcinoembryonic antigen (CEA) positive tumors [78].

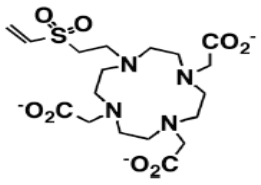

Figure 1.21: Structure of DO3A-VS (1,4,7-tris(carboxymethyl)-10-(vinylsulfone)-1,4,7,10-tetraazacyclododecane)

The biodistribution of ^{64}Cu complexes with Sar, Diamsar and SarAr hexa-aza cages have been evaluated in mice. Figure 1.22 shows a comparison of the blood, liver and kidney uptake for the ^{64}Cu-complexes of hexa-aza cage compounds and free ^{64}Cu pattern in balb/c mice, at 30min p.i. [19].

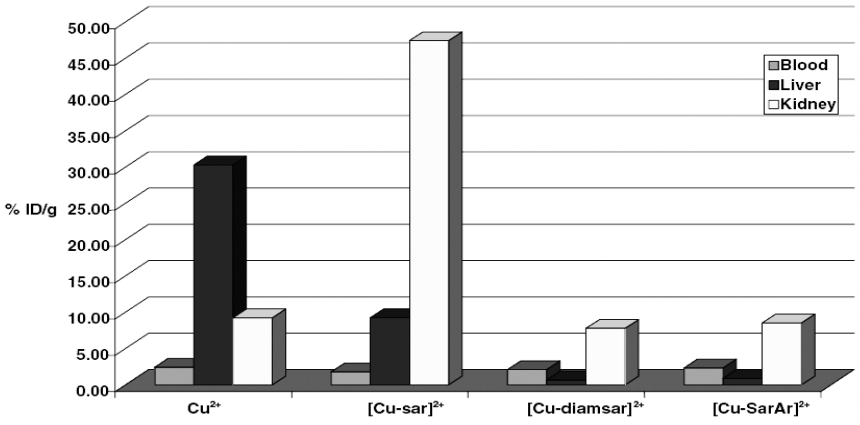

Figure 1.22: Comparison of blood, liver and kidney uptake of ^{64}Cu and ^{64}Cu-heza-aza cage complexes, [19]

The copper hexa-aza cage complexes clear rapidly from the blood, and at a similar rate. Both the $[^{64}Cu(II)$–diamsar$]^{2+}$ and $[^{64}Cu(II)$–SarAr$]^{2+}$ clear also rapidly from liver and kidney. For $[^{64}Cu(II)$–Sar$]^{2+}$ it appears to exist some retention in the kidney and liver, which was appointed to be related to mechanical trap of the complex and not to its charge or decomposition [19, 79]. Nevertheless, it is clear that the introduction of NH_2 or NHR groups in the $\mathbf{R_1}$ and $\mathbf{R_2}$ positions (figure 1.8) improves the biodistribution pattern of the Sar derivatives.

The bifunctional chelator **SarAr** was conjugated to the murine antibody B72.3 or to fragments and the resulting immunoconjugate was quantitatively labelled with ^{64}Cu [19,81]. The kinetics of the labelling was significantly higher than the kinetics found for other macrocyclic BFCAs under the same reaction conditions. However, some model complexes with small biomolecules should be prepared to demonstrate if ^{64}Cu is indeed attached to the macrocycle or simply bonded to the amino acid groups (like histidine and cysteine) of the whole or fragmented B72.3 murine antibody. Animal studies showed that the ^{64}Cu–SarAr–immunoconjugates maintain their specificity for the target and are stable *in vivo* [80].

1.3. Coordination Chemistry of Lanthanides Relevant for Medical Applications

1.3.1. Introduction

Lanthanides are generally considered as the group of elements from lanthanum to lutetium, though strictly speaking they are confined to the 14 *4f-elements* following lanthanum in the periodic table. In contrast to the *d*-block transition metals, the *4f* electrons are inner electrons, shielded from external influences by the overlying $5s^2$, $5p^6$, and $6s^2$ electron shells.

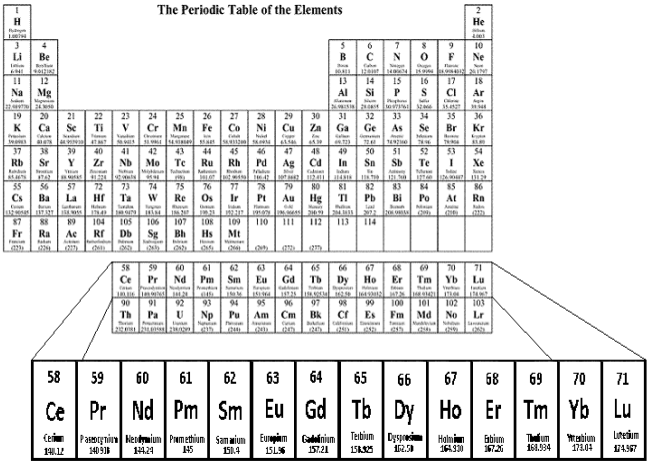

The ligand field effect is relatively weak, and the magnetic properties of these metal ions are not significantly affected by the coordination environment. Since *4f* electrons are not significantly involved in bonding, the interactions between the donor atoms and the lanthanide metal ions are predominately ionic and the ionic radii of these elements contract across the series. Although yttrium and scandium are no real lanthanides, they are added to this group because of their strong chemical similarities (similar charge, ionic radii and coordination chemistry) and important radiodiagnostic and/or therapeutic properties [5,43].

Lanthanides are usually most stable in solution as trivalent ions (M^{3+}), with the exception of cerium and europium which can exist as quadrivalent and bivalent species. Lanthanides in aqueous solution bind to water molecules, and due to their large size, their coordination numbers are typically between 7 and 10. Very few six coordinate species are known, while coordination numbers of 8 and 9 are the most common [5,43]. Lanthanides form stable complexes with oxygen or nitrogen donor chelators.

In general, lanthanides are toxic although its toxicity decreases with increasing atomic number, probably due to a greater solubility, ionic stability and smaller radius [81]. These elements have ionic radii similar to calcium, but have a higher charge, so

they have a high affinity for Ca^{2+} sites on biological molecules and also bind strongly to water molecules. In addition, their spectroscopic properties, resulting from their unusual electronic configuration, make them useful probes for calcium in biological systems using techniques such as NMR, luminescence or fluorescence spectroscopy [82].

Some of the lanthanides have radioactive isotopes interesting for Nuclear Medicine applications. As can be seen in table 1.7, radiolanthanides decay by beta particle emission and have been explored either for therapeutical applications and/or for bone pain palliation. They emit a wide range of beta energies and have also very different half-lifes. These two characteristics give them a high versatility as they can be easily matched with the biological vector and/or medical application [83,84].

Table 1.7: Physical properties of ß⁻-emitting radiolanthanides with potential for therapeutical applications; from ref. [83,84]

Radionuclide	$T_{1/2}$ (days)	$E_{\beta, max}$ (MeV)	$E_{\beta, ave}$ (MeV)	E_{γ} (MeV) (%)
^{153}Sm	1.95	0.81	0.22	0.103 (28) 0.07 (5)
^{165}Dy	0.097	1.30	0.44	0.095 (4)
^{166}Ho	1.12	1.96	0.71	0.081 (6.2)
^{169}Er	9.4	0.35	0.10	---
^{177}Lu	6.71	0.50	0.13	0.208 (11) 0.113 (6.4)
^{90}Y	2.67	2.28	0.93	2.18

Some of these radioisotopes have also been explored for imaging. For example, ^{166}Ho microspheres were proposed for hepatic investigations by SPECT-CT [85].

1.3.2. Coordination Chemistry

Lanthanides are not inherently incorporated in biological systems and their toxic potential has never been in question. For this reason, yttrium and lanthanide compounds used for medical applications are required to be thermodynamically and kinetically very stable. Once the radiopharmaceutical is injected into the blood stream, its concentration may become so low that dissociation of the radiometal from its metal chelate will eventually become favoured. Loss of radiometal may

result in accumulation of radioactivity in non-target organs, and for ^{90}Y and lanthanides it has been reported that they readily deposit on the bone. Thus, the BFCA's must form a metal complex with high stability, to retain its chemical integrity in competition with naturally occurring chelators, such as transferrin [4,86].

Several lanthanide complexes formed with acyclic and cyclic ligands have been prepared and evaluated for radiopharmaceutical applications.

1.3.2.1. Polydentante Acyclic Ligands

The acyclic polydentate chelators more studied with lanthanides were DTPA and EDTMP, figure 1.23.

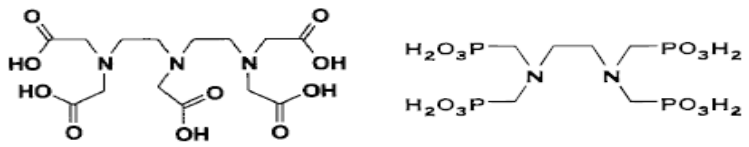

DTPA **EDTMP**

Figure 1.23: Acyclic polydentate ligands studied with lanthanides

These ligands generally form 8 or 9 coordinated complexes. DTPA-based complexes have been extensively explored with Gd as MRI contrast agents and two are in clinical use (Magnevist and Omniscan) [87]. A complex of ^{153}Sm with EDTMP is also in clinical use for bone pain palliation. So far, the structure and defined composition of this complex was not determined. However, some studies have demonstrated that several species are present at physiological pH, namely $[Sm(EDTMP)]^{5-}$ (main species), $[Sm(EDTMP)(OH)]^{6-}$ and $[Sm(HEDTMP)]^{4-}$ [88].

1.3.2.2. Polydentate Cyclic Ligands

Polyazamacrocycles with coordinating pendant arms such as dota, dotp and tritp (figures 1.8 and 1.24) strongly chelate lanthanide ions. Moreover, their thermodynamically stable complexes are usually kinetically inert, which is a desirable feature for *in vivo* use [35,84,89].

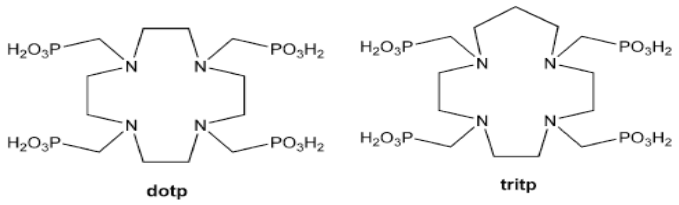

Figure 1.24: Structure of phosphonate ligands: dotp and tritp

The lanthanide complexes formed with 12-membered tetraazamacrocycles are usually 8 or 9 coordinated. The 8-coordinated complexes usually display square anti-prism (SA) and twisted square antiprism (TSA) coordination geometries (figure 1.25). The nine-coordinated complexes present capped SA or TSA coordination geometries. The tricapped trigonal prismatic coordination geometry (TTP), although being also a possible coordination geometry for Ln-complexes, is not usually find in complexes of lanthanides with 12-membered macrocycle ligands [87].

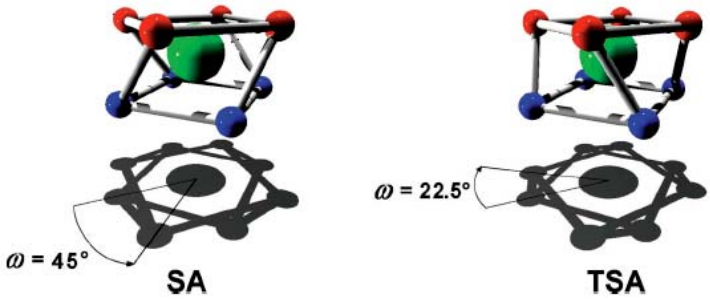

Figure 1.25: Possible geometries of lanthanide-dota/dotp-like complexes: ideal values for the twisted angles (ω) in both geometries are indicated in the figure, adapted from ref. [87]

Colours: ● Lanthanide, ● Nitrogen, ● Oxygen

In dota-like or dotp-like lanthanide complexes, the coordination sphere of the metal is fulfilled by the four nitrogen atoms from the macrocycle backbone and four oxygen atoms from the pendant arms. As an example, are presented in figure 1.26 ORTEP diagrams for $[Tm\text{-}dota]^-$, $[Gd\text{-}dotp]^{5-}$ and $[Eu(dota)(H_2O)]$. Complexes $[Tm\text{-}dota]^-$ and $[Gd\text{-}dotp]^{5-}$ display both TSA geometries. However, for larger lanthanides, complexes such as $[Eu(dota)(H_2O)]$ (figure 1.26c) can also be formed. In these complexes the metal is nine coordinated due to the coordination of an oxygen atom from a water molecule, displaying a capped SA coordination geometry.

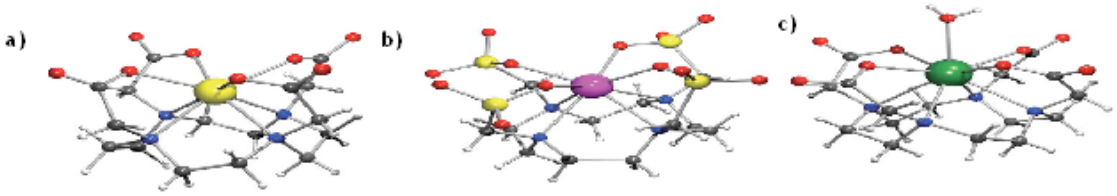

Figure 1.26: Structure of (a) $[Tm(dota)]^-$; (b) $[Gd(dotp)]^{5-}$ and (c) $[Eu(dota)(H_2O)]^-$, from ref. [35]. Colours: Thulium, Gadolinium, Europium, Nitrogen, Oxygen, Carbon, Phosphorus, Hydrogen

Normally, in all these complexes the metal ion is not equidistant from the plane defined by the nitrogen and by the oxygen atoms, being shifted towards the O_4 base.

The targetting of cyclen-based chelators can be based on the conjugation of some vectors to the macrocycle backbone. The labelling of these vectors has been mostly explored with ^{153}Sm, ^{166}Ho and ^{177}Lu, being some of the most promising under clinical evaluation. These vectors can be different biologically active molecule, such as antibodies or their fragments, peptides [45,90-110], or functional groups, such as phosphonates or bisphosphonates, with affinity for bone [111-133].

1.3.3. Labelling of Biomolecules with Radiolanthanides

As stated before, biomolecules such as antibodies, antibody fragments and peptides can be conjugated to tetraazamacrocycles trough covalent bonds between the biomolecule and the BFCA. Examples of some of these studies, mainly the most promising ones, will be briefly described.

Maecke *et al.* have reported on the development of a novel dota peptide conjugate of bombesin (BN). These conjugates should recognize bombesin receptor-positive tumours, such as prostate and breast cancer or gastrointestinal stromal tumours, and could be interesting for targeted radionuclide therapy, using ^{177}Lu (figure 1.27).

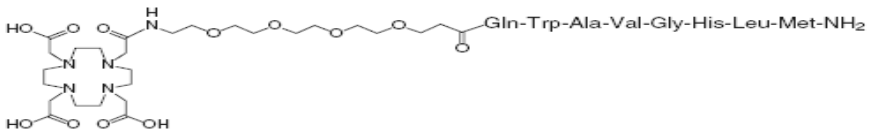

Figure 1.27: Structure of dota-PEG_4-BN or dota-PESIN

The complex ^{177}Lu-dota-PESIN shows suitable pharmacokinetics in the PC-3 tumour-bearing mice model. It presents high tumour uptake and relatively slow washout from the tumour, being this new conjugate suitable for clinical studies. The uptake specificity was demonstrated by blocking the tumour and the pancreas with the cold peptide. Fast clearance was found from blood and all non-target organs, except from kidney. The high tumour-to-normal tissue ratios increased with time. Planar scintigraphic imaging, presented in figure 1.28, showed that the ^{177}Lu-labelled peptide remained in the tumour even 3 days post injection [103].

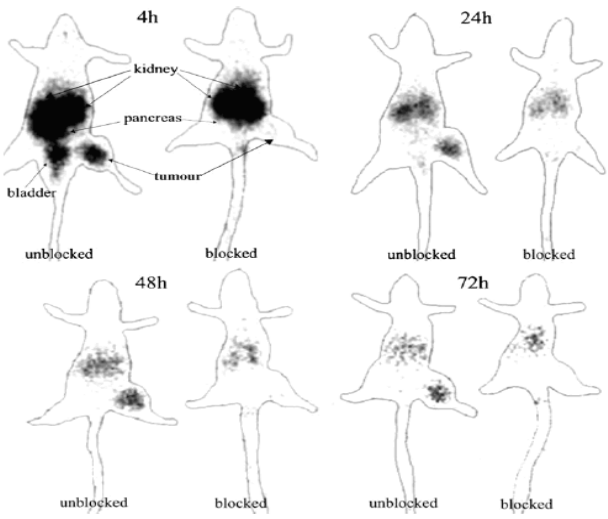

Figure 1.28: Scintigraphic planar images of [^{177}Lu-dota-PESIN] in PC-3 tumour-bearing mice at 4, 24, 48 and 72 h post injection (blocked with 50 μg [Ga^{III}-dota-PESIN]); [103]

Some other ^{177}Lu-dota conjugates are in clinical trials. Lantry *et al.* described a clinically relevant novel GRP-R/NMB-R–binding peptide agonist, ^{177}Lu-do3a-CH_2CO-G-4-aminobenzoyl-Q-W-A-V-G-H-L-M-NH_2 or ^{177}Lu-AMBA (figure 1.29), which demonstrate nanomolar affinity in both human prostate tumor tissue and in the human PC-3 cells. This radiocomplex has shown very low uptake and retention in kidney, unlike other reported peptide-based complexes. These results indicated a very favourable risk–benefit profile for this complex, which is now in phase I clinical trials [107].

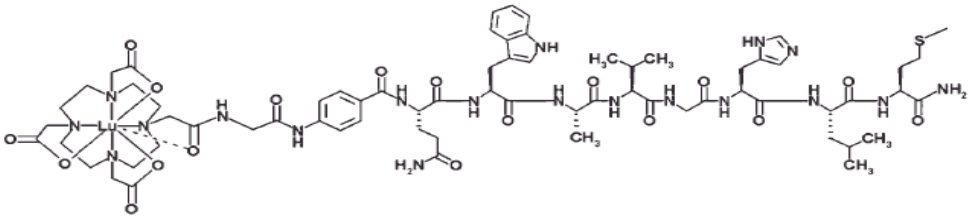

Figure 1.29: Structure of ^{177}Lu-do3a-AMBA

Krenning *et al.* have explored the radiolabeled somatostatin analogue ^{177}Lu-dota-octreotate, figure 1.30. Treatment with this radioconjugate resulted in tumor remission in a high percentage of patients with endocrine gastroenteropancreatic tumors, with rare serious side effects. The time of progression compared favourably with other treatment modalities, namely chemotherapy. Therefore, early treatment with this radioconjugate may be a good choice, even in patients who have no progressive disease. Moreover, there is a benefit in overall survival of several years from time of diagnosis [104,108].

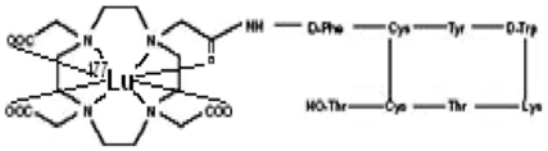

Figure 1.30: Structure of ^{177}Lu-dota-DPhe-Tyr3-octreotate

Jurisson *et al.* have studied the ^{177}Lu, ^{90}Y and ^{111}In labelling of three different B72.3 conjugates, figure 1.31. The B72.3 was used to prolong blood retention so that *in vivo* stability of the radiometallated chelates (NHS-dota, Arm-dota and Back-dota) could be directly compared. In the three chelates studied, the antibody is attached to the macrocycle in different positions: in NHS-dota the antibody is directly attached to one acetate pendant arm, in Arm-dota the antibody is linked trough the alkylation of the CH_2 group of one pendant arm and has a benzyl spacer, while in Back-dota the antibody is linked to the macrocycle backbone trough alkylation with a spacer. The authors conclude that the ^{90}Y-labeled B72.3-DOTA conjugates were less stable than ^{177}Lu-labeled analogue, based on bone uptake. The ^{177}Lu complexes with Arm-DOTA and Back-DOTA were very stable but the NHS-DOTA complex was not so stable [109].

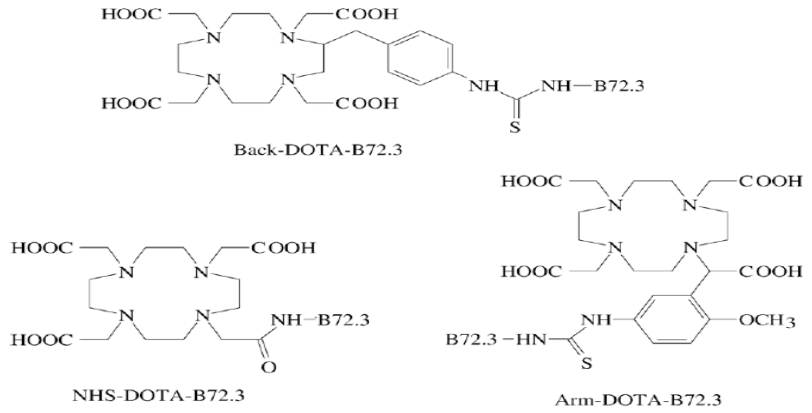

Figure 1.31: Structure of the dota-B72.3 conjugates

Fortin *et al.* have coupled an affibody ($Z_{HER2:342}$) to dota. This affibody binds to HER2/neu with picomolar affinity and can be used for targeting HER2/neu-expressing bladder carcinomas. The authors have labelled this conjugate with ^{177}Lu and ^{90}Y, and the complexes demonstrated high antigen-binding capacity and good cellular retention. Their biodistribution in normal mice demonstrated low uptake in all organs and tissues, except for kidneys, revealing to be a promising targeting conjugate for the treatment of bladder cancer [110].

1.3.4. Radiolanthanide Complexes Bearing Functional Groups with Affinity for Bone

It is well recognized that phosphonate or bisphosphonate groups have affinity for bone [118,122]. If such groups are present in a molecule, the adsorption to hydroxyapatite (inorganic matrix of bone, HA) is usually significant, and correlates with the number of carbon atoms separating the phosphonic acid groups [131]. For example, geminal bisphosphonates show the highest affinities for the HA. This class of bisphosphonates has found important applications in the treatment of diseases connected with disorder of calcium metabolism, including osteoporosis and Paget's disease [131]. Based on this knowledge, the utility of radiocompounds bearing phosphonate or biphosphonate groups has been extensively explored for bone pain palliation or therapy of metastasis, an important pathology which normally appears from primary tumors, such as breast or prostate cancer.

As referred, the only radiolanthanide complex in clinical use for bone pain palliation is ^{153}Sm - Samarium-edtpm (Quadramet®, figure 1.32a). Nevertheless, Quadramet®, although being the most used, due to the physical properties of ^{153}Sm, yet it is not an ideal radiopharmaceutical: ^{153}Sm-edtmp is not kinetically inert, so its preparation requires a large excess of the ligand (≈250-300). If such excess is not used a high liver uptake is found, due to the possible formation of ^{153}Sm-hydroxyl species [133]. Tetraazamacrocycles with phosphonate or bisphosphonate pendant arms form highly stable and kinetically inert complexes with radiolanthanides at a considerable lower ligand:metal ratio (1.5-2:1), justifying the interest of these ligands for the development of bone pain palliation agents. It has been shown that Ln-dotp (Ln= ^{153}Sm, ^{177}Lu, figure 1.32b) present potential to relief pain from bone metastases. The analogous ^{166}Ho-dotp seems to be an effective agent for bone marrow ablation in multiple myeloma patients [111,113, 115-117].

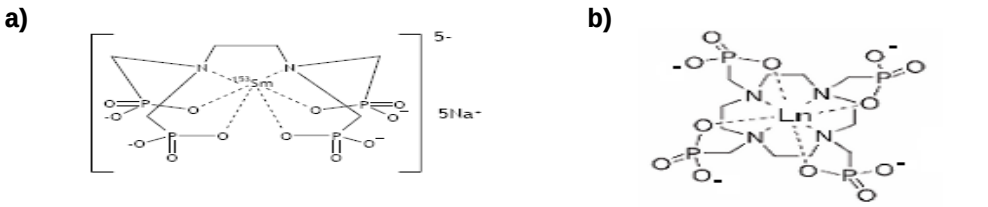

Figure 1.32: Structure of (**a**) ^{153}Sm-EDTMP and (**b**) Sm/Lu-dotp complexes

However, the relatively slow rate of formation of the dotp complexes, the low selectivity for a specific metal ion and the high osmolarity might be a disadvantage for the ^{153}Sm/^{166}Ho-dotp complexes [112,114]. To overcome some of these problems, the synthesis of mixed carboxylate/phosphonate, phosphinate or bisphosphonate dota-like macrocyclic ligands has been explored [119-121, 122-131].

Vitha et al. have comparatively tested lanthanide complexes of BPAMD and BPAPD for application in MRI, radiotherapy, and bone pain palliation (figure 1.33) [130].

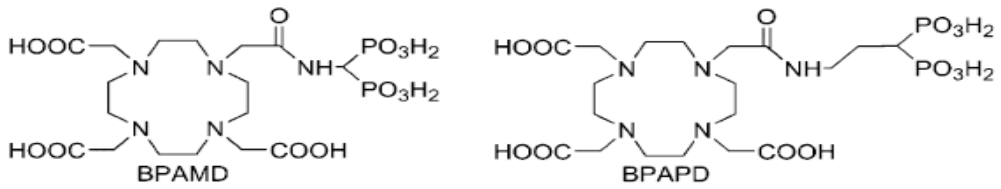

Figure 1.33: Structure of BPAMD and BPAPD

Solution studies performed for the complexes with BPAMD and BPAPD showed that the bisphosphonate moieties are not coordinated to the lanthanide, being predominantly mono- and diprotonated at physiological pH. The complexes are nine-coordinated, with one water molecule in the first coordination sphere of the Ln(III) ion, which remains bound upon adsorption on hydroxyapatite. The Ln(III) complexes formed with both ligands are very selective bone targeting agents. They particularly have shown high selectivity for newly formed bone and, therefore, they are promising diagnostic agents for bone tumors [130].

An *in vivo* γ-ray imaging study showed that the profile of the ^{177}Lu complexes is very similar, but the bone-uptake of the complex with BPAPD (bisphosphonate moiety more far away from the metal) seems to be slightly slower than that of BPAMD. The clearance of both ^{177}Lu-complexes from the body is mainly via the kidneys, but the clearance from the skeleton is probably too slow for application in MRI. Nevertheless, BPAPD might be very useful for radiodiagnosis or for bone pain palliation [130].

As shown along this chapter, several Cu, Sm and Ho-macrocycle-based conjugates have shown good coordination, radiochemical and biological behaviours, and some of them are even in clinical evaluation. Nevertheless, the seek for ideal macrocycle-base conjugates labelled with radiocopper and/or radiolanthanides is still an area of active development.

2. MACROCYCLES FOR STABILIZATION OF *d*-ELEMENTS

In this chapter the synthesis and characterisation of macrocyclic compounds for the stabilisation of *d*-elements is presented. Studies in solution and in the solid state were performed, namely with copper. Radiocopper complexes were also synthesized and evaluated *in vitro*.

Part of the work presented in this chapter has been published:

- S. Lacerda, M.P. Campello, I.C. Santos, I. Santos and R. Delgado, *Polyhedron*, **2005**, *24*, 451-461.
- S. Lacerda, M.P. Campello, I. Santos and R. Delgado, *Polyhedron*, **2007**, *26*, 3763-3773.

2.1. Introduction

As referred in Chapter 1, copper is a very interesting element for medical applications, as it has different isotopes with physical properties interesting for imaging or for therapy. From all the oxidation states of this element, Cu(II) is the more studied for the design of radiopharmaceuticals, due to its stability in aqueous solution [5,17,18]. The coordination chemistry of Cu(II) was explored using acyclic or cyclic chelators, mainly the ones which have nitrogen and oxygen donor atoms [5, 11, 17-19, 23-27]. From literature is clear that Cu(II) forms with tetraazamacrocycles more stable and kinetically more inert complexes than with nitrogen and oxygen donor acyclic ligands. However, the stability with tetrazamacrocycles depends on several parameters such as, rigidity, cavity size, and number and nature of the pendant arms. Bifunctional chelator agents (BFCA) derived from tetraazamacrocycles have been applied for labelling different biomolecules with radiocopper [134-137]. One possibility to conjugate biomolecules to the macrocycle is through a carboxylate group of the pendant arm. The number of 12[ane] tetraazamacrocycles bearing thiol and/or thioether groups as pendant arms for conjugation to biomolecules is scarce. When we started the work presented in this thesis there was only one reported tetraazmacrocycle bearing a thiol pendant arm. However, such compound had been generated and coupled *in situ* to biologically active molecules, without being isolated and characterized [138-141]. More recently, some dota derivatives with thiol functions were reported. They have been conjugated to peptides trough S-S bonds and applied for site-specific labelling of proteins [142], conjugation to antibodies [78,143] and redox-sensitive or blood-pool MRI contrast agents [144-146]. From all the described compounds, ^{64}Cu was only studied with one of those dota derivatives, the DO3A-vinylsulfone derivative [78].

According to the state of the art, we decided to explore in this thesis different tetraazamacrocycles and to evaluate their capability to stabilize Cu(II) complexes. We were interested on evaluating the effect of the cavity size, nature of the pendant arms and rigidity of the macrocycle on the thermodynamic stability and kinetic inertness of the Cu(II) complexes. To achieve such goal, we decided to synthesize and characterize novel cyclam and cyclen derivatives bearing sulphur, or sulphur and carboxylic pendant arms, and also to explore a tetraazamacrocycle having a benzene in its backbone. The coordination capability of these chelators towards Cu(II) and towards Zn^{2+}, an endogenous element which can compete *in vivo* with Cu(II), was also

studied. Thinking on chelation therapy, we have also studied the coordination capability of some of these macrocycles with Cd^{2+}, Pb^{2+} and Ni^{2+}. The results obtained in these studies are presented and discussed in this chapter.

2.2. Cyclam and Cyclen Derivatives

In general, to prepare mono-substituted tetraazamacrocycles, different synthetic methodologies have been described, namely the introduction of the side chain on the amine before cyclisation [139], pH controlled reactions [140], protection/deprotection methods [141] or alkylation of the macrocycle using an excess of the compound *versus* the desired alkylating agent [142]. It has also been reported that it was possible to introduce one oxygen or sulphur pendant arm in the cyclam and cyclen backbone by reacting the macrocycle with stoichiometric amounts of trimethylene oxide or ethylene sulphide, respectively [143-146]. We will present in the following pages the methodologies explored to prepare cyclam and cyclen derivatives as well as the studies performed with the tetraazamacrocycles successfully synthesized.

2.2.1. Cyclam Derivatives Bearing a Thiol Pendant Arm

To prepare mono-thiol derivatives of cyclam we have explored the methodologies shown in schemes 2.1 – 2.3. These methodologies involved direct alkylation methods (scheme 2.1), internal protection with glioxal (scheme 2.2) or tri-protection of the amines of the macrocyclic ring (scheme 2.3).

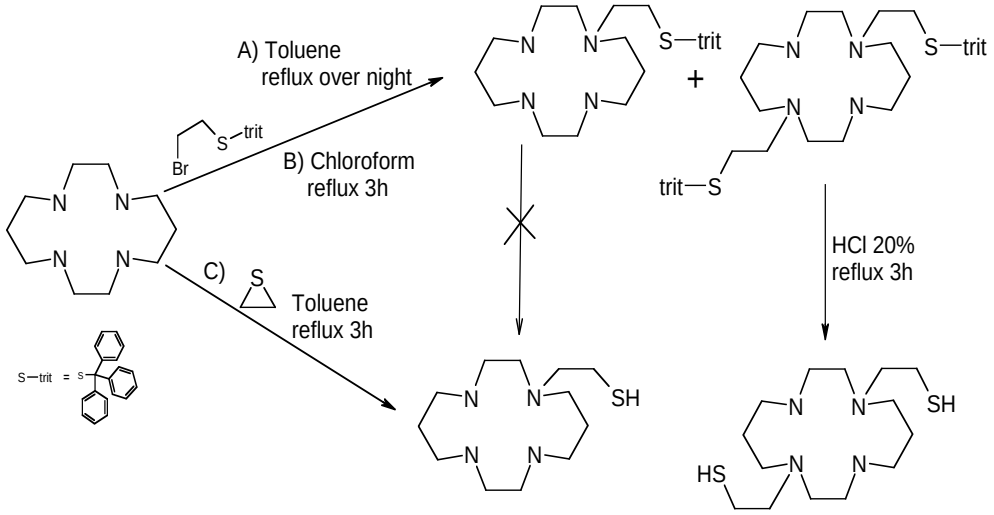

Scheme 2.1: Cyclam derivatives – direct alkylation

As can be seen in scheme 2.1, the direct alkylation of the cyclam with bromoethyl trytilthiol, synthesized according to Meegalla *et al.* [153], or with ethylene sulphide was carried out in different experimental conditions, namely solvents (toluene and chloroform), temperature (20ºC to 110ºC), and reaction time (3h -18h).

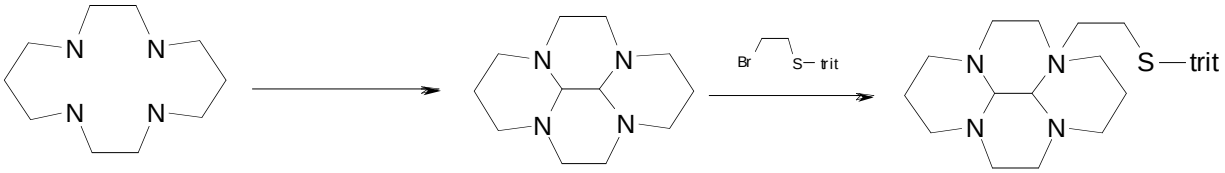

Scheme 2.2: Cyclam derivatives – protection with glioxal

In all these reactions we have obtained a mixture of the mono and bi-substitued cyclam. Attempts to separate those compounds always led to the decomposition of the mono-substituted, while the bi-substituted was recovered in a very low yield. These results led us to test another methodology which consisted on reacting the cyclam protected with glioxal with bromoethyl trytilthiol. Alkylation of cyclam-glioxal is normally run in dry acetronitrile at room temperature, but in these conditions the bromoethyl trityl-thiol is not soluble. Then, different solvents such as dry dichloromethane and a mixture of dry acetonitrile and methanol were also tested. The mono-substituted cyclam could be obtained but the overall yield was so low that we decided not to pursue.

This methodology was then leftover and the synthetic procedures shown in scheme 2.3 were tested. So, we protected the cyclam with either boc (*tert*-Butyloxycarbonyl) or with tfa (trifluoro acetic acid). This protection was successfully achieved, but the alkylation of the remaining amine with bromoethyl trytilthiol or the reaction with ethylene sulphide led to the desired product but in a very low yield and not pure.

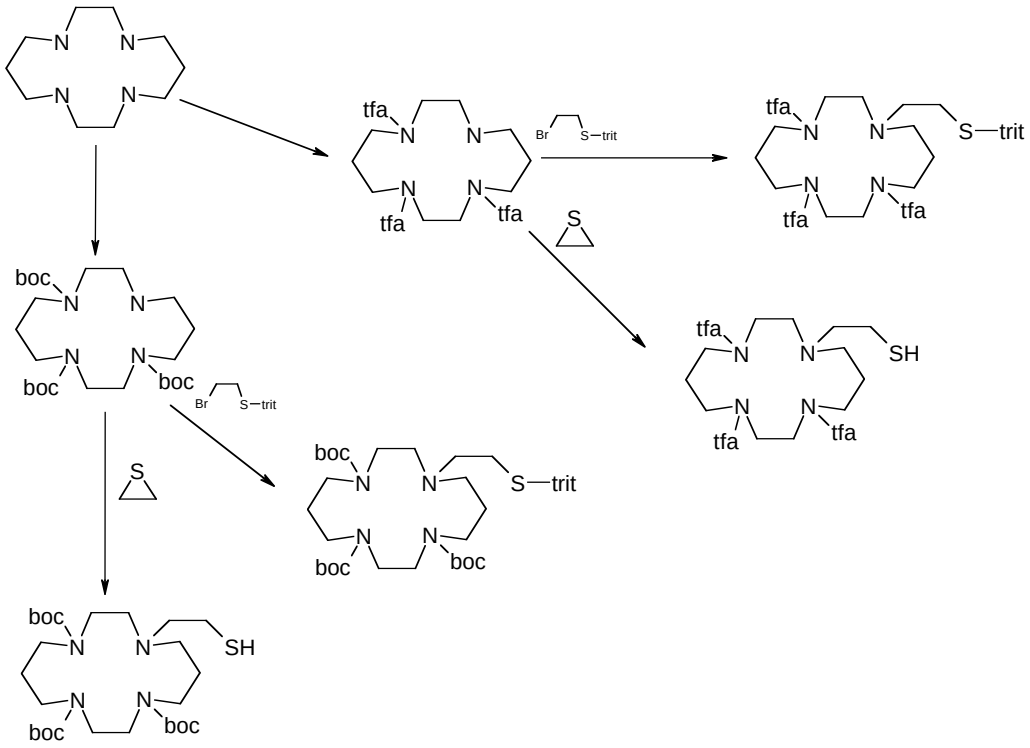

Scheme 2.3: Cyclam derivatives - triprotection of cyclam

From all the attempts described, only the synthetic route presented in Scheme 2.1 led to the formation of a new compound the 1,8-di-substituted thiol cyclam derivative (te2SH). This new macrocycle was isolated in a pure form and in 15% yield, after purification of the crude by column chromatography, using as stationary phase silica gel and as eluent a gradient of EtAcO/MeOH/NH_3. As shown in the experimental section, the characterization of te2SH involved ^{1}H- and ^{13}C-NMR spectroscopy. However, the te1SH was never recovered as a pure compound although its presence in the crude of the reaction could be identified by $^{1}H/^{13}C$-NMR spectroscopy.

2.2.2. Cyclen Derivative Bearing a Thiol Pendant Arm

Taking into account the stability constants of Cu(II) with cyclen, cyclam, dota and teta, as well as the corresponding basicity of each ligand, the pM (-log$[M]_{free}$) values for each complex at physiological pH (7.4) are the following:

dota (15.19) ≈ teta (15.19) > cyclam (10.54) > cyclen (10.02)

As can be seen, such results indicate that there is no difference, in terms of thermodynamic stability, between Cu-dota and Cu-teta. Also, it has been published

that Cu-dota derivatives present a kinetic inertness and a serum stability higher than Cu-teta. These data, together with the experimental difficulties on preparing cyclam derivatives made us to pursue our work based on cyclen.

2.2.2.1. Synthesis and Characterization of 2-[1,4,7,10-tetraazacyclododecan-1-yl] ethanetritylthiol (do1Strit) and 2-[1,4,7,10-tetraazacyclododecan-1-yl] ethanethiol (do1SH)

The synthesis of the mono-N-(2-ethanethiol) cyclen derivative (do1SH) was first tried following the methodology described by Moore et al., which involved the use of ethylene sulphide [138]. In our hands, such synthetic procedure has never worked properly and compound do1SH could never be isolated. Compound do1SH was finally synthesized in 40% overall yield, following the methodology indicated in scheme 2.4.

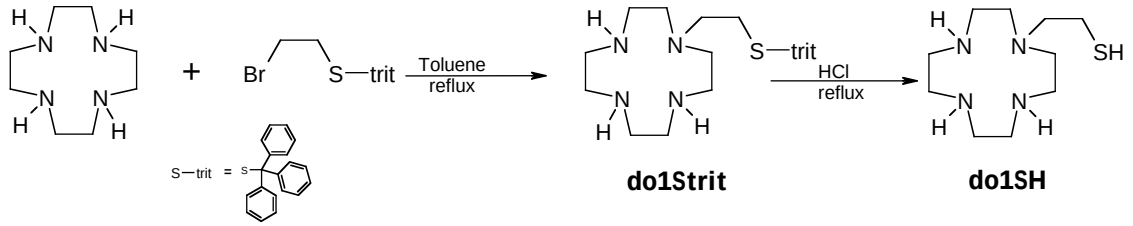

Scheme 2.4: Synthesis of ligands do1Strit and do1SH

As shown in scheme 2.4, we first prepared do1Strit by adding bromoethyl trytilthiol to cyclen in a 1:3 molar ratio. Compound do1Strit was purified by column chromatography, using $MeOH/NH_3$ as eluent. The fractions containing the pure compound were identified by TLC (silica plates, eluent: $MeOH/NH_3$) and analysed by ^1H- and ^{13}C-NMR spectroscopy. The ^1H-NMR spectrum of do1Strit, in $CDCl_3$, presented five resonances: two for the aromatic protons of trytil, one for the methylenic protons of the pendant arm and two multiplets for the protons of the macrocyclic backbone. The ^{13}C-NMR presented eleven resonances: four for the aromatic carbons of trytil group, one for the quaternary carbon of the trytil, one for the carbon of the pendant arm, in β position towards sulphur, four for the carbons of the macrocyclic backbone and another one for the carbon atom in α position towards sulphur.

Slow concentration of some fractions containing the pure do1Strit led to crystals suitable for X-ray crystallography. Compound do1Strit crystallises on the triclinic

system, P-1 space group, with cell parameters a = 8.1242(1) Å, b = 8.8600(1) Å, c = 27.0151(4) Å, α = 81.867(1) ° β = 82.113(1) ° γ = 63.902(1) ° and V = 1722.57(4) Å^3. The asymmetric unit contains one molecule of diprotonated do1Strit ($C_{29}H_{40}N_4S$), one sulphate dianion $(SO_4)^{2-}$ and six water molecules, being the molecular formula the following: $[C_{29}H_{40}N_4S].SO_4.6H_2O$.

Figure 2.1 presents an ORTEP diagram of the compound $[C_{29}H_{40}N_4S].SO_4.6H_2O$.

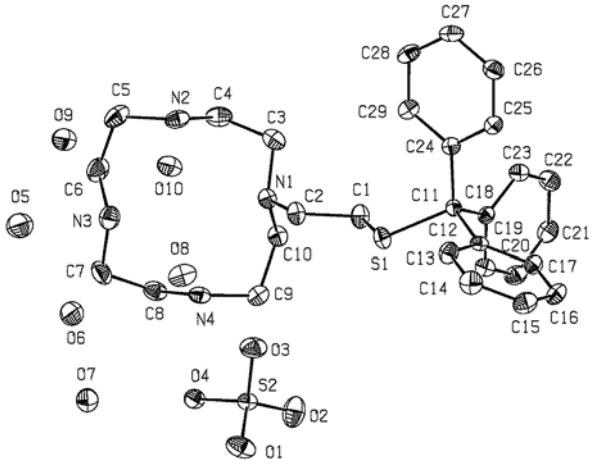

Figure 2.1: ORTEP diagram with atomic numbering scheme of asymmetric unit of $[C_{29}H_{40}N_4S].SO_4.6H_2O$, with thermal ellipsoids at 50% probability level (Hydrogen atoms are omitted for clarity)

The macrocycle was found to be protonated in the N2 and N4 amines. The average C – $N_{protonated}$ bond distances (1.490 Å) are slightly longer than the average C – $N_{unprotonated}$ ones (1.467 Å). These differences compare well with the values previously reported for other protonated macrocyclic ligands [154]. The four nitrogen atoms of the macrocycle are coplanar with a root mean square deviation (Rms) of 0.0306 Å. The CH_2 groups of the backbone are below this plane, while the sulphur arm is above, pointing in the opposite direction. The calculated torsion angle N1-C2-C1-S1 of 178.1° shows the relative position of the pendant arm towards the macrocycle cavity.

Selected bond lengths (Å) and angles (°) for the dication $[C_{29}H_{40}N_4S]^{2+}$ are listed in Table 2.1.

Table 2.1: Selected bond length (Å) and angles (°) for the dication $[C_{29}H_{40}N_4S]^{2+}$

Bond length (Å)			
S(1)-C(1)	1.822(2)	N(2)-C(4)	1.484(3)
S(1)-C(11)	1.862(2)	N(2)-C(5)	1.497(3)
C(1)-C(2)	1.531(2)	N(3)-C(6)	1.459(3)
N(1)-C(2)	1.470(2)	N(3)-C(7)	1.471(3)
N(1)-C(3)	1.472(2)	N(4)-C(8)	1.483(2)
N(1)-C(10)	1.467(2)	N(4)-C(9)	1.497(2)
Angle (°)			
C(1) – S(1) – C(11)	105.14(8)	C(2) – C(1) – S(1)	105.56(12)
C(10) – N(1) –C(3)	111.02(14)	N(1) – C(2) –C(1)	116.56(15)
C(5) – N(2) –C(4)	117.13(16)	C(3)- N(1)-C(2)	113.99(15)
C(7) – N(3) –C(6)	113.57(16)	C(10)- N(1)-C(2)	115.64(14)
C(8) – N(4) – C(9)	114.98(15)		

The crystal packing of do1Strit is shown in Figure 2.2. This packing is characterised by the formation of a bidimensional layer parallel to the bc plane due to several hydrogen bonds between the water molecules and due to intermolecular short N···O and C···O contacts between the SO_4^{2-} units and the macrocycle.

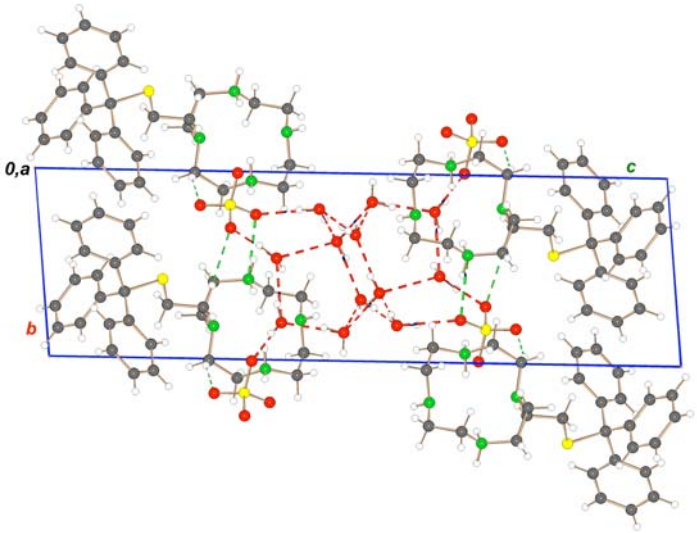

Figure 2.2: Crystal structure of $[C_{29}H_{40}N_4S].SO_4.6H_2O$ viewed along *a*

In table 2.2 are shown selected hydrogen bonds and short contacts in the crystal structure of compound do1Strit.

Table 2.2: Selected hydrogen bonds and short contacts in the crystal structure of $[C_{29}H_{40}N_4S].SO_4.6H_2O$

		Distance (Å)
$O_{sulphate}\cdots N$	O4···N4	2.766(2)
	O4···N2	2.764(3)
$O_{sulphate}\cdots H\text{–}C_{backbone}$	O1···H4b–C4	2.612(2)
	O1···H6b–C6	2.381(2)
	O3···H2a–C2	2.564(1)
$O_{sulphate}\cdots H\text{–}C_{aromatic}$	O2···H14–C14	2.456(2)
	O2···H28–C28	2.688(2)

The deprotection of do1Strit with HCl under reflux, yielded compound do1SH in almost quantitative yield (scheme 2.4).

Compound do1SH is quite soluble in water and stable under aerobic conditions and has been characterised by mass spectrometry and multinuclear NMR spectroscopy (^{1}H, ^{13}C, ^{1}H,^{1}H COSY, ^{1}H,^{13}C HSQC), at different pD values (range 1–14).

In the LDI-positive mass spectrum three main peaks were found at m/z = 233.191, 255.156 and 271.118 corresponding to $[M+H]^+$, $[M+Na]^+$ and $[M+K]^+$, respectively.

^{13}C-NMR spectra of do1SH have been recorded in the pD range 1.05 to 14.00. The spectrum recorded at pD 1.05 exhibit six resonances, consistent with the two-fold symmetry expected for do1SH. At higher pD values the ^{13}C-NMR spectra has shown always the same pattern, while the ^{1}H-NMR spectra became less clear due to the overlapping of some resonances. At pD=1.05, the ^{1}H-NMR spectrum presented five resonances with different multiplicities at 2.54, 2.70, 2.84, 2.97, 3.07 ppm in an intensity ratio of 2:2:4:4:8.

The assignment of the ^{1}H and ^{13}C-NMR resonances was based on 2D-NMR studies (^{1}H,^{1}H and ^{1}H,^{13}C correlations), performed at pD = 1.05. Figure 2.3 shows the g-COSY ^{1}H,^{1}H and the g-HSQC ^{1}H,^{13}C 2D correlations. From these studies it was possible to conclude that the triplets centered at 2.54 and 2.70 ppm correlate with the carbons at 22.03 and 56.81 ppm, respectively. Based on the carbon and proton NMR data of the free arm and on literature data, the resonances at 22.03 and 56.81 ppm were assigned to the α (*C1*) and β (*C2*) carbon atoms of the pendant arm, respectively. The

triplet centred at 2.84 ppm (4H) correlates with the carbon atoms at 50.26 ppm (*C3)*. The multiplet at 2.97 ppm (4H) correlates with the carbon atom at 44.39 ppm and correlates with the multiplet at 3.07 ppm (8H). Based on these data the resonance at 44.39 ppm was assigned to the *C6* carbon atoms and the multiplet at 3.07 ppm (8H) was assigned to the protons bound to the *C4* and *C5* atoms, which appear at 45.64 and 43.92 ppm, respectively.

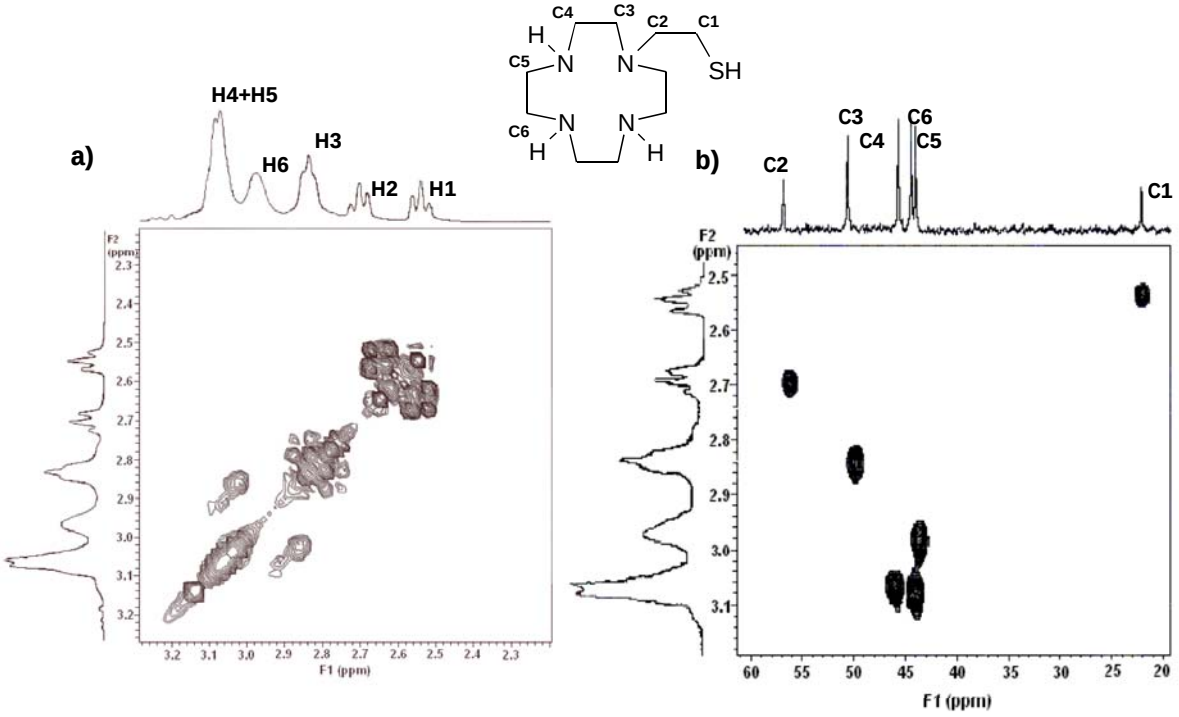

Figure 2.3: g-COSY $^{1}H,^{1}H$ (a) and g-HSQC $^{1}H,^{13}C$ (b) 2D correlations for do1SH, at pD = 1.05

In Table 2.3 are presented the chemical shifts and the corresponding assignment of the resonances for do1SH at pD = 1.05.

Table 2.3: ^{1}H and ^{13}C NMR data for do1SH at pD = 1.05

Assignment	Chemical shift (ppm)	
	^{1}H	^{13}C
C1	2.54 (t, 2 H)	22.03
C2	2.70 (t, 2 H)	56.81
C3	2.84 (t, 4 H)	50.26
C4	3.07 (m, 8 H)	45.64
C5		43.92
C6	2.97 (m, 4 H)	44.39

2.2.2.2. Protonation Constants of do1SH

The protonation constants of do1SH were determined by potentiometry at 25.0 ºC and 0.10 mol dm^{-3} KNO_3 ionic strength, and the protonation sequence of the macrocycle was assigned based on ^{13}C-NMR spectrometry. Compound do1SH has five protonation constants, from which four could be determined by potentiometry, but the remaining one is too low to be determined by this technique. The values found are summarised in Table 2.4, together with the protonation constants of some related tetraazamacrocycles, namely cyclen, N-methyl cyclen (**I**), 2-hydroxyethyl cyclen (**II**) and 3-hydroxypropyl cyclen (**III**) (Figure 2.4) [151,155].

Table 2.4: Protonation constants (log units) of do1SH and other related macrocyclic ligands

Species	do1SH [a]		cyclen [b]	I [c]	II [d]	III [e]
l h	log β_{LH_i}	log K_{LH_i}	log K_{LH_i}	log K_{LH_i}	log K_{LH_i}	log K_{LH_i}
1 1	10.98(2)	10.98	10.97	10.7	10.72	10.56(4)
1 2	20.96(2)	9.98	9.87	9.7	9.28	9.14(4)
1 3	29.11(4)	8.15	1.6	< 2	< 2	<2.3
1 4	31.39(6)	2.28	0.8	< 2	< 2	<2.3

* Values in parentheses are standard deviations in the last significant figures. [a] T = 25.0 ºC, I = 0.10 mol dm^{-3} in KNO_3, this work; [b] I = 0.50 mol dm^{-3} in KNO_3, ref. 155a and I = 0.20 mol dm^{-3} in $NaClO_4$, ref. 155b; [c] I = 0.10 mol dm^{-3} in $NaNO_3$, ref. 155d; [d] I = 0.10 mol dm^{-3} NEt_4ClO_4, ref. 151; [e] I = 0.10 mol dm^{-3} in $NaClO_4$, ref. 155c.

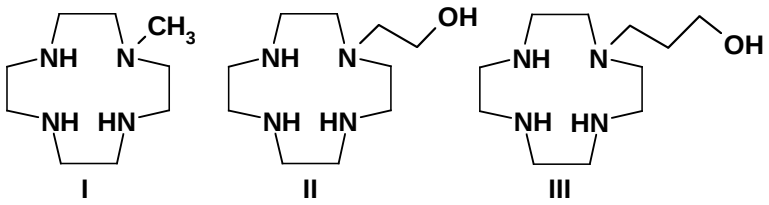

Figure 2.4: Structure of the ligands used for comparison: N-methyl cyclen (**I**), 2-hydroxyethyl cyclen (**II**) and 3-hydroxypropyl cyclen (**III**)

We have found three high protonation constants and one relatively low. Based on the values shown inTable 2.4 it is difficult to ascribe the protonation sequence of do1SH. In order to understand this sequence a ^{13}C-NMR titration was performed.

^{13}C-NMR Studies

As we referred, the ^{1}H- and the ^{13}C-NMR spectra of do1SH have been run at different pD values. These studies were carried out at 20ºC without controlling the ionic strength [156]. The ^{1}H-NMR data are not reported due to the broadness and overlapping of the signals. Considering these results, we have used the ^{13}C-NMR data to predict the protonation sequence of do1SH. For that, we have studied the variation of the ^{13}C chemical shift of do1SH as function of the pD (figure 2.5).

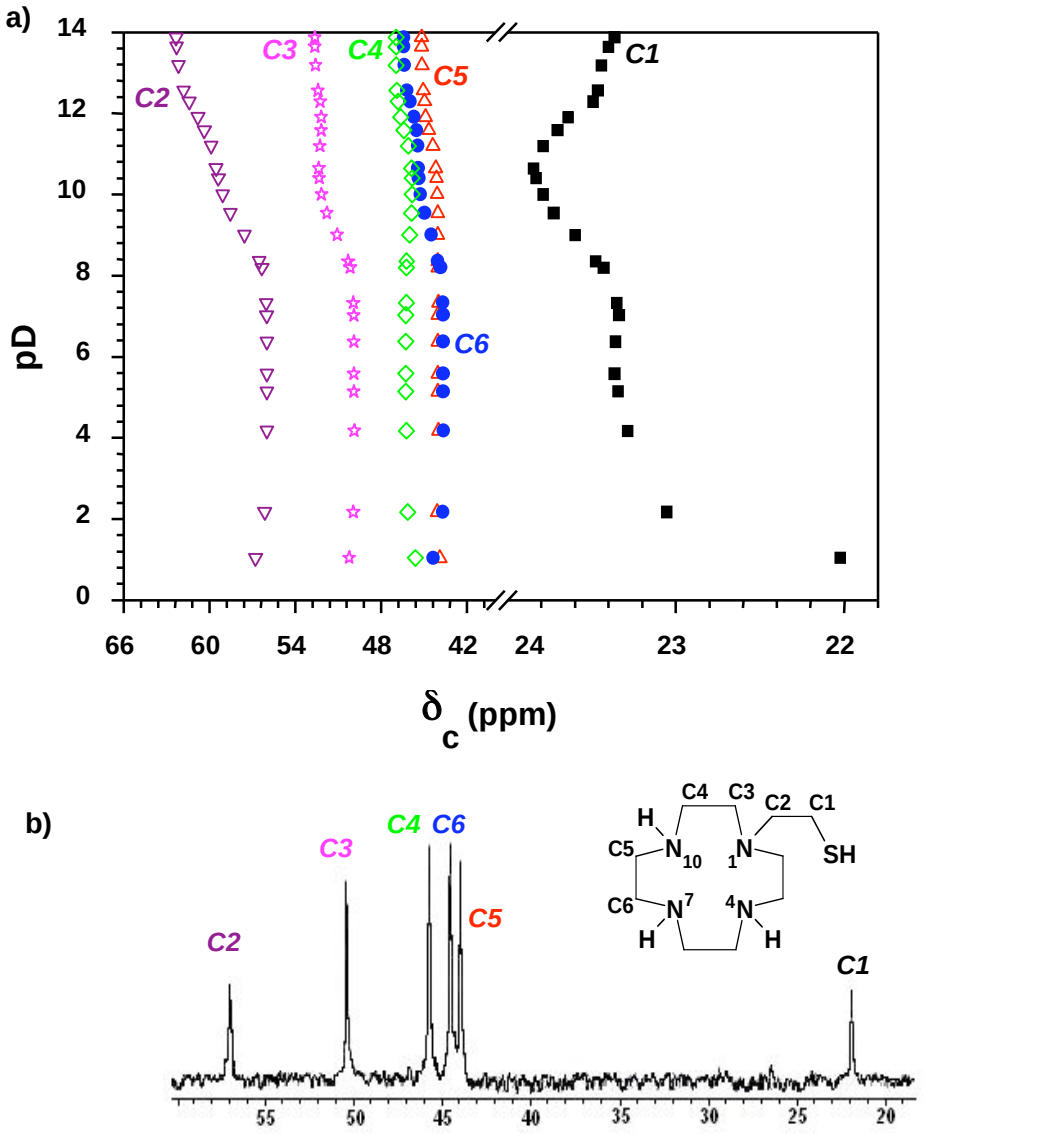

Figure 2.5: a) ^{13}C-NMR titration curves for do1SH (chemical shift (δ_C) in function of pD): ■ ***C1***, ▽ ***C2***, ☆ ***C3***, ◊ ***C4***, Δ ***C5*** and ● ***C6***; **b)** ^{13}C-NMR spectrum of do1SH (D_2O, pD = 1.05)

In the entire pD range the ^{13}C NMR spectra of do1SH exhibit six resonances. Single resonances have been observed for each magnetically equivalent carbon atom which indicates a rapid exchange between protonated species. To analyse these data the pK_H values determined for do1SH (Table 2.4) were converted to pK_D, using the correlation pK_D = 0.11 + 1.10 pK_H, determined for polyaza and polyoxa-polyaza macrocyclic compounds [157]. The calculated values were: pK_{D1} = 12.19, pK_{D2} = 11.09, pK_{D3} = 9.08 and pK_{D4} = 2.62. Analysing the NMR titration curves three pD regions were defined: one comprising two protonation constants (13.0 ≥ pD ≥ 10.5), and the other two comprising one protonation constant each (10.5 ≥ pD ≥ 8.0 and pD ≤ 3.0). The high symmetry of do1SH makes difficult to predict the protonation sequence, but an attempt has been made taking into account that when a protonation occurs at a given site the β-carbons are upfield shifted [158]:

- In the **13.0 ≥ pD ≥ 10.5** region two protonations occur, and their constant values differ only by one log unit, which makes difficult to distinguish the effect of each. However, taking into account that in this range the resonances ***C2***, ***C4*** and ***C5*** are upfield shifted while ***C1*** shifts downfield, it seems that the thiol group is protonated and a second proton may be shared by the **N_1** and **N_7** amines.

- In the region **10.5 ≥ pD ≥ 8.0** a third protonation occurs on one amine of the macrocyclic ring, and this proton together with the one already existing in the macrocycle backbone will be shared by the **N_1**/**N_4**/**N_{10}** amines. This is supported by the upfield shift of the resonances ***C1***, ***C3***, and ***C6***.

- In the pD range **8.0 ≥ pD ≥ 3.0** no significant changes were observed.

- For **pD ≤ 3.0**, the ***C1***, ***C4*** and ***C5*** carbon atoms are upfield shifted, being ***C1*** the most significantly shifted (ca.1 ppm), which may indicate the protonation of the **N_1** centre.

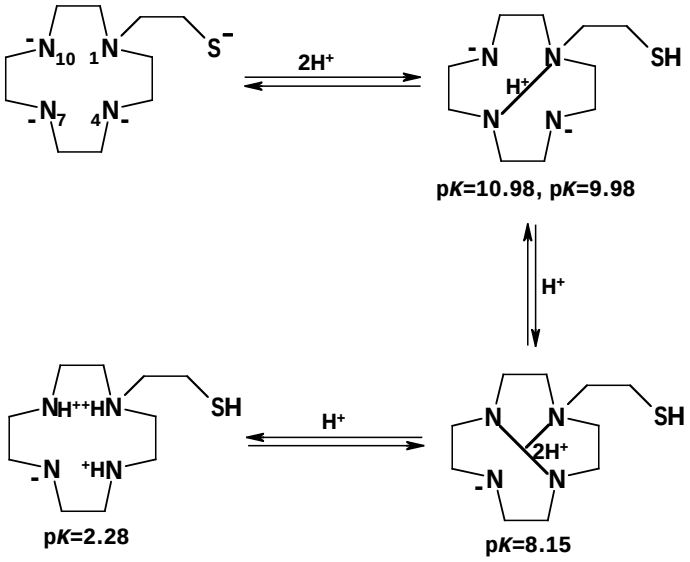

Scheme 2.5: Proposed protonation sequence for do1SH

The first protonation constant corresponds to the protonation of the thiol group, see below, and the remaining constants correspond to the amine centers. As it it possible to see by the values reported in table 2.4 for similar compounds, the difference between the constants found for cyclen and mono-substituted cyclen derivatives is small, being difficult to ascribe, based only in the observation of the values, which constant takes place in the tertiary amine even if the substitution of an hydrogen atom by an R- substituing group in a secondary amine leads to a decrease in its basicity. Nevertheless, in the case of do1SH the third constant is smaller than the ones reported for the similar compounds. This constant may correspond to the tertiary amine center and the lower value may be related to the presence of the thiol group.

2.2.2.3. Stability Constants of do1SH with Copper and Other Metals with Biological Interest

The complexation of do1SH with Cu^{2+}, Zn^{2+} and Cd^{2+} was followed by potentiometry, at 25.0 ºC and 0.1 $moldm^{-3}$ KNO_3, and the corresponding stability constants were determined. The kinetics of formation of the complexes of do1SH with these transition metal ions is relatively slow. The stability constants were determined by the use of a batch method in the pH regions where complexation equilibrium was not attained during in-cell titrations, leading to stability constants with relatively high standard deviations. In Table 2.5 are listed the stability constants of the complexes

of do1SH with Cu^{2+}, Zn^{2+} and Cd^{2+}, together with the constants for other related tetraazmacrocycles [159].

For a better visualisation of the existing species over a pH range, species distribution diagrams can be drawn based on the stability constants determined. Such diagrams are drawn using programs, such as HySS program [160], and are determined for an excess of 100% of ligand.

Table 2.5: Stability constants (log units) for complexes of do1SH and other related ligands with Cu^{2+}, Zn^{2+} and Cd^{2+} ions

Metal	Species m h l	do1SH [a]		cyclen [b]	III [c]
		log β_{MH_iL}	log K_{MH_iL}	log K_{MH_iL}	log K_{MH_iL}
Cu^{2+}	**1 0 1**	21.19(6)	21.17	23.29 / 24.8	17.3(1)
	1 1 1	27.45(4)	6.26	–	–
	1 2 1	30.47(7)	3.02	–	–
	1 -1 1	12.2(1)	8.99	–	10.2
Zn^{2+}	**1 0 1**	18.6(1)	18.6	16.2	13.7(1)
	1 1 1	25.60(2)	7.00	5.74	–
	1 -1 1	8.8(1)	9.8	–	8.3
Cd^{2+}	**1 0 1**	18.8(1)	18.8	14.3	13.0(1)
	1 1 1	25.51(5)	6.71	–	–
	1 2 1	–	–	–	9.8
	1 -1 1	9.2(1)	9.6	–	–
	1 -2 1	-1.7(1)	10.9	–	–

* Values in parentheses are standard deviations in the last significant figures. [a] This work, T = 25.0 °C, I = 0.10 mol dm^{-3} KNO_3, this work; [b] I = 0.1 mol dm^{-3} $NaNO_3$, ref. 155a; [c] T = 25.0 °C , I = 0.1 mol dm^{-3} KCl, ref. 151.

Figure 2.6 shows the species distribution diagrams for M-do1SH (M=Cu^{2+},Zn^{2+},Cd^{2+}).

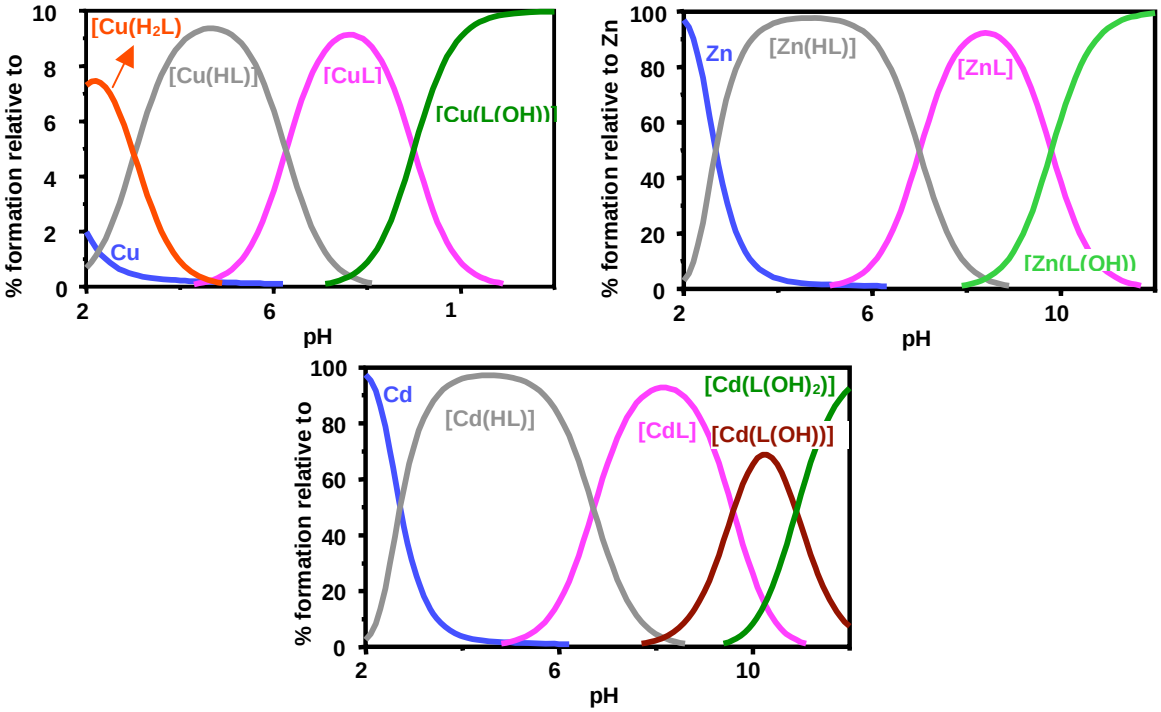

Figure 2.6: Species distribution diagrams for the Cu^{2+}, Zn^{2+} and Cd^{2+} complexes with do1SH, $C_L = 2C_M = 1.0\times10^{-5}$ mol dm^{-3} (charges were omitted)

Only mononuclear species were formed with the studied metal ions, namely [ML], [M(HL)], [$M(H_2L)$], [M(L(OH))] and [$M(L(OH)_2)$]. The latter species is only formed for Cd^{2+}, while [$M(H_2L)$] only exists when M = Cu^{2+}. At physiological pH, the [ML] complex is formed at about 100% for Cu^{2+}, while for Cd^{2+} and for Zn^{2+} only above pH 8 this is the main species (Figure 2.6).

As can be seen in Table 2.5, the stability constants of the complexes studied follow the trend: [Cu-do1SH] > [Zn-do1SH] ≈ [Cd-do1SH]. Such trend is the usually found for cyclen derivatives. However the log $K_{Cu\text{-}do1SH}$/log $K_{Zn\text{-}do1SH}$ and log $K_{Cu\text{-}do1SH}$/log $K_{Cd\text{-}do1SH}$ ratios are smaller than usually found for ligands having only amine donor atoms, such as cyclen or cyclam. This feature, together with the larger values of K_{ML} observed for do1SH, when compared to cyclen, strongly suggests the involvement of the arm in the coordination sphere of the metal centre. For all the metal ions, completely different direct and back titration potentiometric curves were obtained, suggesting structural rearrangements, may be related with the formation and break of the M-S bond.

A direct comparison of stability constants of do1SH and those reported for cyclen, **III** (Figure 2.4) and cyclam can only be made using pM (-log[M^{2+}]) values, due to the different basicity of the ligands. In table 2.6 are listed the pM values for do1SH as well as the ones calculated for related tetraazamacrocycles.

Table 2.6: pM values[a] calculated for do1SH and other related ligands (pH = 7.4)

Ion	do1SH	cyclen	III
Cu^{2+}	14.24	9.27, 10.02	11.59
Cd^{2+}	11.91	4.73	7.29
Zn^{2+}	11.77	5.68	7.99

[a] The values were calculated for 100% excess of free ligand, using the program HySS [160], $C_L = 2C_M = 1\times10^{-5}$ mol dm^{-3} and the stability constants given in Table 2.5.

The data shown in table 2.6 indicate that compound do1SH has higher affinity for Cu^{2+}, Cd^{2+} and Zn^{2+} than the tetraazamacrocycles considered for comparison. More specifically we can say that for the same cavity size, the presence of a coordinating pendant arm increases significantly the stability of the complexes. However, do1SH shows a lower selectivity for Cu^{2+} over Zn^{2+} and Cd^{2+} than the other macrocycles considered for comparison.

2.2.2.4. Solution Structural Studies of Cu- and Zn-do1SH

The structure of a metal complex in solution can be assessed with the help of techniques such as NMR, UV-Vis and EPR spectroscopies. In the case of copper(II) complexes it is not possible to perform NMR spectroscopy because these complexes are paramagnetic. The structure in solution of the Cu(II) complexes can then be assigned using UV-Vis and EPR spectroscopies. NMR studies were performed to study the solution structure of Zn^{2+} complexes.

2.2.2.4.1. UV-vis and EPR Spectroscopic Studies of Copper(II) Complexes

The UV-vis-NIR and the EPR spectra of Cu^{2+}/do1SH were recorded at pH 5, 8 and 12. At these pH values, about 100% of the [Cu(HL)], [CuL] and [Cu(L(OH))] species are respectively formed (Figure 2.6). Similar studies with Cu^{2+}/cyclen were also performed in the same condition, to assess the influence of the thiol pendant arm in the structure of Cu-do1SH.

In table 2.7 the spectroscopic data found for Cu^{2+}/do1SH and Cu^{2+}/cyclen are presented, together with data for related macrocycles and for the aqua-complex $[Cu(H_2O)_6]^{2+}$, taken from the literature.

Table 2.7: Spectroscopic data for the copper(II) complexes of do1SH and other related ligands taken from literature

Cu(II) complexes (pH)	UV-vis-near IR	EPR (10^4 A_i / cm^{-1})					
	λ / nm (ε /$mol^{-1}dm^3cm^{-1}$)	g_x	g_y	g_z	A_x	A_y	A_z
Cu-do1SH (5) [a, b]	612 (112); 277 (4×10^4)	-	-	2.198	-	-	182.14
Cu-do1SH (8) [a]	615 (132); 270 (6×10^4)	2.040	2.055	2.198	16.88	17.68	182.41
Cu-do1SH (12) [a]	620 (220); 273 (8×10^4)	2.041	2.082	2.200	1.92	7.68	186.98
Cu-cyclen (5) [a]	579 (56); 282 (1×10^4)	2.040	2.055	2.197	16.88	21.02	181.97
Cu-cyclen (8) [a]	578 (56); 274 (3×10^4)	2.040	2.055	2.196	16.88	21.02	181.99
Cu-cyclen (12) [a]	581 (80); 274 (3×10^4)	2.052	2.060	2.212	2.30	10.33	180.23
$[Cu(cyclen)Cl]^+$ [c]	599 (220)	2.057		2.198	24.1		184.2
$[Cu(cyclam)]Cl_2$ [c]	513 (100)	2.049		2.186	38.7		205.0
$[Cu(H_2O)_6]^{2+}$ [d]	-	2.08		2.4	-	-	134.0

[a] This work; [b] Species A: g_z = 2.410 and A_z = 131.92; [c] ref. 161; [d] ref. 162.

As can be seen in Table 2.7, the electronic spectra of the Cu^{2+} complexes with do1SH and cyclen exhibit two well defined bands, one in the UV-vis range and another in the charge transfer region. A red-shift of the band in the UV-vis is expected when the geometry of a Cu^{2+} complex changes from a square planar to a penta-coordinated one. For Cu^{2+}/cyclam [161] and Cu^{2+}-1,4,8-trimethyl-11-(2-thioethyl)-1,4,8,11-tetraazacyclotetradecane [139a], which have been considered to be four and five-coordinated, the maximum absorption of the bands has been reported to be at λ_{max} = 513 nm and 622 nm, respectively. Our data for Cu^{2+}/do1SH and Cu^{2+}/cyclen seem to indicate that in the complexes studied in this work the copper centre is five-coordinated. In the pH range studied, both complexes present the same pattern for the UV-vis spectra and the maximum of absorption does not change significantly with the pH. These results may suggest that the environment around the Cu is the same, independently of the protonation of the corresponding ligand. However, the molar absorptivity of the complex Cu^{2+}/do1SH increases with pH, indicating a highest distortion for the complex, most probably due to the deprotonation of the sulphur atom and formation of a strong apical Cu-S bond.

In Figure 2.7 are shown the X-band EPR spectra of Cu^{2+}/do1SH and Cu^{2+}/cyclen complexes and their simulated spectra, at different pH values. All the spectra indicated the presence of only one species, except for Cu^{2+}/do1SH at pH 5, which revealed the presence of two species. All the spectra showed the expected four well-resolved lines at low field, due to the interaction of the unpaired electron spin with the copper nucleus. The hyperfine coupling constants (*A*) and *g* values obtained by the simulation of the spectra [163] are shown in Table 2.7, together with those of other copper(II) complexes taken from literature, for comparison [161,162]. The simulation of the spectra revealed three different *g* values with $g_z > (g_x+g_y)/2$ and the lowest $g \geq 2.04$, which is characteristic of mononuclear copper(II) complexes having rhombic-octahedral with elongation of the axial bonds or distorted square-based pyramidal symmetries, and $d_{x^2-y^2}$ ground state.

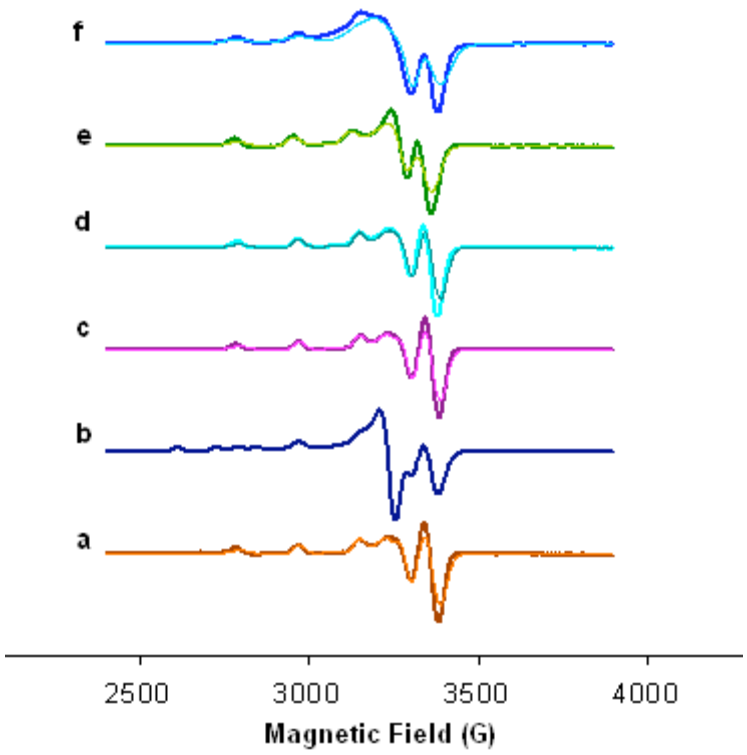

Figure 2.7: X-band EPR spectra of copper complexes of do1SH and cyclen in ≈ 1.5×10^{-3} mol dm^{-3} and 40% DMSO/H_2O solutions (strong lines) and the simulated spectra (smooth lines) at different pH values: (a) Cu^{2+}/Cyclen pH = 5, at 114.5 K; (b) Cu^{2+}/do1SH pH = 5, at 111.6 K; (c) Cu^{2+}/Cyclen pH = 8, at 105.9 K; (d) Cu^{2+}/do1SH pH = 8, at 112.2 K; (e) Cu^{2+}/Cyclen pH = 12, at 119.4 K and (f) Cu^{2+}/do1SH pH = 12, at 107.6 K. All spectra were recorded with microwave power of 2.0 mW, modulation amplitude of 1 mT, and frequency of 9.41 GHz

The two species present, at pH = 5, in the EPR spectrum of Cu^{2+}/do1SH are in about the same proportion, based on the intensity of the bands. The simulation of this spectrum could not be obtained and so is not presented. Nevertheless, the direct analysis of the spectrum and the estimated g_z and A_z parameters suggest that one species (species A) corresponds to the aqua-complex $[Cu(H_2O)_6]^{2+}$, and the other to the species found at pH = 8 (species B).

The EPR parameters of the Cu^{2+}/do1SH and Cu^{2+}/cyclen complexes (at pH ≥ 5) are similar pointing to identical coordination environments. The g_i and A_i values are related to the electronic transitions by the factors derived from the ligand field theory [167,168]: the g_i values increase and the A_i values decrease as the equatorial ligand field becomes weaker or the axial ligand field stronger and this occurs with the simultaneous red-shift of the *d–d* absorption bands in the electronic spectra [164-166].

Additionally the EPR data obtained in this work for the copper(II) complexes of do1SH and cyclen are quite different from those for Cu^{2+}/cyclam also collected in Table 2.7. In the latter complex the copper has a square planar geometry, with the equatorial plane formed by the four nitrogen atoms of the macrocycle and the metal centre included into the cavity [167]. Indeed, the 12-membered cavity of do1SH and cyclen is too small for the copper centre, and therefore the macrocycle take a folded arrangement with the metal out of the cavity. In the cyclen complex a water molecule or other solution ion completes a five-coordination geometry, while in the Cu^{2+}/do1SH the sulphur of the arm certainly do the same effect. A square-pyramidal geometry is expected for do1SH complexes since in the case of a trigonal-bipyramidal a $g_\perp > g_{||}$ and a UV-vis band in the region 800-850 nm would be observed [37]. Thus, considering the UV-vis and the EPR data, a square pyramidal geometry is expected for all the complexes studied in this work, and the small changes observed for Cu^{2+}/do1SH versus Cu^{2+}/cyclen can be most probably only assigned to distortions in the structure, promoted by a stronger coordination of the thiol group at higher pH.

2.2.2.4.2. NMR Studies of Zinc(II) Complexes

Due to the impossibility of studying Cu(II) complexes by NMR spectroscopy we have decided to study the ^{13}C NMR spectra of solutions containing Zn^{2+} and do1SH (1:1

molar ratio) at different pD values. Based on the species distribution diagram (Figure 2.6), we have chosen 5.6, 7.6 and 11.6 pH values to run such studies, which correspond to the [Zn(HL)], [ZnL] and [Zn(L(OH))] species, respectively. In Table 2.8 are collected the chemical shifts of the carbon atoms of the Zn^{2+}/do1SH species formed as well as those for the free do1SH, recorded in the same experimental conditions.

Table 2.8: Chemical shift (δ/ ppm) of the carbon atoms of do1SH and of the species Zn/do1SH at pD 6, 8 and 12

	pD ≈ 6		pD ≈ 8		pD ≈ 12	
	do1SH	Zn/do1SH	do1SH	Zn/do1SH	do1SH	Zn/do1SH
C1	23.36	26.37	23.43	26.02	23.64	25.97
C2	56.02	55.07	56.36	57.22	60.84	57.18
C3	49.93	51.66	50.20	52.22	52.22	52.18
C4	46.30	46.54	46.26	47.22	46.66	47.19
C5	44.04	45.64	44.05	46.18	44.93	44.45
C6	43.69	44.40	43.87	44.49	45.71	46.14

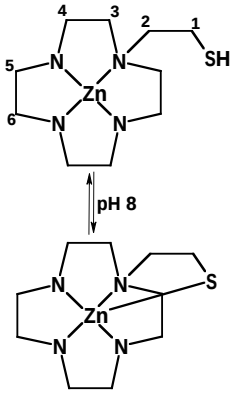

The same number of resonances (six) was found in all the spectra, being this value similar to the number of resonances found for the free ligand. However, most of the carbon atoms of do1SH are significantly downfield shifted upon coordination to the Zn^{2+}. These results are consistent with the formation of a Zn^{2+}/do1SH complex and seem to indicate that all the donor atoms are coordinated to the metal. The significant downfield shift observed for ***C2***, when pD increases from 6 to 8, may be correlated to the deprotonation followed by coordination of the thiol group, in agreement with the potentiometric studies (Table 2.5). Also, in the solution studies performed with Cu(II) we have found that the increase of the pH leads to the coordination of the sulphur atom to the metal ion.

2.2.3. Cyclen Derivative with Thiol/Carboxylate Pendant Arms

2.2.3.1. Synthesis and Characterization of 1,4,7,10-tetraazacyclododecane-1,4,7-triacetic-10-ethanethiol acid (do3aSH)

As indicated in Scheme 2.6, do3aSH has been synthesised by alkylation of do1Strit with ethyl-bromoacetate followed by acidic hydrolisis. Compound do3aSH was obtained in relatively high yield (59%). However, the up-scale of this reaction proof to be difficult, due to the formation of side products during the alkylation reaction. To overcome this problem, we have tried different experimental conditions, namely alkylating reagents ($BrCH_2COO^tBu$ or $BrCH_2COOH$), solvents (CH_2Cl_2, $CHCl_3$, dioxane, toluene), bases ($Cs(CO_3)_2$, DIPEA), temperature and reaction time. The use of do3a, do3Et and do3^{t}Bu as starting material followed by the alkylation with $BrCH_2CH_2Strit$ was also tested. From all the synthetic procedures evaluated, the one described in scheme 2.6 was the best, but up-scaling is not possible without compromising the overall yield of the reaction. This means that in each reaction we must not use more then 300mg of do1SH to alkylate.

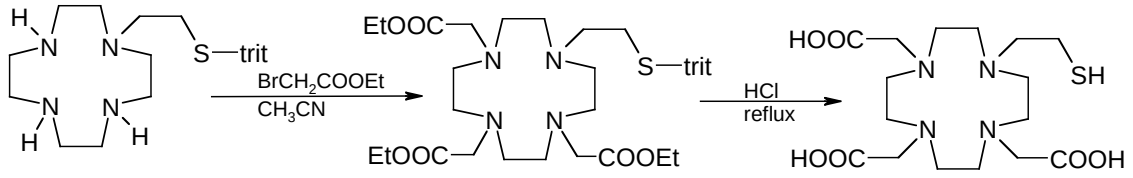

Scheme 2.6: Synthesis of do3aSH

Compound do3aSH is quite soluble in water and stable under aerobic conditions at pH ≤ 8. The formulation of do3aSH was mainly based on mass spectrometry, multinuclear NMR spectroscopy (^1H, ^{13}C, $^1H,^1H$ COSY, $^1H,^{13}C$ HSQC) at acidic pD and elemental analysis.

Mass Spectrometry

The ESI-MS positive mass spectrum of do3aSH is presented in figure 2.8. Four main peaks were found at m/z = 347, 407, 429 and 451 corresponding to $[do3a+H]^+$, $[M+H]^+$, $[M+Na]^+$ and $[M-H+2Na]^+$, respectively. The fragment do3a may result from the loss of the thiol pendant arm, due to the analytical experimental conditions.

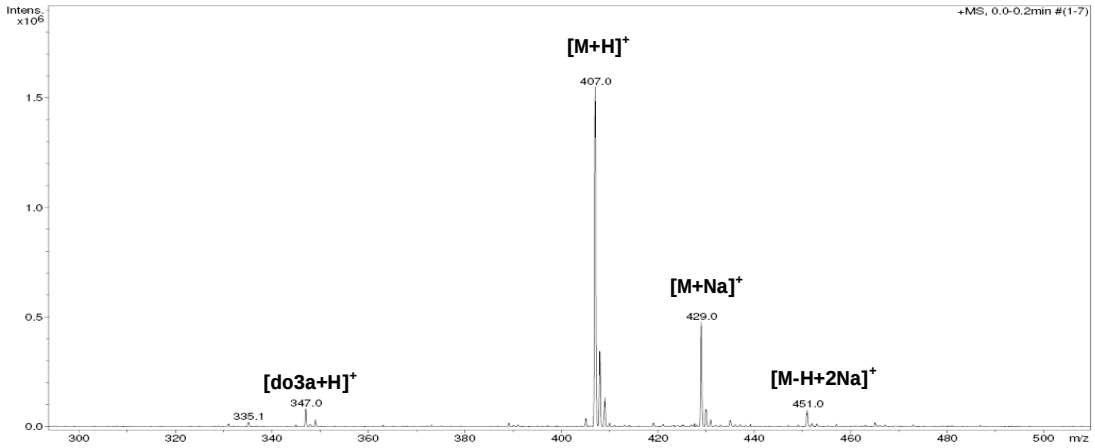

Figure 2.8: ESI-MS spectrum of do3aSH

NMR studies

The ^{1}H and ^{13}C NMR spectra of compound do3aSH were studied at different pD values. At pD = 1.20, the ^{1}H-NMR spectra presented five resonances with different multiplicities at 2.76, 2.95, 3.30-3.37, 3.44 and 4.04 ppm in an intensity ratio of 2:8:10:4:2. The ^{13}C-NMR spectra recorded at the same pD exhibit ten resonances, a pattern consistent with the two-fold symmetry expected for do3aSH: four resonances were assigned to the carbon atoms of the macrocyclic backbone, two to the carbon atoms of the carboxylate pendant arms, two to the carbon atoms of the thiol pendant arm and the other two to the carbon atoms of the carbonyl groups.

From 2D-NMR studies (*g*-COSY $^{1}H,^{1}H$ and *g*-HSQC $^{1}H,^{13}C$ correlations) performed at pD= 1.20 (Figure 2.9) was possible to conclude that the triplet centered at 2.76 ppm (2H) correlates with the carbon atom at 19.71 ppm. Based on the carbon and proton NMR data of the free arm and on our previous results [168], the resonance at 19.71 ppm was assigned to the α carbon atom of the thiol pendant arm, *C1*. The triplet at 2.76 ppm correlates also with the multiplet at 3.30-3.37 ppm (10H) and this correlates with the carbon atom at 58.04 ppm, which was assigned to the β carbon atom of the thiol pendant arm, *C2*. *g*-COSY $^{1}H,^{1}H$ indicates that the singlets found at 3.44 ppm (4H) and 4.04 ppm (2H) do not correlate with any other resonances, indicating that they can only correspond to the methylene protons of the acetate pendant arms. Based on *g*-HSQC $^{1}H,^{13}C$, these singlets correlate with the carbons at 56.68 and 55.07 which were assigned as *C3* and *C4*, respectively. The resonances at 53.69 and 51.94 ppm were assigned to the *C5* and *C6* atoms, as they correlate with the multiplet

appearing in the range 3.30-3.37 ppm. The multiplet at 2.95 ppm (8H) correlates with the carbon resonance at 50.47 ppm which also correlates with the multiplet at 3.30-3.37 ppm. Based on these data the resonance at 50.47 was assigned to the *C7* and *C8* carbon atoms and the multiplet at 2.95 ppm (8H) was assigned to the protons bound to these carbon atoms.

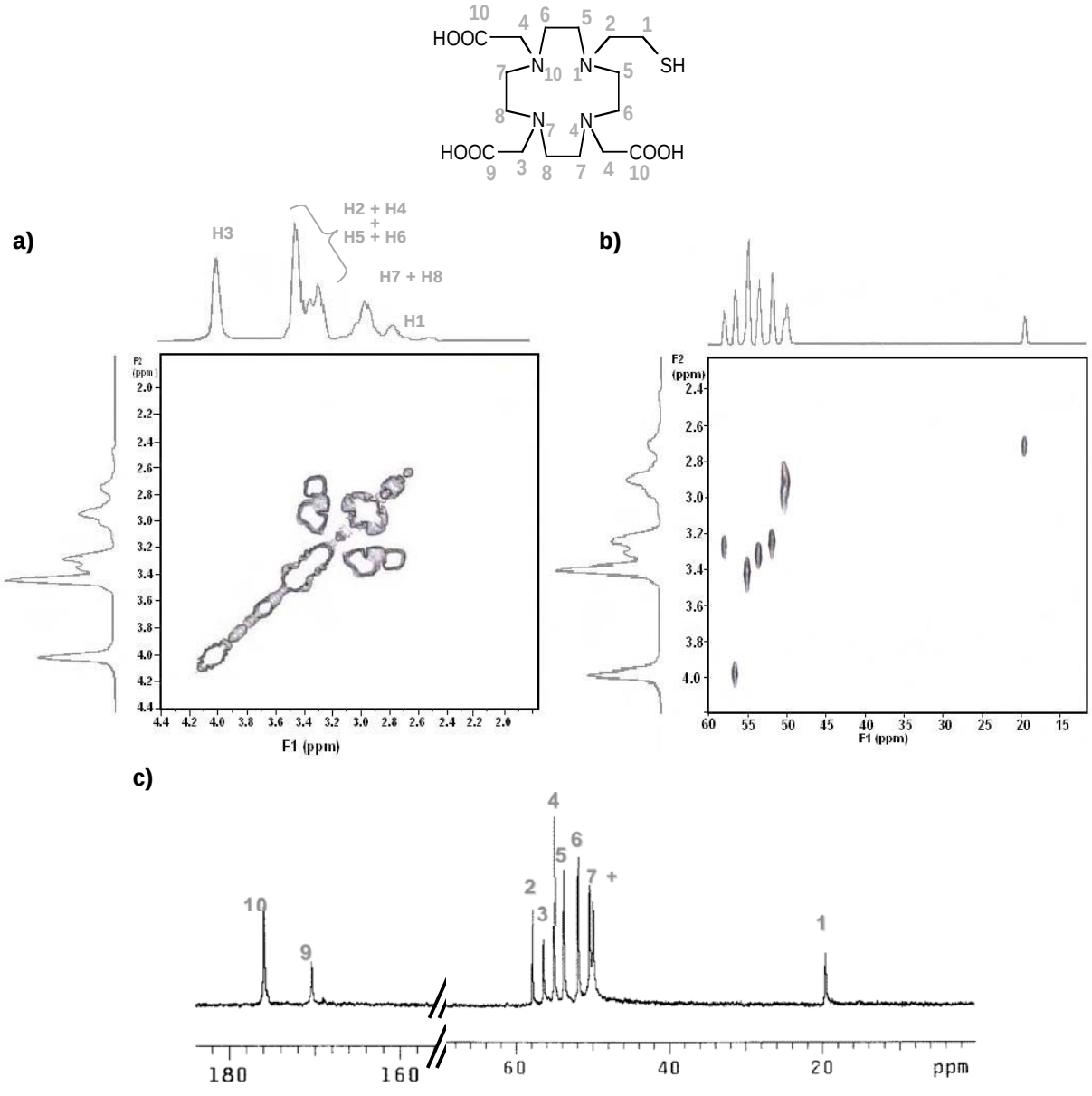

Figure 2.9: (**a**) g-COSY $^{1}H,^{1}H$ and (**b**) g-HSQC $^{1}H,^{13}C$; (**c**) final attribution of ^{13}C-NMR spectrum for do3aSH at pD = 1.20

Table 2.9 summarizes the ^{1}H and ^{13}C NMR data for do3aSH, at pD = 1.20.

Table 2.9: ^{1}H and ^{13}C NMR data for do3aSH at pD = 1.20

Assignment	Chemical shift (ppm)	
	^{1}H	^{13}C
C10	---	176.05 (2C)
C9	---	170.87 (1C)
C3	4.04 (s, 2 H)	56.68 (C)
C4	3.44 (s, 4 H)	55.07 (C)
C2	3.30 - 3.37 (m, 10 H)	58.04 (C)
C5		53.69 (C)
C6		51.94 (C)
C7	2.95 (m, 8 H)	50.47 (C)
C8		50.47 (C)
C1	2.76 (t, 2 H)	19.71 (C)

2.2.3.2. Protonation Constants of do3aSH

The acid-base behaviour of do3aSH was investigated by potentiometry, in the pH range 1.7-11.5 at 0.1 mM KCl ionic strength, and also by ^{1}H and ^{13}C-NMR spectroscopy in the pD range 1.20-10.40 (pH range: 0.80-10.00), without control of the ionic strength.

The protonation of the Ca-do3aSH complex was determined by potentiometry to assess about the protonation of the thiol group, as the sulphur atom is not involved in the coordination of calcium.

Six out of the eight protonation constants have been determined. From these, five were determined by potentiometry and the lowest one by NMR spectroscopy. This technique was also used to propose a protonation sequence for the ligand. A direct comparison of these two techniques is not possible due to the experimental conditions used in each one. The potentiometric studies were run under N_2 with control of the ionic strength, and in the pH range 1.7 – 11.5. In the NMR studies we did not control the ionic strength and the pH range explored was also different (0.80 – 10.00) due to the sensitivity of the thiol pendant arm at high pH values, under aerobic conditions.

In table 2.10 are summarized the protonation constants determined for do3aSH, by potentiometry and by ^{1}H and ^{13}C NMR spectroscopy.

Table 2.10: Protonation constants (log units) determined for do3aSH

Species	Potentiometry [a]		$^{1}H/^{13}C$-NMR spectroscopy [b]	
l h	log β_{LH_i}	log K_{LH_i}	log β_{LH_i}	log K_{LH_i}
1 1	12.22 (0.02)	12.22	12.22 *	12.22
1 2	22.95 (0.01)	10.73	22.88 (0.01)	10.66
1 3	31.82 (0.02)	8.81	31.74 (0.02)	8.86
1 4	36.12 (0.02)	4.31	36.09 (0.03)	4.35
1 5	38.67 (0.02)	2.55	38.64 (0.03)	2.55
1 6	----	---	40.43 (0.04)	1.79

Charges were ignored; [a] 25.0ºC, *I* = 0.1mM KCl, determined with OPIUM program [169]; [b] 25.0 ºC, without ionic strength control, determined with HypNMR program [170]; * value fixed according to potentiometric data.

As indicated in Table 2.10, for NMR studies we have used the highest protonation constant of do3aSH determined by potentiometry (log*K*=12.22) as a fixed parameter. As can be seen in table 2.10, the values obtained by NMR are in good agreement with the ones calculated by potentiometry and a sixth constant in the more acidic region was possible to determine based on the multinuclear NMR data.

Figure 2.10 shows the chemical shifts of the carbon and the proton atoms of do3aSH, as a function of the pH.

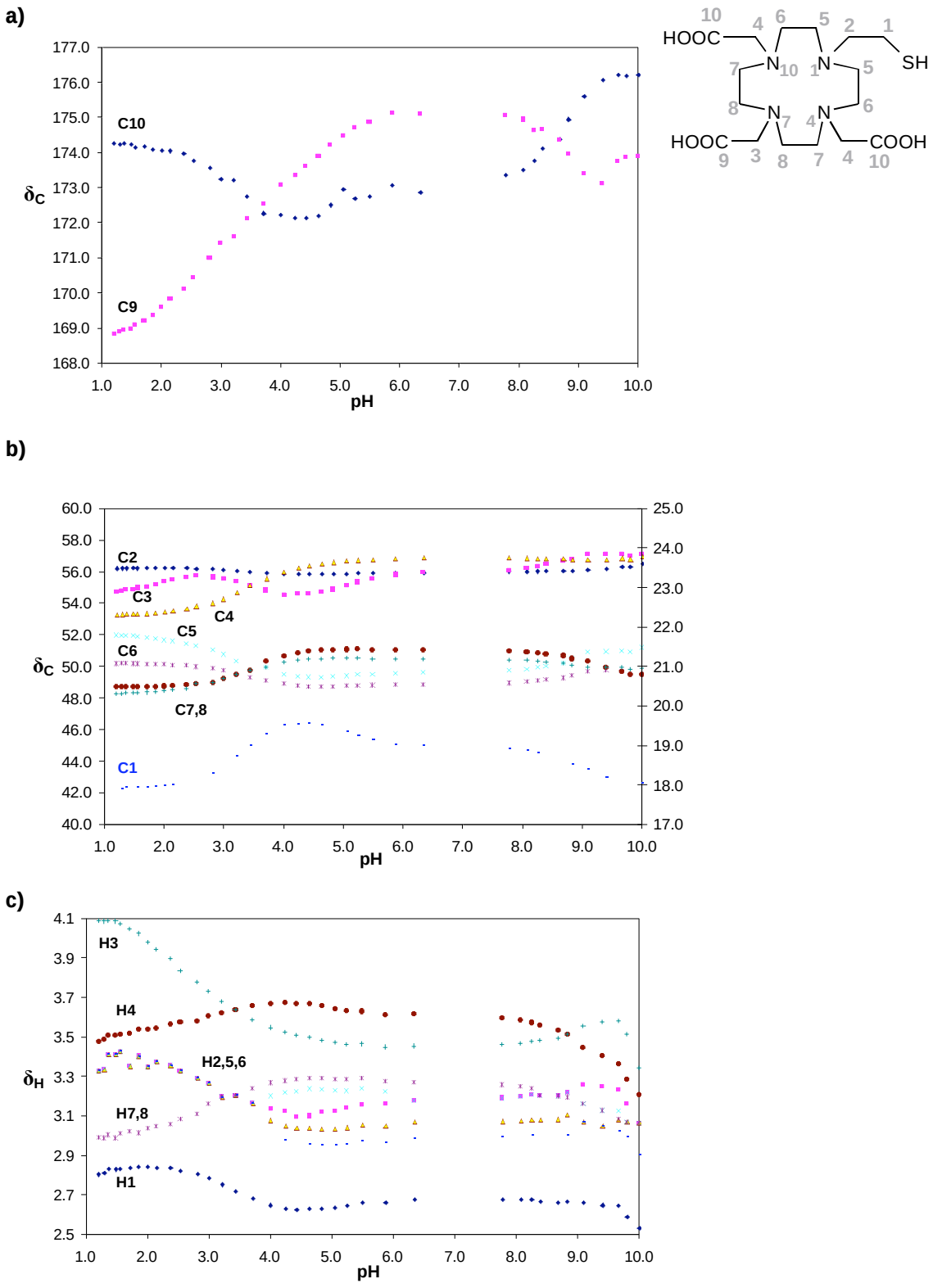

Figure 2.10: $^{13}C/^{1}H$-NMR titration of do3aSH: (**a**) ^{13}C carbonyl resonances; (**b**) other ^{13}C resonances; (**c**) ^{1}H, all resonances

Based on these NMR titration curves a protonation sequence for the ligand is tentatively proposed, and summarized in scheme 2.7. It is generally assumed that when a given site is protonated, the β-carbons are upfield shifted while the adjacent protons undergo a downfield shift [158]. In accordance with the logK_H values determined by potentiometry, four pH regions can be distinguished in the NMR titration curves: two including two protonation constants each (14.0 ≥ pH ≥ 10.0 and pH ≤ 4.0) and two comprising one protonation constant each (10.0 ≥ pH ≥ 7.5 and 5.0 ≥ pH ≥ 4.0):

- **14.0 ≥ pH ≥ 10.0 -** This region was not studied by NMR, due to the sensitivity of the thiol group under aerobic conditions at basic pH. However, based on potentiometric studies and according to data published for other related macrocycles (do3a and dota), the two highest protonation constants are easily ascribed to the protonation of two nitrogen atoms of the tetraazamacrocycle. Due to electrostatic repulsion, this protonation takes place in opposite nitrogen atoms inside the cavity, most probably one at **N_1** (the nitrogen atom bearing the pendant thiol group) and at **N_7**.

- **10.0 ≥ pH ≥ 7.5 -** In this region, the resonances ***C1*** and ***C9*** are first shifted upfield (until pH=9.4) and then downfield, while ***C10*** shifts upfield from pH ~9.50. **H1**, **H3** and **H4** also undergo a downfield shift. Therefore, the third protonation constant (logK_{H3}=8.81) can be ascribed to the thiol group. This agrees with logK_H values reported in the literature for thiols, though in some cases the protonation constants for thiol groups might be highly dependent on the ligand structure and number and nature of adjacent donor atoms [172,176]. The attribution of logK_{H3}=8.81 to the thiol group was further confirmed by measuring the protonation constant of Cado3aSH complex. The thiol group is not expected to be coordinated to Ca^{2+}, so its protonation should not be significantly influenced by the coordination of this cation to the macrocycle. Indeed, the protonation constant of the Ca^{2+} complex was logK_{HCaL} = 8.5 ± 0.1, a value very close to the logK_{H3}=8.81 determined for the ligand itself.

- **10.0 ≥ pH ≥ 7.5 –** In this region, the NMR data also indicate that the two protons attached to **N_1** and **N_7** undergo a redistribution to **N_4** and **N_{10}**.

- **7.5 ≥ pH ≥ 5.0 –** In this region no significant changes are observed, though the protonation of the carboxylic groups probably starts in this region as shown by the smooth upfield shift of ***C9***.

- **5.0 ≥ pH ≥ 4.0** – Only *C9*, *C3* and *C4* are upfield shifted and *H3* is downfiled shifted, therefore in this region the carboxylic group opposite to the thiol pendant arm seems to be protonated.

- **pH ≤ 4.0** – Two protonation steps take place in this region. The *C9* and *C1* carbon atoms and *H4, H7, H8* proton atoms are upfield shifted, while *C10*, *C5*, *C6*, *H1*, *H2*, *H3*, *H5* and *H6* are downfield shifted. In this region, *C3* is first downfield and then upfield shifted. These variations indicate that first a protonation of a carboxylate group attach to *C4* occurs and simultaneously there is a redistribution of the nitrogen protons from $\mathbf{N_4/N_{10}}$ to $\mathbf{N_1/N_7}$ amines and a transfer of the proton of the carboxylate group attach to *C3* to the other carboxylate group attached to *C4*. After this, another protonation occurs on the carboxylic group attached to *C3*, and a new redistribution from $\mathbf{N_1/N_7}$ to $\mathbf{N_4/N_{10}}$ amines takes place. The protonations of the last two nitrogen atoms are not detected even by NMR, as it must occur under very acidic conditions.

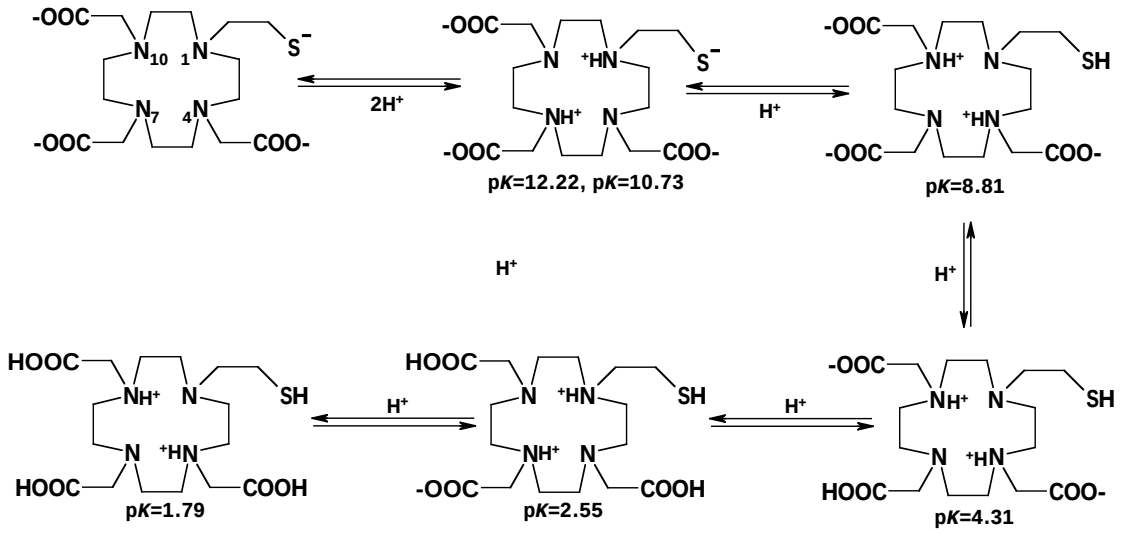

Scheme 2.7: Proposed protonation sequence for do3aSH

Table 2.11 presents the protonation constants of do3aSH together with those described in the literature for other related macrocycles, namely do1SH, do3a and dota.

Table 2.11: Protonation constants (log units) determined for do3aSH, together with those for similar macrocyclic ligands

Species l h	log K_{LH_i}			
	do3aSH [a]	do1SH [b]	do3a [c]	dota [c]
1 1	12.22	10.98	11.55	11.14
1 2	10.73	9.98	9.15	9.50
1 3	8.81	8.15	4.48	4.61
1 4	4.31	2.28	---	4.30
1 5	2.55	---	---	---
1 6	1.79 *	---	---	---

[a] this work, 25.0ºC, *I* = 0.1mM KCl; [b] this work, 25.0ºC, I = 0.1M KNO_3; [c] 25.0ºC, I = 0.1M KCl, ref. [171]; * determined by $^1H/^{13}C$ NMR spectroscopy, without ionic strength control.

The first and the second protonation constants found for do3aSH have been assigned to two amines of the macrocyle backbone, as well as the two first constants reported for do3a and dota. There are several sets of protonation constant reported in the literature for dota and do3a [33,171,172]. Nevertheless, we have chosen to compare our values with a set of values determined in the same conditions (25.0ºC and using KCl as electrolyte). In fact, in these conditions, the first two constants found for dota and do3a are lower than the one determined for do3aSH, which is certainly due to the presence of the thiol group. The third protonation constant of do3aSH has been assigned to the thiol group. The difference between the protonation of the thiol group in do3aSH and in do1SH (8.81 and 10.98 respectively) certainly results from the presence of the three carboxylic groups in do3aSH. The remaining three constants have been attributed to protonations of the carboxylate groups and these values are in the same range of the corresponding reported values for do3a and dota (p*K*a<4.6). The proposed protonation sequence for do3aSH it's similar to the reported sequences for do3a and dota ligands, for which the first two protonations correspond to amines in *trans* position, logK_{H3} and logK_{H4} occur in COOH groups in opposite position towards the protonated NH^+ and the remaining protonations in the other COOH groups [173,174].

2.2.4. A Benzodioxo-Cyclen Derivative

To evaluate the effect of the rigidity of the tetraazamacrocycle on its capability to form Cu(II) complexes, we have isolated and characterized the dioxo-1,4,7,10-tetraazabicyclo[1.10.1]hexadeca-1(11),13,15-triene-4,7-diacetic acid (bz2ac). It is well known that the introduction of a benzene ring in the molecular skeleton of a macrocycle confers spatial pre-organization to the donor atoms, leading usually to a more efficient complexation and slower complex dissociation [175]. Moreover, functionalization of the benzene ring can be easily achieved, for further coupling to any type of biomolecule (e.g., peptide or antibody), not affecting the coordination capability of the ligand towards the metal [176].

2.2.4.1. Synthesis and Characterization of dioxo-1,4,7,10-tetraazabicyclo[1.10.1]hexadeca-1(11),13,15-triene-4,7-diacetic acid (bz2ac)

To synthesize compound bz2ac we have followed the methodology previously described [177]. Such methodology consisted on the condensation of *o*-phenylenediamine with ethylenedianime tetraacetic dianhydride in dry tetrahydrofluran (THF) (Scheme 2.8).

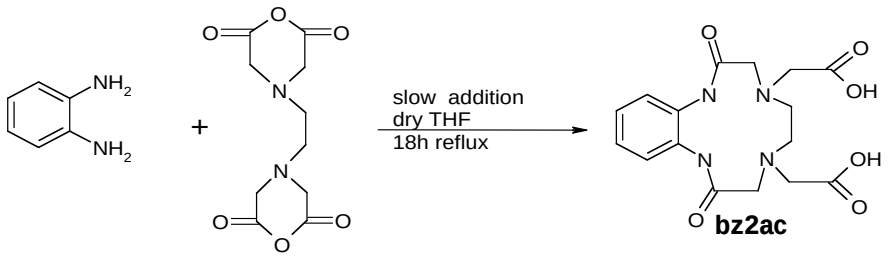

Scheme 2.8: Synthesis of the benzodioxotetraazamacrocycle bz2ac, [177]

Compound bz2ac was characterized by the usual techniques in chemistry, namely multinuclear NMR spectroscopy and HPLC. The ^{1}H and ^{13}C-NMR spectra (figure 2.11) obtained were in agreement with the expected values [177,178].

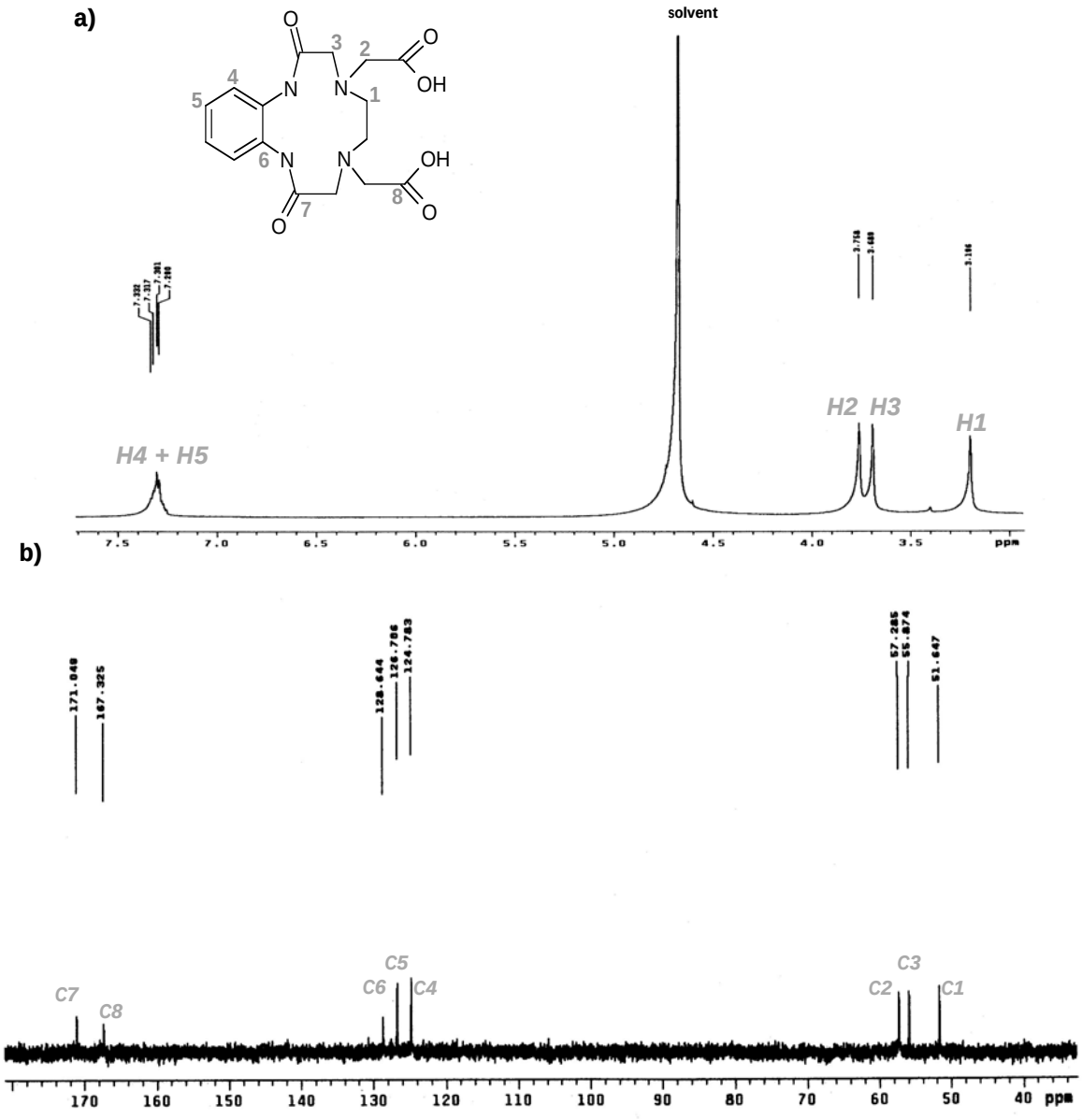

Figure 2.11: ^{1}H-NMR (**a**) and ^{13}C-NMR spectra (**b**) of bz2ac at pD ≈ 2.5

As shown in figure 2.11, in both spectra the number of resonances found was the expected taking into account the symmetry of the molecule. In the ^{13}C-NMR spectrum eight resonances could be found. The resonances appearing at 172.73 and 169.07 ppm are due to the two C=O group of the amide (***C7***) and of the carboxylate (***C8***), respectively. The resonances found at 130.43 ppm (***C6***), 128.50 ppm (***C4***) and 126.57 ppm (***C5***) correspond to the carbon atoms of the benzenic ring. We have also found three resonances at 59.06 ppm (***C2***), 57.55 ppm (***C3***) and 53.41 ppm (***C1***) which were assigned to the CH_2 groups of the macrocycle. At low pD values, the ^{1}H-NMR presented four resonances appearing at 7.33-7.29 (m), 3.76 (s), 3.69 (s) and 3.20 (s), integrating all for 4 protons each which correspond to ***H4+H5***, ***H2***, ***H3*** and ***H1*** respectively. At high pD values the spectrum also shows four resonances, in an

intensity ratio of 2:2:4:2, but with a different pattern: two multiplets assigned to the aromatic protons (***H4*** and ***H5***) and two singlets, assigned to the ***H2+H3*** and ***H1*** protons, respectively.

2.2.4.2. Protonation Constants of bz2ac

For this compound Fernando et al. have only reported two of the six possible protonation constants [178]. Bearing in mind that different experimental conditions and the use of methodologies other then potentiometry may allow the determination of more protonation constants, we decided to study bz2ac by NMR spectroscopy and potentiometry. The stability constants of bz2ac with Cu and other metal ions were also determined using the same techniques. To get a better insight on the solution structure of Cu-bz2ac, UV-vis and X-band EPR spectra at different pH values were also studied.

The protonation constants of bz2ac were determined by potentiometry at 25.0 ºC and 0.10 M ionic strength in KNO_3 and the first protonation constant was confirmed by ^{1}H-NMR spectroscopy. The constants were determined with the program HYPERQUAD [179] and the species distribution diagrams were plotted with the program HySS [160]. Four out of six protonation constants were determined for bz2ac. The remaining two constants are either very high or very low to be determined. In our experimental conditions only one amide centre can be deprotonated, and even this one at very high pH value, so the corresponding constant was determined by ^{1}H-NMR spectroscopy (see below). In Table 2.12 are shown the protonation constants of bz2ac, as well the values published in literature for other related tetraazamacrocyclic ligands, which are depicted in Figure 2.12.

Table 2.12: Protonation constants (log units) for bz2ac and other related macrocycles

Species	bz2ac [a]		bz2ac [b]	IV [c]	V [c]	VI [d]	VII [d]
l h	log β_{LH_i}	log K_{LH_i}	log K_{LH_i}	log K_{LH_i}	log K_{LH_i}	log K_{LH_i}	log K_{LH_i}
1 1	12.8(2)[‡]	12.8	-	-	-	11.56	11.51
1 2	18.84(1)	6.03	6.07	6.50	6.41	6.13	6.82
1 3	22.24(1)	3.40	3.27	3.54	3.40	2.85	5.50
1 4	24.35(3)	2.11	-	-	-	-	-

[a] This work, 25.0 ºC, I = 0.10 mol dm^{-3} KNO_3, values in parenthesis are standard deviations in the last significant figures. [‡] determined by ^{1}H-NMR. [b] 25 ºC, I = 0.1 mol dm^{-3} KCl, ref. [178]. [c] 25º C, I = 0.1 mol dm^{-3} KCl, refs. [180,181]. [d] 25.0ºC, I = 0.10 mol dm^{-3} KNO_3, ref. [182].

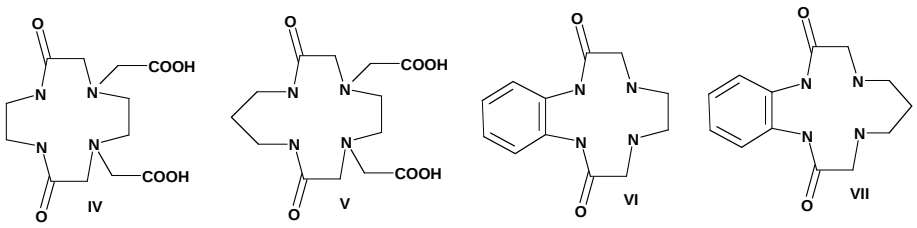

Figure 2.12: Tetraazamacrocyclic ligands related with bz2ac: **IV** = 2,9-dioxo-1,4,7,10-tetraazacyclododecane-4,7-diacetic acid **V** = 2,9-dioxo-1,4,7,10-tetraaza-cyclotridecane-4,7-diacetic acid, **VI** = 2,9-dioxo-1,4,7,10-tetraazabicyclo[10.4.0]1,11-hexadeca-1(11),13,15-triene, **VII** = 2,10-dioxo-1,4,8,11-tetraazabicyclo[11.4.0]1,12-heptadeca-1(12),14,16-triene

The first protonation constant (log*K*=12.8) due to its high value was determined by ^{1}H NMR titration in the pD range 8 – 15 (about 25 points).

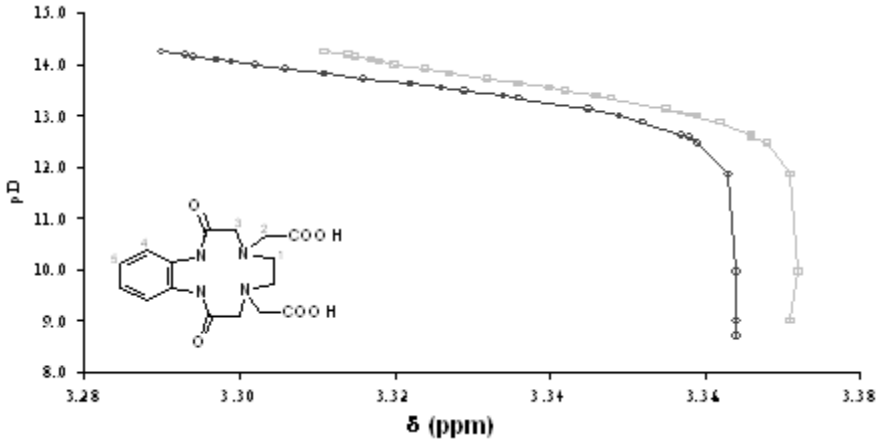

Figure 2.13: ^{1}H NMR titration curves of bz2ac: proton ***H3*** (O) and proton ***H2*** (□)

For this study we have used the chemical shift (δ) of the ***H2*** and ***H3*** protons as a function of pD values. As shown in the titration curve, Figure 2.13, the resonances due to ***H2*** and ***H3*** are upfield shifted when the pD increases. Taking into account the structure of bz2ac, results published in the literature and our ^{1}H NMR data, we expect that the first protonation occurs at one amide nitrogen atom. Nevertheless, as the resonances of the protons closer to the protonation site are overlapped in the pD region of interest, we have studied the variation of the chemical shifts of the resonances ***H2*** and ***H3***. The variation of their chemical shift with the pD is small, but significantly different to be used for calculations. Based on these data two pK_D values were determined independently. These values were converted to pK_H, and the final pK_H given by the average. The conversion of the pK_D values in pK_H was made using the correlation $pK_D = 0.11+1.10\ pK_H$ [157]. The average pK_H value found was 12.81 ± 0.04.

However, if all the experimental errors for the determination of this value were taken into account a standard deviation of about 0.2 should be indicated as more realistic.

The first protonation occurs in one amide group. The second protonation occurs at one amine, in spite of being low, compares well with values previously found for amine centres in close proximity of electron-withdrawing amide groups [183,184]. The third constant corresponds to the protonation of the acetate group of the arm bound to the non-protonated nitrogen amine [183]. Finally, the fourth constant can be assigned to the remaining nitrogen amine or to the remaining acetate or to both simultaneously. Moreover, the difference found between the log K_4 of bz2ac and the log K_3 of **VI** (attributed to an amine) is certainly due to the conversion of a secondary amine into a tertiary one. Scheme 2.9 summarizes the protonation sequence proposed for bz2ac.

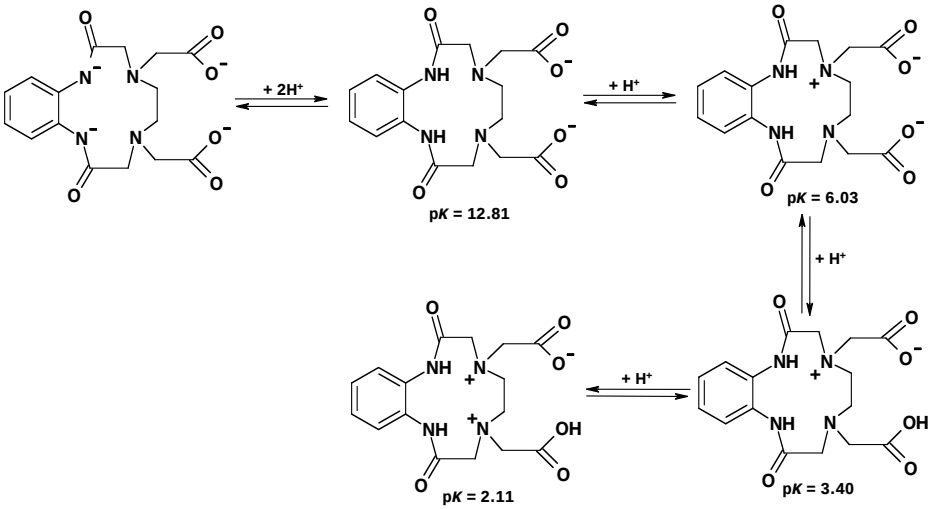

Scheme 2.9: Proposed protonation sequence for bz2ac

In general, we can say that our values for the second and the third constants compare with the values previously reported by Cathala *et al.* and Q. Fernando et al. [177,178]. In our case, most probably due to the presence of the benzene ring in the bz2ac backbone**,** we have successfully also determined the protonation constant of one amide centre. A similar result was later reported by Antunes et al. when they studied compounds **VI** and **VII** [182]. For compounds **IV** and **V,** certainly due to the less acidic character of the amides, no protonation constants were reported by Q. Fernando and co-workers [180,181,184]. Comparing our constants with the ones recently reported for compound **VI**, is clear that logK_3 corresponds to the protonation of a carboxylate pendant, being the other values similar to the ones determined in this work for bz2ac.

Based on our results, we can say that the macrocycle bz2ac has an overall basicity which is about 15 log units higher then the basicity previously described by Q. Fernando et al. for the same compound. Obviously such difference will have a significant influence on the stability constant values of its metal complexes.

2.2.4.3. Stability Constants of bz2ac with Copper and Other Metals with Biological Interest

Potentiometric studies of bz2ac with Cu^{2+}, Ni^{2+}, Zn^{2+}, Cd^{2+} and Pb^{2+} were performed at 25.0 ºC and 0.10 M ionic strength in KNO_3, in order to determine the corresponding stability constants (Table 2.13).

Table 2.13: Stability constants (log units) for complexes of bz2ac and other related ligands with several divalent metal ions

Ion	Species	bz2ac [a]		bz2ac [b]	IV [c]	V [c]	VI [d]	VII [d]
	m l h	log β_{MLH_i}	log K_{MLH_i}	log K_{MLH_i}	log K_{MLH_i}	log K_{MLH_i}	log K_{MLH_i}	log K_{MLH_i}
Cu^{2+}	**1 1 0**	17.13(5)	17.13	9.04	11.34	10.46	9.17	16.3
	1 1 1	21.72(4)	4.59	-	1.29	1.09		
	1 1 -1	8.54(6)	8.59	4.53	7.3	7.38		
	1 1 -2	-2.70(7)	11.24	8.84	10.41	6.05		
Zn^{2+}	**1 1 0**	13.23(4)	13.23	7.56	8.98	9.13	-	-
	1 1 1	20.40(2)	7.17	-	1.47	2.36	-	-
	1 1 -1	2.68(6)	10.55	7.14	9.56	9.97	-	-
	1 1 -2	-	-	11.26	11.94	11.24	-	-
Ni^{2+}	**1 1 0**	17.73(8)	17.73	9.4	11.27	10.08	-	-
	1 1 1	22.81(3)	5.08	-	1.55	1.60	-	-
	1 1 2	27.04(6)	4.23	-	-	-	-	-
	1 1 -1	8.76(5)	8.97	6.9	9.30	10.68	-	-
	1 1 -2	-	-	-	13.90	9.78	-	-
Cd^{2+}	**1 1 0**	12.68(5)	12.68	-	7.3	7.4	-	-
	1 1 1	19.84(2)	7.16	-	2.6	2.6	-	-
	1 1 -1	2.48(6)	10.20	-	10.4	10.6	-	-
	1 1 -2	-9.42(4)	11.90	-	12.3	12.0	-	-
Pb^{2+}	**1 1 0**	13.43(2)	13.43	-	-	-	-	-
	1 1 1	20.88(1)	7.45	-	-	-	-	-
	1 1 -1	3.60(3)	9.83	-	-	-	-	-

[a] This work; 25.0 ºC, I = 0.10 mol dm^{-3} KNO_3; values in parenthesis are standard deviations in the last significant figures. [b] 25 ºC, I = 0.1 mol dm^{-3} KCl, ref. [181]. [c] 25º C, I = 0.1 mol dm^{-3} KCl, ref. [180,181]. [d] 25.0ºC, I = 0.10 mol dm^{-3} KNO_3, ref. [182].

The species distribution diagrams for all the metals studied are shown in Figure 2.14.

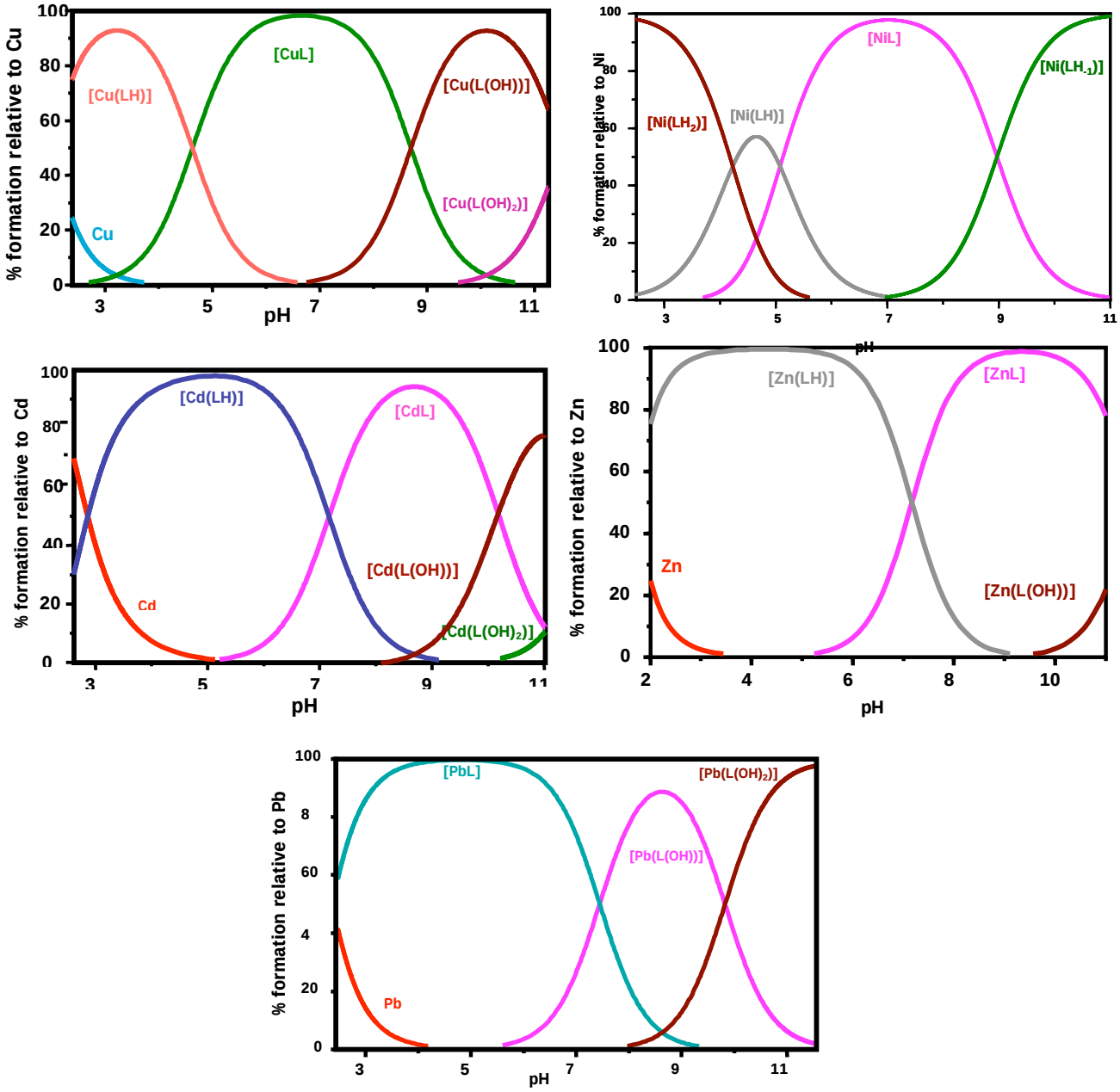

Figure 2.14: Species distribution diagrams for the Cu^{2+}, Ni^{2+}, Cd^{2+}, Zn^{2+} and Pb^{2+} complexes with bz2ac in water, $C_L = C_M = 4.2\times10^{-5}$ mol dm^{-3}

As can be seen in Table 2.13 and Figure 2.14, only mononuclear species were formed with the metal ions studied, namely [ML], [M(HL)] and [$M(H_{-1}L)$]. The [$M(H_2L)$] species only appears with Ni^{2+}, while [$M(H_{-2}L)]^{3-}$ is formed with Cu^{2+} and Cd^{2+}. At physiological pH the [ML] complex is formed at about 100% for Cu^{2+} and Ni^{2+}, while for Pb^{2+} and

Zn^{2+} this species is the main complex only at pH ≥ 9. For Cd^{2+} the amount of [CdL] formed is low at physiological pH, being [ML] always present.

This information suggests that Ni^{2+} and Cu^{2+} easily deprotonate the first amide centre while the other studied metal ions only manage to do it at higher pH values. Based in these experiments is also impossible to realize if a structural arrangement occurs upon deprotonation of the amide centre for the nickel and copper complexes. However a slow reaction occurs after the deprotonation of the first amide centre for nickel, because we found completely different potentiometric curves when the solution containing the metal and the ligand (1:1 molar ratio) is titrated with base (formation of complexes) or with acid upon the complete formation of complexes. These results clearly suggest a structural rearrangement (Figure 2.15).

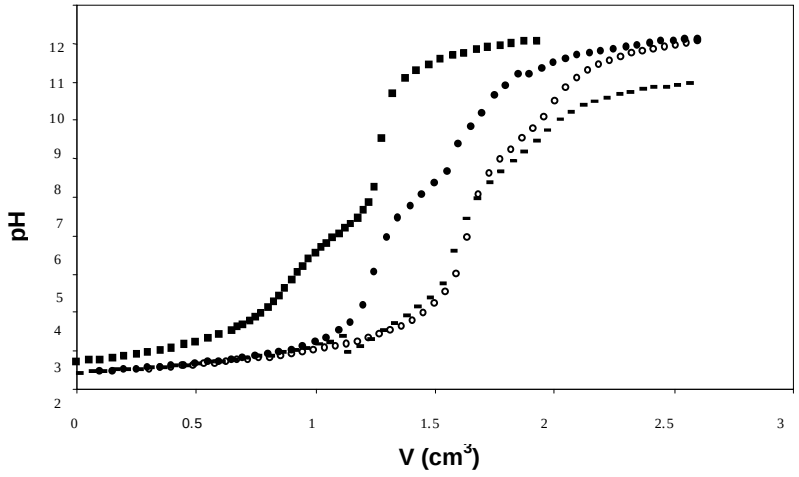

Figure 2.15: Potentiometric titration curves of a solution of the bz2ac alone (▪), the ligand in presence of Ni^{2+}, in 1:1 ratio, using KOH as titrant (direct titration) (•), the same titration using HNO_3 as titrant, starting at high pH value (backtitration) (▫), and, direct / backtitration of bz2ac in presence of Cu^{2+} (1:1 ratio) (‾)

The Ni(II) complex [M(L)] exhibits the highest thermodynamic stability constant followed by Cu(II), being the corresponding values significantly lower for the other three metal ions (Pb(II), Zn(II) and Cd(II)). The trend [NiL] > [CuL] >> [PbL] > [ZnL] > [CdL] does not follow the usual Irving-Williams order of stability [185]. However, analogous trends have already been reported. In general, steric requirements of the ligands on complex formation (macrocyclic type or other) or coordination geometry preferences are on the basis of the inversion of stability for the nickel and copper complexes [186].

The stability constant values of bz2ac with all the metals studied are significantly higher than the values previously reported by Fernando et al for Cu, Zn and Ni (table 2.19) [178]. This difference is certainly due to the values found the protonation constants of bz2ac. The direct comparison of values of this work and the previously reported ones can be made by the calculation of pM (-log [M^{2+}]) values. In Table 2.14 are shown the pM values for the different complexes together with those calculated from the potentiometric data for other related ligands (see Figure 2.12) [160]. The pCu and pZn values for bz2ac, calculated using our stability constants, are comparable to the values found for compounds **IV** and **V**. However, we have found a pNi value higher than the reported ones. By comparing the pM values for bz2ac, VI and VII we can clearly say that the presence of carboxylic pendant arms is very important for 12[N_4] cavity macrocycles but when larger cavity sizes, such as 13[N_4], is used the presence of the pendant arms is not that important.

Table 2.14: pM (-log [M^{2+}])* values determined for metal complexes of bz2ac at physiological pH

Ion	bz2ac [a]	bz2ac [b]	IV	V	VI	VII
Cu^{2+}	11.73	11.91	11.64	11.83	5.2	17.1
Ni^{2+}	12.32	9.99	11.67	10.04	-	-
Zn^{2+}	8.00	7.99	8.93	9.09	-	-
Cd^{2+}	7.45	-	7.88	7.90	-	-
Pb^{2+}	8.33	-	-	-	-	-

* The values were calculated using the program HySS [163], $C_L = 2C_M = 1 \times 10^{-5}$ mol dm^{-3}, and the stability constants given in Table 2.13; [a] this work; [b] ref. [178].

The discrepancy found for our pNi values and the ones reported for the related ligands, probably results from the very high value of its stability constant togheter with its slow kinetic formation. Indeed this constant, as well as that for the copper complex, was determined by a competition reaction (see experimental section) because the complex is completely formed at the beginning of the titration, this means at very low pH values, see Figure 2.14. The ligand **V** presents lower pM values when compared with those of bz2ac, except for zinc. The lower values for **V** are expected due to the larger cavity size of this macrocycle, although the high value presented for Zn is not expected. The pM values for bz2ac and **IV** are very similar suggesting that the introduction of the benzene ring into the framework of bz2ac has a minor influence on complex formation, or that the donor atoms involved in the

coordination to the metal are not specially affected by the presence of the benzene ring.

2.2.4.4. Structural Studies in Solution

The UV-vis-near IR and the X-band EPR spectra of Cu(II) complexes were recorded at pH values of about 3, 6.5 and 10. The selected pH values correspond to the maximum percentage of [M(HL)], [ML] and [M(L(OH))] species (figure 2.14). The spectra of **C1**, a Cu(II) crystal of the ligand ($[C_{18}H_{23}N_4O_6ClCu]$, page 89) were also performed.

UV-vis-near IR and EPR Spectroscopic Studies of Cu(II) Complexes

The electronic spectra of the copper complexes at the different pH values were studied and the values of the main bands are reported in Table 2.15.

Table 2.15: Spectroscopic EPR parameters and UV-Vis-near IR data for Cu(II) complexes of bz2ac and other related ligands taken from literature (shown in figures 2.12 and 2.17)

complex (pH)		EPR (10^4 A_i / cm^{-1})						UV-Vis-near IR
		g_x	g_y	g_z	A_x	A_y	A_z	λ / nm [h] (ε / $mol^{-1}dm^3cm^{-1}$)
Cu-bz2ac (3.51) [a]		2.060	2.088	2.338	1.7	7.9	155.1	752 (65), 487 (sh., 24), 382 (69)
Cu-bz2ac (6.37) [a]		2.050	2.080	2.293	3.1	12.8	161.4	1020 (sh., 22), 670 (61), 444 (sh., 60), 375 (450)
Cu-bz2ac (10.26) [a]		2.039	2.064	2.194	2.5	13.5	186.8	643 (sh., 160), 560 (186), 384(197)
C1 (3.23) [a]	**A**	2.060	2.088	2.336	1.4	6.4	153.6	704 (54), 382 (133)
	B	2.050	2.081	2.293	2.5	11.9	163.8	
Cu-bz2ac (6.6) [b]		2.035	2.090	2.290	-	-	165.1	700 (60)
Cu-bz2ac (12.0) [b]		2.040		2.195	-	-	190.2	605 (220)
Cu-V (<7) [c]		2.039	2.073	2.336	-	-	147.0	
Cu-V (>7) [c]		≈ 2.0		2.190	-	-	188.0	
Cu-VIII [d]		2.045	2.073	2.251	5.4	16.6	187.8	
[Cu(cyclen)Cl] [e]		2.057		2.198	24.1		184.2	599 (220)
[Cu(cyclam)]Cl_2 [e]		2.049		2.186	38.7		205.0	513 (100)
Cu-dota [e]		2.062		2.300	-	-	150.3	
Cu-teta [e]		2.050		2.249	-	-	168.0	
[Cu(VI)(H_2O)] (10.0) [f]		2.038	2.052	2.193	0.32	14.97	193.12	
[Cu(VII)] (10.0) [f]		2.018	2.058	2.166	5.28	18.64	209.01	
[Cu(H_2O)$_6$] [g]		2.08		2.4	-	-	134.0	

[a] This work, [b] ref. [178], [c] ref. [180], [d] ref. [187], [e] ref. [37,161], [f] ref. [182], [g] ref. [162], [h] aqueous solution, **C1** dissolved in water.

All the UV-Vis-near IR spectra presented one main band in the visible region and one in the near-IR region. It is possible to observe that the visible band suffers a blue shift with the increase of the pH – changing from 752 to 643nm. The spectrum of the **C1** shows also one band in the visible at 704nm. Although the UV-vis-near IR spectra of Cu(II) complexes are not especially informative about the adopted geometry in solution, the band in the near-IR region togheter with the blue shifts of the visible band indicates that a distorted geometry is expected for all the complexes analysed.

The EPR spectra of copper complexes in solution at different pH indicated the presence of only one species, while the EPR spectrum of the solution obtained by dissolving the crystals of **C1** ($C_{18}H_{23}N_4O_6ClCu$, page 92) in DMSO/H_2O indicated the presence of two species, see Figure 2.16.

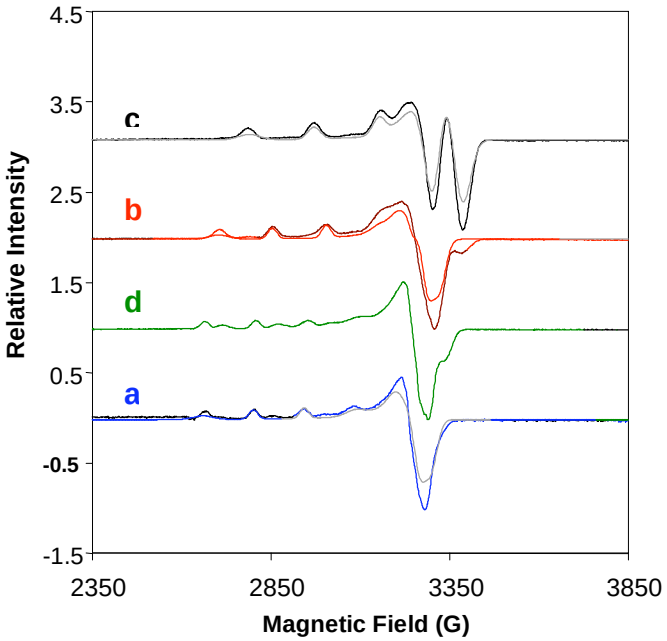

Figure 2.16: X-band EPR spectra of copper complexes of bz2ac in ≈ 2×10^{-3} moldm^{-3} and 1:1 H_2O/DMSO solutions (black lines) and its simulated spectra (grey lines) at different pH values: (**a**) pH = 3.51; (**b**) pH = 6.37 and (**c**) pH = 10.26. The spectrum of a solution of **C1** in 1:1 H_2O/DMSO (pH = 3.23) is also shown (**d**). All the spectra were recorded at 96 K, microwave power of 2.0 mW and modulation amplitude of 1 mT. The frequency was 9.405 GHz, 9.407 GHz, 9.408 GHz and 9.407 GHz, respectively

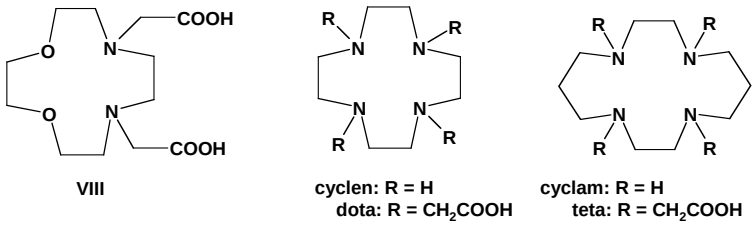

VIII | **cyclen: R = H** **dota: R = CH_2COOH** | **cyclam: R = H** **teta: R = CH_2COOH**

Figure 2.17: Tetraazamacrocyclic ligands related with bz2ac: **VIII** = 1,4-dioxa-7,10-diazacyclododecane-7,10-diacetic acid, cyclen, dota, cyclam and teta

All spectra showed the expected four well-resolved lines at low field, due to the interaction of the unpaired electron spin with the copper nucleus. The hyperfine coupling constants (A) and *g* values obtained by the simulation of the spectra [163] are also shown in Table 2.15, together with the parameters obtained for other copper(II) complexes taken from literature for comparison (figure 2.17).

The simulation of the spectra indicates three different *g* values with $g_z > (g_x+g_y)/2$ and the lowest $g \geq 2.04$, which is characteristic of mononuclear copper(II) complexes having rhombic-octahedral with elongation of the axial bonds or distorted square-based pyramidal symmetries, and $d_{x^2-y^2}$ ground state.

At the three pH studied, the complexes have g_z and A_z parameters consistent with different type of donor atoms close lying the metal. At pH 3.51 these parameters are consistent with N_2O_2 equatorial coordination sphere [188]. The differences between them can be visualised in the diagram g_z *versus* A_z presented in the Figure 2.18, and rationalised in terms of different axial field for each complex. Indeed, the g_i and A_i values are related to the electronic transitions by the factors derived from the ligand field theory [166,189]: the g_i values increase and the A_i values decrease as the equatorial ligand field becomes weaker or stronger the axial ligand field and this occurs with the simultaneous red-shift of the *d-d* absorption bands in the electronic spectra (see Table 2.15) [164-166]. Herein, when the pH increases a blue-shift is observed, and simultaneously the g_z decrease and the A_z values increase, which is consistent with the increase of the equatorial field. These features are also consistent with the potentiometric results which have shown that the deprotonation of one amide nitrogen atom occurs at $pH \approx 6$.

The EPR spectrum of **C1** crystals ($C_{18}H_{23}N_4O_6ClCu$, page 92) indicated the presence of two species, in different proportions. The g_z and A_z parameters suggest that crystals of **C1** have a different structure in solution and in the solid state, most probably because the chloride atom can be replaced by an oxygen of a water molecule. The resulting parameters are consistent with a mixture of species A and B, being the first in a higher proportion (about 75%). This suggests that an equilibrium between the two corresponding structures is responsible by the observed EPR spectrum.

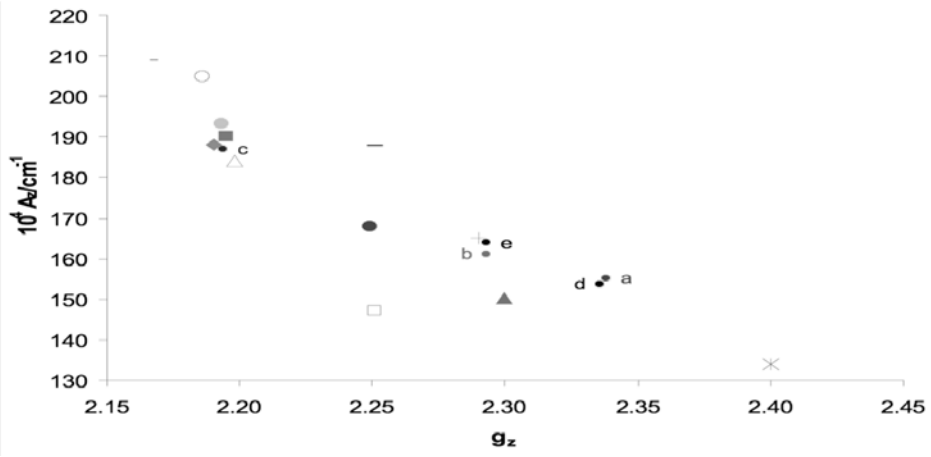

Figure 2.18: Diagram A_z *versus* g_z EPR parameters for the copper(II) complexes studied (×) and others from literature formed with the following ligands: • **a Cu/bz2ac** (pH 3.51), • **b Cu/bz2ac** (pH 6.37), • **c Cu/bz2ac** (pH 10.26), • **d C1** (species A), • **e C1** (species B), **+ Cu/bz2ac** (pH 6.6), ■ **Cu/bz2ac** (pH 12), ◆ **[Cu(V)]** (pH>7), □ **[Cu(V)]** (pH <7), **_ [Cu(VIII)]**, ○ **[Cu(cyclam)]Cl**, Δ **[Cu(cyclen)Cl]$^+$**, ▲ **[Cu(dota)]**, ● **[Cu(teta)]**, ● **[Cu(VI)(H_2O)]** (pH 10), **⁻ [Cu(VII)]** (pH 10) and ✳ **[Cu(H_2O)$_6$]**

The A_z *vs.* g_z diagram shown in Figure 2.18, together with the known geometries of some of the complexes taken from the literature [37,161,162,182,187], allow the following considerations:

1) The right region of the diagram, higher g_z and lower A_z values, is occupied by complexes with oxygen atoms in the equatorial plane, such as $[Cu(H_2O)_6]$;

2) In the middle of the diagram, complexes with octahedral geometry are found. The coordination being provided by four nitrogen atoms of the macrocycle and two oxygens, such as teta;

3) The complexes anchored on four nitrogen atoms of the macrocyclic ring (equatorial plane) are located in the left part of the diagram and exhibit square-

planar ([Cu(cyclam)]Cl, [Cu(VII)]) or square pyramidal ([Cu(cyclen)Cl]$^+$, [Cu(VI)(H_2O)]) geometries.

The parameters of the copper complexes of bz2ac change considerably with the increase of the pH, with the decrease of g_z, the increase of A_z and a corresponding blue shift, accounting a stronger equatorial ligand field. Indeed, at pH 3.5 these parameters are consistent with a N_2O_2 coordination sphere, while those for the complexes at pH ≈ 6 and ≈ 10 point to arrangements with stronger equatorial ligand fields, in agreement to the presence of an increased number of nitrogen as donor atoms.

2.3. Reactions of do1SH, do3aSH and bz2ac with Inactive and Radioactive Copper

We have studied reactions of the macrocycles do1SH, do3aSH and bz2ac with $Cu(NO_3)_2.H_2O$, $Cu(OAc)_2$ or $CuCl_2$ to see whether we could obtain well defined species to be characterised by MS, HPLC or TLC and X-ray diffraction analysis. Such species, if well characterised at the macroscopic level, would be used for the characterisation of the $^{64/67}$Cu(II) complexes formed with the corresponding tetrazamacrocycles. In fact, the radioactive complexes do not have mass to be characterized by the normal techniques in chemistry, being usual to characterize such compounds by comparing their TLC or HPLC with those of the compounds prepared at the macroscopic level.
The ^{64}Cu used in this work was produced at the FZ Dresden-Rossendorf using the cyclotron "Cyclone 18/9". The ^{64}Cu and the ^{67}Cu are obtained by irradiating with protons ^{64}Ni and ^{67}Zn, respectively. The nuclear reactions which take place are the following:

$$^{64}\text{Ni} \xrightarrow{(p,n)} {}^{64}\text{Cu}$$

$$^{67}\text{Zn} \xrightarrow{(p,n)} {}^{67}\text{Cu}$$

After chemical treatment and purification, the two radioisotopes are obtained as dichlorides $^{64/67}CuCl_2$. This compound is then diluted in 0.1M NH_4OAc, yielding $^{64/67}Cu(OAc)_2$ – the starting materials used in the reactions with the different tetraazamacrocycles. The ^{64}Cu used in our studies had a very high specific activity (1.840 MBq/mmol), while the ^{67}Cu was obtained with an unexpected very low specific activity. In this case we were forced to use relatively high ligand concentration and long reaction times to reach complexation.

2.3.1. do1SH

The reaction of do1SH with $Cu(NO_3)_2.H_2O$ at room temperature was followed by TLC. We have found a quite slow kinetic rate, a result which was in agreement with the potentiometric solution studies (see page 50). Even using long reaction times we have never obtained a pure compound, and the reaction was never complete, being free Cu^{2+} always present. Increasing the temperature all the free Cu^{2+} disappeared, but the TLC chromatographic analysis indicated the presence of several species, which we have not been able to identifiy.

These results at the macroscopic level did not encourage reactions of do1SH with radioactive copper.

2.3.2. do3aSH

Other research groups have explored the chemistry and radiochemistry of Cu(II) with do3a and dota. They have shown that it was possible to prepare complexes with high thermodynamic stability ($pM_{Cu\text{-}do3a}$=16.84; $pM_{Cu\text{-}dota}$=15.2, at pH 7.4) and they also labelled these chelators quantitatively with ^{64}Cu [36b,136,190]. Such results, together with the favourable features of do3aSH for conjugation to biomolecules through the sulphur atom, led us to explore the possibility of preparing copper complexes with do3aSH, at the macroscopic and non-carrier added level.

To prepare Cu^{2+} complexes anchored by do3aSH we studied reactions of do3aSH with $Cu(OAc)_2$ at pH 7 and at room temperature. The progress of these reactions was followed by TLC and HPLC. After 18h of reaction, the TLC (RP-18, Methanol/10% NH_4OAc (1:1)) identified the presence of 3 spots, visualized by UV detection (λ=254 nm). The first spot had a Rf = 0 and was identified as free Cu^{2+}. The other two spots had Rf of 0.2 and 0.8, and may correspond to new copper species, as the free ligand in the same experimental conditions migrates with Rf = 0.65 (iodine revelation). This reaction was also controlled by HPLC. As shown in figure 2.19, the HPLC analysis also indicated the presence of three main peaks with retention times of 2.40, 11.81 and 14.71min.

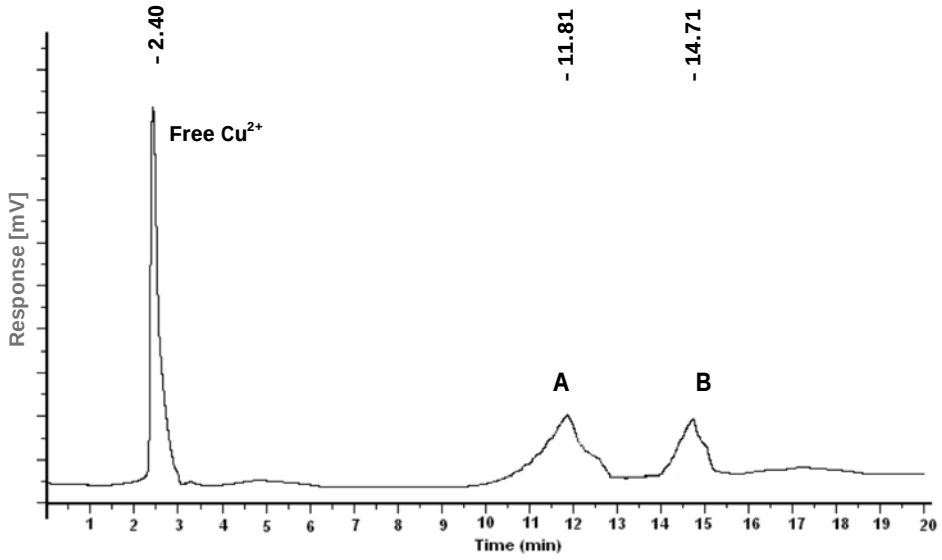

Figure 2.19: HPLC chromatogram of the reaction mixture of do3aSH with $Cu(OAc)_2$

The analysis of a solution of $Cu(OAc)_2$, using the same HPLC conditions, revealed that the peak at 2.40 min corresponds to unreacted Cu^{2+}. The other two peaks were separated by HPLC and analysed by ESI-MS. Unexpectedly, the ESI-MS spectra of both samples were similar, presenting five main peaks at *m/z* 421.0, 443.0, 466.0, 931.1 and 953.1 (figure 2.20).

The peak at m/z 931.1 may correspond to the dimeric complex $[Cu(do3aS)]_2$. From the structural point of view this dimer could be as indicated in figure 2.21: two (Cu-do3aS) units linked by an S-S bond. The peak at m/z 953.1 corresponds to $[M-2H+Na]^-$, being M the dimeric complex $[Cu(do3aS)]_2$. The peak at m/z 466.0 corresponds to unit [Cu-do3aS] and the other two can correspond to fragments of this monomeric species. The ESI-MS spectrum presented the isotopic distribution expected for Cu(II) complexes. In figure 2.20 are shown the theoretical isotopic distribution calculated for the main species, as well as the profile of the peaks obtained experimentally.

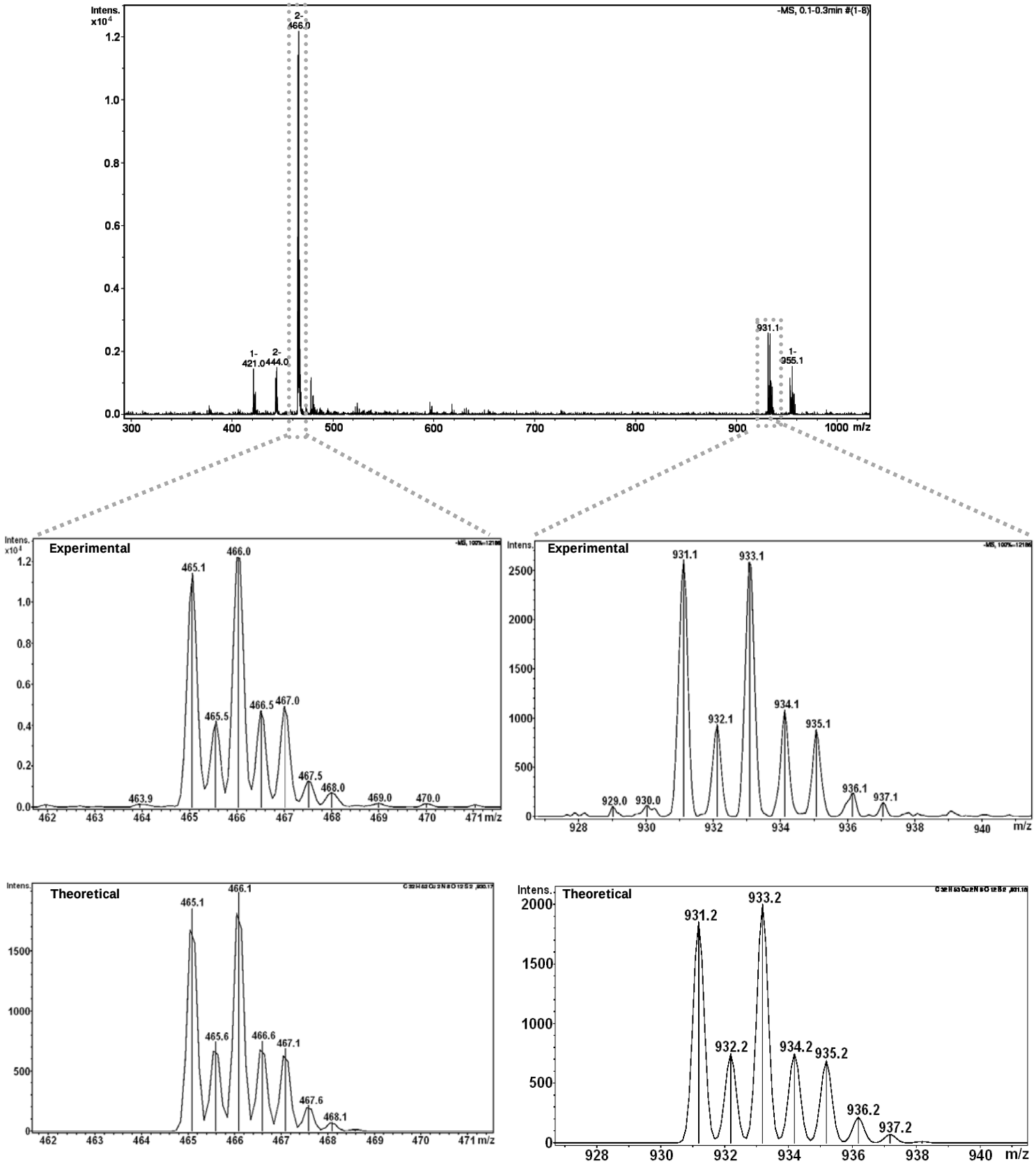

Figure 2.20: ESI-MS spectrum of the species isolated

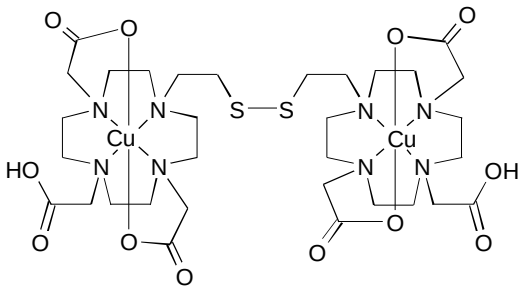

Figure 2.21: Probable structure of the complex [(Cu-do3aS)$_2$]

Based on HPLC and ESI-MS we would say that the two species found by HPLC are certainly isomers, resulting from the different position of the arms towards the metal ion. The identification and separation of different isomers of Y^{3+}-dota like complexes by HPLC has also recently been reported [191]. In fact, the formation of isomers in Ln/Y-dota like complexes is common and can be easily distinguishable by NMR spectroscopy. Unfortunately, Cu(II) complexes do not have NMR spectra, so the identification of such isomers is not possible using this technique. The UV-vis and EPR spectroscopy would not also be adequate as they are sensitive to the nature of atoms coordinated to the metal, and in this case they are the same. So, the only possibility would be to be lucky and to obtain monocrystals for each isomer for X-ray crystallographic analysis.

To find the best reaction conditions to prepare the ^{64}Cu complexes, different parameters have been evaluated namely, pH, reaction time, temperature and concentration of do3aSH.

We reacted 50 µL of $^{64}Cu(OAc)_2$ (5 MBq) with 100 µL of an aqueous solution of do3aSH in different buffers (final concentration of ligand 10^{-3}M or 10^{-4}M). The radiochemical composition of the reaction mixture along the time and the yield of the reactions were evaluated by thin layer chromatography (TLC). As an example, we present in figure 2.22 the radiochromatograms obtained for some of the reactions.

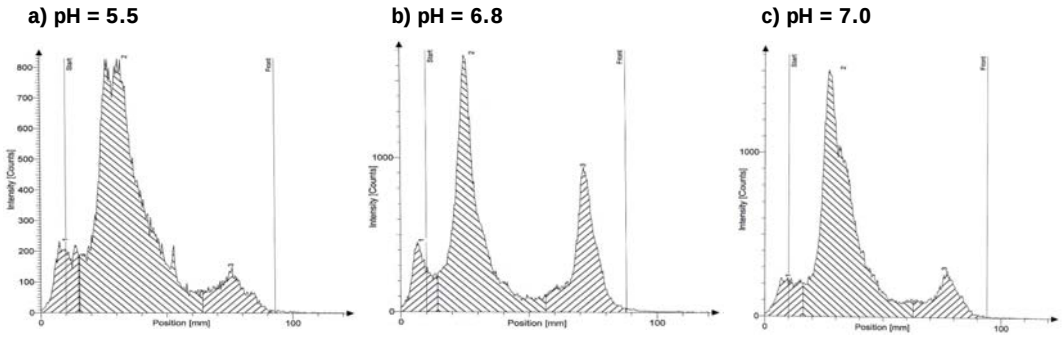

Figure 2.22: Radiochromatograms for reactions of $^{64}Cu(OAc)_2$ (5 MBq) with do3aSH (10^{-3}M) in different buffers (time=30min, t=20ºC): **a**) MES buffer, pH = 5.5; **b**) Ammonium Acetate buffer, pH = 6.8; **c**) HEPES buffer, pH = 7.0

From the chromatographic analysis it was possible to conclude that under the experimental conditions indicated in table 2.16 three main species could be found. By comparison with the behaviour of $^{64}Cu(OAc)_2$ in the same chromatographic conditions, the species with Rf=0 was assigned to the $^{64}Cu^{2+}$. The other two species were not identified but it is clear that the major species was the one with Rf=0.2.

In table 2.16 are listed the results obtained when we studied the effect of the pH on the labelling of do3aSH with ^{64}Cu.

Table 2.16: pH dependence of ^{64}Cu-do3aSH labelling efficiency

pH	do3aSH 10^{-3}M, r.t., 30 min		
	Peak	Rf	%
5.5 MES	Free ^{64}Cu	0	10.1
	species A	0.2	80.5
	species B	0.8	9.5
6.0 MES	Free ^{64}Cu	0	10.1
	species A	0.2	80.3
	species B	0.8	9.6
6.8 Ammonium Acetate	Free ^{64}Cu	0	11.1
	species A	0.2	59.0
	species B	0.8	29.9
7.0 HEPES	Free ^{64}Cu	0	8.9
	species A	0.2	78.3
	species B	0.8	12.7
7.4 HEPES	Free ^{64}Cu	0	7.8
	species A	0.2	74.5
	species B	0.8	17.7
8.0 HEPES	Free ^{64}Cu	0	10.5
	species A	0.2	55.2
	species B	0.8	34.3

Based on the results presented in Table 2.16 and on the interest on physiological conditions, we have decided to pursue our studies using pH 7 (HEPES buffer) and pH 6 (MES buffer).

Using HEPES buffer (pH 7) and MES buffer (pH 6) we evaluate the effect of the temperature on the kinetics of the labelling. The results obtained are presented in Tables 2.17-2.19. As an example, we also show in Figure 2.23 the radiochromatogram obtained for one of the labelling reactions.

Table 2.17: Kinetics of formation of ^{64}Cu-do3aSH, at room temperature and pH 7

Time (h)	do3aSH 10^{-3} M, pH 7 (HEPES), r.t.		
	Peak	**Rf**	**%**
1	Free ^{64}Cu	0	15.4
	species A	0.2	73.4
	species B	0.9	10.8
2	Free ^{64}Cu	0	25.9
	species A	0.2	57.4
	species B	0.8	16.7
4	Free ^{64}Cu	0	0
	species A	0.2	86.4
	species B	0.8	13.6

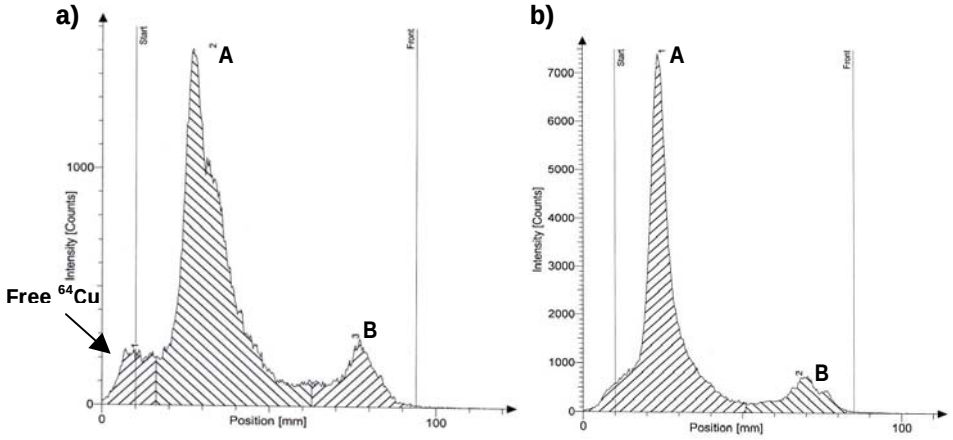

Figure 2.23: Radiochromatogram of ^{64}Cu-do3aSH at pH 7, room temp. (a) t = 1h; (b) t = 4h

Table 2.18: Kinetics of formation of ^{64}Cu-do3aSH, 37ºC and pH 7 (HEPES buffer)

Time (h)	do3aSH 10^{-3} M, pH 7 (HEPES), 37ºC		
	Peak	Rf	%
0.25	species A	0.2	83.7
	species B	0.8	16.3
0.50	species A	0.2	84.2
	species B	0.8	15.8
1	species A	0.2	88.0
	species B	0.8	12.0
24	species A	0.2	80,4
	species B	0.8	19,6

Table 2.19: Kinetics of formation of ^{64}Cu-do3aSH, 37ºC and pH 6 (MES buffer)

Time (min)	do3aSH 10^{-3} M, pH 6 (MES), 37ºC		
	Peak	Rf	%
15	Species A	0.2	89.2
	species B	0.8	10.8
30	Species A	0.2	86.2
	species B	0.8	13.8
60	Species A	0.2	87.8
	species B	0.8	12.2

Independently of the buffer, we found that at 37ºC the reaction was faster: all the free $^{64}Cu^{2+}$ disappeared after 15 minutes and the species with Rf=0.2 was the major one.

The effect of the concentration of do3aSH on the labelling was also evaluated. As can be seen in table 2.20, at pH 7 (HEPES buffer) and at 37ºC, the final concentration of do3aSH did not influence the yield of the reaction.

Table 2.20: Effect of the Ligand concentration on the labelling reaction of ^{64}Cu-do3aSH

[do3aSH]	do3aSH pH 7 (HEPES), 37ºC, 20 min		
	Peak	Rf	%
10^{-3} M	Species A	0.2	84.2
	Species B	0.8	15.8
10^{-4} M	Species A	0.2	83.3
	Species B	0.8	16.7

The results obtained with $^{64}Cu^{2+}$ can be compared with the results obtained at the macroscopic level. This means that, in both cases, we have the formation of two species. As discussed before, we have considered these species to be isomers, based on HPLC and ESI-MS analysis (see page 82). At the radioactive level one of the isomers seems to be more stable. As can be seen in Tables 2.16–2.20 the species with

Rf=0.2 is the major one, and can be obtained in about 80% yield. At the macroscopic level, the two possible isomers seem to present similar stability and in the mixture we have about 50% of each.

Stability in Rat Plasma

The stability of ^{64}Cu-do3aSH was tested in the presence of rat plasma after 2 and 24h of incubation at 37ºC. For this, we have run a reaction of do3aSH with ^{64}Cu at pH 7 (HEPES buffer), 37ºC, 20 min. The yield of the reaction was checked by TLC and after complete disappearance of free Cu^{2+}, an aliquot of the reaction mixture was incubated at 37ºC in the presence of rat plasma. Aliquots of this solution were then taken and analysed by TLC after 2h and 24h and the results are shown in table 2.21.

Table 2.21: *In vitro* stability of ^{64}Cu-do3aSH in the presence of rat plasma

Time (h)	do3aSH $2.4x10^{-2}$ M, pH 7 (HEPES), 37ºC		
	Peak	**Rf**	**%**
0	species A	0.2	84.2
	species B	0.8	15.8
2	species A	0.2	65.9
	species B	0.8	34.1
24	Free ^{64}Cu	0.0	12.6
	species A	0.2	57.8
	species B	0.8	28.9

After 2h we only could detect the presence of the two species normally formed in these studies (Rf 0.2 and Rf 0.8), but after 24h, the presence of free ^{64}Cu could be found (12.6%). These results indicate a moderate stability of the complexes.

2.3.3. bz2ac

To prepare Cu-bz2ac complexes at macroscopic level we have studied reactions of bz2ac with Cu(II) using different experimental conditions, namely different Cu(II) starting materials, different solvents and reaction temperatures, see scheme 2.10.

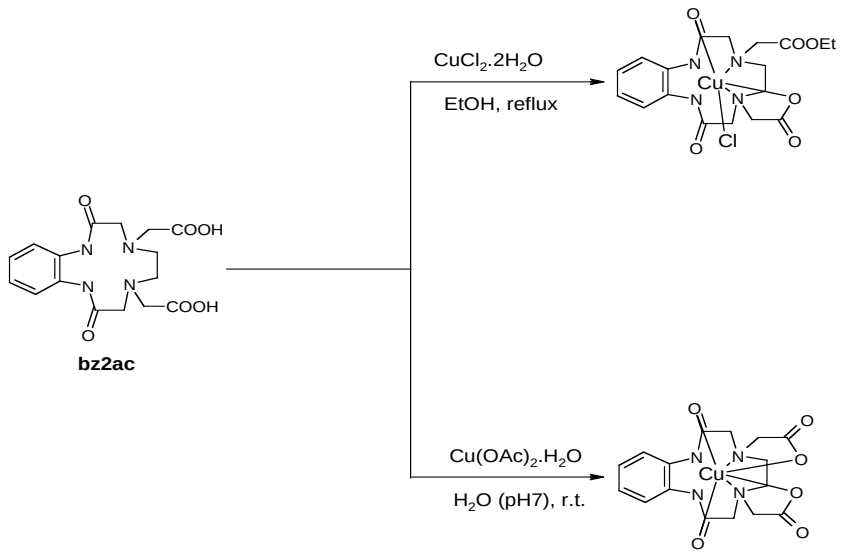

Scheme 2.10: Preparation of Cu-bz2ac complexes

As can be seen in scheme 2.10, the reaction of $CuCl_2.2H_2O$ with bz2ac in the molar ratio 1:1 and using ethanol as solvent was studied. The reaction mixture was refluxed for 2h resulting in a brown solution. After filtration, the filtrate was concentrated and a small amount of methanol added. Upon slow diffusion of MeOH, green monocrystals suitable for X-ray crystallographic analysis were obtained. These crystals have been characterised by X-ray diffraction as $C_{18}H_{23}N_4O_6ClCu$ or [Cu(bz2ac')Cl] (**C1**). As shown in figure 2.24 and 2.25 the ligand has been modified as one acetate arm has been esterified into an ethylesther.

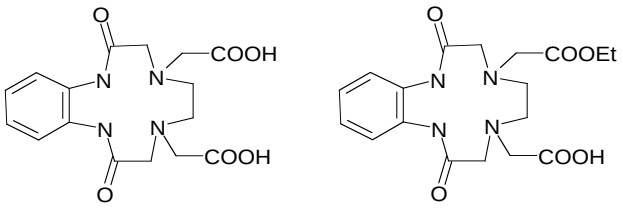

bz2ac **bz2ac'**

Figure 2.24: 2,9-dioxo-1,4,7,10-tetraazabicyclo(1.10.1(hexadeca-1(11),13,15-triene-4,7-diacetic acid (bz2ac) and its monoethylesther (bz2ac')

In this complex, Cu is five-coordinated by two nitrogen atoms of the macrocyclic backbone, two oxygen atoms, one from one amide group and the other from an acetate arm, and a chloride atom, displaying a square pyramidal coordination geometry. The second acetate arm of the macrocycle does not coordinate to the Cu, as it has suffered *in situ* an ethanolic esterification reaction. The ORTEP drawing of the final Cu(II) complex (**C1**) is shown in Figure 2.25.

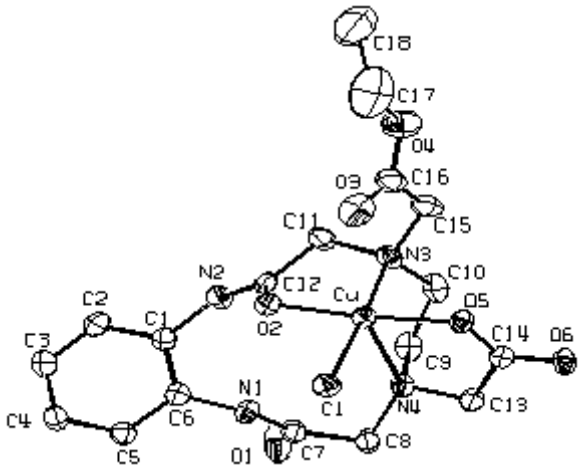

Figure 2.25: ORTEP view of the complex **C1;** thermal ellipsoids are drawn at 40% probability level

Selected bond lengths and angles of **C1** are listed in Table 2.22.

Table 2.22: Selected bond length (Å) and angles (°) for **C1**

Bond length (Å)		Angles (°)	
Cu – O5	1.942(4)	O5 – Cu – Cl	96.10(14)
		O2 – Cu – Cl	91.12(13)
Cu – O2	1.964(4)	N3 – Cu – Cl	173.54(17)
		O5 – Cu – N4	81.25(18)
Cu – N3	2.100(6)	O2 – Cu – N4	99.27(17)
		N4 – Cu – N3	81.10(18)
Cu – N4	2.420(5)	O5 – Cu – O2	172.66(18)
		O5 – Cu – N3	89.30(17)
Cu – Cl	2.2540(19)	O2 – Cu – N3	83.60(17)
		Cl – Cu – N4	96.17(14)

The basal plane is defined by the N3, O2, O5 and the chloride atoms, while the apical position is occupied by the N4 atom.

Most of the Cu(II) five-coordinate complexes known display either distorted square pyramidal (SP) or distorted trigonal bipyramidal (TBP) coordination geometries. To evaluate the degree of distortion from the ideal polyhedron mainly two methods have been developed. The simplest method, which can be applied when there is an apical bond distance longer then the others, is based on the ratio of the two basal angles of the square plane, which is given by the expression $\tau = [(\theta - \phi)/60]\times100$ (%),

being τ = 0 for an ideal SP and τ = 100 for an ideal TBP coordination geometries [192]. For complex **C1** the angles considered were Cl–Cu–N3 and O2–Cu–O5, and the value calculated for τ was 1.46 %. The square plane is folded along the axis defined by Cl, Cu and N3, yielding a dihedral angle between the planes [Cl, N3, O5] and [O2, Cl, N3] of 5.65(23)°. The angle between basal plane and the apical line Cu–N4 is 78.91(15)°. The copper is 0.0217(24) Å above the basal plane and the apical N4 atom is 2.348(6) Å below this plane, yielding a Cu–N4 apical bond distance of 2.420(4) Å, which is longer than the copper nitrogen bond distance in the basal plane (Cu–N3, 2.100(6) Å). The dihedral angle between the aromatic ring and the plane defined by the nitrogen atoms of the macrocyclic backbone is 14.45(30)°, being the copper atom 1.6750(31) Å above this plane. The Cu–N3 bond distance is in the expected range of 1.99–2.08 Å, normally found for five coordinated Cu(II) complexes stabilized by amines [192a,193].

In complex **C1**, the Cu–O2 and Cu–O5 bond lengths are 1.964(4) and 1.942(4) Å, respectively. As in other five-coordinated Cu(II) complexes the bond Cu-O_{amide} is slightly longer than Cu-$O_{carboxylate}$. The Cu-Cl bond length of 2.254(2) Å in **C1** is in the expected range [194].

The formation of the monomeric complex **C1** is certainly related with the reaction conditions used for the synthesis and recrystallization of this complex (1:1 bz2ac/$CuCl_2.2H_2O$, pH = 6, ethanol, 2h reflux, slow diffusion of MeOH), which certainly were also responsible for the *in situ* sterification of one carboxylic acid arm. In fact, a dimer copper complex, isolated by Q. Fernando and co-workers [178], has been obtained by reacting bz2ac with $CuCl_2.2H_2O$ in basic aqueous conditions and slow concentration of this solution (Figure 2.26). In the dimer the Cu atom is six-coordinated by two oxygen atoms of the carboxylate arms, an oxygen from an amide group and two nitrogen atoms from the macrocyclic backbone. The sixth coordination position being occupied by an oxygen atom of a carboxylate arm from an adjacent molecule. It is clear that the pH also plays an important role in the definition of the coordination sphere. Indeed, in our hands the reaction of the bz2ac in aqueous solution at different pH conditions (pH=7) led to the formation of a monomeric species.

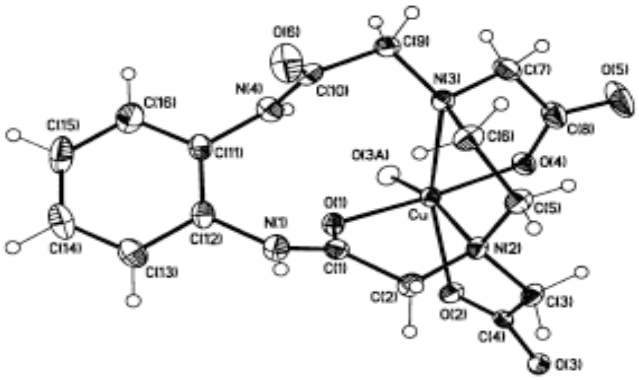

Figure 2.26: X-ray structure of [Cu-bz2ac]. The coordination of carboxylate oxygen atom O(3a) from the neighboring metal chelate molecule results in the formation of a polymeric structure. Taken from ref. [178]

Nevertheless, the solution studies performed with our complex have shown that once it is dissolved in water, the coordination around the metal changes, becoming probably six-coordinated and with replacement of the chloride ion by a water molecule. To prepare a complex Cu-bz2ac to be used as a reference for the radioactive reactions, we have tried the synthesis of Cu-bz2ac using experimental conditions close to the ones usually used in the radiochemical studies: $Cu(OAc)_2$ as starting material, water (pH 7) as solvent and room temperature (Scheme 2.10). After overnight reaction, a green solution was obtained which was analysed by TLC and HPLC. Using these two chromatographic methods we have concluded that a new and well defined species was formed. As shown in figure 2.27, the HPLC chromatogram obtained presented only one peak with a retention time of 3.44 min and no free Cu^{2+} or free ligand could be found (Rt 4.22 min and 2.70 min, respectively; chromatographic profiles also shown in figure 2.27).

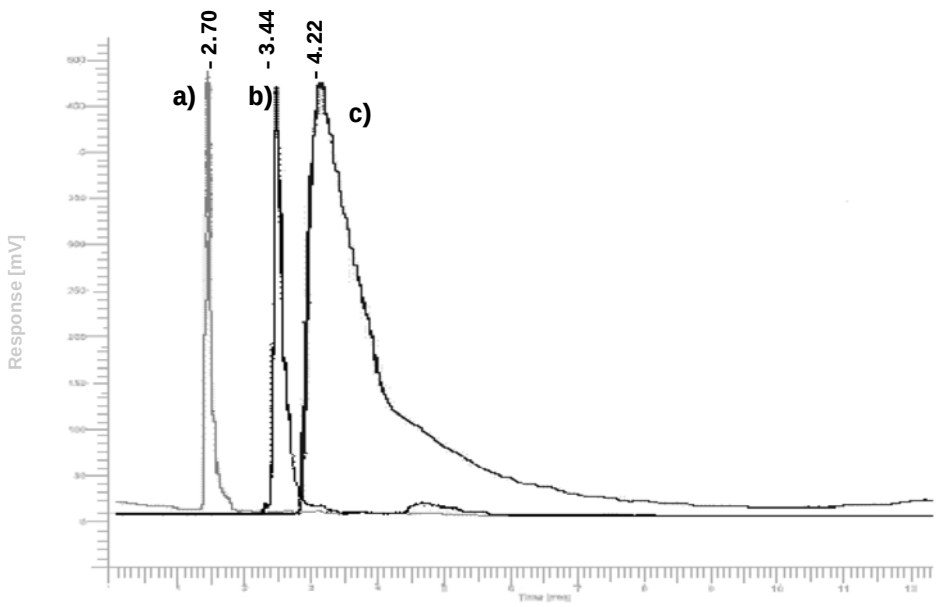

Figure 2.27: HPLC profile of the reaction of bz2ac with $Cu(OAc)_2$: **a)** bz2ac (2.70 min); **b)** new species (3.44 min); **c)** $Cu(OAc)_2$ (4.22 min)

This new species had an Rf = 0.79 in the TLC. An aliquot of the reaction was analysed by ESI-MS (negative mode). The ESI-MS spectrum of the reaction mixture presented only one main peak at *m/z* -424 (figure 2.28). This species corresponds to the neutral complex, which we have formulated as [Cu-bz2ac] (m/z_{calc} = 425.5). The isotopic distribution found for this peak is in agreement with the expected one, also shown in figure 2.28.

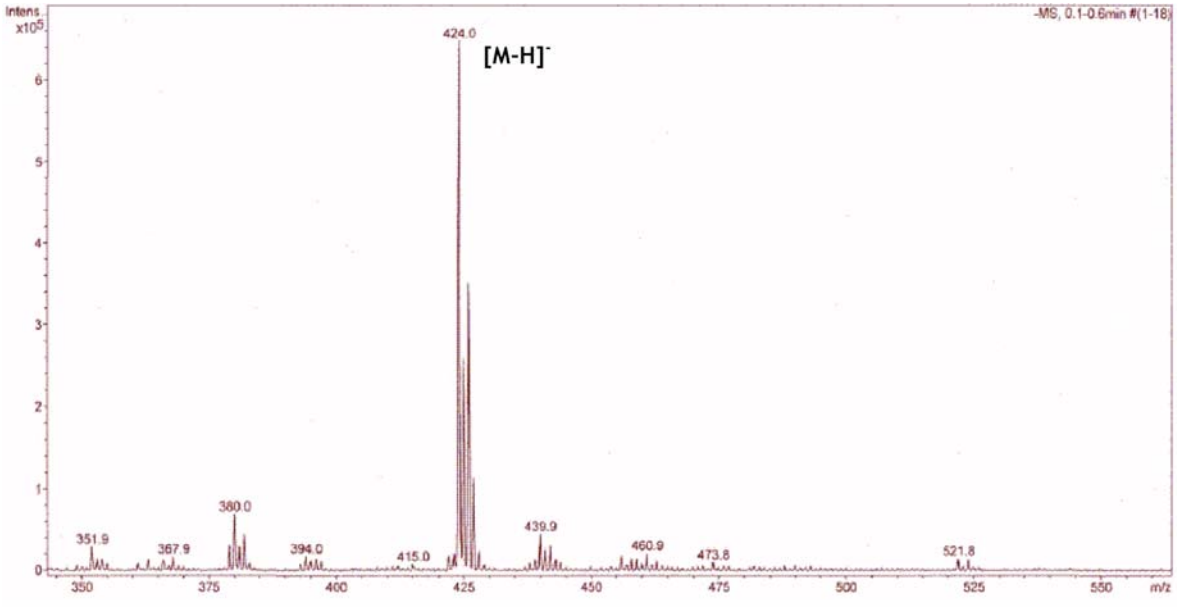

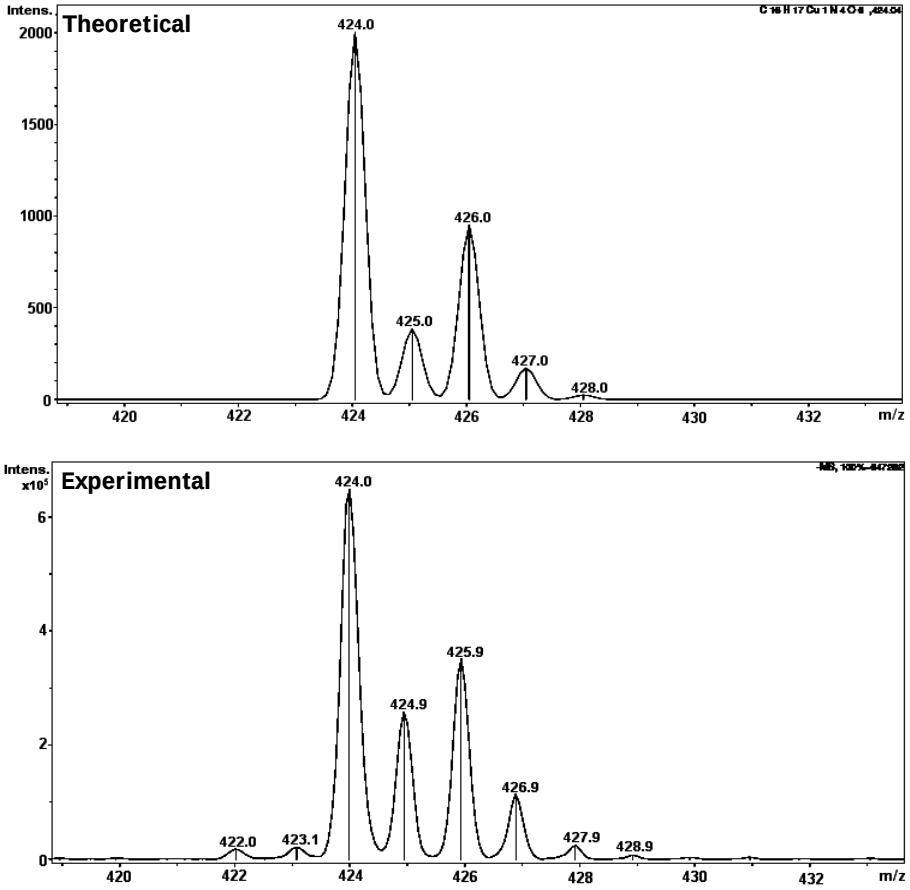

Figure 2.28: ESI-MS spectrum of the reaction mixture

Unfortunately no mono crystals suitable for X-ray diffraction analysis were obtained. So, is difficult only based on ESI-MS to assign the real structure of the complex. However, if we consider the pH at which this reaction has been performed, pH 7, and if we take into consideration the species distribution diagram (figure 2.14), we can say that most probably the species formed is [ML]. Moreover, based on the solution studies performed, we expect that at this pH the two nitrogen atoms of the amides are protonated. Taking all this into consideration we propose for this Cu-bz2ac complex the structure shown in figure 2.29.

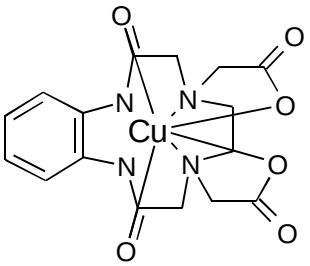

Figure 2.29: Probable structure of the complex [Cu-bz2ac]

In this structure the Cu^{2+} would be six-coordinated by two nitrogen atoms of the macrocycle, by two oxygen atoms of the amide groups and by two oxygen atoms from the carboxylate arms. Taking into account literature data, the metal ion is expected to be out of the plane defined by the nitrogen atoms. More recently, after the publication of this work, Antunes *et al* have reported a crystal structure of a Cu(II) complex anchored by a similar macrocycle **VI** (see figure 2.12). The reaction has been performed at pH 10 and in water, conditions at which the nitrogen atoms of the amide groups are probably deprotonated. They have found that in the complex [Cu-VI] the Cu^{2+} is five-coordinated, being anchored by the 4 nitrogen atoms of the macrocyclic backbone and one oxygen atom from a water molecule [182].

To check about the stability of [Cu-bz2ac], this compound was incubated with a 10 fold excess of cyclam. Cyclam is a tetraazamacrocycle with very well known affinity for Cu^{2+} ($\log K_{Cu\text{-}cyclam}$=26.5) [19]. This reaction mixture Cu-bz2ac/cyclam was analysed by TLC at different time points (30 and 180 min). The chromatograms indicated the presence of only one species with an Rf=0.79, indicating that no transchelation or transmetallation have occurred.

To find the best reaction conditions to prepare the ^{64}Cu complexes, different parameters have been evaluated: pH, reaction time, temperature and concentration of the ligand bz2ac. To start our studies we have added 50 µL of $^{64}Cu(OAc)_2$ (5 MBq) to 100 µL of aqueous solutions of bz2ac (final concentration of ligand 10^{-3} M to 10^{-6}M). The radiochemical composition of the reaction mixture and the yield of the reaction were evaluated by thin layer chromatography (TLC). Figure 2.30 shows the radiochromatogram obtained. As can be seen, only one main species could be found with an Rf=0.8.

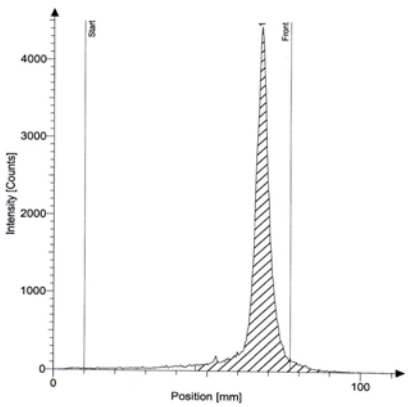

Figure 2.30: Radiochromatogram of the ^{64}Cu-bz2ac: 1min, 20ºC, HEPES buffer (pH7)

In table 2.23 are listed the results obtained when we studied the effect of the pH in the labelling of bz2ac with ^{64}Cu.

Table 2.23: Effect of pH in the labelling of bz2ac with ^{64}Cu

pH Buffer	bz2ac 10^{-3}M, r.t., 30 min		
	Peak	Rf	%
5.5 MES	Species A	0.8	84.9
	Species B	1.0	15.1
6.0 MES	Species A	0.8	88.0
	Species B	1.0	12.0
6.8 Ammonium Acetate	1 species	0.8	100
7.0 HEPES	1 species	0.8	100
7.4 HEPES	1 species	0.8	100
7.4 Phosphate	1 species	0.8	100
8.0 HEPES	1 species	0.8	100

Comparing the results obtained at diferent pH values, it is possible to see that only in the case of pH 5.5 and 6.0 two species were formed – one that corresponds to the ML species with Rf ≈ 0.8 and another with Rf = 1.0. In fact, these results are somehow unexpected taking into account the species distribution diagram, shown in figure 2.14. At pH 6.0 one major species, ML, would be expected being the species MHL still present at this pH, although in a percentage smaller than 5%. Nevertheless, at pH 8.0 the species LM(OH) may be present, in about 10%, what has not been observed in the radiochemical studies.

We have decided to work at pH 7.0, using HEPES buffer. In table 2.24 are summarized the results found for different reaction times.

Table 2.24: Effect of time in the labelling of bz2ac with ^{64}Cu

Time (min)	bz2ac 10^{-3} M, pH 7 (HEPES), r.t.		
	Peak	Rf	%
1	1 species	0.8	100
5	1 species	0.8	100
10	1 species	0.8	100
15	1 species	0.8	100
30	1 species	0.8	100

The labelling reaction takes place quite fast (figure 2.30) and the species formed is stable up to 24h.

The effect of the concentration of ligand was also tested. Table 2.25 shows the results obtained when we have tried the labelling using different final concentrations of bz2ac.

Table 2.25: Effect of the ligand concentration in the labelling of bz2ac with ^{64}Cu

[bz2ac]	bz2ac pH 7, r.t., 30 min		
	Peak	**Rf**	**%**
10^{-3} M	1 species	0.8	100
10^{-4} M	Species A	0	82
	Species B	0.5	18
10^{-5} M	1 species	0.1	100
10^{-6} M	1 species	0.1	100

The analysis of these data indicated that the best conditions for a quantitative labelling involve: 10^{-3}M final ligand concentration, room temperature, HEPES buffer, pH 7-8, and 1 min. reaction time.

The high labelling efficiency for bz2ac and the fact that the Rf of the labelled species is the same as the one found for Cu-bz2ac in the same experimental conditions, led us to assume that the radioactive complex has the same structure as the inactive one.

In vitro Stability in Rat Plasma

The stability of the ^{64}Cu-bz2ac complex was tested in the presence of rat plasma, after 2h and 24h of incubation at 37ºC. The stability was followed by TLC. The results obtained are shown in table 2.26.

Table 2.26: *In vitro* stability of ^{64}Cu-bz2ac in rat plasma

Time (h)	bz2ac $3.4x10^{-2}$ M, pH 7 (HEPES), r.t.		
	Peak	**Rf**	**%**
2	1 species	0.8	100
24	species A	0.3	6,0
	species B	0.7	91,7

We have found that ^{64}Cu-bz2ac is stable up to 2 hours in the presence of rat plasma. At 24 hours the formation of 6% of a different species was observed. This new species has an Rf = 0.3 and does not correspond to free ^{64}Cu.

Further studies were carried out using ^{67}Cu, another isotope interesting for medical purposes. Using the experimental conditions optimised for ^{64}Cu we have performed studies with ^{67}Cu. The labelling of bz2ac with ^{67}Cu has been quantitative but the reaction is slower than with ^{64}Cu. We were forced to use a concentration of the ligand higher than the one used with ^{64}Cu. We consider that the difficulties found in these reactions are due to the unexpected low specific activity of $^{67}CuCl_2$, which was tested by reacting ^{67}Cu with teta, which is a macrocycle presenting high stability towards copper and the labelling reaction is quantitative and very fast. Nevertheless, some stability and challenge studies were preformed.

In vitro Stability in Human and Rat Plasma

For the stability studies in human and rat plasma, the labelling was preformed with [L] = $3.4x10^{-2}$ M, pH 7 (HEPES buffer), 30 min. at room temperature. These studies were performed as described for the assessment of the *in vitro* stability of ^{64}Cu-bz2ac in rat plasma. The results are shown table 2.27.

Table 2.27: *In vitro* stability of ^{67}Cu-bz2ac in human and rat plasma

Time (h)	Human plasma			Rat plasma		
	Peak	Rf	%	Peak	Rf	%
2	1 species	0.8	100	1 species	0.8	100
24	1 species	0.8	100	1 species	0.8	100

In vitro Stability in Phosphate Buffer and Saline Solution

For the challenge studies towards phosphate buffer and saline solution a preparation of ^{67}Cu-bz2ac (~6 MBq) at pH 7 was used. The yield of the reaction was checked by TLC, before the addition of the challenge agent. The mixtures were incubated at 37ºC and the stability checked by TLC after 0.5, 2 and 24 hours. The results are presented in table 2.28.

Table 2.28: *In vitro* stability of ^{67}Cu-bz2ac in phosphate buffer (pH 7.4) and saline

Time (h)	Phosphate buffer (pH 7.4)			Saline (NaCl 0.9%)		
	Peak	Rf	%	Peak	Rf	%
0.5	1 species	0.8	100	1 species	0.8	100
2	1 species	0.8	100	species A	0.8	88.2
				species B	0.9	11.8
24	1 species	0.8	100	species A	0.8	79.0
				species B	0.9	21.0

In vitro Stability in the Presence of Cyclam

The use of cyclam, as a possible transquelating agent, is due to the well recognised stability of the Cu-cyclam complexes.

Table 2.29: *In vitro* stability of ^{67}Cu-bz2ac in the presence of cyclam (100 excess fold)

Time (h)	Cyclam (100 excess)		
	Peak	Rf	%
1	species A	0.8	85.5
	species B	0.9	14.5
24	species A	0.8	81.5
	species B	0.9	18.5

From the results shown in table 2.29, it is possible to conclude that a different species appears in the presence of cyclam, with a slightly higher Rf value (≈ 0.90). This new species doesn't correspond to the Cu-cyclam complex (Rf=0.4), but the result certainly indicates some instability of our complex.

2.4. Conjugation of a Model Peptide to bz2ac

To explore the potential interest of the ligand bz2ac as a bifunctional chelator agent (BFCA), we decided to conjugate this ligand to a lysine protected with a Fmoc group (figure 2.31).

This conjugation was important due to two main reasons:
1. The labelling of this conjugate could predict future results with a biologically active peptide;
2. The conjugate bz2ac-lysine could be used for conjugation to such peptide.

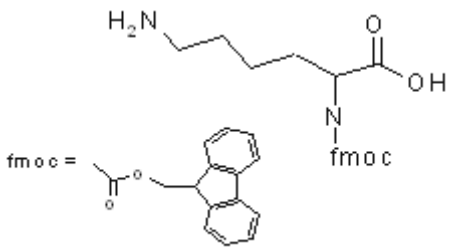

Figure 2.31: Structure of the Lysine-Fmoc

2.4.1. Synthesis and Characterization of bz2ac-Lysine-Fmoc Conjugates

The conjugation of a Fmoc protected Lysine to the bz2ac ligand was performed using an experimental procedure analogous to what is normally used for conjugation of peptides [43-45]. Such procedures consisted in the reaction of the primary amine of the lysine with a carboxylic group of the macrocycle. The carboxylic group of the macrocycle was activated with HBTU, in the presence of a base (DIPEA), followed by the addition of 1 eq of Fmoc-Lysine, at room temperature. After 3h, an aliquot of the reaction mixture was analysed by HPLC (RP-18 column, CH_3CN/H_2O with 0.1% TFA gradient, see experimental part for more details). The HPLC chromatogram indicates the presence of 5 main species. These species were separated by HPLC, and each fraction analysed by $^1H/^{13}C$ spectroscopy and by ESI-MS.

Based on these two techniques we have concluded that the fraction with a retention time (Rt) of 33.5min corresponds to the bz2ac conjugated to one Lysine-Fmoc (figure 2.32a). The fraction which had a Rt of 41.5min corresponds to the bz2ac conjugated to two Lysine-Fmoc (figure 2.32b)

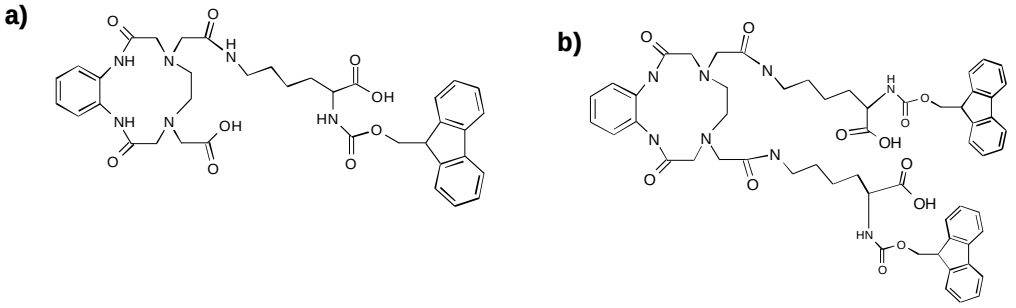

Figure 2.32: Structure of the bz2ac conjugates: **a)** bz2ac-Lys-Fmoc, **b)** bz2ac-$(Lys\text{-}Fmoc)_2$

The ESI-MS spectra obtained for bz2ac-Lys-Fmoc and bz2ac-$(Lys\text{-}Fmoc)_2$ are shown in figure 2.33. The spectrum of bzac-Lys-Fmoc (figure 2.33a) shows one main peak at m/z = 737.47, corresponding to $[M+Na]^+$. The spectrum found for bz2ac-$(Lys\text{-}Fmoc)_2$ (figure 2.33b) shows one main peak at m/z 1065.65, corresponding to $[M+H]^+$. This spectrum also shows a peak at m/z 719 corresponding to bz2ac-FmocLys.

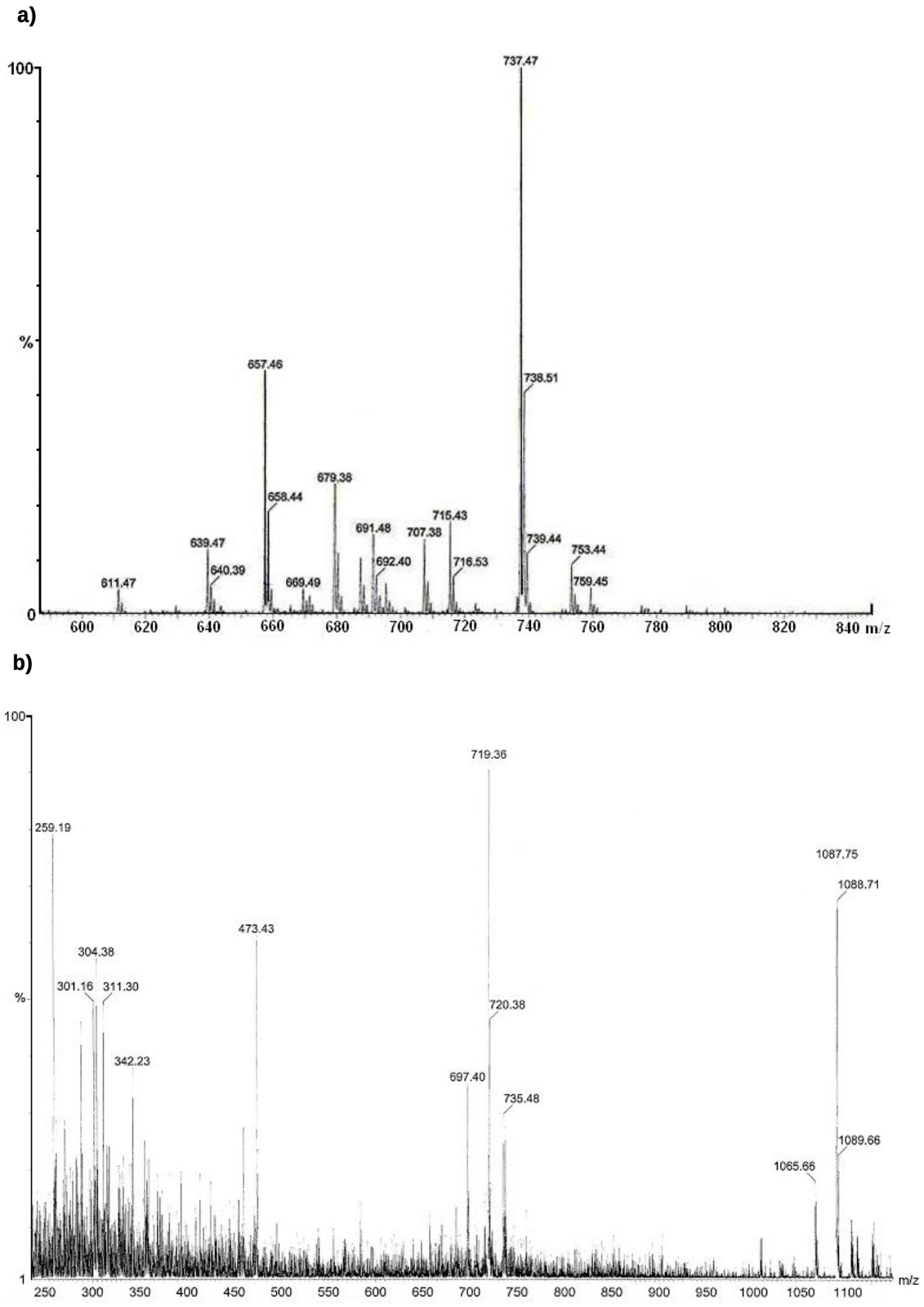

Figure 2.33: ESI-MS spectra of ligands **(a)** bz2ac-Lys-Fmoc and **(b)** bz2ac-(Lys-Fmoc)$_2$

It was clear that we have activated one or two carboxylate groups from the bz2ac.

2.4.2. Reactions of bz2ac-Lys-Fmoc and bz2ac-(Lys-Fmoc)$_2$ with Inactive and Radioactive Copper

A solution of 1 eq of each conjugate in 1:1 CH_3CN/H_2O was reacted with 0.8 eq of $Cu(NO_3)_2.3H_2O$ for 18h, at room temperature. Several TLC conditions were tested and in all the cases the presence of free copper was observed. The reactions were followed by HPLC analysis (RP-18 column, $MeOH/H_2O$ gradient). In this system, the free copper has a retention time of 2.47 min and the complex [Cu-(bz2ac-Lys-Fmoc)] appears at 11.91 min. In the case of the [Cu-(bz2ac-(Lys-Fmoc)$_2$)], the free copper appears at 2.03 min and the Cu(II) complex at 13.78 min.

To prepare the radioactive complexes of the conjugates we started using the same experimental conditions previously followed for bz2ac: 10^{-3}M solution, pH 7, 5 min., room temperature. The progress of the labelling was followed by HPLC. The Rt of the species formed was found to be 14.93min and the Rt of free Cu^{2+} was 3.27min. Under these conditions a complete labelling was never achieved, and the final concentration of the conjugates had to be increased to $3.64x10^{-3}$M. For [^{64}Cu-bz2ac-Lys-Fmoc] a labelling yield of ≈90% after 1.5h of reaction at pH 7 and at room temperature was obtained, while for [^{64}Cu-bz2ac-(Fmoc-Lys)$_2$] the formation of 2 different species (18.40 min, 22.3% and 18.93 min, 26.6%), and about 45% of free ^{64}Cu was observed.
The low labelling yields found for the lysine conjugates indicate that the carboxylate pendant arms are needed to stabilize Cu^{2+}.

2.5. Concluding Remarks

A novel mono-substituted thiol cyclen derivative, do1SH, was successfully obtained and its protonation constants were determined by potentiometry. ^{13}C-NMR titrations were also performed to assess the protonation sequence of the ligand. The stability constants of do1SH with Cu^{2+}, Zn^{2+} and Cd^{2+} were determined by potentiometry and the values found follow the trend [Cu-do1SH]>[Zn-do1SH]≈[Cd-do1SH]. The introduction of one thiol pendant arm in the cyclen backbone has improved the affinity for Cu^{2+} but its selectivity towards the other d-elements has decreased. Solution structural studies of [Cu-do1SH] and [Zn-do1SH] showed that do1SH forms penta-coordinated complexes with these metals and that the sulphur atom only coordinates to the metal ion at pH>8.

A new carboxylate/thiol cyclen derivative, do3aSH, was also successfully synthesised and characterized by the usual analytical techniques, which included 2D-NMR studies, mass spectrometry and elemental analysis. The protonation constants of the ligand were determined by potentiometry and $^{1}H/^{13}C$-NMR spectroscopy. Based on these techniques, a protonation sequence was proposed. Reactions of do3aSH with Cu^{2+} and $^{64/67}Cu^{2+}$ were performed and the formation of two new Cu^{2+} species was always observed. The ESI-MS spectrum of the two inactive isolated species were identical and consistent with the presence of the dimer $[Cu\text{-}do3aS]_2$. So, one possibility is that the two species found in solution may correspond to isomers.

The previously reported bz2ac (a $12N_4$ macrocycle bearing a benzene ring on the cyclen backbone and two carboxylate pendant arms) was also studied. The protonation and stability constants of bz2ac with Cu^{2+} and with other *d*-elements were determined by potentiometry. The increase of the rigidity of the macrocycle, imposed by the benzene ring, didn't raise the pM values for Cu^{2+} relatively to other *d*-metals. Reactions of bz2ac with Cu^{2+} and with $^{64/67}Cu^{2+}$ have been studied and the formation of a single species formulated as [Cu-bz2ac] has been found. Recrystalization of the complex prepared at the macroscopic level, from ethanol/methanol, led to crystals suitable for X-ray diffraction. The crystallographic analysis showed the formation of a monomeric benzodioxochlorocomplex [Cu(bz2ac')Cl] (bz2ac' = monoethylesther of bz2ac), where the Cu^{2+} is five-coordinated by two nitrogen and two oxygen atoms of the macrocycle and by a chloride, displaying a square pyramidal coordination geometry. One of the acetate arms does not coordinate to the Cu^{2+} and has suffered an *in situ* ethanolic esterification reaction.

3. MACROCYCLES FOR STABILIZATION OF *f*-ELEMENTS

In this chapter the synthesis and characterisation of macrocyclic compounds suitable for the stabilization of *f*-elements is presented. Solution and solid state studies with some *f*-elements were performed. Radiolanthanide complexes of ^{153}Sm and ^{166}Ho were also synthesized and biologically evaluated.

Part of the work described in this chapter has been already published or is in preparation:

- F. Marques, L. Gano, M.P. Campello, S. Lacerda, I. Santos, L.M.P. Lima, P. Antunes, J. Costa and R. Delgado, *J. Inorg. Biochem.* 2006, 100: 270-280.
- M.P. Campelo, S. Lacerda, L. Gano, F. Marques and I. Santos, *Radiochimica Acta*, 2007, 95, 329-334.
- F. Marques, M.P. Campello, S. Lacerda, L. Gano and I. Santos, *Radiochimica Acta*, 2007, 95, 335-342.
- L. Gano, F. Marques, M.P. Campello, M. Balbina, S. Lacerda and I. Santos, *Q. J. Nucl. Med. Mol. Imaging*, 2007, 51: 6-15.
- S. Lacerda, M.P. Campello, F. Marques, L. Gano, P. Fousková, V. Kubíček, E. Toth and I. Santos, Dalton Trans., in press
- S. Lacerda, F. Marques, L. Gano, V. Kubíček, P. Hermann and I. Santos, *to be submitted*
- M.P. Campello, S. Lacerda, I.C. Santos, C. Geraldes, P. Hermann, J. Kotek, I. Lukes, P. Lubal, V. Kubíček, E. Toth and I. Santos, manuscript in preparation

3.1. Introduction

Lanthanides have isotopes with physical properties interesting for medical applications. From all the lanthanides, ^{153}Sm, ^{166}Ho and ^{177}Lu are the most explored for potential application in nuclear medicine [84,198]. As referred before, polyazamacrocycles with different pendant arms, such as dota, dota –derivatives or dotp strongly chelate lanthanide ions. Moreover, the thermodynamically stable complexes formed with such chelators are also, in general, kinetically inert, a desirable feature for their *in vivo* application, as bifunctional chelating agents (BFCA´s) [89, 199,200]. As discussed in chapter 1, the properties and utility of this class of compounds can be modulated by changing the nature and number of their pendant arms, the cavity size and rigidity of the tetraazamacrocycle.

With the work described in this chapter we intended to explore the coordination capability of the cyclen-derivative do3aSH (synthesis described in Chapter 2, page 58) towards different lanthanides, mainly the ones with isotopes interesting for Nuclear Medicine. According to the state of the art, trivalent lanthanides, despite their large ionic size, have been stabilized by do3a [201]. Such result predicted that do3aSH would be able to stabilize those ions, remaining the thiol pendant arm free for conjugation to biologically relevant molecules. Herein, we will present solution studies of do3aSH with different lanthanides, reactions of this cyclen-derivative with $^{153}Sm^{3+}$ and $^{166}Ho^{3+}$ and *in vitro* and *in vivo* evaluation of the radioactive species formed.

As also referred in Chapter 1, is also important to find complexes with bone affinity without the limitations of ^{153}Sm - Samarium-edtpm (Quadramet®) and ^{153}Sm-dotp. A possibility would be to prepare samarium or holmium complexes anchored by cyclen-derivatives bearing mixed carboxylate-phosphonate or carboxylate-phosphinic pendant arms. The Radiopharmaceutical Sciences Group/ITN and other research groups have been involved in such study. These groups tried to prepare lanthanide complexes anchored on different macrocycles bearing phosphonate or phosphinic and/or carboxylate pendant arms. The ITN group tried to evaluate the effect of the number of phosphonates and their relative position on the stability of samarium and holmium complexes, as well as on their pharmacokinetics and affinity for bone. During my thesis I have been involved on studies with the new *trans*-do2a2p. I have isolated and fully characterized, in the solid state and in solution, this compound.

Studies of *trans*-do2a2p with inactive and radioactive lantahnides were also performed and the biological behaviour of some of the radioactive complexes was studied. I have also studied the radiochemical and biological behaviour of Sm and Ho complexes anchored by tetraazamacrocycles bearing phosphinic and carboxylate pendant arms. These chelators were isolated and characterized by Prof. Lukes's Group in Prague, and supplied to our group under a bilateral collaboration.

3.2. Cyclen Derivative with Thiol/Carboxylate Pendant Arms

3.2.1. Stability Constants of do3aSH with Lanthanides

The stability constants of the cyclen-derivative do3aSH (mixed thiol/carboxylate pendant arms) with Ce^{3+}, Sm^{3+} and Ho^{3+} were determined by potentiometry (at 25.0ºC and 0.1mM KCl ionic strength) and UV-Vis spectroscopy. The synthesis and characterization of this new compound, as well as the protonation constants were presented and discussed in chapter 2 (table 2.10, page 62). Calculations to determine the stability constants of do3aSH with lanthanides were performed with OPIUM program [169]. The kinetics of formation of the lanthanide complexes with do3aSH is relatively slow. Therefore, the stability constants were determined by the use of a batch method in the pH regions where complexation equilibrium was not attained during in-cell titrations.

In order to get information on the formation kinetics of the lanthanide complexes, namely samarium and holmium complexes, studies with Ce^{3+} were also performed. The complexes formed with this lanthanide usually have an intense UV-Vis band at about 300 nm, easy to follow. Thus, UV-Vis spectra (245-350 nm) of buffered solutions of the Ce^{3+}/do3aSH at pH 4.7, 6.0 and 7.6 ([Ce] = [L] = 10^{-3} M) were recorded. Under these conditions, the complex was completely formed after 2h (pH 4.7), 15 min (pH 6.0) and 3 min (pH 7.6). The stability constant of the Ce-do3aSH complex was determined by UV-Vis spectrophotometry at 25.0 ºC and 0.1 M KCl ionic strength (figure 3.1).

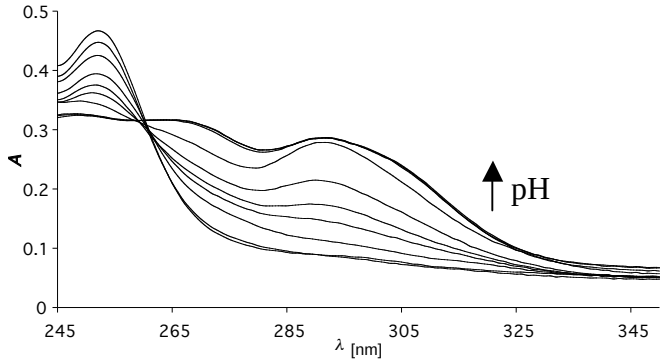

Figure 3.1: UV-VIS titration of the Ce^{3+}/do3aSH system. $c_L = c_M =$ 0.5 mM at 25°C, I = 0.1 M KCl and variable pH (3.01; 3.27; 3.82; 4.16; 4.41; 4.35; 5.66; 6.84; 7.63; 8.08)

Given the slow formation observed below pH ≈ 4, where the complexation is less than 100%, a batch method was used to determine the stability constant. The UV-vis spectra of the Ce^{3+} complex show only negligible changes upon the deprotonation, therefore only the overall stability constant of the Ce-do3aSH complex protonated on the thiol group could be determined by UV-Vis spectrophotometry (β_{HML} = [HML]/[M][H][L]). Then the value of the protonation constant, K_{HML} = [HML]/[ML][H], was obtained from pH-potentiometric titrations of the complex, prepared prior to the titration. The stability constant was calculated as $K_{ML} = \beta_{HML}/K_{HML}$.

The stability constants of the Sm^{3+} and Ho^{3+} complexes were then determined by UV-Vis spectrophotometry in batch samples *via* competition with the Ce^{3+} ion. Similarly to the Ce^{3+} analogue, protonation constants of both Sm^{3+} and Ho^{3+} complexes were obtained by potentiometry. The stability and protonation constants determined for Ce^{3+}, Sm^{3+} and Ho^{3+} are listed in Table 3.1.

Table 3.1: Protonation and stability constants for the Ln(III)-do3aSH complexes

	Ce(III)	Sm(III)	Ho(III)
$\log\beta_{MHL}$ [a]	27.21 ± 0.03	28.0 ± 0.1	27.4 ± 0.1
$\log K_{MHL}$ [b]	5.97 ± 0.03	6.0 ± 0.1	6.4 ± 0.1
$\text{Log}\beta_{ML}$	21.24	22.0	21.0

[a] determined by UV-Vis; [b] determined by potentiometry.

The three different lanthanides, roughly representing the beginning, the middle and the last part of the lanthanide series, have very similar stability constants without any specific trend.

The invariance of the UV-Vis spectrum of the Ce^{3+} complex on deprotonation of the SH group shows that the deprotonated thiol does not coordinate to the lanthanide ion. Thus, the protonation constants of the complexes correspond to protonation of the thiol group.

Table 3.2 presents the stability constant values obtained for do3aSH and for related macrocycles, do3a and dota, as well as the pM values (pM = -log$[M]_{free}$) calculated at pH 7.4.

Table 3.2: Stability constants and pM determined for Ln(III) complexes of do3aSH, do3a and dota

	do3aSH[a]		do3a		dota	
	logK_{ML}	pM*	logK_{ML}	pM*	logK_{ML}	pM*
Ce^{3+}	21.24(0.03)	8.84	19.7[b]	9.28	23.0[b]	10.75
Sm^{3+}	22.0(0.1)	9.22	---	---	23.0[d]	10.75
Eu^{3+}	---	---	20.69[c]	9.77	23.7[e]	11.35
Gd^{3+}	---	---	21.0[b]	9.93	24.6[b]	11.55
Ho^{3+}	21.0(0.1)	8.72	---	---	24.8[d]	11.65
Lu^{3+}	---	---	23.0[b]	10.93	25.5[b]	12.00

[a] This work, 25.0ºC, I = 0.1mM KCl; [b] 25.0ºC, I = 0.1 M NMe_4Cl, ref. [201a]; [c] det. by Laser-Excited Eu^{3+} Luminescence Excitation Spectroscopy, 25.0ºC, ref. [201b]; [d] 25.0ºC, I = 1 M in NaCl, ref [202a]; [e] 37ºC, ref [202b]. *pM = -log$[Ln]_{free;}$ $c_L = c_M = 10^{-6}$ M; pH 7.4.

The values found for do3aSH are two to three orders of magnitude lower than those found for the corresponding Ln-dota complexes, being however somewhat higher than the constants reported for Ln-do3a. As explained before, the pM values allow a better comparison of the affinity of different ligands towards the same metal ion, as it takes into account the different basicity of the ligands. The values found for do3aSH are about 1 log unit lower then the ones found for dota, but are only slightly lower than the ones determined for do3a. This difference reflects mainly the higher protonation constants of do3aSH, in particular the high values of logK_{H2} and logK_{H3}. Nevertheless, the lower value determined for pHo is somehow unexpected as usually the stability constants of the Ho-dota-like complexes are of the same order or higher than the corresponding constants with Sm^{3+} [35].

In figure 3.2 are presented the species distribution diagrams found for Sm-do3aSH and Ho-do3aSH, showing that the ML species exists as unique species for pH > 8.

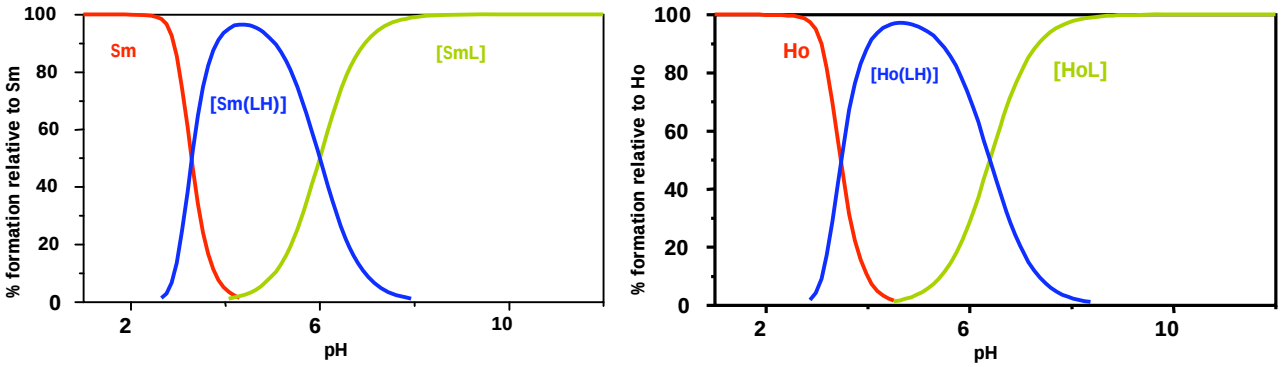

Figure 3.2: Species distribution diagram of Sm-do3aSH and Ho-do3aSH

To confirm if the sulphur atom coordinates or not to the metal, relaxivity measurements on the corresponding Gd^{3+} complex were made. The Gd complexes formed with dota-like compounds are usually 9 coordinated having at least one water molecule coordinated to the metal [87]. In the case of do3aSH, if the sulphur atom is not coordinated, at least two water molecules are expected to be coordinated to the metal ion. In figure 3.3 is presented a model of a Gd-dota like complex.

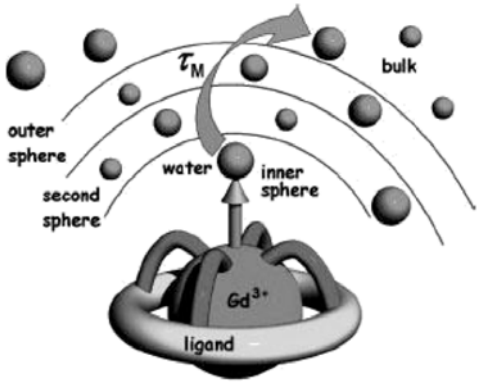

Figure 3.3: Model of Gd-dota like complexes, showing the exchange of one water molecule from the inner sphere to the bulk: τ_M= residence time of the water molecule; adapted from ref [87]

In fact, changing the pH from 4.9 to 7.4, range where the deprotonation of the SH function occurs, the relaxivity decreases only 10%. If the deprotonated thiol coordinates to the Gd^{3+} ion, upon coordination we would expect the elimination of one inner sphere water molecule from the complex and, consequently, a more important decrease of the proton relaxivity would be found. Thus, the experimental data indicates that even in its deprotonated form, the thiol does not replace a water molecule in the inner coordination sphere of the lanthanide. This is an interesting

result as we are mainly interested on leaving the thiol group free for conjugation to different biomolecules.

3.2.2. Reactions of do3aSH with Radiolanthanides and Biological Studies

3.2.2.1. Synthesis of ^{153}Sm/^{166}Ho-do3aSH

^{153}Sm ($t_{1/2}$ 46.8h; β_{max} 0.67MeV, 34%; 0.71MeV, 44%; 0.81MeV, 21%; γ 0.103MeV, 38%) and ^{166}Ho ($t_{1/2}$ 26.8h; β_{max} 1.85MeV, 51%; 1.77MeV, 48%; γ 80.6keV, 7.5%; 1.38MeV, 0.90%) were produced in the ITN Portuguese Research Reactor (RPI), by thermal neutron bombardment of isotopically enriched ^{152}Sm$(NO_3)_3$ or natural Ho$(NO_3)_3$, respectively [209,210]. The specific activities of the radionuclides, after 3h irradiation and at EOB, were 110-150MBq/mg for ^{153}Sm and 220-260MBq/mg for ^{166}Ho. The radionuclidic purity of the ^{153}Sm and ^{166}Ho solutions was assessed by γ-ray spectrometry using a Ge(Li) detector coupled to an Accuspec B Canberra multichannel analyzer [203]. The spectra were processed, following efficiency calibration with a ^{152}Eu source. The ^{153}Sm and ^{166}Ho activities produced after irradiation were measured in a dose calibrator (Aloka Curiemeter IGC-3).

The complexes ^{153}Sm/^{166}Ho-do3aSH were prepared by reacting ^{153}Sm/^{166}Ho$(NO_3)_3$ with the corresponding ligand in water, using a 1:2 metal/ligand molar ratio, at different pH values and temperature. We also studied reactions of ^{153}Sm$(NO_3)_3$ with the ligand do3a**.** These studies were performed to provide a better insight on the role of the thiol pendant arm on the labelling yield and also on the *in vitro* and *in vivo* behaviour of the radioactive complexes.

The ligand do3a was prepared from the do3Et, upon acidic hydrolisis of the ester groups with HCl, and was obtained in 60% yield [205].

The yield of the reactions was followed by ITLC-SG, using an eluent system in which the ^{153}Sm/^{166}Ho$(NO_3)_3$ stay at the origin (R_f = 0) and the ^{153}Sm/^{166}Ho-do3aSH (R_f = 1) or ^{153}Sm-do3a (R_f = 0.8) complexes migrate, figure 3.4.

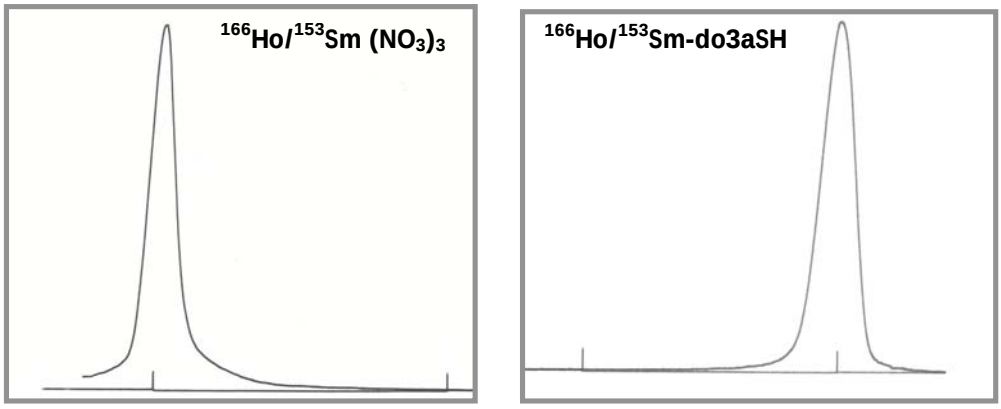

Figure 3.4: Radiochromatogram of $^{153}Sm/^{166}Ho(NO_3)_3$ and $^{153}Sm/^{166}Ho$-do3aSH

The optimized experimental conditions to prepare $^{153}Sm/^{166}Ho$-do3aSH and ^{153}Sm-do3a with high yield and high radiochemical purity are presented in Table 3.3. Just for comparison, we also present in table 3.3 the optimal conditions for preparing $^{153}Sm/^{166}Ho$-dota [204].

Table 3.3: Labelling conditions for do3aSH, do3a and dota with ^{153}Sm and ^{166}Ho

Ligand	^{153}Sm-macrocyclic complexes		^{166}Ho-macrocyclic complexes	
	Labelling conditions *	Labelling Efficiency	Labelling conditions*	Labelling efficiency
do3aSH [a]	5 min r.t., pH 6	> 98%	60 min r.t., pH 6	> 98%
do3a [a]	5 min r.t., pH 6-8	> 98%	-----	
dota [b]	5 min r.t., pH 6-9	> 98%	5 min r.t., pH 6-9	> 98%

* r.t. = room temperature; [a] This work; [b] ref. [204].

As can be seen in table 3.3, $^{153}Sm/^{166}Ho$-do3aSH were obtained in quantitative yield at pH 6. Looking at the species distribution diagram of Sm-do3aSH shown in Figure 3.2 (Ho-do3aSH is not shown, but is similar), at this pH two different protonated species coexist in about 50% each: [Sm(Hdo3aSH)] and [Sm(do3aSH)]. In the TLC chromatogram we only see a well defined peak (Figure 3.4), either because at the radioactive level the two species have different kinetics of formation or because they have similar behaviour in the experimental conditions used for TLC. The formation kinetics of ^{153}Sm-do3aSH and ^{153}Sm-do3a compare with that found for $^{153}Sm/^{166}Ho$-dota, while ^{166}Ho-do3aSH forms more slowly.

The quantitative reaction of do3aSH with $^{153}Sm/^{166}Ho(NO_3)_3$ and the potentiometric and relaxitivity studies which indicate that the thiol group was not involved on the coordination sphere of the metal encouraged the *in vitro* and *in vivo* evaluation of $^{153}Sm/^{166}Ho$-do3aSH complexes.

3.2.2.2. *In vitro* Studies

The *in vitro* stability of the radiolanthanide complexes under physiological conditions was studied at 37 ºC, in order to detect any radiochemical impurities or free radioactive metal. The physiological media studied were saline, 0.1 M phosphate buffer (pH 7.4) and human serum. After incubation, samples were collected at various time points (up to five days) and analysed by ITLC. Typically, 50 μL of each ^{153}Sm- or ^{166}Ho-complexes were added to 100 μL of different solutions namely: saline, 0.1 M phosphate buffer (pH 7.4), 0.1 M tris HCl (tris(hydroxymethyl)aminomethane hydrochloride) buffer (pH 7.4), 0.1 M glycine-HCl (pH 4.0) and human serum. Daily, an aliquot of each mixture was removed and evaluated by ITLC analysis, as described above. The percentage of radiochemical impurities was then calculated. In terms of stability *in vitro*, we have found that ^{153}Sm-do3aSH is stable, at least up to five days, at 37ºC in saline, phosphate buffer (pH 7.4) and human serum. The ^{166}Ho analogue is only stable up to 3 days in saline, 1 day in the presence of PBS and 2 days in human serum. These results indicate that ^{153}Sm-do3aSH is more stable than ^{166}Ho-do3aSH.
As we have shown in Table 3.2, the thermodynamic stability constants and pM values of Sm-dota ($\log K_{ML}$=23; pM=10.75) and Sm-do3aSH ($\log K_{ML}$=22; pM=9.22) are somewhat different. However, this difference seems not to affect the *in vitro* kinetic inertness of Sm-do3aSH comparatively to Sm-dota, at least up to 5 days.

Partition coefficients at physiological pH were determined using the shake-flash method between octanol and PBS (pH=7.4). The logD values found were -2.11 and -1.63 for ^{153}Sm-do3aSH and ^{166}Ho-do3aSH, respectively.

The protein binding of these hydrophilic complexes was determined using a trichloroacetic acid (TCA) precipitation method. The values found for protein binding were 2.1% and 6.7% for samarium and holmium complexes, respectively. These are relatively low values, which predict a relatively fast blood clearance *in vivo*.

Challenge studies in the presence of Cysteine and GSH at pH 7.4

Due to high level of circulating biomolecules containing thiol groups in healthy human plasma, namely cysteine (201μM) and glutathione (GSH, 3.60μM) [206], it is very important to evaluate the kinetic inertness of the radiocomplexes in the presence of an excess of those substrates. The complexes ^{153}Sm/^{166}Ho-do3aSH (1.6 μmol) were incubated with cysteine solutions in PBS (pH 7.4), and aliquots of these mixtures analysed by ITLC chromatography, at different time points. The ^{153}Sm complex was stable up to 24h in 0.5 mM and 2 mM cysteine solutions, while for ^{166}Ho-do3aSH only 50% of intact compound could be identified after 24h of incubation. Due to the relatively low *in vitro* stability of ^{166}Ho-do3aSH, we only proceeded with the evaluation of ^{153}Sm-do3aSH in 1mM GSH solution. We have found that this complex is resistant to transchelation and/or reaction with GSH, up to 24h.

3.2.2.3. *In vivo* Studies

Owing to the high stability of ^{153}Sm-do3aSH, compared with ^{166}Ho-do3aSH, the *in vivo* studies were only performed for the samarium complex. To have an idea of the effect of the thiol pendant arm, the biological behaviour of ^{153}Sm-do3a was also studied. Biodistribution studies of the complexes were performed in female CD-1 mice after 30min. and 2h post intravenous (i.v.) injection through tail. The experimental data obtained are presented in tables 4.4 and 4.5 in the experimental part (chapter 4).

Tissue distribution data for ^{153}Sm-do3aSH, ^{153}Sm-do3a and ^{153}Sm-dota complexes for the most relevant organs as a function of time, after i.v. administration in female CD-1 mice, are summarized in Figure 3.5.

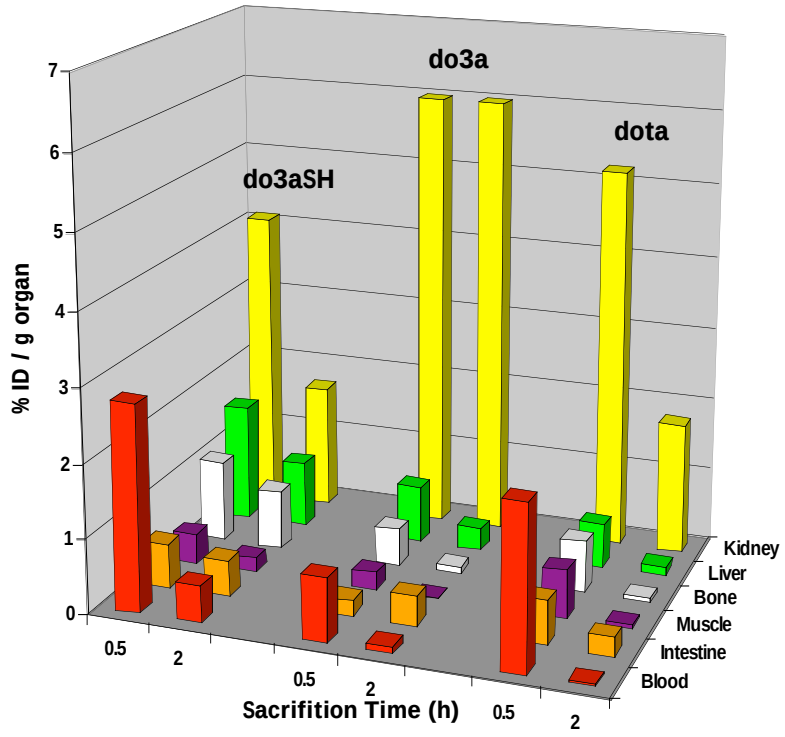

Figure 3.5: Biodistribution of ^{153}Sm-do3aSH, ^{153}Sm-do3a and ^{153}Sm-dota in the main organs (%I.D./g organ)

Total animal body radioactivity excretion over time is shown in Table 3.4.

Table 3.4: Excretion of ^{153}Sm complexes (% ID)

Complex	Time (h)	
	0.5	2
^{153}Sm-do3aSH	49.2 ± 8.9	79.7 ± 3.9
^{153}Sm-do3a	76.8 ± 7.6	90.3 ± 2.2
^{153}Sm-dota	60.2 ± 9.9	97.2 ± 1.0

These data point out a comparable pattern for both complexes with no significant accumulation of radioactivity in any major organs, except for the kidneys. A relatively rapid washout from blood stream and most important organs and a high rate of total excretion was found (> 79% of the radioactivity is excreted at 2h p.i.), a behaviour which correlates well with the high hydrophilic character of the radioactive complexes. In spite of the biodistribution similarities, ^{153}Sm-do3aSH complex presents a slightly slower clearance from blood and most organs than ^{153}Sm-do3a. Moreover, there was a small difference in the percentage of injected dose

taken by the hepatobiliar tract. Actually, the total radioactivity was quite efficiently excreted mainly *via* urinary excretory route for both complexes but there was also some hepatobiliar uptake that is slightly higher for ^{153}Sm-do3aSH (0.9 ± 0.1 %ID/g organ, 2h p.i.) than for ^{153}Sm-do3a (0.3 ± 0.1 %ID/g organ, 2h p.i.).

Chromatographic analysis of urine samples, collected at different sacrifice time, indicated a high *in vivo* stability for both complexes, as no metabolites were detected and/or no free metal was found. This *in vivo* behaviour, rapid washout from main organs, high rate of whole body excretion and high stability is similar to that found for ^{153}Sm-dota in the same animal model [204].

The favourable biodistribution profile of the ^{153}Sm-complex indicates that ^{153}Sm-do3aSH is a promising candidate for further studies towards biological applications. Moreover, its kinetic inertness remains sufficiently high to avoid *in vivo* transmetallation or transchelation. Our results seem to indicate that the conjugation of the complex *via* the thiol sulphur atom to a biomolecule would not compromise the stability and kinetic inertness of the ^{153}Sm-labelled conjugate.

3.3. Cyclen Derivatives with Phosphonate/Phosphinic and Carboxylate Pendant Arms

3.3.1. 1,4,7,10-tetraazacyclododecane-1,7-bis(acetic acid)-4,10-bis(methylphosphonic acid) (trans-do2a2p)

3.3.1.1. Synthesis and Characterization of *trans*-do2a2p

The synthesis of the novel macrocyclic ligand *trans*-do2a2p has been performed by a Mannich reaction, followed by acidic hydrolysis.
As indicated in scheme 3.1, 1,7-bis(acetic acid tert-butyl ester)-1,4,7,10-tetraazacyclododecane [148] was reacted with triethylphosphite and dry paraformaldehyde in benzene. The reaction mixture was vacuum dried and the yellow pale oil obtained was purified by silica-gel column chromatography. The pure fractions were collected and vacuum dried, yielding the compound 1,7-bis(acetic acid tert-butyl ester)-4,10-bis(methanephosphonic acid diethyl ester)-1,4,7,10-

tetraazacyclododecane (do2^{t}Bu2PO(OEt)$_2$, in 42% yield. Acidic hydrolysis of do2^{t}Bu2PO(OEt)$_2$ with HCl 20% (reflux over 24h), cleaved the ester groups from the phosphonate and acetate pendant arms yielding the compound *trans*-do2a2p in 90% yield, after recrystallization from water/ethanol. The white powder obtained was formulated as 1,4,7,10-tetraazacyclododecane-1,7-bis(carboxymethyl)-4,10-bis(methylphosphonic acid) (*trans*-do2a2p) based on multinuclear NMR spectroscopy and X-ray crystallographic analysis.

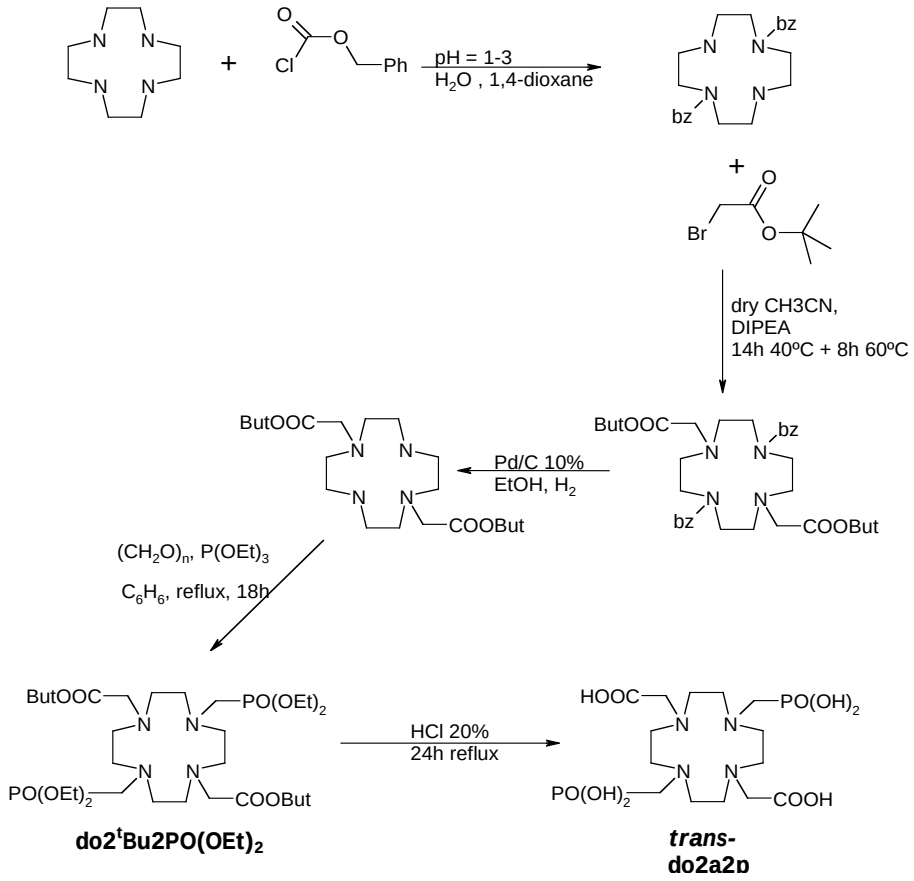

Scheme 3.1: Synthesis of do2^{t}Bu2PO(OEt)$_2$ and *trans*-do2a2p

NMR Characterization

The ^{1}H NMR spectra in D_2O at acidic pD (figure 3.6a), consist of two resonances integrating for eight protons each assigned to the methylenic protons of the macrocycle backbone, and two other resonances, integrating for four protons each, corresponding to the methylenic protons of the methylcarboxylate and methylphosphonate pendant arms. In the ^{13}C NMR spectrum five resonances were observed for the fourteen carbon nuclei, figure 3.6b. The resonance at 176.3 ppm

was assigned to the carbons of the two carboxylate groups, while the resonances at 54.9 and 53.1 ppm are due to the methylenic carbons of the carboxylate and phosphonate pendant arms, respectively. The carbons of the macrocycle backbone appear as two resonances at 53.9 and 52.4 ppm. In acidic conditions the ^{31}P NMR spectrum presents only one very broad resonance for the two phosphours nuclei, but this resonance sharpened significantly at basic pD, as evidenced in figure 3.7. At pD≈13 the spectrum shows one resonance at 20.5 ppm. The pattern of the ^{1}H, ^{13}C and ^{31}P NMR spectra agrees with the C_2 symmetry expected for *trans*-do2a2p.

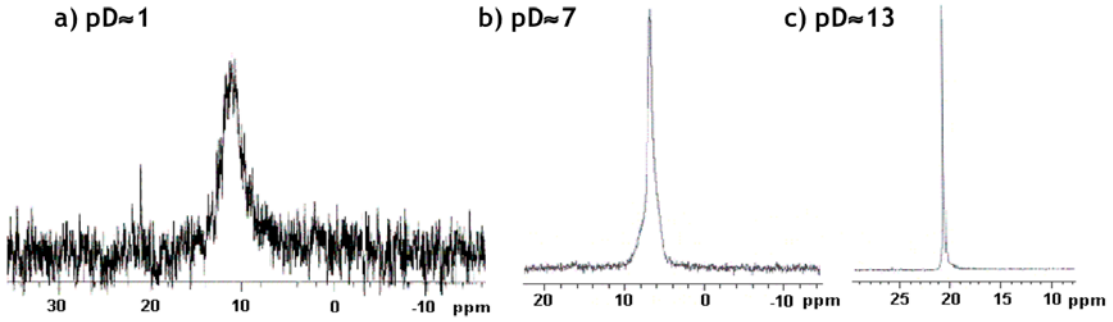

Figure 3.6: Multinuclear spectra of trans-do2a2p: (**a**) ^{1}H-NMR spectrum at pD ≈ 1; (**b**) ^{13}C-NMR spectrum at pD ≈ 1

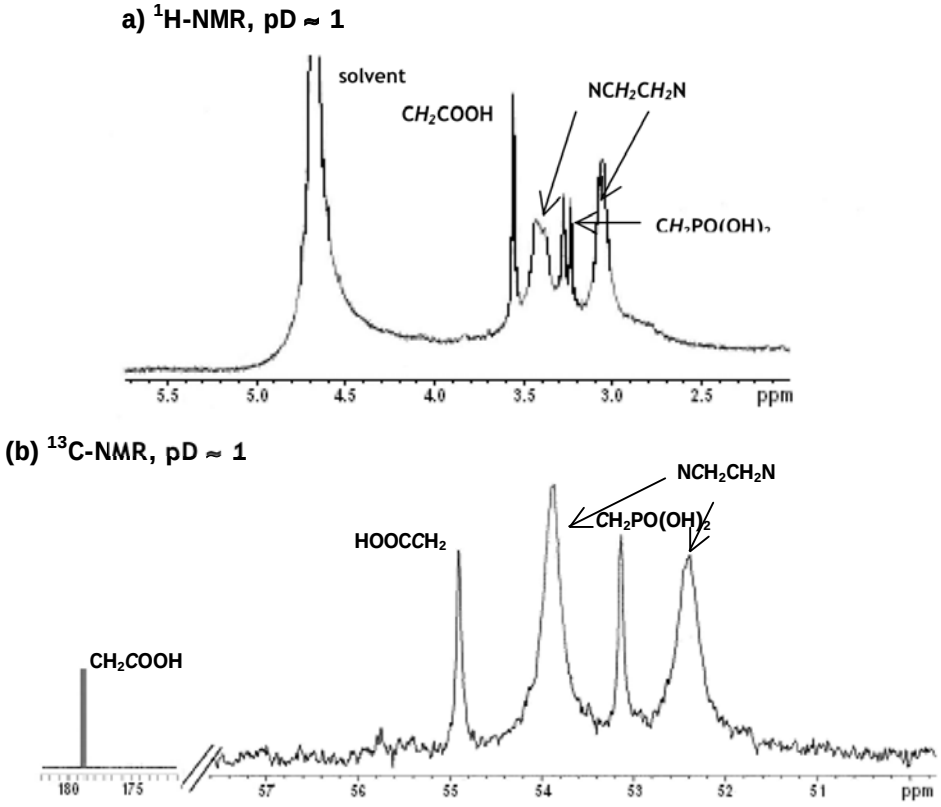

Figure 3.7: ^{31}P-NMR spectra of *trans*-do2a2p: (**a**) pD ≈ 1; (**b**) pD ≈ 7; (**c**) pD ≈ 13

In order to perform solution studies with *trans*-do2a2p, it was desirable to have the ligand in the zwiterionic form, which means to remove any traces of HCl (arising from the last step of the synthesis, see scheme 3.1) or other solvents/salts. To achieve such goal we have dissolved the product in water and purified on a Dowex 50 column (H^+ form) using water and 10% aqueous pyridine as eluents. The fractions containing the product were vacuum dried and the residue purified on an Amberlite CG50 column (H^+ form) using water as eluent. The fractions containing the pure product (analysed by ^1H, ^{13}C and ^{31}P-NMR spectroscopy) were combined and the solvent evaporated under vacuum.

X-ray crystallographic analysis

Single crystals suitable for X-ray crystallographic analysis were obtained by slow concentration of solutions of the purified *trans*-do2a2p in water. Figure 3.8 shows an ORTEP diagram for *trans*-H_6do2a2p and the most relevant bond distances and angles are presented in table 3.5.

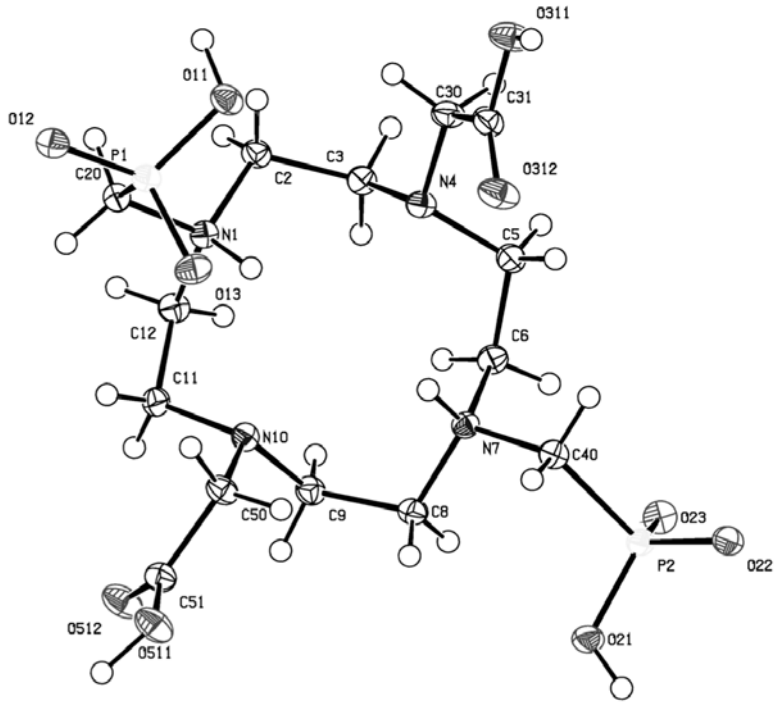

Figure 3.8: Crystal structure of *trans*-H_6do2a2p

From the X-ray analysis it was clear that the two nitrogen atoms N1 and N7, in *trans* position and near the phosphonate groups, were protonated. This protonation comes

from the increase of the electronic density in these amines, due to the deprotonation of one oxygen atom of the phosphonic acid group. The two oxygen atoms of the two carboxylic groups are also protonated and the N4 and N10 nitrogen atoms are non-protonated. This mode of protonation is preserved in aqueous solution (see below). The protonation of N1 and N7 results in NH-C bond lengths which are longer than those involving the non-protonated N4 and N10 nitrogen atoms (NH-C_{ave}= 1.532 Å and N-C_{ave}= 1.471 Å). The existence of short C=O (d_{ave}= 1.197 Å) and long C-O (d_{ave}= 1.314 Å) bond distances also indicate the protonation of the carboxylate groups. These differences compare well with the values previously reported for other protonated tetraazamacrocycles [207].

Table 3.5: Selected bond length (Å) and angles (°) for *trans*-H_6do2a2p

Bond Lenght (Å)			
P1–O11	1.587	N1(H11)-C2	1.512
P1–O12	1.564	N1(H11)-C12	1.488
P1–O13	1.518	N1(H11)-C20	1.566
P1–C20	1.776	N7(H71)-C6	1.499
P2–O21	1.566	N7(H71)-C8	1.499
P2–O22	1.515	N7(H71)-C40	1.530
P2–O23	1.470	N4-C3	1.464
P2-C40	1.887	N4-C5	1.541
C31-O311	1.308	N4-C30	1.460
C31-O312	1.215	N10-C9	1.510
C51-O511	1.320	N10-C11	1.502
C51-O512	1.179	N10-C50	1.450
Angle (°)			
O13 – P1 – O12	120.58(7)	O23 – P2 – O22	113.38(8)
O13 – P1 –O11	106.12(8)	O23 – P2 – O21	112.89(8)
O12 – P1 –O11	112.34(7)	O23 – P1 – O22	110.02(7)
C20 – P1 –O11	106.33(8)	C40 – P2 –O21	103.44(8)
C20 – P1 – O12	105.32(8)	C40 – P2 – O22	107.41(8)
C20 – P1 – O13	105.11(8)	C40 - P2 - O23	109.07(8)

The structural parameters of the phosphonate groups in *trans*-H_6do2a2p are comparable to those of the deprotonated phosphonate groups in do3ap and dotp, indicating the protonation of only one oxygen atom *per* phosphonate group [208,209]. The four nitrogen atoms of the *trans*-H_6do2a2p backbone are coplanar. The

arrangement of the pendant arms is singular relatively to those observed in dota, do3ap and dotp. In *trans*-H_6do2a2p, the carboxylate groups and one of the phosphonate groups are positioned above the plane defined by the nitrogen atoms, while the other phosphonate group (P2) is oriented away from the ring.

In dota and in do3ap (not shown), all the four pendant arms are positioned above the plane defined by the ring nitrogen atoms, while in dotp two of the phosphonate groups are positioned above this plane and the other two are pointed away from the N4-ring [209,210]. Figure 3.9 shows the orientation of the pendant arms in dota, *trans*-do2a2p and dotp.

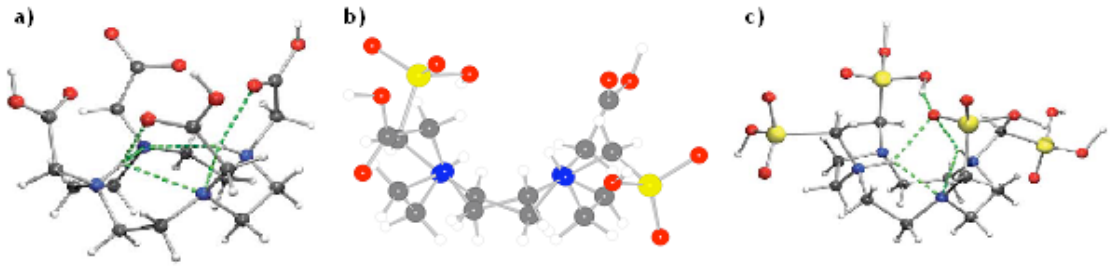

Figure 3.9: Crystal structures of (a) H_6dota^{2+} (ref. [35]); (b) *trans*-H_6do2a2p and (c) H_8dotp (ref. [35]) Colours: ● Nitrogen, ● Oxygen, ● Carbon, ● Phosphorus, ● Hydrogen

Moreover, the relative position of the pendant arms towards the macrocycle cavity in *trans*-H_6do2a2p can also be seen based on the calculated torsion angles: P1-C20-N1-N7, 36.1°; P2-C40-N7-N1, -173.2°; C31-C30-N4-N10, 63.5°; C51-C50-N10-N4, -176.3°.

3.3.1.2. Solution Studies of trans-do2a2p with Lanthanides and with Other Metals with Biological Interest

Protonation constants of *trans*-do2a2p and stability constants with some *f*- and *d*-elements were determined. The protonation sequence of *trans*-do2a2p was also evaluated, based on potentiometric and NMR titrations.

3.3.1.2.1. Acid-base Behaviour

The protonation constants of *trans*-do2a2p, presented in table 3.6, were determined by potentiometry at 25.0 °C with 0.10 M NMe_4Cl ionic strength, and by ^{31}P-NMR

spectroscopy, without ionic strength control. We have determined six protonation constants. From these, five were determined by potentiometry and one by ^{31}P-NMR studies in the pH range 11-13.3 (about 15 points). These data were fitted together with the program OPIUM [169]. The other NMR data were fitted with the program HypNMR [170].

Table 3.6: Protonation constants (log units) of *trans*-do2a2p and other related macrocyclic ligands

Species	*trans*-do2a2p [a]		*trans*-do2a2p [b]		*trans*-do2a2p [c]	dota [d]	do3ap [e]	dotp [f]
l h	log β_{LHi}	log K_{LH_i}	log β_{LHi}	log K_{LH_i}	log K_{LH_i}	log K_{LH_i}	log K_{LH_i}	log K_{LH_i}
1 1	13.02 (0.05)*	13.02 (0.05)*	13.17 (0.07)	13.17	12.60 (0.01)	11.9 (0.2)	13.83	14.65 (0.02)
1 2	11.82 (0.01)	11.82 (0.01)	25.43 (0.06)	12.25	11.43 (0.01)	9.72 (0.03)	10.35	12.40 (0.02)
1 3	18.16 (0.01)	6.34 (0.01)	31.90 (0.07)	6.47	5.95 (0.01)	4.60 (0.05)	6.54	9.28
1 4	24.49 (0.01)	6.33 (0.01)	38.34 (0.06)	6.44	6.15 (0.01)	4.13 (0.03)	4.34	8.09
1 5	27.62 (0.01)	3.13 (0.01)	41.48 (0.08)	3.13	2.88 (0.01)	2.36 (0.05)	3.09	6.12
1 6	30.26 (0.01)	2.64 (0.01)	44.5 (0.1)	3.02	2.77 (0.01)	---	1.63	5.22
1 7	---	---	---	---	---	---	1.07	---

* Determined by ^{31}P-NMR. [a] T = 25.0 ºC, I = 0.10 mol dm^{-3} in NMe_4OH, this work; [b] determined by ^{31}P-NMR, T = 25.0ºC, no ionic strength control, this work; [c] I = 1.0 mol dm^{-3} in KCl, ref [211]; [d] I = 0.10 mol dm^{-3} in Me_4NNO_3/Cl, ref. [33]; [e] T = 25.0 ºC; I = 0.10 mol dm^{-3} in NMe_4Cl, ref.[209]; [f] T = 25.0 ºC; I = 0.10 mol dm^{-3} in NMe_4NO_3, ref.[204].

As expected, *trans*-do2a2p is much more basic than dota and do3ap and less then dotp. The high value found for the first protonation constant of all the cyclen-derivatives bearing phosphonate pendant arms is usually ascribed either to the spreading the of high electron density of the fully deprotonated phosphonate group(s) to the nearest nitrogen atom(s) and/or to the establishment of a five-membered ring, due to the formation of strong intramolecular hydrogen bonds between protonated nitrogen atoms and the deprotonated phosphonate groups. The first protonation constant found for *trans*-do2a2p is slightly lower than the value found for do3ap. This difference is most probably due to the formation of weaker

intramolecular hydrogen bonds in *trans*-do2a2p than in do3ap, due to the high flexibility of the phosphonate groups in *trans*-do2a2p [154a, 212].

To get a better insight on the protonation sequence of *trans*-do2a2p, we investigated the dependence of δ_P and δ_H of N-C*H*$_2$-*P*O(OH)$_2$ with the pH in the range 13.8<pH <1.9. Figure 3.10 shows the variation of δ_H and δ_P with the pH.

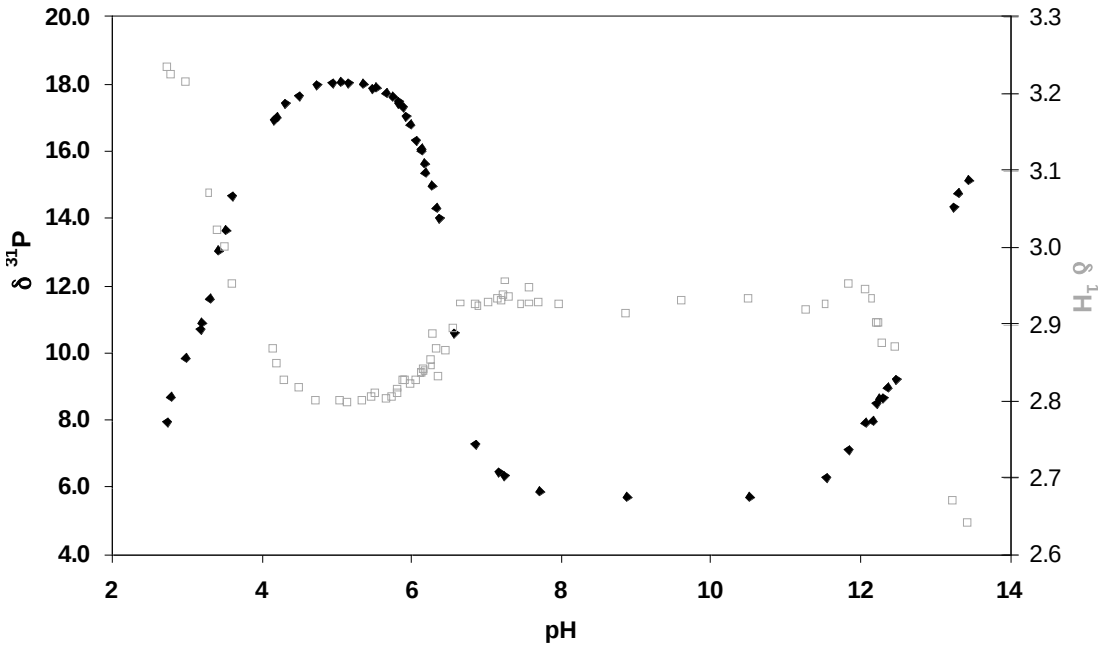

Figure 3.10: NMR studies of *trans*-do2a2p: ^{31}P (♦) and ^{1}H NMR (□) titration curves for N-C*H*$_2$-*P*O$_3$H$_2$

Based on the variation of the chemical shift of the ^{31}P and of the ^{1}H of the pendant arm N-C*H*$_2$-*P*O(OH)$_2$ with the pH, we concluded that in solution six protonations take place in the pH range studied. The first two protonation constants occur in two *trans* nitrogen atoms N1 and N7. The third and the fourth, which occur in the pH range of 7.0-5.5, must take place in the phosphonate groups with a redistribution of the NH protons from N1 and N7 to N4 and N10. Finally the last two constants, in the pH range 4.0-2.0, must occur in the carboxylate groups with a new redistribution of the NH protons to the amines bearing the phosphonate groups. Scheme 3.2 shows the proposed protonation sequence for *trans*-do2a2p.

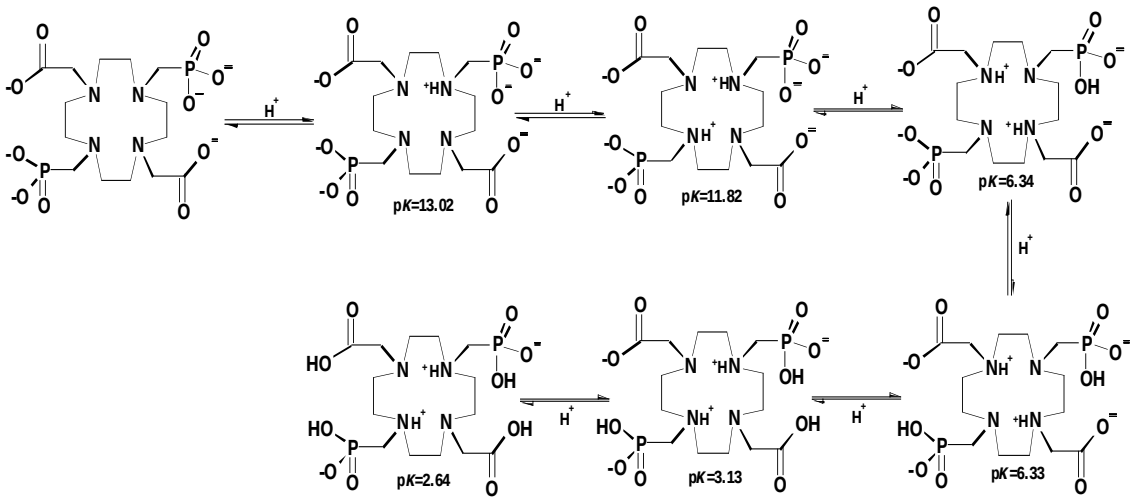

Scheme 3.2: Proposed protonation sequence for *trans*-do2a2p

The same number and sequence of protonation was described by Kálmán *et al.* In fact, while this work was in progress and after the publication of the synthesis of *trans*-do2a2p by our group, Kálmán *et al*., independently, reported again the synthesis of this ligand as well as some solution and complexation studies [211]. However, there are two important differences in the values presented in this work and the values reported by Kálmán *et al*. First, all the six protonations determined in this work are somewhat higher than those determined by Kálmán *et al*, especially the first three protonation constants (Table 3.6). These results are certainly related with the different experimental conditions used by us and by Kálmán *et al*., namely the nature of the electrolyte for the ionic strength control. Actually, we have used tetramethyl ammonium chloride (NMe_4Cl) as background salt in order to avoid the possible formation of stable complexes of *trans*-do2a2p with alkali metal ions. Kálmán *et al.* controlled the ionic strength with KCl and, certainly, the formation of stable complexes with K^+ ions may have occurred [171,172,213]. Kálmán et al. also found a $\log K_{H4}$ (6.15) higher than $\log K_{H3}$ (5.95), and justified this unusual trend with the peculiar structure of the tri-protonated $H_3do2a2p^{3-}$ which leads to the formation of strong H-bonds between the NH^+ and PO_3^{2-} groups. In our case, these constants follow the normal decreasing order, although the differences between the $\log K_{H4}$ and $\log K_{H3}$ are relatively small. For cyclam and cyclen-derivatives there are also sometimes differences on protonation constants reported by different groups. Normally, such differences are considered to be due to different experimental conditions, as they may lead to different sterical arrangements in the intermediate structures [213].

3.3.1.2.2. Stability Constants of *trans*-do2a2p with Lanthanides and with Other Elements with Biological Interest

Stability constants of *trans*-do2a2p with Sm^{3+}, Ho^{3+}, Y^{3+}, Cu^{2+}, Zn^{2+}, Cd^{2+} and Ca^{2+} were determined by potentiometry.

The stability constants determined with Sm^{3+}, Ho^{3+} and Y^{3+} are presented in table 3.7, together with the ones reported for related ligands.

Table 3.7: Stability constants (log units) of Sm^{3+}, Ho^{3+} and Y^{3+} with *trans*-do2a2p and other related ligands

Metal	Species	*trans*-do2a2p [a]		*trans*-do2a2p [b]	dota	dotp [e]
	m h l	log β_{MH_iL}	Log K_{MH_iL}	log K_{MH_iL}	log K_{MH_iL}	log K_{MH_iL}
Sm^{3+}	1 0 1	26.9 (0.1)	26.9	---	23.0 [c]	28.1
	1 1 1	33.02 (0.09)	6.10	---	---	7.6
	1 2 1	37.96 (0.03)	4.94	---	---	6.3
	1 3 1	---	---	---	---	5.4
	1 4 1	43.33 (0.04)	5.36	---	---	---
	2 0 1	32.36 (0.09)	5.44			
Ho^{3+}	1 0 1	27.5 (0.1)	27.5	---	24.8 [c]	29.2
	1 1 1	33.3 (0.1)	5.87	---	---	8.3
	1 2 1	38.23 (0.06)	4.89	---	---	6.9
	1 4 1	43.13 (0.07)	4.90	---	---	4.5
	2 0 1	32.9 (0.2)	5.53			
	2 1 1	36.9 (0.2)	3.94			
Y^{3+}	1 0 1	26.54 (0.08)	26.54	26.6 (0.09)	24.4 (0.1) [d]	---
	1 1 1	32.19 (0.09)	5.65	5.19 (0.09)	---	---
	1 2 1	37.01 (0.04)	4.82	4.27 (0.09)	---	---
	1 4 1	42.70 (0.04)	5.69	---	---	---
	2 0 1	32.02 (0.09)	5.48	3.10 (0.05)	---	---
	2 1 1	35.9 (0.1)	3.92	---	---	---

* Values in parentheses are standard deviations. [a] This work, T = 25.0 °C, I = 0.10 mol dm^{-3} NMe_4OH; [b] I = 1.0 mol dm^{-3} KCl, ref. [211]; [c] I = 0.10 mol dm^{-3} NMe_4NO_3, ref. [204]; [d] ref.[214]; [e] I = 0.10 mol dm^{-3} NMe_4NO_3, ref. [215].

The value of the stability constant of the Sm^{3+} complex is about one log$K$ unit lower than the one found for Ho^{3+}. The increase of the stability constant with the decrease

of the Ln^{3+} ionic radius agrees with what has been observed for other macrocyclic ligands, namely dota, do3ap and dotp [35, 87]. The value found for Y^{3+} agrees with the reported value by Kálmán et al. for logK_{ML}, but the values reported for the other step constants are lower than the ones determined in this work. As already observed for the protonation constants, the values found are lower than the ones reported for dotp and higher than the ones reported for dota.

In figure 3.11 are presented the species distribution diagrams for the complexes of *trans*-do2a2p with Sm^{3+} and Ho^{3+}.

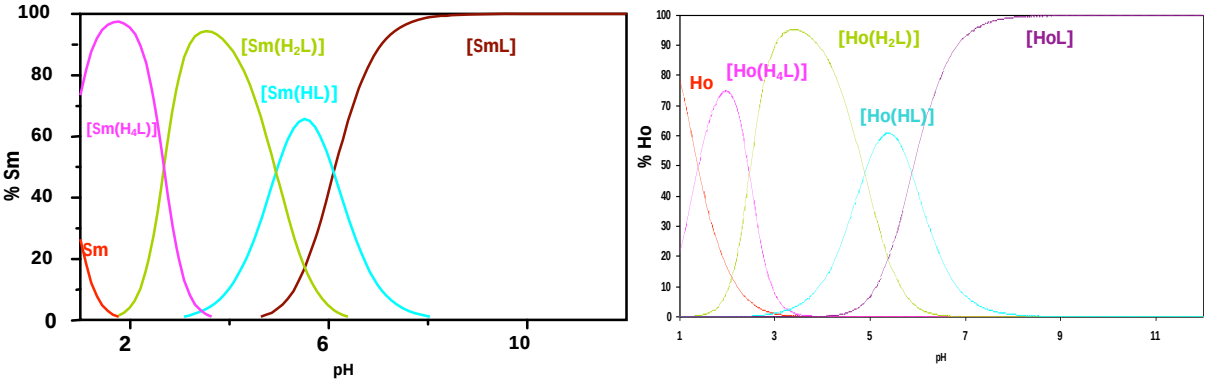

Figure 3.11: Species distribution diagram of Sm-do2a2p and Ho-do2a2p

The species distribution diagrams for the complexes Sm-do2a2p and Ho-do2a2p are quite similar. As can be seen in figure 3.11, the type of species formed is similar. At physiological pH (7.4), the main species in solution are [ML] and [MLH], being [ML] the predominating one (95% for Sm^{3+} and 97% in the case of Ho^{3+}).

The elements copper, zinc and calcium are present in the organism, and although in low concentration they can compete with other injected complexes. So, it is important to determine the stability constant of *trans*-do2a2p with these elements and to compare with the stability constants found for lanthanides, as these analysis will predict the stability *in vivo* of Sm/Ho/Y-do2a2p towards transmetalation. Another potential application of macrocyclic ligands is their use for quelataion therapy, removal of toxic elements from the organism. Therefore, the stability of cadmium was also evaluated.

The stability constants determined with Cu^{2+}, Zn^{2+}, Cd^{2+} and Ca^{2+} are presented in table 3.8, together with the ones reported for related ligands.

Table 3.8: Stability constants (log units) for complexes of *trans*-do2a2p with *d*-metals and other related ligands

Metal	Species	*trans*-do2a2p [a]		*trans*-do2a2p [b]	dota [c]	dotp
	m h l	log β_{MH_iL}	log K_{MH_iL}	log K_{MH_iL}	log K_{MH_iL}	log K_{MH_iL}
Cu^{2+}	**1 0 1**	25.17 (0.03)	25.17	24.9 (0.04)	22.3 (0.1)	25.4 [d]
	1 1 1	32.40 (0.04)	7.23	6.79 (0.05)	4.30 (0.09)	7.41
	1 2 1	39.06 (0.02)	6.67	6.30 (0.03)	3.55 (0.09)	6.42
	1 3 1	41.57 (0.02)	2.51	---	---	6.16
	2 0 1	31.36 (0.03)	6.19	3.05 (0.07)	---	---
	2 1 1	36.98 (0.04)	5.62	---	---	---
	2 -1 1	23.60 (0.04)	7.77	---	---	---
Zn^{2+}	**1 0 1**	23.26 (0.02)	23.26	22.5 (0.03)	20.8 (0.2)	24.8 [e]
	1 1 1	30.71 (0.03)	7.45	6.92 (0.03)	4.24 (0.08)	---
	1 2 1	37.387 (0.009)	6.68	6.34 (0.01)	3.51 (0.04)	---
	1 3 1	39.71 (0.02)	2.33	---	---	---
	2 0 1	27.73 (0.02)	4.48	3.47 (0.08)	---	---
	2 -1 1	19.34 (0.04)	8.84	---	---	---
	2 -2 1	9.67 (0.06)	9.68	---	---	---
Cd^{2+}	**1 0 1**	22.78 (0.03)	22.78	---	21.3 (0.1)	---
	1 1 1	30.54 (0.03)	7.76	---	4.39 (0.04)	---
	1 2 1	36.91 (0.02)	6.37	---	3.03 (0.05)	---
	1 3 1	39.93 (0.01)	3.02	---	---	---
	1 4 1	42.45 (0.02)	2.52	---	---	---
Ca^{2+}	**1 0 1**	14.74 (0.01)	14.74	15.1 (0.07)	17.2 (0.1)	10.3 [f]
	1 1 1	23.14 (0.02)	8.40	7.33 (0.01)	3.7 (0.1)	---
	1 2 1	30.466 (0.006)	7.32	6.40 (0.04)	---	---
	1 3 1	34.95 (0.02)	4.48	---	---	---
	2 0 1	19.89 (0.01)	5.15	3.05 (0.07)	---	---
	2 1 1	26.86 (0.02)	6.98	---	---	---

* Values in parentheses are standard deviations. [a] This work, T = 25.0 °C, I = 0.10 mol dm^{-3} NMe_4OH; [b] I = 1.0 mol dm^{-3} KCl, ref. [211]; [c] I = 0.1 mol dm^{-3} NMe_4NO_3, ref. [33]; [d] I = 0.10 mol dm^{-3} NMe_4NO_3, ref. [215]; [e] ref. [216]; [f] ref. [217].

The values of the first and second protonation constants (log K_{MHL} and log K_{MH_2L}) of the complexes of *trans*-do2a2p with Ca^{2+}, Cu^{2+}, Cd^{2+} and Zn^{2+} are higher than the values of the protonation constants related with the phosphonate groups (log K_{LH_3}, log K_{LH_4}) in the free ligand. This is in accordance with what has been observed by Kálmán *et al* and suggests that also in the complex formed with Cd^{2+} the protonations

occurs first in the carboxylate groups. On the other hand the same constants (log K_{MLH}, log K_{LMH_2}) for the lanthanide complexes are grater than log K_{LH_3}, log K_{LH_4} in the free ligand, which indicates the protonation of the coordinated phosphonate groups in these complexes.

The distribution species diagram for the complexes of *trans*-do2a2p with Ca^{2+} and Cu^{2+} are presented in figure 3.12.

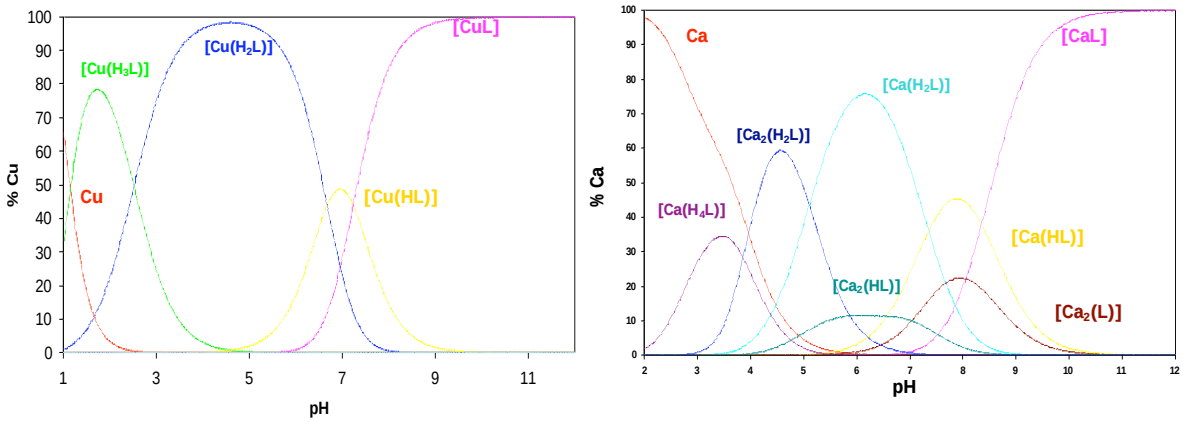

Figure 3.12: Species distribution diagram of Cu-do2a2p and Ca-do2a2p

From tables 3.7 and 3.8 it is clear that *trans*-do2a2p form very stable complexes with all the metal ions studied. As expected, the stability constants of the complexes formed with *trans*-do2a2p are larger than those found for dota complexes and smaller than those of dotp complexes, except in the case of Ca^{2+}. This observation is in agreement with the previous order of basicity found for these three ligands, (see above). For the same metal ions, our values are slightly higher than the ones reported before by Kálmán *et al* [211]. This fact is certainly related with the different electrolyte used for the ionic strength control and probably reflects the effect of K-do2a2p formation.

The pM values for *trans*-do2a2p are presented in table 3.9, these values were calculated based on the protonation and stability constants reported in tables 3.6-3.8, at physiological pH (7.4) and $C_L=2C_M=10^{-3}$M.

Table 3.9: pM values for *trans*-do2a2p and related ligands (pH 7.4)

Metal	*trans*-do2a2p
Cu^{2+}	15.36
Zn^{2+}	13.56
Cd^{2+}	13.25
Ca^{2+}	5.97
Sm^{3+}	16.87
Ho^{3+}	17.40
Y^{3+}	16.47

As expected, the pM values reveal that *trans*-do2a2p has a higher affinity for *f*- than for *d*-elements. So, no transmetalation of Ln-do2ap with the endogenous metal ions may occur.

3.3.1.3. Structural Studies of Sm-do2a2p

3.3.1.3.1. Solid State Structural Analysis

Reactions of *trans*-do2a2p with $SmCl_3$ in water (pH 8) were performed. The reaction mixtures were filtered trough a SEP-PAK C18 cartridge. The pH of the filtrate solution was then lowered to 4-5 (with HCl) and the resulting solution was slightly concentrated under vacuum. Slow diffusion of *iso*-propanol/ethanol into concentrated solutions of Sm-do2a2p in water, over 3-4 months, led to the formation of crystals suitable for X-ray diffraction analysis. During X-ray diffraction analysis we have found that two different crystals were formed. The analysis of these crystals showed that one corresponds to $H[Sm(H_2do2a2p)(H_2O)].8.5H_2O.2.5HCl$ and the other to $H[Sm(H_2do2a2p)].5H_2O.3HCl$. Moreover, the structural analysis also showed that for $H[Sm(H_2do2a2p)(H_2O)].8.5H_2O.2.5HCl$ two crystallographic independent molecules were found *per* asymmetric unit.

In the anion $[Sm(H_2do2a2p)]^-$ the metal is eight coordinated by the four nitrogen atoms of the macrocycle backbone and by four oxygen atoms: two from the carboxylic groups and another two from the phosphonates. The coordination geometry around the metal is better ascribed as TSA. For the anion $[Sm(H_2do2a2p)(H_2O)]^-$ the metal is nine coordinated by the four nitrogen atoms of the macrocycle backbone, four oxygen atoms from the pendant arms and by one water molecule in the capping position. The coordination geometry around samarium is better ascribed as CTSA. Figure 3.13 shows the ORTEP diagrams for the anions $[Sm(H_2do2a2p)]^-$ and $[Sm(H_2do2a2p)(H_2O)]^-$.

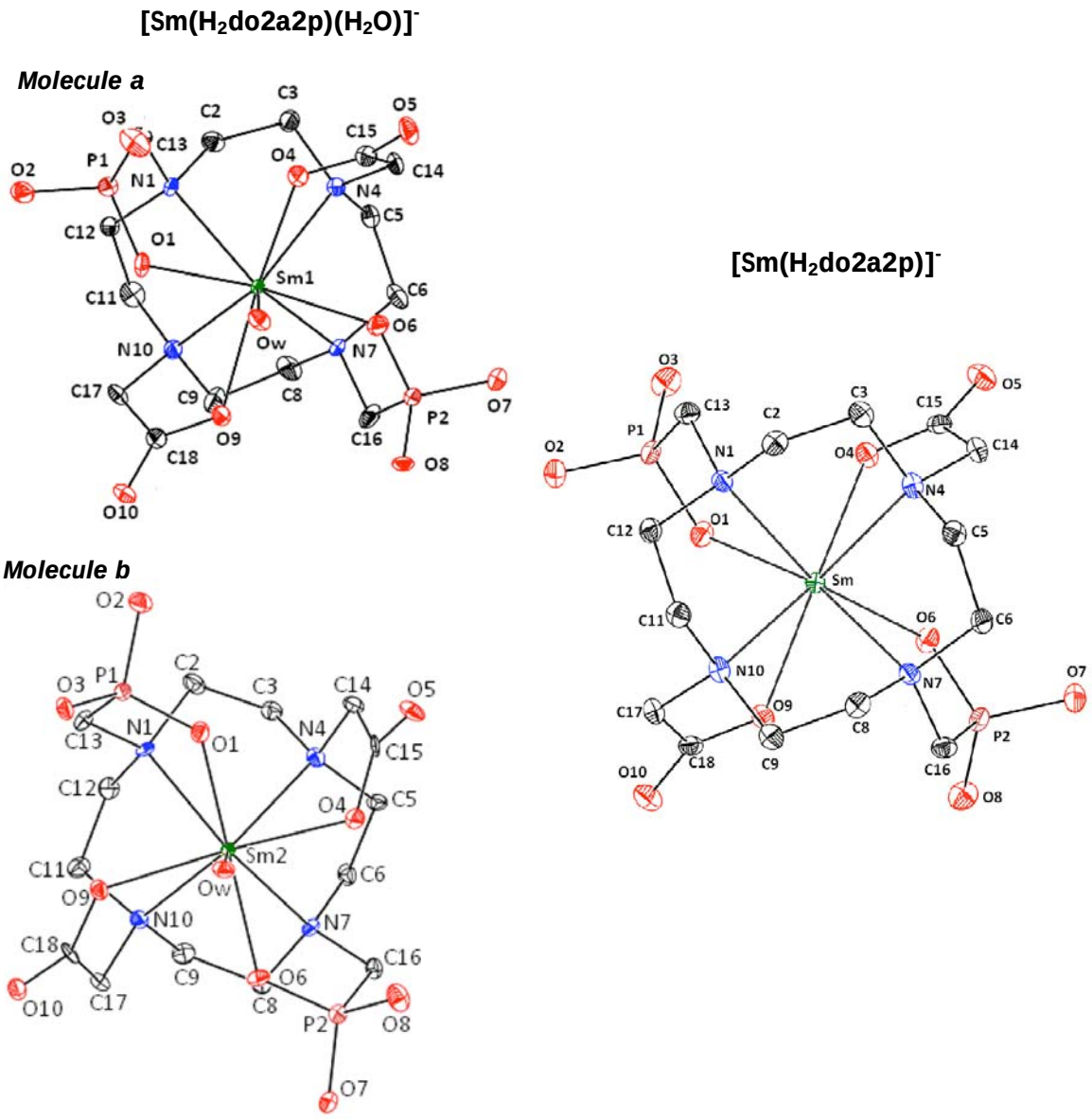

Figure 3.13: ORTEP diagrams of the anions: $[Sm(H_2do2a2p)(H_2O)]^-$ (molecules ***a*** and ***b***) and $[Sm(H_2do2a2p)]^-$; Colours: ● Samarium, ● Nitrogen, ● Oxygen, ● Carbon, ● Phosphorus

In table 3.10 are listed selected bond lengths and angles for the complexes.

Table 3.10: Selected bond length and angles for the anions $[Sm(H_2do2a2p)(H_2O)]^-$ (molecules ***a*** and ***b***)and $[Sm(H_2do2a2p)]^-$

	$[Sm(H_2do2a2p)(H_2O)]^-$		$[Sm(H_2do2a2p)]^-$
	a	***b***	
bond length (Å)			
Sm-Ow	2.607(15)	2.578(15)	---
Sm-O1	2.341(15)	2.342(14)	2.299(4)
Sm-O4	2.369(15)	2.389(14)	2.395(4)
Sm-O6	2.342(14)	2.351(14)	2.299(4)
Sm-O9	2.450(15)	2.426(13)	2.395(4)
Sm-N1	2.761(18)	2.714(8)	2.631(5)
Sm-N4	2.697(19)	2.690(8)	2.633(5)
Sm-N7	2.707(17)	2.707(9)	2.631(5)
Sm-N10	2.709(18)	2.690(8)	2.633(5)
P1-O1	1.526(15)	1.510(15)	1.531(4)
P1-O2	1.525(15)	1.566(16)	1.536(4)
P2-O6	1.518(16)	1.531(15)	1.531(4)
P2-O7	1.557(16)	1.541(16)	1.536(4)
Angle (º)			
O1-Sm-O4	86.3(5)	80.8(5)	81.10(14)
O1-Sm-O6	135.2(5)	137.3(5)	116.2(2)
O1-Sm-O9	80.2(5)	85.9(5)	75.56(14)
O4-Sm-O6	81.7(5)	85.3(5)	75.56(14)
O4-Sm-O9	143.7(5)	143.8(5)	135.0(2)
O6-Sm-O9	84.6(5)	82.0(5)	81.10(14)
O1-Sm-N1	66.4(5)	66.6(5)	71.32(15)
O4-Sm-N1	82.7(5)	121.9(5)	122.19(14)
O6-Sm-N1	151.9(6)	149.7(5)	162.21(15)
O9-Sm-N1	121.0(5)	82.0(5)	85.68(14)
O1-Sm-N4	125.5(5)	82.3(5)	124.52(15)
O4-Sm-N4	62.9(5)	62.9(5)	153.96(14)
O6-Sm-N4	86.1(6)	125.8(5)	94.24(15)
O9-Sm-N4	149.2(5)	147.9(5)	64.23(14)
O1-Sm-N7	149.8(5)	148.3(5)	162.21(15)
O4-Sm-N7	120.5(5)	81.9(5)	85.68(14)
O6-Sm-N7	67.7(5)	66.7(5)	71.32(15)
O9-Sm-N7	84.0(5)	122.6(5)	122.19(14)
O1-Sm-N10	82.7(5)	125.9(5)	94.24(15)
O4-Sm-N10	148.5(5)	148.5(5)	64.23(14)
O6-Sm-N10	125.9(5)	83.8(5)	124.52(15)
O9-Sm-N10	62.7(5)	63.0(5)	153.96(14)
N1-Sm-N4	66.0(6)	66.0(5)	69.17(15)
N1-Sm-N7	101.2(5)	101.4(5)	106.6(2)
N1-Sm-N10	65.9(5)	66.0(5)	68.31(15)
N4-Sm-N7	65.3(5)	66.2(5)	68.31(15)
N4-Sm-N10	100.6(6)	100.8(5)	105.4(2)
N7-Sm-N10	62.7(5)	66.6(5)	69.17(15)
P1-O1-Sm	124.1(9)	123.2(8)	126.8(2)
P2-O6-Sm	125.7(9)	122.1(8)	126.8(2)
C15-O4-Sm	119.7(12)	116.1(13)	121.6(4)
C18-O9-Sm	119.5(13)	119.9(13)	121.6(4)

As can be seen in Figure 3.13, in molecule ***a*** the acetate pendant arms and phosphonates are twisted in the *anti-sense* way, presenting the Δ configuration (orientated counter-clockwise), while in the molecule ***b*** those pendant arms adopt

the Λ orientation (orientated clockwise). The average of the torsional angles Sm-N-C-C(O)/Sm-N-C-P(O) and N-C-C-O/N-C-P-O are 42.30/46.21° and -12.77/-18.11° in molecule ***a***, while they are -41.99/-44.85 and 14.59/19.88° for the molecule ***b***. The quadrangular conformations of the tetraazamacrocycles are enantiomeric for the two independent molecules: the average torsional angles N-C-C-N, C-C-N-C and C-N-C-C- are, respectively, -56.3, -80.6 and 161.7 ° in molecule ***a*** and 58.0, and 78.9 -161.5° in the molecule ***b***. Corresponding values for the above torsional angles in the tetraazacyclododecane macrocycle are: -63, -75 and 166° respectively [218e]. In solution, the interconversion between these two conformational rearrangements of the tetraazacyclododecane ring and the interconversion of the pendant arms, involving a consecutive binding and unbinding process for each acetate and phosphonate pendant arm, are fast on the NMR time-scale, yielding to an average structure.

The Ln-N bond distances are longer then those of Ln-O. The nitrogen and oxygen atoms form N_4 and O_4 bases which are planar and parallel within an experimental error. The Ln(III) cation lies between these two bases, being the lanthanide closer to the O4 plane, as observed in other Ln(III)-dota like complexes [218a-c].

Dota-like complexes of lanthanides usually display square-antiprismatic (SA) or twisted-square-antiprimatic (TSA) coordination geometries (represented in figure 1.21). These geometries are ruled by the torsion of the macrocyclic chelate rings and by the position of the pedant arms. Moreover, an ideal SA structure presents a twisted angle of 45° and an ideal TSA presents one of 22.5°. When there is one water molecule in the capping position, the geometries are denominated as CSA or CTSA [219].

The mean twist angle ω of the N4 and O4 planes is -28.40° in molecule ***a*** and 27.02° in molecule ***b*** (Table 3.12). Thus, the arrangement should be termed a TSA, being the rearrangement Λ(δδδδ) and Δ(λλλλ) in molecules ***a*** and ***b***, respectively.

As it was just pointed out, a water molecule capping the O4 base completes the coordination sphere of the Sm(III). The bond length Sm-O_W is significantly different in the two molecules: Sm(a)-O_W 2.607Å and Sm(b)-O_W 2.578Å. However, these values are in the range of those found for similar complexes, such as [Ln(dota)(H_2O)] and [Ln(Hdo3ap)(H_2O] [203,218b,218c]. In the two molecules, the opening angles are

similar, but in both cases the O-Sm-O bond angle for the phosphonates is slightly smaller than the corresponding carboxylate (Table 3.10). Based on the P-O bond lengths, in molecules ***a*** and ***b*** most probably only one of the two coordinated phosphonate group is protonated (O7 in molecule ***a***, O2 in molecule ***b***).

Table 3.11: Major differences between the anions $[Sm(H_2do2a2p)(H_2O)]^-$ (molecules ***a*** and ***b***) and $[Sm(H_2do2a2p)]^-$

	$[Sm(H_2do2a2p)(H_2O)]^-$ ***a***	$[Sm(H_2do2a2p)(H_2O)]^-$ ***b***	$[Sm(H_2do2a2p)]^-$
Sm-Ow	2.617(7)	2.558(7)	---
Sm-Q(O)	0.798	0.817	1.066
Sm-Q(N)	1.711	1.735	1.586
Q(N)-Q(O)	2.509	2.551	2.652
Twist angle (ω)	-29.87, -29.26, -27.10, -27.37	25.99, 28.03, 28.19, 26.86	-24.79, -20.85

O_W = Water Oxygen; Q(O) = Centroid of the O_4 plane; Q(N) = Centroid of the N_4 plane.

The opening angle between the *trans* O-acetates, O4-Sm-O9 is 135.0(2)° in the complex $[Sm(H_2do2a2p)]^-$, which reinforces the idea that both opening angle have to be larger than 135° for coordination of a water molecule [218d]. The bond lengths between the central ions and the donor atoms of the ligand are in the range expected for this type of complexes. The differences between the bond lengths of the P-O clearly indicate that both coordinated phosphonate groups are protonated (Table 3.10).

3.3.1.3.2. Solution Structural Analysis

A solution containing equimolar amounts of *trans*-do2a2p (at pH 6) and $SmCl_3$ was prepared in D_2O. The mixture was allowed to react at room temperature and the pH was slowly raised until full formation of the complex. The full formation of the complex was checked by ^{31}P-NMR spectroscopy. As can be seen in Figure 3.14, at pH 8.38 only one peak was found in the ^{31}P-NMR spectrum (20.74 ppm), significantly shifted relatively to the chemical shift of the free ligand (6.49 ppm).

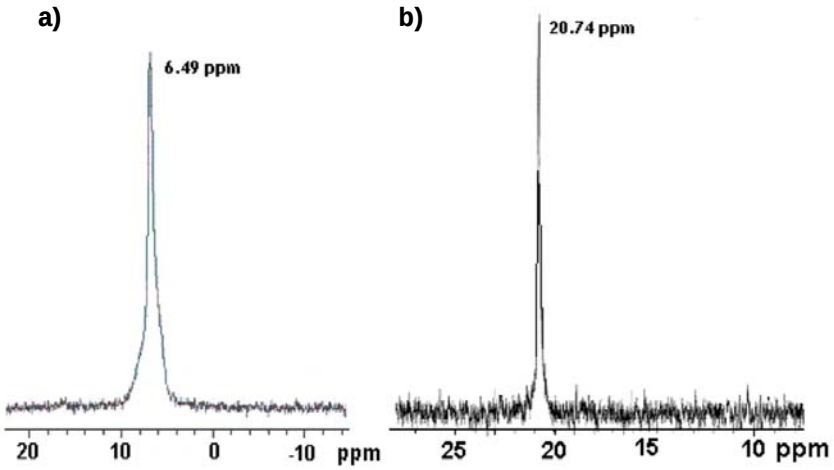

Figure 3.14: ^{31}P-NMR spectra: **a**) *trans*-do2a2p, pH 8; **b**) $[Sm(do2a2p)]^{3-}$, pH 8.38

After full formation of the complex, we have recorded the ^{1}H and ^{13}C NMR spectra (figure 3.15) and we have run 2D-NMR studies (^{1}H,^{1}H COSY, ^{1}H,^{13}C HSQC, figure 3.16) to assign all the resonances found in the spectra.

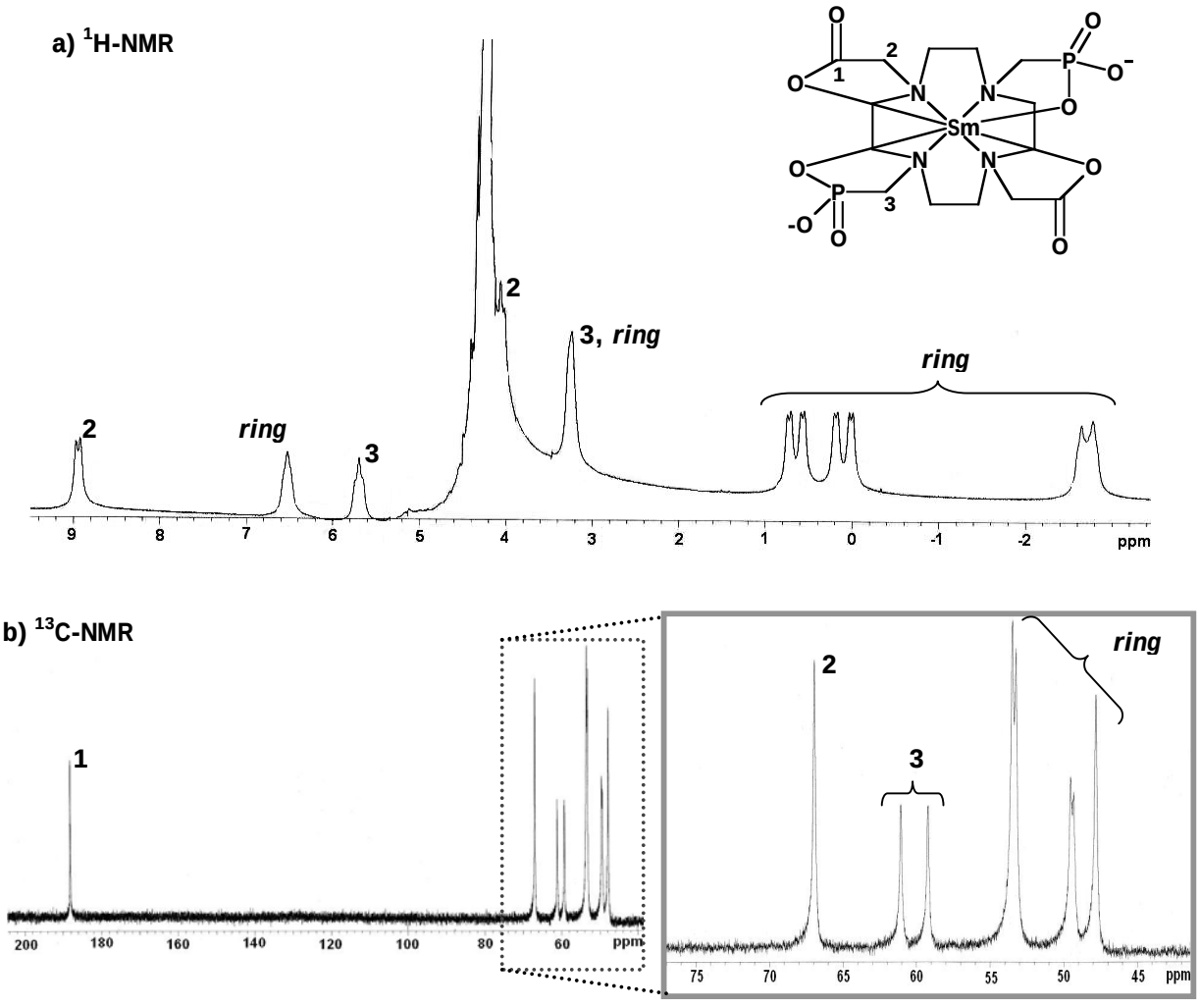

Figure 3.15: Multinuclear NMR spectra of $[Sm(do2a2p)]^{3-}$ (pH 8.38): (**a**) ^{1}H-NMR; (**b**) ^{13}C-NMR

The ^{1}H NMR spectrum of the complex $[Sm(do2a2p)]^{3-}$ presented ten resonances with different multiplicities at -2.72(d), 0.02(d), 0.19(d), 0.57(d), 0.73(d), 3.25(s), 4.08(t), 5.70(t), 6.53(t) and 8.95(d) ppm in an intensity ratio of 4:2:2:2:2:4:2:2:2:2 (figure 3.15a). For the same pH, all the ^{1}H-NMR resonances found for the free ligand are in the range 3.0-3.5 ppm (spectrum not shown), and present a pattern similar to the one shown in figure 3.6a. It is known from the ^{1}H NMR studies of Sm(dota) and Sm(dotp) complexes that the ring axial protons are coupled with the geminal and vicinal axial protons, while the equatorial protons are coupled with the geminal protons only. Due to these couplings, the axial and equatorial protons appear as triplets and doublets, respectively. For the complex $[Sm(do2a2p)]^{3-}$ the splitting found for the different resonances must also be related with such coupling [220].

The ^{13}C-NMR spectrum (figure 3.15b), recorded at the same pH, exhibit six resonances: 188.11, 66.93, 60.12 (d, $^{1}J_{CP}$=140Hz), 53.35(d, $^{3}J_{CP}$=18Hz), 49.41(d, $^{3}J_{CP}$=15Hz), 47.80ppm. Three resonances were assigned to the carbon atoms of the macrocyclic backbone (*ring*), one to the carbon atoms of the carboxylate pendant arms (*2*), one to the carbon atoms of the phosphonte pendant arms (*3*) and one to the carbonyl carbon atoms (*1*).

For almost all the Ln(III) complexes with dota-like chelators the NMR data show the presence of different isomers in solution (SA and TSA) which normally do not interconvert on the NMR time scale [220]. Nevertheless, as can be seen in figure 3.15, for $[Sm(do2a2p)]^{3-}$ only one isomer was observed in solution. Such result may be due to the presence of only one isomer in solution or to a fast interconversion between the two possible isomers. Taking into account the solid state structural analysis, we consider that most probably the first hypothesis is the real one. In fact, as explained before, in the solid state we have only found the TSA isomer, certainly the most stable.

The assignment of the resonances obtained in the NMR spectra was based on 2D-NMR studies (*g*-COSY ^{1}H,^{1}H and *g*-HSQC ^{1}H,^{13}C correlations) at pH 8.38 (figure 3.16).

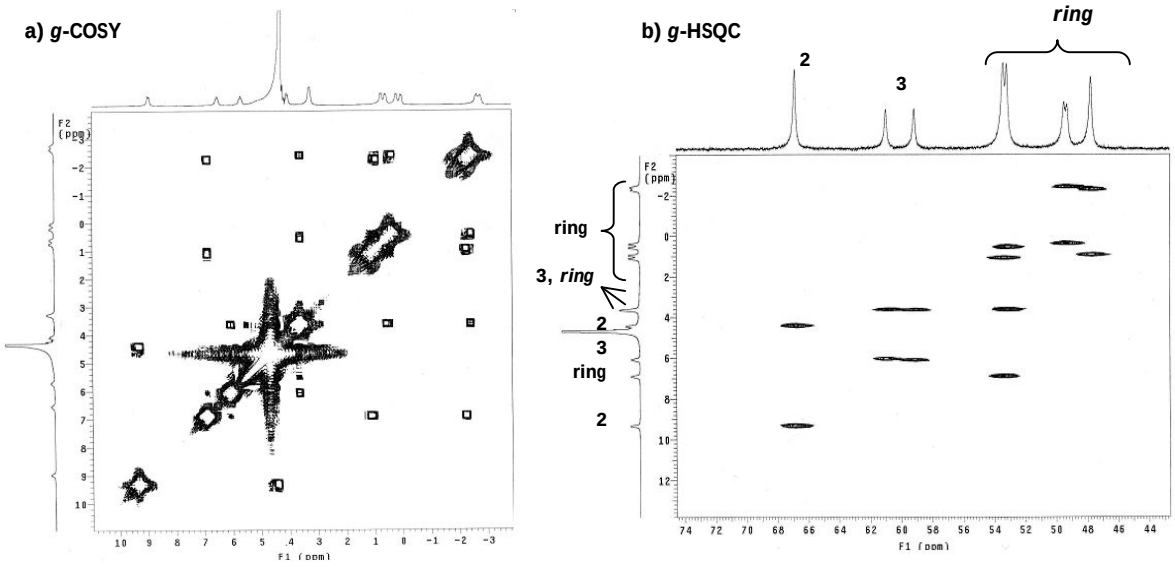

Figure 3.16: 2D-NMR studies of $[Sm(do2a2p)]^{3-}$ (pH 8.38): (**a**) g-COSY and (**b**) g-HSQC

3.3.1.4. Reactions of *trans*-do2a2p with ^{153}Sm and ^{166}Ho and Biological Evaluation

3.3.1.4.1. Synthesis of ^{153}Sm/^{166}Ho-do2a2p

The radioisotopes ^{153}Sm and ^{166}Ho were prepared as nitrates, following the methodology described in 3.2.2. (page 114).

^{153}Sm/^{166}Ho-*trans*-do2a2p complexes were obtained by reacting ^{153}Sm/^{166}Ho$(NO_3)_3$ solutions with *trans*-do2a2p in a 1:2 metal to ligand molar ratio. Aliquots of the reaction mixture were analysed by ascending ITLC, using silica gel ITLC strips developed with the mobile phase: MeOH:H_2O:NH_3 (4:4:0.2). In this system the ^{153}Sm/^{166}Ho complexes migrate with R_f = 1.0, while ^{153}Sm$(NO_3)_3$ and ^{166}Ho$(NO_3)_3$ remain at the origin. After trying different experimental conditions, the radiocomplexes were obtained quantitatively (> 98%) and with high radiochemical purity at pH 8/9, 2 hours reaction at room temperature or 30 min reaction at 70ºC.

3.3.1.4.2. In Vitro Studies

In vitro studies, such as stability of the complexes in physiological media, lipophilicity, plasmatic protein and hydroxyapatite binding were performed. The results obtained are summarized in table 3.12 and in figure 3.19.

Table 3.12: *In vitro* studies of ^{153}Sm/^{166}Ho-do2a2p complexes

Ligand	^{153}Sm complexes					^{166}Ho complexes				
	% prot. binding	log *P*	*In vitro* stability (days) *			% prot. binding	log *P*	*In vitro* stability (days) *		
			HS	S	PB			HS	S	PB
dota [a]	7.0	-2.02	5	5	5	1.4	-1.64	5	5	5
do2a2p	1.5	-1.93	2	4	4	1.5	-1.32	2	4	4
dotp [a]	---	-2.02	4	4	4	---	-1.90	4	4	4

[a] from ref. [204]; ***** 100% of radiocomplex present; Physiological Media: **HS** = Human Serum; **S** = Saline and **PB** = PO_4^{2-} Buffer.

These complexes are stable up to four days at 37ºC in physiologic conditions, namely in saline and phosphate buffer (pH 7.4). In human serum they are only stable up to 2 days. In 0.1 M Tris-HCl buffer (pH 7.4), the solution used for the hydroxyapatite binding studies and for electrophoresis, both complexes have proven to be stable during at least 2h. The complexes are hydrophilic (log *P* = -1.93 and -1.32, for ^{153}Sm-do2a2p and ^{166}Ho-do2a2p, respectively) and present a low binding to plasmatic proteins (1.5% for ^{153}Sm/^{166}Ho-do2a2p).

The overall complex charge was determined by electrophoresis using: paper strips, phosphate buffer (pH 7.4) or Tris-HCl buffer (pH 7.4) as electrolyte and applying a constant voltage (300 V) for 1h. Radioactive distribution on the ITLC strips was detected using a Berthold LB 505 γ detector coupled to a radiochromatogram scanner. In figure 3.17 we present the radiochromatogram obtained for ^{153}Sm-do2a2p, showing that this complex migrates towards the anode (~2.3 cm). In these studies we always used a compound with known charge as a reference. These studies indicate that, under these conditions, both complexes are negatively charged, as expected.

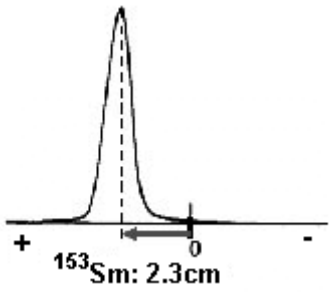

Figure 3.17: Radiochromatogram of an electrophoresis strip

The *in vitro* binding of $^{153}Sm/^{166}Ho$-do2a2p onto hydroxyapatide (HA), the main mineral component of bone, was studied.

Bone is a dynamic and metabolic active organ, in continuous renovation and remodelation mainly due to the osteoblasts and osteoclasts. The first are responsible for the synthesis of the organic component of the bone and the second reabsorbs bone. A third type of cells is responsible for the production of the inorganic matrix – the osteocytes [221]. This inorganic matrix consists in crystalline hydroxyapatite (HA) with chemical formula $Ca_{10}(PO_4)_6(OH)_2$ having an ideal Ca:P stoichiometric ratio of 1.67:1 (figure 3.18A). However, the analysis of biological bone mineral shows a Ca:P ratio ranging from 1.3:1 to 1.9:1.24, being this deviation mainly attributed to the carbonated groups present which distort the crystal structure of most biological apatites (figure 3.18B). Studies with this inorganic matrix can predict the *in vivo* bone uptake.

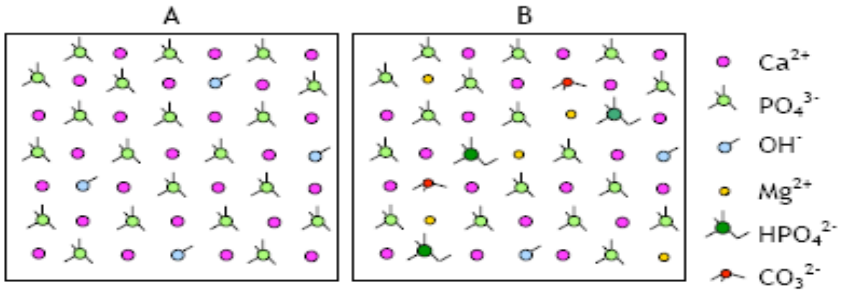

Figure 3.18: Schematic representation of Hydroxyapatite: **A.** Synthetic stoichiometric hydroxyapatite [HA; $Ca_{10}(PO_4)_6(OH)_2$]; **B.** Biological HA, with presence of other cations (e.g., Mg^{2+}) and anions (e.g., HPO_4^{2-}or CO_3^{2-}). Adapted from ref. [221a]

Binding to hydroxyapatite (50 and 100 mg in Tris-HCl buffer) was found to be 13.1%, 20.7% and 34%, 47% for ^{153}Sm-do2a2p and ^{166}Ho-do2a2p, respectively. In Figure 3.19 are graphically represented the HA adsorption curves of both complexes as a function of the amount of HA.

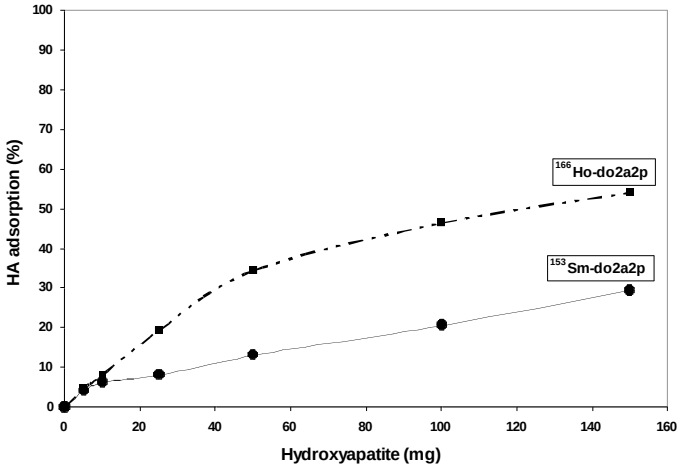

Figure 3.19: Percentage of ^{153}Sm/^{166}Ho-do2a2p hydroxyapatite adsorption as a function of the hydroxyapatite amount (in mg)

Analysis of these curves has clearly demonstrated that the ^{166}Ho has a significantly higher adsorption onto HA than observed for the ^{153}Sm complex, a trend which has also been found for other macrocyclic complexes with the same radiometals [126-128,204]. According to these results, it was reasonable to expect for ^{166}Ho-do2a2p an *in vivo* bone uptake higher than for ^{153}Sm-do2a2p.

3.3.1.4.3. In Vivo Studies

Biodistribution studies of ^{153}Sm/^{166}Ho-do2a2p were performed in female CD-1 mice after i.v. administration of the complexes. The complete experimental data are presented in table 4.6 (chapter 4). Figure 3.20 presents the percentage of injected dose/g organ for the most relevant organs and figure 3.21 presents the whole animal body radioactivity excretion.

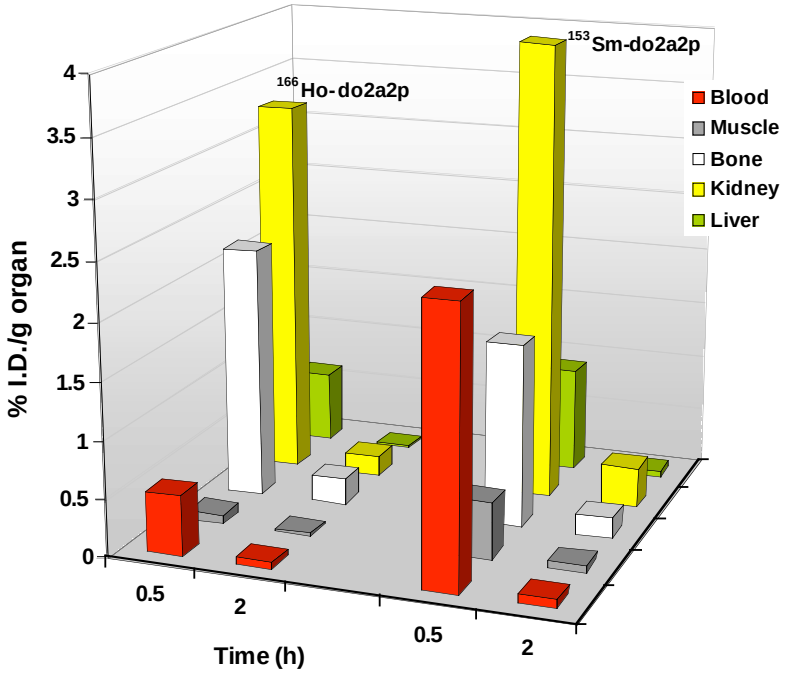

Figure 3.20: Biodistribution data (% I.D./g organ) for ^{153}Sm/^{166}Ho-do2a2p, at 30 min and 2h after i.v. administrationin CD-1 mice (*n*=4-5).

As can be seen in figure 3.20, the complexes present both a rapid blood clearance, with no significant uptake in any of the major organs except in kidneys, which is in agreement with the relatively low plasmatic protein binding found *in vitro*.

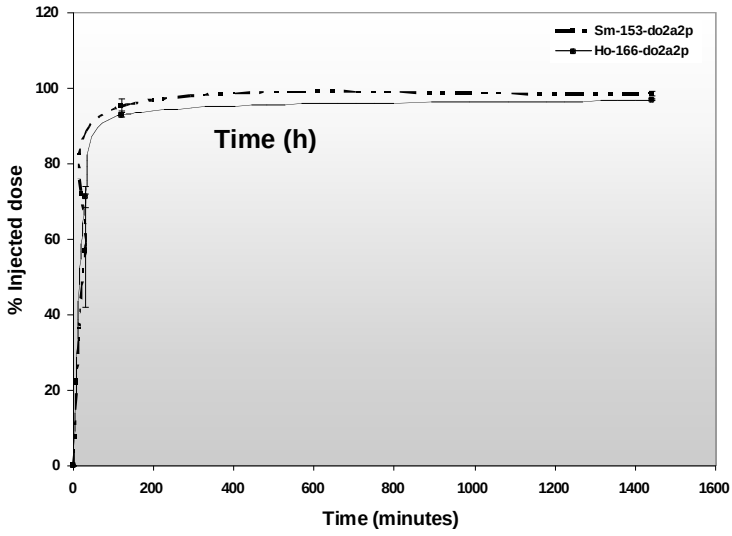

Figure 3.21: Excretion data (% I.D.) for ^{153}Sm/^{166}Ho-do2a2p, at 30 min and 2h after i.v. administration in CD-1 mice (*n*=4-5)

Figure 3.21 shows that for both complexes more than 93% of the radioactivity is excreted via urinary pathway, at 2h after injection. Chromatographic analysis of urine samples collected at different time points indicated a high *in vivo* stability for these complexes as no metabolites could be identified.

The biodistribution profile of these complexes, a rapid total excretion and faster washout from main organs, in addition to the high *in vitro* and *in vivo* stability are attractive features. However, the radioactivity taken by bone decreases rapidly, which does not make these complexes promising for bone pain palliation and/or therapy.

3.3.2. Reactions of 1,4,7,10-tetraazacyclododecane-1,4,7-triacetic-10-(methylphosphonic acid) (do3ap), 1,4,7,10-tetraazacyclododecane-4,7,10-triacetic acid-1-{[(2-carboxyethyl)hydroxyphosphoryl]methyl} (do3ap^{PrA}) and 1,4,7,10-tetraazacyclododecane-4,7,10-triacetic-1-{methyl[(4-aminophenyl)methyl] phosphinic acid} (do3ap^{ABn}) with Radiolanthanides and Biological Evaluation

The synthesis and characterization of the ligands do3ap, do3ap^{PrA} and do3ap^{ABn} have been previously described by the group of Professor Lukeš in Prague (figure 3.22) [121,123,124]. Under a bilateral research project, these compounds have been prepared in Prague and sent to our laboratory for labelling and biological evaluation.

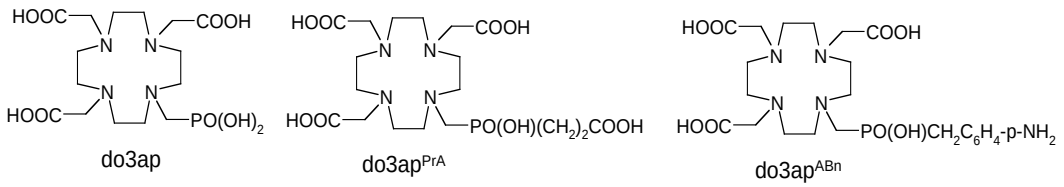

Figure 3.22: Structures of the ligands do3ap^{R}.

3.3.2.1. Synthesis of ^{153}Sm/^{166}Ho-do3ap^{R}

The radiolanthanide complexes with do3ap, doa3p^{PrA} and do3ap^{ABn} were prepared by reacting ^{153}Sm/^{166}Ho$(NO_3)_3$ with the corresponding ligands (1:2 M/L molar ratio) in

water at different pH and temperature. The labelling efficiency was evaluated by ascending ITLC-SG. The reaction conditions were optimized in order to obtain ^{153}Sm and ^{166}Ho complexes with a high radiochemical purity. In figure 3.23 the kinetics of labelling for do3ap^{ABn} and ^{153}Sm at room temperature and different pH values is shown (similar results were found for ^{166}Ho). The maximum complexation yields with ^{153}Sm and ^{166}Ho were achieved at room temperature and pH values in the range 6–9 for do3ap and do3ap^{PrA} and pH 6–7 for do3ap^{ABn}. These labelling conditions are comparable to the ones found for dota with the same radiolanthanides (pH 6–7, 5 min., room temperature) [204].

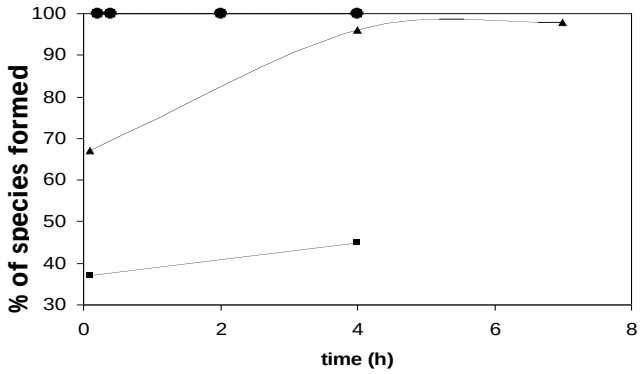

Figure 3.23: Influence of the pH of reaction in the labelling of do3ap^{ABn} with ^{153}Sm and ^{166}Ho, at room temperature: ■ pH 3.5; ● pH 6 and 7; ▲ pH 9

According to the species distribution diagrams (not shown), the fully deprotonated [ML] species is the one formed at the pH values used for the labelling reactions.

3.3.2.2. *In Vitro* Studies

The ^{153}Sm and ^{166}Ho complexes with the do3ap^{R} ligands have negative overall charge, are hydrophilic and present a low human serum protein binding (table 3.13). When these results are compared with those obtained for ^{153}Sm/^{166}Ho-dota complexes under the same experimental conditions the set of ligands does not show significant differences [204].

Table 3.13: *In vitro* studies

Ligand	^{153}Sm complexes					^{166}Ho complexes				
	% protein binding	log *P*	*In vitro* stability (days) *			% protein binding	log *P*	*In vitro* stability (days) *		
			HS	S	PB			HS	S	PB
do3ap	3.1	-2.49	2	3	3	2.9	-1.80	1	3	3
doa3p^{PrA}	4.0	-2.46	2	3	2	3.0	-1.88	1	3	2
do3ap^{Abn}	2.3	-2.43	2	3	3	2.7	-2.05	2	3	3

***** 100% of radiocomplex present; physiological media: **HS** = Human Serum; **S** = Saline and **PB** = PO_4^{2-} Buffer.

As can be seen in table 3.13, the stability of the ^{153}Sm/^{166}Ho-do3ap^{R} complexes in physiological solutions is significantly different from what has been found for analogous complexes with dota. The most relevant differences were found for ^{166}Ho-do3ap^{PrA}. In fact, in the presence of human serum, we have observed a relatively low stability. A new radioactive species (with lower R_f) is formed and increases along the time, while the percentage of the main species decreases (figure 3.24a (B)).

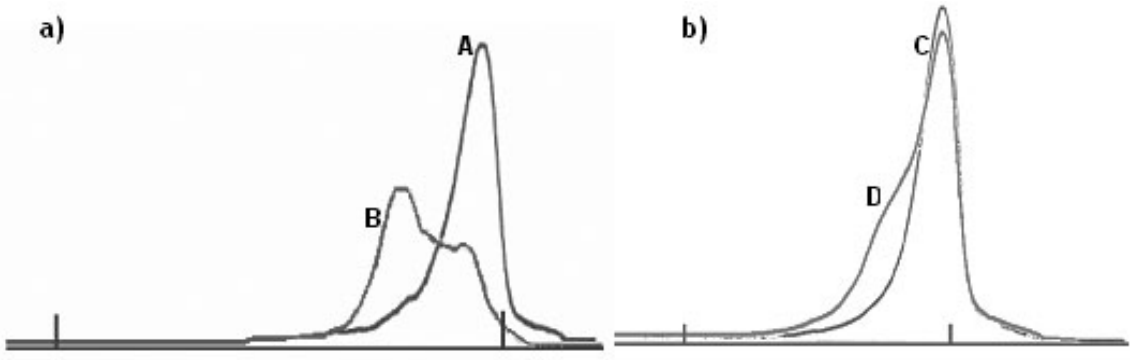

Figure 3.24: ^{166}Ho-do3ap^{PrA} chromatographic profile: a) **A:** after labelling, **B:** in human serum, after 3 days; b) **C:** before injection, **D:** in urine, 30 min post injection

After incubation of the ^{153}Sm/^{166}Ho-do3ap^{R} complexes with HA in Tris-HCl buffer (pH 7.4, 0.1 M), we have found relatively low HA binding: ^{153}Sm: 0.7% for all complexes; ^{166}Ho: 1.5% for do3ap, 2.4% for doa3p^{PrA} and 1.7% for do3ap^{ABn}. These results led us to conclude that the replacement of one pendant arm in dota by a phosphonic or phosphinic pendant arm do not have any effect on the HA uptake. The low binding values found led us to conclude that no *in vivo* bone uptake is expected, due the presence of one phosphonic/phosphinic acid pendant arm of do3ap^{R}.

3.3.2.3. *In Vivo* Studies

The biodistribution studies of all ^{153}Sm/^{166}Ho complexes were performed in female CD-1 mice, at 30min and 2h after intravenous (i.v.) injection through the tail vein. Results were then compared with data for the corresponding dota-complexes, obtained in the same animal model [204]. The experimental data obtained are presented in tables 4.7-4.9 (chapter 4). Tissue distribution data for the most relevant organs, expressed as percentage of injected dose *per* gram of organ, are graphically presented in Figures 3.25 and 3.26, for ^{153}Sm and ^{166}Ho-complexes, respectively.

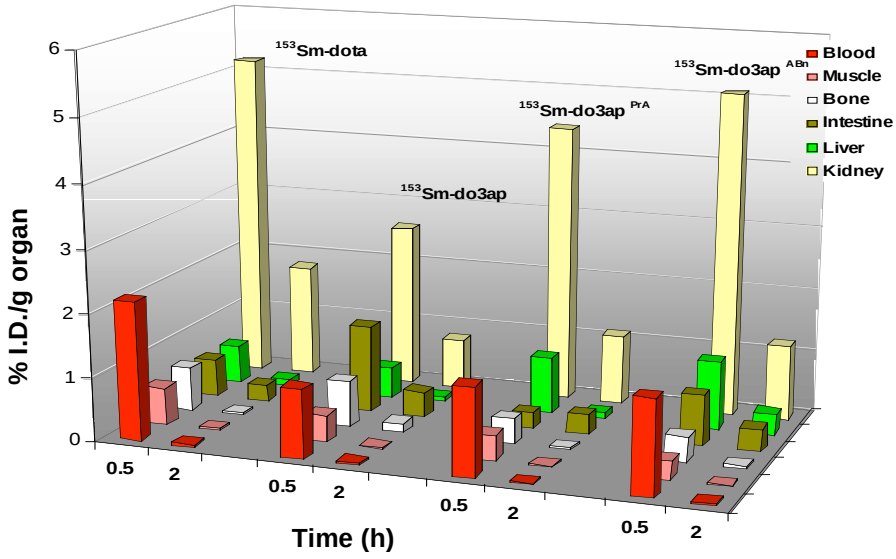

Figure 3.25: Biodistribution results for ^{153}Sm-do3ap^{R} complexes (% I.D./g organ) in comparison with ^{153}Sm-dota in mice (*n*=4-5)

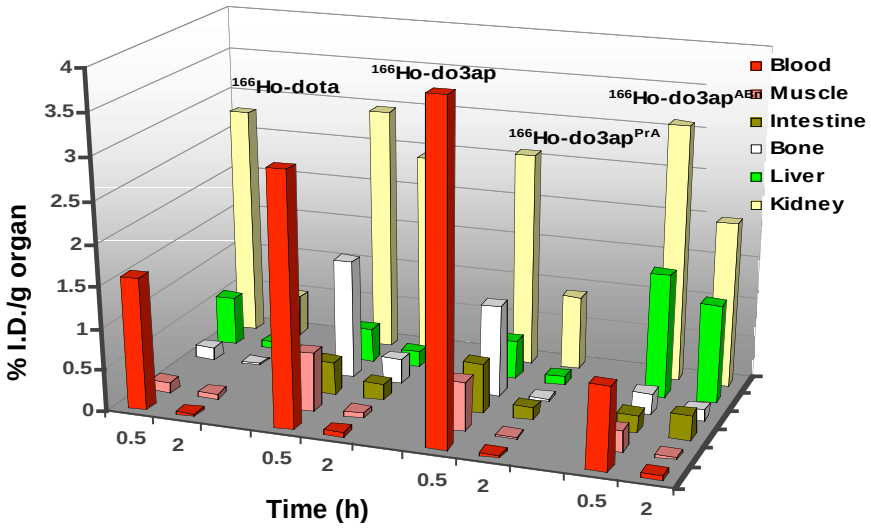

Figure 3.26: Biodistribution results for ^{166}Ho-do3ap^{R} complexes (% I.D./g organ) in comparison with ^{166}Ho-dota in mice (*n*=4-5)

In general, the *in vivo* studies showed a similar biodistribution profile for all ^{153}Sm/^{166}Ho complexes under study with a rapid clearance from main organs, including the blood stream and soft tissues, in agreement with their hydrophilic character and low plasmatic protein binding. At 2h after administration there was only radioactivity localization in organs involved in the excretion routes especially in the kidney. In spite of the presence of one methylphosphonate pendant arm in do3ap, the bone uptake of both radiolanthanide complexes with this ligand is low (0.14 and 0.3 % ID/g organ, at 2h for ^{153}Sm- and ^{166}Ho-do3ap, respectively) and rapidly decreases over time, which agrees with the low HA binding observed *in vitro*. These findings make evident that these complexes are not promising for bone targeting, but the ligands may be useful as an alternative to the common dota-like ligands for labelling biologically active molecules.

Figure 3.27 shows the total excretion as a function of time. The main difference is perhaps the slightly faster excretion of the ^{166}Ho complexes. However, for all the complexes most of the injected activity (> 92 %) was excreted 2h after administration.

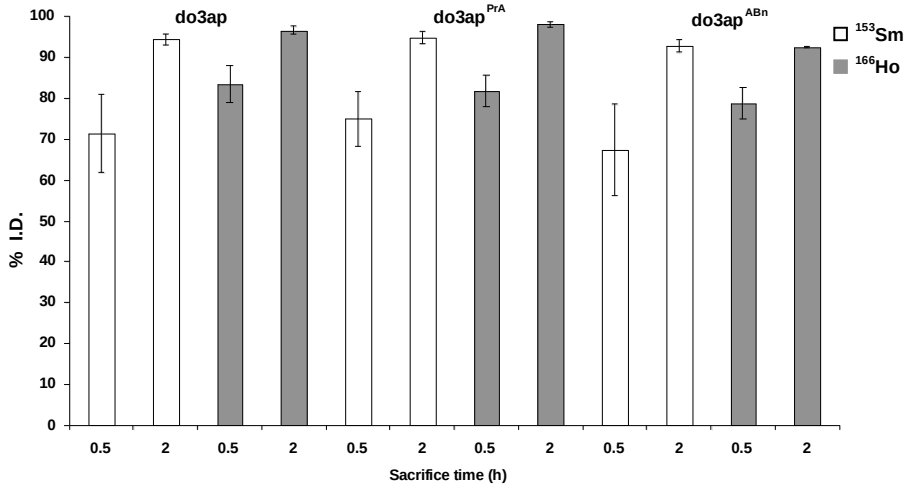

Figure 3.27: Total excretion (% I.D.) of the ^{153}Sm/^{166}Ho-do3ap^{R} complexes in mice at 30 min and 2h after i.v. injection

Chromatographic analysis (ITLC-SG) of urine and blood samples taken at the sacrifice time indicated a high *in vivo* stability for ^{153}Sm/^{166}Ho-do3ap and ^{153}Sm/^{166}Ho-do3ap^{ABn} complexes, since no other radiochemical species than the corresponding intact complexes were detected. The *in vivo* stability and biodistribution profiles of the ^{153}Sm/^{166}Ho complexes with these ligands are comparable to those obtained with ^{153}Sm/^{166}Ho-dota in the same animal model [204]. In the case of ^{166}Ho-do3ap^{PrA} it was

possible to see some degradation of the complex. Figure 3.24b show the chromatographic profile of an aliquot of urine taken 30min post injection (D) together with the profile of the injected radiocomplex (C). It has been reported that trivalent lanthanides may behave *in vivo* similarly to Fe^{3+}. In blood the main carrier protein for Fe^{3+} is transferrin, which also forms complexes with lanthanides [93]. The stability constants for the two binding sites of transferrin with lanthanides(III) are smaller then the ones for Fe^{3+} [222]. However, the serum transferrin is not normally saturated with iron and some binding can occur with other hard metal ions.

3.4. 12-Membered Tetraazamacrocycles Bearing Carboxylate and Phosphonate/Phosphinic Pendants Arms: A Comparative Analysis

Taking into account our results on cyclen-derivatives bearing phosphonate/phosphinic pendant arms and other studies performed in the Radiopharmaceutical Sciences Group/ITN with chelators of the same family, we decided to perform a comparative analysis of the *in vitro*/*in vivo* behaviour of $^{153}Sm/^{166}Ho$ complexes anchored on this set of ligands (figure 3.28).

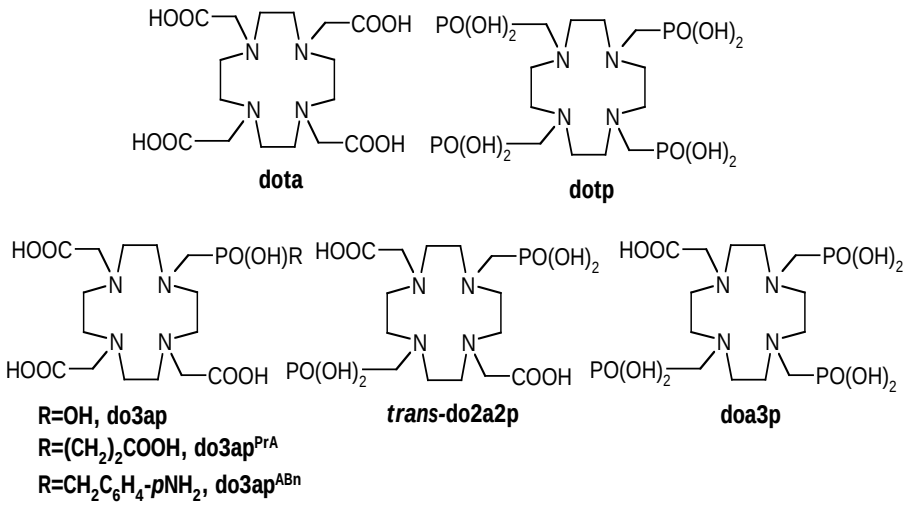

Figure 3.28: Family of macrocycles containing phosphonate pendant arms

Table 3.14 shows the stability constants and pM values (pH 7.4, determined with HySS program [160]) for the Sm^{3+} and Ho^{3+} complexes with this family of chelators.

Table 3.14: Stability constants (Log *K*) and pM values for dota and macrocyclic ligands bearing phosphonate/phosphinic arms with Sm^{3+} and Ho^{3+}

Ligand	Number of PO(OH)R	Sm^{3+}		Ho^{3+}	
		Log *K*	pM*	Log *K*	pM*
dota [a]	**0**	23	16.25	24.8	17.75
do3ap [b]	**1**	28.67	19.23	28.51	19.07
doa3p^{PrA} [b]	**1**	25.11	17.78	25.12	17.79
do3ap^{ABn} [b]	**1**	24.28	16.93	24.49	17.14
do2a2p [c]	**2**	26.92	16.87	27.46	17.40
doa3p [d]	**3**	---		---	
dotp [a]	**4**	28.1	14.76	29.2	16.49

* pM values were calculated with HySS program [160] for $C_L=2xC_M = 10^{-3}M$; [a] ref. [210]; [b] ref. [120]; [c] this work; [d] constants not determined.

From the data in table 3.14, is clear that the pM values decrease when the number of phosphonate pendant arms increases. The replacement of one phosphosnate by phosphinic groups leads also to significantly lower pM value, but, the nature of the phosphinic group does not seem to have any significant effect on the pM value.
Table 3.15 shows the experimental conditions used for a quantitative labelling of the chelators with ^{153}Sm and ^{166}Ho.

Table 3.15: Experimental conditions for quantitative synthesis (> 98%) of the radiolanthanide complexes

Ligand	^{153}Sm-macrocyclic complexes	^{166}Ho-macrocyclic complexes
dota [a]	5 min, r.t., pH 6-9	5 min, r.t., pH 6-9
do3ap [b]	15 min, r.t., pH 6-9	15 min, r.t., pH 6-9
doa3p^{PrA} [b]	15 min, r.t., pH 7-9	15 min, r.t., pH 7-9
do3ap^{ABn} [b]	15 min, r.t., pH 7	15 min, r.t., pH 7
do2a2p [b]	30 min, r.t., pH 6-9	30 min, r.t., pH 6-9
doa3p [c]	15 min, r.t., pH 8	15 min, r.t., pH 8
dotp [a]	60 min, 60-70ºC, pH 8	60 min, 60-70ºC, pH 8

[a] ref. [204]; [b] this work; [c] ref. [128].

Based on the stability constants and on species distribution diagrams of the Sm/Ho-complexes formed with all these ligands, we can say that the best labelling pH corresponds to the region where LM is the main species. In fact, all the radiolanthanide complexes were quantitatively formed at pH 6-9, using 1:2 M:L molar

ratio. Except for dotp, all the labelling reactions were run at room temperature and the maximum complexation was obtained after 5-30 min. For dotp, the maximum yield was possible only after 1h of reaction at 60-70ºC.

The i*n vitro* results obtained for the complexes are shown in table 3.16.

Table 3.16: *In vitro* studies for $^{153}Sm/^{166}Ho$-tetraazamacrocyclic complexes

Ligand	^{153}Sm complexes					^{166}Ho complexes				
	% protein binding	log *P*	*In vitro* stability (days) *			% protein binding	log *P*	*In vitro* stability (days) *		
			HS	S	PB			HS	S	PB
dota [a]	7.0	-2.02	5	5	5	1.4	-1.64	5	5	5
do3ap [b]	3.1	-2.49	2	3	3	2.9	-1.80	1	3	3
doa3p^{PrA} [b]	4.0	-2.46	2	3	2	3.0	-1.88	1	3	2
do3ap^{ABn} [b]	2.3	-2.43	2	3	3	2.7	-2.05	2	3	3
do2a2p [b]	1.5	-1.93	2	4	4	1.5	-1.32	2	4	4
doa3p [c]	1.3	-1.68	4	4	4	1.2	-1.57	4	4	4
dotp [a]	---	-2.00	4	4	4	---	-1.90	4	4	4

***** 100% of radiocomplex present; physiological media: **HS** = Human Serum; **S** = Saline and **PB** = PO_4^{2-} Buffer. [a] ref. [204]; [b] this work; [c] ref. [128].

From the analysis of table 3.15 it is possible to say that: 1) the protein binding decreases when increases the number of phosphonate/phosphinic pendant arms; 2) in general, the more stable complexes are the ones with dota and with the ligands with more phosphonate pendant arms.

Binding to 50 mg of HA for all the complexes studied is graphically represented In Figure 3.29.

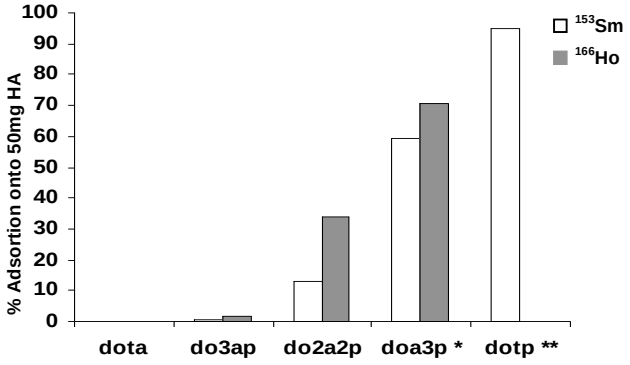

*** Gano, L., Santos, I., *et al*, *Q.J. Nucl. Med. Mol. Imaging*, 2007, 51: 6-15**
**** Alves, F.C., Geraldes, C., *et al*, *Invest. Radiol.*, 2003, 38: 750-760**

Figure 3.29: Adsortion of $^{153}Sm/^{166}Ho$ complexes onto 50 mg of Hydroxyapatite

From the analysis of figure 3.29 it is clear that the adsorption onto hydroxyapatite matrix is higher for Holmium complexes than for samarium ones and that the increase of the number of the phosphonate pendant arms is directly correlated with this parameter.

Tissue distribution data for $^{153}Sm/^{166}Ho$ complexes with all the ligands as a function of time are summarized in Figures 3.30 and 3.31.

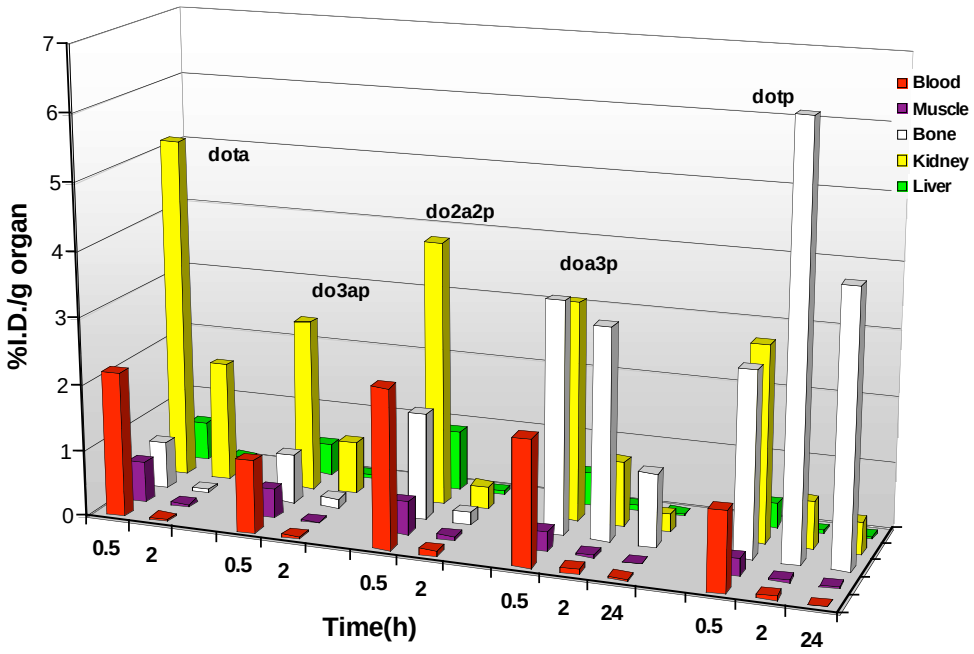

Figure 3.30: Biodistribution of ^{153}Sm complexes on some organs

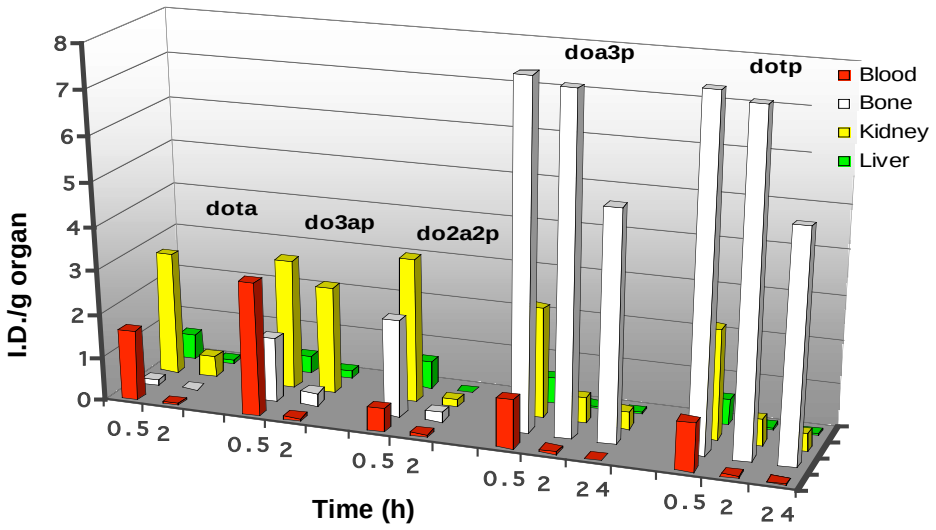

Figure 3.31: Biodistribution of ^{166}Ho complexes on some organs

These results indicated a rapid clearance of the injected activity from blood stream with no significant uptake in any of the major organs except in kidneys.
The biological profile of ^{153}Sm/^{166}Ho-do3ap and ^{153}Sm/^{166}Ho-do2a2p complexes is very similar to that found for ^{153}Sm/^{166}Ho-dota in the same animal model. The main difference is related with the degree of activity taken by bone. Complex Ho-doa3p presents a relatively high bone uptake which is comparable to the uptake found for Ho-dotp. The bone uptake for all the ^{166}Ho complexes is normally higher than that observed for ^{153}Sm.

Table 3.17 summarizes the overall excretion results obtained for the radiocomplexes studied.

Table 3.17: Excretion (%ID) for the ^{153}Sm/^{166}Ho complexes studied

Ligand	^{153}Sm		^{166}Ho	
	Time (h)			
	0.5	2	0.5	2
dota	60.2 ± 9.9	97.2 ±1.0	82.1 ± 4.3	94.4 ± 2.3
do3ap	71.5 ± 9.6	94.5 ± 1.4	83.6 ± 4.5	96.7 ± 1.0
doa3p^{PrA}	75 ± 6.7	94.9 ± 1.5	81.9 ± 3.8	98.2 ± 0.6
do3ap^{ABn}	67.4 ± 11.1	92.8 ± 1.5	78.9 ± 3.9	92.5 ± 0.1
do2a2p	57.0 ± 15.1	95.3 ± 1.8	71.2 ± 2.8	93.1 ± 0.9
doa3p	67.3 ± 8.8	87.9 ± 2.6	51.1 ± 5.2	71.2 ± 3.1
dotp	62.7 ± 9.0	79.8 ± 2.3	54.5 ± 13.1	77.7 ± 0.3

As observed in table 3.16, the excretion of the radiocomplexes slightly decreases with the increase of the number of phosphonate pendant arms.

3.5. Concluding Remarks

The stability constants of do3aSH with Ce^{3+}, Sm^{3+} and Ho^{3+} have been determined by potentiometry and UV-Vis spectrophotometry. The values found for these lanthanides, roughly, representing the beginning, the middle and the last part of the Ln series, are comparable, being in a narrow range ($logK_{Ln\text{-}do3aSH}$: Ce=21.24, Sm=22.0 and Ho=21.0). Based on the protonation constants of the complexes, the UV-vis spectroscopy and relaxativity measurements on Gd-do3aSH, it was found that the thiol group does not coordinate to the Ln(III) ions, even when deprotonated (pH>8). The radiocomplexes ^{153}Sm/^{166}Ho-do3aSH have been quantitatively prepared in

relatively mild conditions. Complex ^{153}Sm-do3aSH is more stable *in vitro* than ^{166}Ho-do3aSH. These findings led us to perform *in vivo* studies only for the ^{153}Sm-do3aSH. To better understand the possible role of the sulphur atom, the do3a chelator was also synthesized and studied with ^{153}Sm. We have found similar biological profiles and *in vivo* stability for ^{153}Sm-do3aSH and ^{153}Sm-do3a. The fast blood clearance, rapid and high overall excretion and the non involvement of the thiol group on the stabilization of the lanthanide, pointed out the potential use of the new do3aSH as a bifunctional chelating agent for labeling biomolecules with ^{153}Sm.

The new carboxylate/phosphonate compound, *trans*-do2a2p, was also synthesized and characterized, including by X-ray crystallographic analysis and multinuclear NMR spectroscopy. Protonation and stability constants of *trans*-do2a2p with Sm^{3+}, Ho^{3+} and Y^{3+}, as well as with other biologically relevant *d*-elements (Ca^{2+}, Cu^{2+}, Zn^{2+} and Cd^{2+}), were determined by potentiometry and/or by ^{31}P-NMR spectroscopy. The *trans*-do2a2p forms more stable complexes with lanthanides than with *d*-transition elements. Reactions of Sm^{3+} with *trans*-do2a2p at the macroscopic and radioactive level have shown the formation of stable complexes. For Sm^{3+}, monocrystals have been obtained and X-ray diffraction analysis has shown the presence of two different complexes: $H[Sm(H_2do2a2p)(H_2O)].8.5H_2O.2.5HCl$ and $H[Sm(H_2do2a2p)].5H_2O.3HCl$. In the anion $[Sm(H_2do2a2p)(H_2O)]^-$ the metal is 9 coordinated, presenting a capped-twisted square-antiprismatic (CTSA) coordination geometry and in $[Sm(H_2do2a2p)]^-$ the samarium is 8 coordinated and displays a twisted square-antiprismatic (TSA) coordination geometry. Multinuclear NMR studies have shown the presence of only one isomer and the data indicate that all the pendant arms are coordinated to the metal ion, in accordance with the solid state X-ray structural analysis. Complexes ^{153}Sm/^{166}Ho-do2a2p have been quantitatively obtained and their *in vitro* and *in vivo* stability is high. The biological profile is identical: high overall excretion, low liver and kidney uptake and also low-to-moderate bone uptake.

The previously described chelators do3ap^R (R=$P(O)(OH)_2$, $P(O)(OH)(CH_2)_2COOOH$ or $P(O)(OH)CH_2C_6H_4$-*p*NH_2) have also been quantitatively labeled with ^{153}Sm and ^{166}Ho. *In vivo* studies have shown identical biological profile for all the complexes, with no bone uptake.

CONCLUSIONS AND OUTLOOK

Herein the most important conclusions of this work are highlighted and some perspectives are pointed out.

The work presented in this thesis involved the synthesis and characterization of novel cyclen-based macrocyclic compounds to stabilize *d*- or *f*- elements. Our main interest was to get an idea about the possibility of using such ligands for preparing stable inactive and radioactive Cu^{2+}, Sm^{3+} and Ho^{3+} complexes.

The novel chelators synthesised were 2-[1,4,7,10-tetraazacyclododecan-1-yl] ethanethiol (do1SH), 1,4,7,10-tetraazacyclododecane-1,4,7-triacetic-10-ethanethiol acid (do3aSH) and 1,4,7,10-tetraazacyclododecane-1,7-bis(acetic acid)-4,10-bis(methylphosphonic acid (*trans*-do2a2p) as well as the previously reported dioxo-1,4,7,10-tetraazabicyclo[1.10.1]hexadeca-1(11),13,15-triene-4,7-diacetic acid (bz2ac).

do1SH was characterized by multinuclear NMR spectroscopy and by X-ray crystallographic analysis of the do1SH Trytil protected precursor (do1STrit). The protonation constants of do1SH were determined by potentiometry (25.0ºC, 0.10M KNO_3) and ^{13}C-NMR spectroscopy. ^{13}C-NMR titrations showed that the highest protonation takes place on the thiol group and the remaining three determined constants occur on the amine groups of the macrocycle backbone.

The stability constants with Cu^{2+}, Zn^{2+} and Cd^{2+} have been determined by potentiometry and the values found follow the trend [Cu-do1SH]>[Zn-do1SH]≈[Cd-do1SH]. The presence of the thiol group has improved the stability towards Cu^{2+} in comparison to cyclen: $pM_{Cu\text{-}do1SH}$=14.24 and $pM_{Cu\text{-}cyclen}$=10.02. Nevertheless, the selectivity of do1SH for Cu^{2+} relatively to other endogenous elements, like zinc, has decreased: $pM_{Zn\text{-}do1SH}$=11.77 and $pM_{Zn\text{-}cyclen}$=5.68.

Solution structural studies of do1SH with Cu^{2+} and Zn^{2+} were performed to assess the nature of the inner sphere of the respective complexes. UV-vis and EPR spectra of Cu-do1SH and ^{13}C-NMR spectra of Zn-do1SH at different pH values were evaluated and the studies indicated that the thiol group only coordinates to the metal ions at pH > 10.

Taking into account that the introduction of a thiol pendant arm in the cyclen backbone has improved the affinity for Cu^{2+} but its selectivity has decreased, and taking also into account the results obtained when do1SH reacted with Cu^{2+}, we decided not to pursue studies with $^{64/67}Cu$.

The novel do3aSH was then prepared by alkylation of do1STrit with ethylbromoacetate. Compound do3aSH was characterized by multinuclear NMR spectroscopy, mass spectrometry and elemental analysis. Six out of the eight

protonation constants were determined by potentiometry (25.0ºC, 0.10mM KCl). Based on the $^{1}H/^{13}C$-NMR spectroscopic titration curves it was possible to assess that: the first two protonations occur in two amine centers, the third protonation occurs on the thiol group (also confirmed by protonation studies with Ca-do3aSH) and the other three protonation constants take place on the carboxylate groups.
Reactions of do3aSH with Cu^{2+} and with $^{64/67}Cu^{2+}$ were studied. The TLC and HPLC analysis of the reactions mixtures obtained revealed the presence of two copper species. The HPLC analysis enabled the separation of these two species and their ESI-MS spectra were identical. The main molecular ion and isotopic distribution agree with the formation of the dimer [(Cu-do3aS)$_2$]. One possibility for the structure of such species would be: two [Cu-do3aS] units linked by an S-S bond. The two identical species formed may be two isomers of [(Cu-do3aS)$_2$]. The conclusion that we can get from these results is that the sulphur atom may be not needed for stabilization of the Cu^{2+} being possible its conjugation to a biomolecule, without compromising the coordination set for copper.

We have chosen compound bz2ac to evaluate the effect of the rigidity (by the introduction of a benzene ring on the cyclen cavity) of the macrocycle on the selectivity for Cu^{2+}, relatively to other *d*-metals. For bz2ac, four out of six protonation constants were determined by potentiometry (25.0ºC, 0.10M KNO_3) and ^{1}H-NMR spectroscopy. The protonation sequence proposed for the compound was: the highest protonation at one amide group, the second on one amine group, the third may occur in the carboxylate arm attached to the unprotonated amine and the last one can occur on the remaining amine or on the remaining carboxylate or in both at the same time. The stability constants with Cu^{2+}, Zn^{2+}, Ni^{2+}, Cd^{2+} and Pb^{2+} have been determined by potentiometry. The presence of the benzene has improved the stability towards Cu^{2+} in comparison to cyclen: $pM_{Cu\text{-}bz2ac}$=11.73 and $pM_{Cu\text{-}cyclen}$=10.02. Nevertheless, the selectivity of this ligand for Cu^{2+} relatively to other endogenous elements, like zinc, has decreased: $pM_{Zn\text{-}bz2ac}$=8.00 and $pM_{Zn\text{-}cyclen}$=5.68. The possible use of bz2ac as a therapeutic chelating agent to remove toxic ions (such as Cd^{2+} or Pb^{2+}) was also discarded due to the relatively low stability of such complexes and also due to the low selectivity towards *d*-metals: $pM_{Cd\text{-}bz2ac}$=7.45 and $pM_{Pb\text{-}bz2ac}$=8.33.
Solution structural studies with Cu^{2+} were performed to assess the coordination structure of Cu-bz2ac at different pH values. UV-vis and EPR spectra of Cu-bz2ac were evaluated and the studies indicated that the amide group coordinates to the metal ion at pH > 10.

Reactions of bz2ac with $CuCl_2$ were performed in ethanol. The recrystallization from ethanol/methanol led to the formation of monocrystals suitable for X-ray analysis. The X-ray diffraction analysis revealed the formation of the monomeric benzodioxochlorocomplex [Cu(bz2ac')Cl] anchored by a modified tetraazamacrocycle. In this complex, Cu is five-coordinated by two nitrogen atoms of the macrocyclic backbone, two oxygen atoms, one from one amide group and the other from an acetate arm, and a chloride atom, displaying a square pyramidal coordination geometry. One of the acetate arms has been esterified *in situ* into an ethylesther and does not coordinate to the metal. Reactions of bz2ac with $Cu(OAc)_2$, in water, led to the formation of one species which has been analysed by mass spectrometry and formulated as [Cu-bz2ac]. The structure proposed was: Cu six coordinated by two amine nitrogens, by two oxygen atoms from the amide groups and two oxygen atoms from the carboxylates (figure 2.29).
We have also explored the synthesis of $^{64/67}$Cu-bz2ac complexes. The radiocomplexes were quantitatively obtained in mild conditions: 10^{-3}M, pH 7, 1 min., room temperature. The good *in vitro* stability observed (including in rat and human plasma) led us to evaluate the possibility of using one of the pendant arms for the conjugation of a biomolecule. We have tried to conjugate bz2ac to a Fmoc protected lysine. Two lysine conjugates were obtained and formulated as: bz2ac-Lys-Fmoc and bz2ac-$(Lys\text{-}Fmoc)_2$. Reactions of these conjugates with Cu^{2+} and with $^{64}Cu^{2+}$ were performed, but the results have always shown the presence of free Cu^{2+}. These results may indicate that the carboxylates used on conjugation are needed to stabilize the metal.

For the stabilization of *f*-elements, the studies were based on the novel compounds do3aSH and *trans*-do2a2p, as well as on the previously reported do3ap (1,4,7,10-tetraazacyclododecane-1,4,7-triacetic-10-(methylphosphonic acid)), do3ap^{PrA} (1,4,7,10-tetraazacyclododecane-4,7,10-triacetic acid-1-{[(2-carboxyethyl)hydroxyphosphoryl]methyl}) and do3ap^{ABn} (1,4,7,10-tetraazacyclododecane-4,7,10-triacetic-1-{methyl[(4-aminophenyl)methyl]phosphinic acid}).
The stability constants of do3aSH with Ce^{3+}, Sm^{3+} and Ho^{3+} were determined by potentiometry (25.0ºC, 0.10mM KCl) and UV-vis spectroscopy. The complexes showed relatively high stability constants, when compared with the corresponding dota and do3a analogues: $pM_{Ce\text{-}do3aSH}$=8.84, $pM_{Ce\text{-}do3a}$=9.28 and $pM_{Ce\text{-}dota}$=10.75. Unexpectedly, the pM value obtained for Ho-do3aSH is lower than the one obtained for Sm-do3aSH:

$pM_{Ho\text{-}do3aSH}$=8.72 and $pM_{Sm\text{-}do3aSH}$=9.22. Uv-vis studies of Ce-do3aSH and relaxation studies with Gd-do3aSH showed that the thiol group is not coordinated to the metal ion, even in its deprotonated form.

^{153}Sm/^{166}Ho-do3aSH complexes were quantitatively obtained at pH 6, room temperature and 1:2 M/L molar ratio. The radiocomplex ^{153}Sm-do3a was also studied to better understand the effect of the thiol group. The kinetics of ^{153}Sm-do3aSH and ^{153}Sm-do3a compare with that found for ^{153}Sm/^{166}Ho-dota, while ^{166}Ho-do3aSH forms more slowly. The high *in vitro* stability found with ^{153}Sm led us to perform *in vivo* studies with ^{153}Sm-do3aSH. The biological profile found for ^{153}Sm-do3aSH is similar to the ones found for ^{153}Sm-do3a and ^{153}Sm-dota. These results together with the indication that the sulphur atom is not involved in the coordination to the lanthanide ion, pointed out the potential of do3aSH to be conjugated to a biomolecule through the thiol group and the labeling of the conjugate with ^{153}Sm.

The new *trans*-do2a2p was synthesized and characterized by multinuclear NMR spectroscopy and X-ray crystallography. The X-ray structural analysis showed that two amines in *trans* position are protonated, as well as the carboxylate groups and two of the oxygen atoms of the phosphonates. Six out of ten protonation constants were determined by potentiometry (25.0ºC, 0.1M NMe_4Cl) and by ^{31}P-NMR spectroscopy. Based on the ^{1}H/^{31}P-NMR spectroscopic titration curves, we concluded that the first two protonations occur in two amine centers, the third and fourth protonations occur in two phosphonate groups attached to the unprotonated amines, and the last two protonations occur in the carboxylate groups.

The stability constants of *trans*-do2a2p with Y^{3+}, Sm^{3+}, Ho^{3+}, Ca^{2+} and with some *d*-elements were evaluated. Compound *trans*-do2a2p forms with *f*-elements more stable complexes than with *d*-transition elements: $pM_{Sm\text{-}do2a2p}$=16.87 and $pM_{Cu\text{-}do2a2p}$=15.36 (table 3.9). Reactions of Sm^{3+} with *trans*-do2a2p have been performed at the macroscopic level. Monocrystals for X-ray crystallography have been obtained and their analysis indicated the presence of two different complexes: $H[Sm(H_2do2a2p)].5H_2O.3HCl$ and $H[Sm(H_2do2a2p)(H_2O)].8.5H_2O.2.5HCl$. In the anion $[Sm(H_2do2a2p)]^-$ the metal is 8 coordinated by the four nitrogen atoms of the macrocycle backbone and by four oxygen atoms of the pendant arms, displaying TSA coordination geometry. In $[Sm(H_2do2a2p)(H_2O)]^-$ the metal is 9 coordinated, due to the additional coordination of a water molecule and displays a CTSA coordination geometry. In solution, only one isomer was present and multinuclear NMR data

showed that all the pendant arms are coordinated to the metal ion, in agreement with the solid state data.
Radiochemical studies of *trans*-do2a2p with ^{153}Sm and ^{166}Ho showed that these complexes are formed quantitatively at room temperature and pH 8, being very stable *in vitro*. Their *in vivo* biological profile is similar to the one found for ^{153}Sm/^{166}Ho-dota in the same animal model. Moreover, the complexes only present a low-to-moderate bone uptake, which fast decreases after 2h pos injection.

The ligands do3ap, do3ap^{PrA} and do3ap^{ABn} were also studied with ^{153}Sm and ^{166}Ho. These three ligands were quantitatively labeled in mild conditions (pH 6). The radiocomplexes have moderate *in vitro* stability. No effect of the nature of the phophonate group on the radiochemical and *in vivo* biological profile was observed.

Comparing our radiochemical and biological results with other previously reported for ^{153}Sm/^{166}Ho-dota, ^{153}Sm/^{166}Ho-dotp and ^{153}Sm/^{166}Ho-doa3p we can say that the bone uptake depends on the number of phosphonate pendant arms present in the macrocycle and it seems that the relative position of the arms also affects the bone uptake of the radiocomplexes.

From all the ligands studied do3aSH is the most interesting one. It is a novel $12N_4$ macrocycle bearing one thiol pendant arm and three carboxylate groups. This chelator can stabilize either *d*- or *f*-elements. Moreover, the thiol group is not involved on the coordination to the metal being free to be conjugated to a biomolecule. Further studies should involve the coupling of a biomolecule through the thiol group and a re-analysis of the radiochemical and biological behaviour of the conjugate.

4.
EXPERIMENTAL PART

4.1. Reagents

Chemicals and solvents were of reagent grade and were used without further purification, unless stated otherwise. Natural Ho_2O_3 (99.9%) was purchase from Strem Chemicals and enriched Sm_2O_3 (98.4% ^{152}Sm) was obtained from Campro Scientific. Bromoethyl tritylthiol ($Br(CH_2)_2STrit$), 1,4,7-tris(ethoxycarbonylmethyl)-1,4,7,10-tetraazacyclododecane (do3Et) and 1,7-bis(acetic acid tert-butyl ester)-1,4,7,10-tetraazacyclododecane (do2^{t}Bu) were synthesised as previously described [148,153,205].

4.2. Analytical methods

NMR Spectroscopy

^1H (300 MHz), ^{13}C (75.5 MHz) and ^{31}P (121.5 MHz) NMR spectra were recorded in a Varian Unit Inova-300 spectrometer at about 20ºC. The spectra were performed in $CDCl_3$ (δ/ppm: ^1H: 7.24; ^{13}C: 77.00) or D_2O *versus* an external reference of 1,4-dioxane (δ/ppm: ^1H: 3.75; ^{13}C: 69.30). ^{31}P NMR spectra were recorded in $CDCl_3$ or in D_2O, referenced to external 85% aqueous H_3PO_4 solution (δ/ppm: ^{31}P: 0.00). Deuterated potassium hydroxide (KOD) was freshly prepared. Abbreviations used to describe the resonances for NMR spectra are as follows: s (singlet), d (doublet), t (triplet), q (quadruplet), m (multiplet), or br (broad signal).

Mass Spectrometry

Positive-ion mass spectra were obtained in a Finnigan FT/MS 2001-DT FTICR mass spectrometer by laser desorption ionization or on a Micromass Platform II Quadrupole Mass Spectrometer fitted with an electrospray source.

pH Measurements

pH measurements were performed in a ORION SA 720 potentiometer. The solutions used for the NMR titrations were measured directly in the NMR-tube with a combination microelectrode Mettler-Toledo U402-M3-S7/200. The final pD was calculated from pD = pH* + (0.40 ± 0.02) [***Equation 4.1***], where pH* corresponds to the reading of the pH meter [157].

UV-Vis Spectroscopy

UV-Vis spectra were done in a Cary 500 Spectrophotometer.

EPR Spectroscopy

EPR spectroscopic measurements of the copper complex were recorded with a Bruker ESP 380 spectrometer equipped with continuous-flow cryostats for liquid nitrogen, operating at X-band.

HPLC

HPLC of compounds were performed on a Perkin-Elmer device consisting of a Turbo LC System with a quaternary pump (series 200 LC Pump), a programmable absorbance detector model 785A (Perkin-Elmer Instruments GmbH, Germany), and a homemade *γ*-ray detector (well-type, NaI(Tl) crystal), for the detection of the radioactive samples, or on a Perkin Elmer LC pump 200 coupled to a Shimadzu SPD 10AV UV/Vis detector.

Columns:

I) EC 250/4 Nucleosil 100-5 C-18 (Macherey-Nagel);

II) Jupiter (Phenomenex) 4 µ Proteo 90Å, RP-18, 250×4.6 mm;

III) Zorbax (Agilent) SB-C18, 300Å, 5 µm, 250×9.4 mm;

IV) Polymer (Phenomenex) 10 µ 100Å, RP-1, 250×10 mm;

V) EC 250/3 Nucleosil 100-5 C-18 (Macherey-Nagel) ;

VI) Waters µ Bondapak C18, 150 x 19 mm.

Eluent systems:

A = MeOH, **B** = 10% NH_4OAc, **C** = H_2O, **D** = CH_3CN + 0.1% TFA, **E** = 0.1% TFA, **F** = CH_3CN.

Methods:

Method 1: 0-20 min: 50% A / 50% B; λ = 254 nm; $flow_{analytic\ run}$ = 1 mL/min.

Method 2: 0-2 min: 100% C, 2-17 min: 50% A / 50% C, 17-20 min: 50-100% A, 20-22 min: 100% A; λ = 214 nm; $flow_{analytic\ run}$ = 0.5 mL/min.

Method 3: 0 min: 10% D/90% E, 0-45 min: 10 - 70% D, 45-50 min: 70-100% D, 50-55 min: 100% D, 55-56 min: 100-10% D; λ = 220 nm; $flow_{analytic\ run}$ = 1 mL/min, $flow_{preparative\ run}$ = 8 mL/min.

Method 4: 0 min: 10% D/90% E, 0-40 min: 10%-70% D, 40-42 min: 70-100% D, 42-43 min: 100% D, 43-45 min: 100-10% D; λ = 220 nm; $flow_{analytic\ run}$ = 1 mL/min, $flow_{preparative\ run}$ = 8 mL/min.

Method 5: 0 min: 10% D/90% E, 0-20 min: 10-70% D, 20-22 min: 70-100% D, 22-24 min: 100% D, 24-25 min: 100-10% D, 25-26 min: 10% D/90% E; λ = 220 nm; $flow_{analytic\ run}$ = 1 mL/min.

Method 6: 0-20 min: 10% F/90% C; λ = 220 nm; $flow_{analytic\ run}$ = 5 mL/min.

Column Chromatography

Ligands were purified by column chromatography. The columns were of silica-gel 60 (70-230 mesh, pH range = 6.5-7.5, obtained from Merck), Dowex 50WX4 – 100 Ion-exchange resin (H^+ form, Sigma) and Amberlite 50CG/ H AR carboxylic resin (H^+ form, 100-200 mesh, Gegeion: H, Serva).

Thin Layer Chromatography Analysis

The purity of the compounds was assessed by TLC on silica-coated aluminium sheets 0.25 mm UV sensitive or RP-18 (both from Merck). The plates were revealed by UV irradiation (254 nm), exposure to iodine vapours or by spraying with Ninhydrin or Draggendorff's reagent.

Radiocopper complexes were assessed by neutral RP-18 TLC plates (Merck), developed with the mobile phase NH_4OAc 10% / MeOH (1:1). The TLC plates were recorded on a Radioisotope Thin Layer Analyzer (Rita Star, Raytest Isotopenmessgerät GmbH, Straubenhardt, Germany).

Radiolanthanide complexes were assessed by ascending silica gel ITLC plates (Polygram, Macherey-Nagel), developed with the mobile phase MeOH:H_2O:NH_4OH (2:4:0.2) or saline. The ITLC plates were developed using a Berthold LB 505 γ detector coupled to a radiochromatogram scanner.

X-Ray Structural Analysis of Cu-bz2ac ($C_{18}H_{23}N_4O_6ClCu$)

Data were collected at room temperature with the crystal mounted in a glass capillary. An Enraf-Nonius CAD4 diffractometer equipped with graphite monochromatised Mo-Kα radiation (λ = 0.71069 Å) in the ω-2θ scan was used for measurements. Lorentz, polarisation effects and empirical absorption correction based on psi-scans [223] were applied to the collected intensities.

The structure was solved by direct methods using SIR97 [224] and refined by full-matrix least-squares on F^2 methods using the program SHELXL97 [225] and the winGX software package [226]. All non-hydrogen atoms were refined anisotropically. Hydrogen atoms were placed in calculated positions. Molecular graphics were prepared with ORTEP3 [227].

X-Ray Structural Analysis of do1Strit ([$C_{29}H_{40}N_4S$].SO_4.6H_2O) and Sm^{3+}/do2a2p complexes (H[Sm(do2a2p)].5H_2O.3HCl and H[Sm(do2a2p)(H_2O)].8.5H_2O.2.5HCl)

X-ray diffraction experiments were performed with a Bruker AXS APEX CCD detector diffractometer using graphite monochromated Mo Kα radiation (λ = 0.71073 Å), at

150 K in the φ and ω scans mode. A semi empirical absorption correction was carried out using SADABS [228]. Data collection, cell refinement and data reduction were done with the SMART and SAINT programs [229]. The structures were solved by direct methods using SIR97 [224] and refined by fullmatrix least-squares methods using the program SHELXL97 [225] and the winGX software package [226]. Non-hydrogen atoms were refined with anisotropic thermal parameters. The H atoms of the CH and CH_2 were placed at calculated positions using a riding model, with distances C–H = 0.95 Å (aromatic) and C–H = 0.99 Å (CH_2) and with *U*iso(H)=1.2*U*eq(C) of the parent atom. The H atoms in the water, NH_2 and NH were located in difference Fourier maps and their coordinates and isotropic thermal parameters were refined. The residual electronic density ranging from 0.393 to -0.392 e $Å^{-3}$ was within expected values. The final refinement of 472 parameters converged to final R and R_W indices R_1 = 0.0408 and wR_2 = 0.0972 for 7020 reflections with $I > 2\sigma(I)$. Molecular graphics were prepared using ORTEP 3 [227].

X-Ray Structural Analysis of trans-H_6do2a2p ($C_{14}H_{30}N_4O_{10}P_2.4H_2O$)

Selected crystals were mounted on glass fibres in random orientation and cooled to 150(1) K. The diffraction data were collected at 150(1) K (Cryostream Cooler, Oxford Cryosystem) using a Nonius Kappa CCD diffractometer and Mo-Ka radiation (*k* = 0.71073 Å) and analyzed using the HKL DENZO program package [230]. The structures were solved by direct methods (SIR92) [231], and refined by full-matrix least-squares techniques (SHELXL97) [225,232]. The scattering factors used for neutral atoms were included in the SHELXL97 program. All non-hydrogen atoms were refined anisotropically. All hydrogen atoms attached to carbon and nitrogen atoms and oxygen atoms of carboxylate pendants were located in the electron difference map; however, they were fixed in theoretical or original positions with thermal parameters *U*eq(H) = 1.2*U*eq(C) or 1.3*U*eq(N or O) as their free refinement dramatically increases the number of parameters and in some cases leads to unrealistic bond lengths. Some hydrogen atoms belonging to co-crystallized water molecules were also found, and were treated using the AFIX 3 instruction and *U*eq(H) = 1.3*U*eq(O).

4.3. Production of Radionuclides

4.3.1. Production of ^{64}Cu and ^{67}Cu

^{64}Cu ($t_{1/2}$ 12.7 h; $ß^-_{max}$ 0.573 MeV, 39.6%; $ß^+_{max}$ 0.655 MeV, 19.3%; EC 41%; γ 1.35 MeV, 0.6%; 0.511 MeV, 38.6%) was produced on the PET cyclotron "Cyclone 18/9" of the FZ Dresden-Rossendorf. ^{67}Cu ($t_{1/2}$ 62.0 h; $ß^-_{max}$ 0.577 MeV, 20%; 0.484 MeV, 35%; 0.395

MeV, 45%; γ 0.184 MeV, 40%; 0.092 MeV, 23%) was obtained from Switzerland. The products have been purified according to the procedure reported previously [233].

4.3.2. Production of ^{153}Sm and ^{166}Ho

^{153}Sm ($t_{1/2}$ 46.8 h; β_{max} 0.67 MeV, 34%; 0.71 MeV, 44%; 0.81 MeV, 21%; γ 0.103 MeV, 38%) and ^{166}Ho ($t_{1/2}$ 26.8 h; β_{max} 1.85 MeV, 51%; 1.77 MeV, 48%; γ 80.6 keV, 7.5%; 1.38 MeV, 0.90%) were produced in the ITN Portuguese Research Reactor (RPI) (Sacavém, Portugal), by thermal neutron bombardment of isotopically enriched $^{152}Sm(NO_3)_3$ or natural $Ho(NO_3)_3$, respectively, as target materials.

Nitrate targets were prepared from the corresponding oxides. Briefly, 10mg-sized samples of enriched $^{152}Sm_2O_3$ or natural Ho_2O_3 were dissolved in conc. HNO_3 (2 mL) and evaporated to dryness. The samples were taken up in 2 mL of 2% HNO_3 (v/v) and again evaporated to dryness in order to obtain the corresponding nitrate forms. Irradiation was typically performed as follows: power, 1000 kW; thermal neutron flux, ~$1.2x10^{13}$ n/cm^{2}s; epithermal neutron flux, ~$2.6x10^{11}$ n/cm^{2}s. After irradiation, the targets were reconstituted in H_2O to produce a stock solution for complex preparation. The specific activities of the radionuclides, after 3h irradiation and at end of bombardment, were 110-150 MBq/mg for ^{153}Sm and 220-260 MBq/mg for ^{166}Ho. The radionuclidic purity of the ^{153}Sm and ^{166}Ho solutions was assessed by γ-ray spectrometry using a Ge (Li) detector coupled to an Accuspec B Canberra multichannel analyzer. The spectra were processed, following efficiency calibration with a ^{152}Eu source. The ^{153}Sm and ^{166}Ho activities produced after irradiation were measured in a dose calibrator (Aloka Curiemeter IGC-3).

4.4. Synthesis of the ligands

Synthesis of 1,8-di-(2-ethanetritylthiol)-1,5,8,11-tetraazacyclotetradecane (te2Strit)

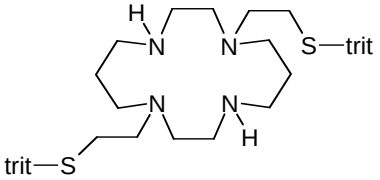

To a solution of cyclam (500 mg, 2.5 mmol) in toluene (50mL) was slowly added bromoethyl tritylthiol [153] (210 mg; 0.5 mmol) in toluene (50mL). The reaction mixture was refluxed overnight and then a solution of NaOH (20%) added. The organic phase was separated and the solvent evaporated under vacuo. The solid obtained was purified by silica-gel chromatography, using as eluent a mixture of

EtOAc/MeOH/aq.NH_3 (gradient 100:0:0 → 0:100:0 → 0:80:20, R_f = 0.3 in 80:20 MeOH/ aq.NH_3 solution). The product obtained was formulated as **te2Strit** (88 mg, 22% yield).

^{1}H-NMR ($CDCl_3$), δ/ppm: 7.25-7.04 m (arom., 30H); 2.79 br (arm, 8H); 2.21-1.98 m(br) (ring, 20H)
^{13}C-NMR ($CDCl_3$, δ/ppm): 144.43, 129.52; 128.03; 126.89; 67.23; 50.91; 49.16; 46.94; 44.16; 26.62; 23.17; 15.26

Synthesis of 1,8-di-(2-ethanethiol)-1,5,8,11-tetraazacyclotetradecane (te2SH)

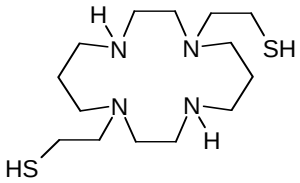

Compound **te2Strit** was refluxed in 20% HCl, for 8h. After cooling to room temperature, the resulting solution was washed with dichloromethane. The aqueous extracts were separated and vacuum dried, yielding a white solid **te2SH** (23 mg, 65%).

^{1}H-NMR (D_2O, pH≈1), δ/ppm: 3.63-3.18 m(br) (ring + arm, 24H); 2.14 br ($CH_2\underline{C}H_2CH_2$ ring, 4H)
^{13}C-NMR (D_2O, pH≈1), δ/ppm: 60.05; 50.64; 47.89; 43.99; 39.86; 20.58

Synthesis of 2-[1,4,7,10-tetraazacyclododecan-1-yl] ethanetritylthiol (do1Strit)

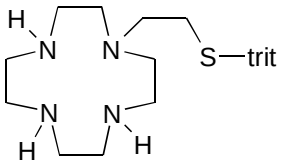

To a solution of cyclen (285 mg, 1.5 mmol) in toluene (50mL) was slowly added bromoethyl tritylthiol [153] (210 mg; 0.5 mmol) in toluene (50mL). The reaction mixture was refluxed overnight and then a solution of NaOH (20%) added. The organic phase was separated and the solvent evaporated under vacuum. The solid obtained was purified by silica-gel chromatography, using as eluent a mixture of $CHCl_3$/MeOH/aq.NH_3 (gradient 100:0:0 → 0:100:0 → 0:80:20, R_f = 0.2 in 80:20 MeOH/ aq.NH_3 solution). Compound **do1Strit** was obtained in 43% yield (100 mg).

X-Ray single crystals were obtained by slow concentration of the fractions containing the ligand, which were obtained after purification by column chromatography.

^{1}H-NMR ($CDCl_3$), δ/ppm: 7.37 (d, 6H), 7.26-7.14 (m, 9H), 2.89-2.84 (m, 4H), 2.52-2.48 (m, 8H), 2.36-2.32 (m, 8H)

^{13}C-NMR ($CDCl_3$), δ/ppm: 144.9 (Ph), 129.6 (Ph), 127.8 (Ph), 126.5 (Ph), 66.8 ($SCPh_3$), 53.5 ($CH_2CH_2SCPh_3$), 50.80 (C_{ring}), 46.9 (C_{ring}), 46.1 (C_{ring}), 44.9 (C_{ring}), 29.4 ($CH_2CH_2SCPh_3$)

Crystal data for do1Strit: $C_{29}H_{52}N_4O_{10}S_2$, M_r = 680.87, triclinic, space group P-1, a = 8.1242(1) Å, b = 8.8600(1) Å, c = 27.0151(4) Å, α = 81.8670(10)°, β = 82.1130(10)°, γ = 63.9020(10)°, U = 1722.57(4)Å^3, Z = 2, D_c = 1.313 g cm^{-3}, μ (Mo Kα) = 1.260 mm^{-1}.

Synthesis of 2-[1,4,7,10-tetraazacyclododecan-1-yl] ethanethiol (do1SH)

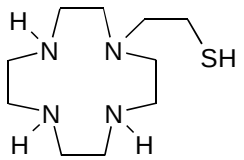

Compound **do1Strit** was refluxed in 20% HCl, for 2h. After cooling to room temperature, the resulting solution was washed with dichloromethane. The aqueous extracts were then separated and vacuum dried yielding a white solid which was formulated as **do1SH** (75 mg, 80%).

^{1}H-NMR (D_2O, pD = 1.05), δ/ppm: 2.54 (t, 2H, C(1)H); 2.70 (t, 2H, C(2)H); 2.84 (t, 4H C(3)H); 2.97 (br m, 4H, C(6)H); 3.07 (br m, 8H, C(4)H + C(5)H)

^{13}C-NMR (D_2O/ 1,4-dioxane, pD = 1.05), δ/ppm: 56.8 (***C2***); 50.3 (***C3***); 45.6 (***C4***); 44.4 (***C6***); 43.9 (***C5***); 22.0 (***C1***)

MS-LDI: *m/z* calc. for $[C_{10}H_{25}N_4S]^+$: 233.179, $[C_{10}H_{24}N_4SNa]^+$: 255.161, $[C_{10}H_{25}N_4SK]^+$: 271.135; found: $[M+H]^+$: 233.191, $[M+Na]^+$: 255.156, $[M+K]^+$: 271.118.

Synthesis of 1,4,7,10-tetraazacyclododecane-4,7,10-tris(ethoxycarbonylmethyl)-1-ethanetritylthiol (do3EtStrit)

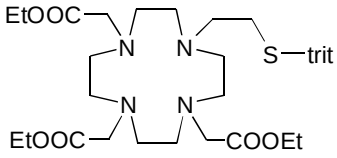

To a suspension of **do1Strit** (300 mg, 0.65 mmol) and K_2CO_3 (540 mg; 3.9 mmol) in dry acetonitrile (50mL), ethylbromoacetate (360 mg; 2.1 mmol) was added. The reaction mixture was stirred for 3 days at room temperature. The crude of the reaction was filtered, the supernatant evaporated to dryness. The resulting oil was purified by silica-gel chromatography, using as eluent a mixture of CH_2Cl_2/MeOH (gradient 100:0 → 100:20, R_f = 0.2 in 90:10 CH_2Cl_2/MeOH). Then compound **do3EtStrit** was recovered (334 mg, 70%).

^{1}H-NMR ($CDCl_3$), δ/ppm: 7.37 (d, 6H), 7.27-7.14 (m, 9H), 4.19-4.09 (m, 6H), 3.15-3.10 (d, 6H), 2.81 (m, 8H), 2.30-2.06 (m, 8H), 1.26-1.18 (m, 9H)

^{13}C-NMR ($CDCl_3$), δ/ppm: 173.58 (*C*=O), 173.13 (*C*=O), 144.12 (Ph), 129.07 (Ph), 127.54 (Ph), 126.36 (Ph), 67.77 (S*C*Ph_3), 66.46 ($CO_2CH_2CH_3$), 61.36 (CH_2CO_2Et), 61.11 (CH_2CO_2Et), 60.66 ($CH_2CH_2SCPh_3$), 55.49 (C_{ring}), 54.93 (C_{ring}), 53.27 (C_{ring}), 52.73 (C_{ring}), 51.59 (C_{ring}), 50.49 (C_{ring}), 49.17 (C_{ring}), 27.03 ($CH_2CH_2SCPh_3$), 13.75 ($CO_2CH_2CH_3$), 13.69 ($CO_2CH_2CH_3$)

Synthesis of 1,4,7,10-tetraazacyclododecane-1,4,7-triacetic-10-ethanethiol acid (do3aSH)

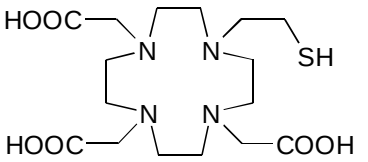

Compound **do3EtStrit** was refluxed in 20% HCl, for 18h. After cooling to room temperature, the resulting solution was washed several times with dichloromethane. Then, the aqueous extracts were separated and vacuum dried. The solid obtained was formulated as **do3aSH** (158 mg, 85%).

^{1}H-NMR (D_2O, pD=1.05), δ/ppm: 4.04 (s, 2H, C(3)H); 3.44 (s, 4H, C(6)H); 3.30-3.37 (m, 10H, C(4)H + C(5)H); 2.95 (m, 8H, C(2)H); 2.76 (t, 2H, C(1)H)

^{13}C-NMR (D_2O/ 1,4-dioxane, pD=1.20), δ/ppm: 176.05 (*C10*); 170.87 (*C9*); 58.04 (*C2*); 56.68 (*C3*); 55.07 (*C4*); 53.69 (*C6*); 51.94 (*C5*); 50.47 (d, *C7+C8*); 19.71 (*C1*)

ESI-MS: *m/z* calc. for $[C_{16}H_{30}N_4O_6S]^+$: 406.50, $[C_{16}H_{29}N_4O_6SNa]^+$: 428.49, $[C_{16}H_{28}N_4O_6SNa_2]^+$: 450.46; found: $[L+H]^+$: 407, $[L+Na]^+$: 429, $[L-H+2Na]^+$: 451.

Anal. Calc. for $C_{16}H_{30}N_4O_6S.4.5H_2O.4HCl$: C, 30.24; H, 6.65; N, 8.50; S, 4.30. Found: C, 30.34; H, 6.84; N, 8.85; S, 5.06.

Synthesis of 1,4,7,10-tetraazacyclododecane-1,4,7-triacetic acid (do3a)

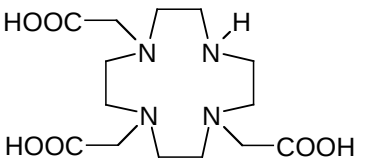

Compound **do3Et** [205] was refluxed in 20% HCl, for 24h. After cooling to room temperature, the resulting solution was washed with dichloromethane. The aqueous extracts were separated and vacuum dried. The resulting oil was purified by HPLC, yielding a yellow solid which was formulated as **do3a** based on NMR spectra.

^{1}H-NMR (D_2O, pD=1.05), δ/ppm: 3.70 (s, 2H); 3.32 (t, 8H); 3.11-2.87 (m, 12H)

^{13}C-NMR (D_2O/ 1,4-dioxane, pD=1.05), δ/ppm: 176.76; 170.25; 56.10; 55.36; 52.77; 51.81; 49.53; 48.54; 42.75.

Rt: 10.76 min (column VI, method 6)

Synthesis of 2,9-dioxo-1,4,7,10-tetraazabicyclo[1.10.1]hexadeca-1(11),13,15-triene-4,7-diacetic acid (bz2ac)

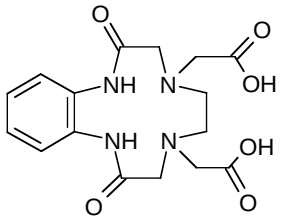

A suspension of ethylenediaminetetraacetic dianhydride (2.5 mmol, 0.641 g) in 250 mL of tetrahydrofuran freshly destilled was heated, under nitrogen atmosphere, and *o*-phenyldiamine (2.5 mmol, 0.270 g) was added dropwise during 4-5h. The reaction mixture was refluxed for 18h. The solvent was then removed under vacuum yielding a white solid which was formulated as **bz2ac** (0.870 g, 95%).

^{1}H-NMR ($CDCl_3$), δ/ppm: 7.332-7.290 (m, 4H), 3.758 (s, 4H), 3.689 (s, 4H), 3.196 (s, 4H)
^{13}C-NMR ($CDCl_3$), δ/ppm: 172.726, 169.072, 130.430, 128.500, 126.569, 59.056, 57.553, 53.406
Rt: 2.70 min (column I, method 1)

1,7-bis(acetic acid tert-butyl ester)-4,10-bis(methanephosphonic acid diethyl ester)-1,4,7,10-tetraazacyclododecane (do2^{t}Bu2PO(OEt)$_2$)

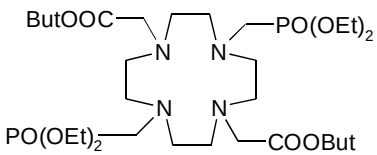

1,7-bis(acetic acid tert-butyl ester)-1,4,7,10-tetraazacyclododecane [148] (550 mg, 1.37 mmol) and triethylphosphite (1.57 g, 9.47 mmol) were dissolved in 20 mL of dry benzene, and the resulting solution refluxed. Dry paraformaldehyde (330 mg, 10.98 mmol) was slowly dropped into the refluxing solution, over a period of 4 h. The mixture was refluxed overnight. The solvent was removed under vacuum and the clear pale yellow oil kept under high vacuum at 40-50ºC for 12 h, to remove volatile impurities. The resulting oil was purified by column chromatography on silica gel (EtOH: 25% aq.NH_3). The fractions containing **do2^{t}Bu2PO(OEt)$_2$** were collected, dried under vacuum and the resulting slightly yellow oil analysed. Yield: 403 mg (42%).

^{1}H-NMR ($CDCl_3$), δ/ppm: 3.99 (q, 8H, P(O)O*C*H_2CH$_3$, $^3J_{HH}$=$^3J_{PH}$= 7,5Hz), 2.89-277 (br m, 24H, cyclen- *C*H_2-N and N*C*H_2COOtBu and *C*H_2P), 1.25 (t, 18H, *C*H_3 t-Bu), 1,89 (t, 12H, P(O)OCH$_2$*C*H_3).

^{13}C-NMR ($CDCl_3$), δ/ppm: 170.0 (*C*OOt-Bu), 81.0 (*C*(CH$_3$)$_3$), 61.6 (P(O)O*C*H_2CH$_3$, $^2J_{PC}$= 3Hz), 55.8 (*C*H_2COOt-Bu), 52.3 (N*C*H_2*C*H_2N), 51.9 (N*C*H_2*C*H_2N and *C*H_2(P(O)OCH$_2$CH$_3$), 27.9 (C(*C*H$_3$)$_3$), 16.3 (P(O)OCH$_2$*C*H_3).

^{31}P NMR ($CDCl_3$), δ/ppm: 26.8.

1,4,7,10-tetraazacyclododecane-1,7-bis(carboxymethyl)-4,10-bis(methylphosphonic acid) (*trans*-do2a2p)

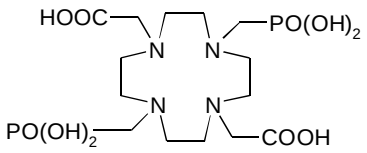

do2^{t}Bu2PO(OEt)$_2$ (400 mg, 0.57 mmol) was dissolved in HCl (20%, 50 mL) and the mixture was refluxed for 24h. After removing the HCl under vacuum, a clear oil was obtained. This oil was dissolved in H_2O and vacuum dried. After repeating this procedure 3 times a white powder was obtained. The residue was dissolved in water and the solution was poured onto a Dowex 50 column (H^+ form, 100 mL). The column was washed with (500 mL) and the amines were eluted out with another 500 mL of water and 10% pyridine solution (500 mL). The solvent was removed in vacuum and the residue was chromatographed using an Amberlite 50CG carboxylic resin (column 6x20 cm, H^+ form) and water as eluent. Fractions containing the desired product were collected and evaporated to dryness. Yield: 238 mg (90%). X-Ray quality single crystals were obtained by slow concentration of the fractions containing the ligand.

^{1}H-NMR (D_2O), δ/ppm: 3.55 (d, 4H, N*C*H_2COOH), 3.43-3.38 (br m, 8H, N*C*H_2*C*H_2N), 3.27 (d, 4H, N*C*H_2P(O)(OH)$_2$, $^2J_{PH}$= 12Hz), 3.06 (br m, 8H, N*C*H_2*C*H_2N).

^{13}C-NMR (D_2O/tert-butyl alcohol), δ/ppm: 176.3 (*C*OOH), 54.9 (*C*H_2COOH), 53.9 (N*C*H_2*C*H_2N) 53.1 (*C*H_2P(O)(OH)$_2$, $^1J_{CP}$=4Hz), 52.4 (N*C*H_2*C*H_2N).

^{31}P-NMR (D_2O/KOD, pD=10), δ/ppm: 20.5.

Crystal data for [*trans*-H_6do2a2p].4H_2O: $C_{14}H_{38}N_4O_{14}P_2$; M= 548.42 g mol^{-1}; Orthorhombic, P21/c, a=8.4668(2), b=18.7663(4), c= 15.5783(2) Å, V = 2402.21(8) Å^3, Z = 4, Dcalc = 1.516 g/cm^3, μ = 0.256 mm^{-1}.

4.5. Conjugation of a Protected Aminoacid to bz2ac

Synthesis of the Lysine conjugates bz2ac-Lys-Fmoc and bz2ac-(Lys-Fmoc)$_2$

A solution containing 1.5 eq of ligand, 3 eq HBTU and 7 eq of DIPEA in 500 μL of 1-methyl-2-pirrolidone was allowed to react for 30 min at room temperature. After this time, 3.3 mg of Fmoc-Lysine in 1-methyl-2-pyrrolidone (250 μL) were added and the reaction mixture was stirred for 3h. The reaction mixture was purified by HPLC, using the column III and method 2. The HPLC chromatogram revealed 5 main peaks, which were collected and sent to MS analysis. The MS analysis allowed the identification of

two of these peaks. The species with retention time (Rt) equal to 33.50min was assigned to bz2ac-Lys-Fmoc (30%) and the peak with a Rt= 41.48min was identified as bz2ac-(Lys-Fmoc)$_2$ (11%).

bz2ac-Lys-Fmoc

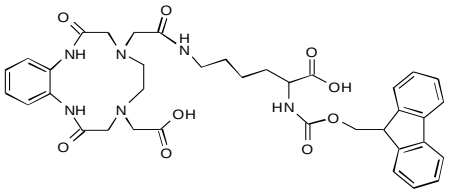

^{1}H-NMR (CD_3CN), δ/ppm: 8.66 (s); 7.83-7.81 (d); 7.65 (t); 7.47-7.29 (m); 6.81 (m); 6.07-6.05 (d); 4.32-4.31 (d); 4.22 (t); 4.11-4.06 (q4); 3.97 (s); 3.93 (s); 3.78-3.77 (d); 3.74-3.73 (d); 3.34 (s); 3.21-3.18 (m); 3.07-3.05 (d); 2.80 (s); 1.80-1.74 (m); 1.69-1.63 (m); 1.50 (m); 1.41-1.36 (m); 1.31-1.26 (m);

^{13}C-NMR (CD_3CN), δ/ppm: 173.57; 171.23-171.20 (d); 170.58; 169.61; 160-158 (q, TFA); 156.54; 144.44-144.38 (d); 141.43; 134.33; 131.39; 130.13; 129.67; 128.26; 128.04; 127.65; 127.44; 125.52; 66.58; 61.88; 58.33; 55.92; 54.07; 51.95; 47.32; 38.81; 31.12; 28.86; 22.89.

MS-ESI: 714.4 found $(M+Na)^+$ 737.47

Rt: 33.50 min (column III, method 3); 18.10 min (column II, method 5)

bz2ac-(Lys-Fmoc)$_2$

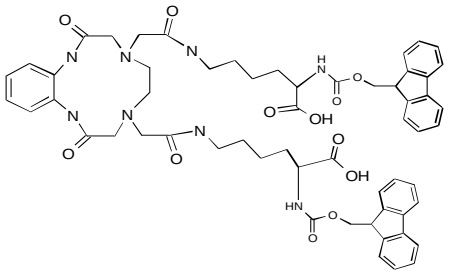

^{1}H-NMR (CD_3CN), δ/ppm: 8.56 (s); 7.79-7.77 (d); 7.62 (t); 7.42-7.24 (m); 6.85 (s); 6.70 (s); 6.40 (m, br); 6.17-6.16 (d); 5.99-5.98 (d); 4.30-4.25 (m); 4.19 (q4); 4.18 (s); 4.16 (s); 4.06 (s); 3.96 (s); 3.91-2.99 (m); 2.66 (s); 1.76-1.63 (m); 1.47-1.38 (m); 1.30-1.23 (m).

^{13}C-NMR (CD_3CN), δ/ppm: 173.54; 172.23; 171.58; 170.34; 156.51; 144.45; 144.35; 141.44; 134.53; 131.25; 130.02; 129.58; 128.21; 128.02; 127.47; 127.42; 125.53; 66.53; 62.05; 57.99; 55.55 d; 54.15; 54.03-53.97 d; 52.27; 47.37-47.31 d; 38.78; 31.94; 30.99; 28.92-28.86 d; 22.85.

MS-ESI: 1064 found $(M+H)^+$ 1065.66; $(M+Na)^+$ 1087.75

Rt: 41.48 min (column II, method 3); 19.96 min (column III, method 5)

4.6. Synthesis of Copper(II) complexes

Synthesis of [Cu^{II}bz2ac]

A solution of 10 mg of **bz2ac** in 500µL of methanol was added to 0.8 eq of $Cu(NO_3)_2.H2O$ in 500µL of methanol. The final solution was stirred in a vortex and allowed to stand overnight.

MS-ESI: *m/z* calc. for $[C_{16}H_{30}N_4O_6Cu]$: 425.5, found $(M)^-$ 424.0
HPLC: Rt = 3.44 min (column I, method 1)

Synthesis of [Cu^{II}(bz2ac')Cl] (C1)

A solution of $CuCl_2.2H_2O$ (0.11 g, 0.651 mmol) in 2 cm^3 of ethanol was added to a solution of **bz2ac** (0.237 g, 0.651 mmol) in 8 cm^3 of ethanol. The resulting brown mixture was refluxed for 2 hours. After cooling to room temperature the solution was filtered through diatomaceous earth and washed with methanol. X-ray-quality green single crystals were obtained by slow diffusion of methanol.

Anal. for $C_{18}H_{23}ClCuN_4O_6.H_2O$: Calc.: C, 42.44; H, 5.14; N, 11.00. Found: C, 42.45; H, 4.63; N, 11.02.
UV: 704 nm (54 $mol^{-1}dm^3cm^{-1}$), 382 nm (133 $mol^{-1}dm^3cm^{-1}$).
Crystal data for C1: $C_{18}H_{23}N_4O_6ClCu$; M= 490.39 g mol^{-1}; Orthorhombic, P212121, a = 10.6410(13), b=13.0690(16), c= *14*.505(2) Å, V = 2017.2(4) $Å^3$, Z = 4, Dcalc = 1.615 g/cm^3.

Synthesis of [Cu-do3aSH]

A solution of 10 mg of **do3aSH** in 500 µL of water was added to 0.8 eq of $Cu(OAc)_2.H_2O$ in 500 µL of methanol. The final solution was stirred for 3h at room temperature and allowed to stand overnight. The green solution was analysed by TLC and HPLC and two species were observed. These species were then separated by HPLC (column I, method 2) and analysed by ESI-MS.

Species A

MS-ESI: *m/z* calc. for $[Cu_2C_{32}H_{54}N_8O_{12}S_2]$: 932, found $(M)^-$ 931.0; $[Cu_2C_{32}H_{54}N_8O_{12}S_2Na]$: 954, found $(M)^-$ 953.0; $[Cu_2C_{32}H_{52}N_8O_{12}S_2]^{2-}$: 466, found $(M)^-$ 465.0; $[CuC_{16}H_{27}N_4O_6SNa_2]$: 513, found $(M)^-$ 512.0
TLC: Rf = 0.2 ((RP-18, Methanol/NH_4OAc 10% (50:50))
HPLC: Rt = 11.81 min (column I, method 2)

Species B

MS-ESI: *m/z* calc. for $[Cu_2C_{32}H_{54}N_8O_{12}S_2]$: 932, found $(M)^-$ 931.0; $[Cu_2C_{32}H_{54}N_8O_{12}S_2Na]$: 954, found $(M)^-$ 953.0; $[Cu_2C_{32}H_{52}N_8O_{12}S_2]^{2-}$: 466, found $(M)^-$ 465.0

TLC: Rf = 0.8 ((RP-18, Methanol/NH_4OAc 10% (50:50))

HPLC: Rt = 14.71 min (column I, method 2)

Synthesis of [Cu-bz2ac-Lys-Fmoc]

A solution of 5 mg of **bz2ac-Lys-Fmoc** in 1mL of acetonitrile and 250 µL of water was added to 0.8 eq of $Cu(NO_3)_2.H_2O$ in 500 µL of water. The light green solution was stirred in a vortex and allowed to stand overnight.

HPLC: Rt = 11.91 min (column III, method 5)

Synthesis of [Cu-bz2ac-(Lys-Fmoc)$_2$]

A solution of 5 mg of **bz2ac-(Lys-Fmoc)$_2$** in 1mL of acetonitrile and 250 µL of water was added to 0.8 eq of $Cu(NO_3)_2.H_2O$ in 500 µL of water. The light green solution was stirred in a vortex and allowed to stand overnight.

HPLC: Rt = 13.78 min (column III, method 5)

4.7. Synthesis of Lanthanide(III) complexes

[Sm(do2a2p)]$^{3-}$ for NMR studies

5 mg of ligand were dissolved in 0.3 mL of D_2O. The pH of the ligand solution was set to 6 by the addition of freshly prepared KOD. An equimolar amount of samarium chloride dissolved in 0.2 mL of D_2O was added and the solution was allowed to stand overnight. The pH of the final solution was raised until no changes in the ^{31}P-NMR were observed. Both ^{1}H, ^{13}C and ^{31}P-NMR spectra were then recorded (pH=8.38).

^{1}H-NMR (D_2O), δ/ppm: 8.95 (d, 2H, NCH_2COOH), 6.53 (t, 2H, NCH_2CH_2N), 5.70 (t, 2H NCH_2P(O)$(OH)_2$), 4.08 (t, 2H, NCH_2COOH), 3.25 (s, 4H, NCH_2CH_2N and NCH_2P(O)$(OH)_2$), 0.73 (d, 2H, NCH_2CH_2N), 0.57 (d, 2H, NCH_2CH_2N), 0.19 (d, 2H, NCH_2CH_2N) 0.02 (d, 2H, NCH_2CH_2N), -2.72 (d, 4H, NCH_2CH_2N).

^{13}C-NMR (D_2O/tert-butyl alcohol), δ/ppm: 188.1 (COOH), 66.9 (CH_2COOH), 60.1 (d, CH_2P(O)$(OH)_2$, $^1J_{CP}$=140Hz), 53.4 (d, NCH_2CH_2N,. $^3J_{CP}$=18Hz), 49.4 (d, $^3J_{CP}$=15Hz, NCH_2CH_2N), 47.8 (NCH_2CH_2N).

^{31}P-NMR (D_2O), δ/ppm: 20.74.

Synthesis of Sm^{3+}/do2a2p complexes for X-ray diffraction analysis

To 5 mL of a 10 mM aqueous solution of *trans*-do2a2p, at pH 8-9, was added a stoichiometric amount of $SmCl_3$. The solution was heated to 50ºC for 3h, with continuous adjustment of the pH to 8 with a diluted solution of NaOH (1 M). After this time, the reaction mixture was allowed to stand at room temperature for 18h, and filtered trough a SEP-PAK C_{18} cartridge (to remove any free Sm^{3+}). Then, the pH of the filtered solution was lowered to 5-4, with diluted HCl, and the volume reduced to 2mL. The solution was transferred to a small vial, which was maintained in *iso*-propanol/ethanol solution environment. After 3-4 months, X-ray quality crystals were obtained.

Crystal data for Sm^{3+}/do2a2p complexes:

1. **$H[Sm(do2a2p)].5H_2O.3HCl$:** $C_{14}H_{36}Cl_3N_4O_{15}P_2Sm$; M= 819.11 $gmol^{-1}$; Monoclinic, C2/m; a = 17.4326(6), b = 18.3213(7), c = 8.9789(3) Å; V = 2867.50(18) $Å^3$, Z = 4; Dcalc= 1.897 g/cm^3.
2. **$H[Sm(do2a2p)(H_2O)].8.5H_2O.2.5HCl$:** $C_{28}H_{95}Cl_5N_8O_{39}P_4Sm_2$; M= 1769.95 $gmol^{-1}$; Triclinic, P-1; a = 11.6092(3), b = 15.2134(4), c = 19.2251(5) Å; V = 3237.10(15) $Å^3$, Z = 2; Dcalc= 1.816 g/cm^3.

4.8. Solution Studies

The potentiometric solution studies with the different ligands were studied in different places, and therefore different equipments were used.

Potentiometry for the ligands do1SH and bz2ac was performed under the supervision of Dr. Rita Delgado, at the Instituto de Tecnologia Química e Bioquímica (ITQB), Oeiras, Portugal. Potentiometric studies for *trans*-do2a2p were performed under the supervision of Dr. Petr Hermann, at the Department of Inorganic Chemistry of the Universita Karlova (UK), Prague, Czech Republic. Finally, the studies of the ligand do3aSH were done by Dr. Petra Fousková and Dr. V. Kubíček, under the supervision of Dr. Eva Toth's laboratory at Centre de Biophysique Moléculiare, Orléans, France. These studies were performed under a FCT project ITN/ITQB (coordination: I. Santos, ITN), a Bilateral project between Portugal (ITN)/Czech Republic (UK) and under the COST D38.

4.8.1. bz2ac and do1SH

Reagents and solutions

Metal ion solutions were prepared at about 2.5×10^{-3} mol dm^{-3} from the nitrate salts of the metals and were titrated using standard methods [234]. Deionised (Millipore/Milli-Q System) distilled water was used. Carbonate-free solutions of the KOH titrant were prepared, maintained and discarded when the percentage of carbonate was about 0.5% of the total amount of base [235].

Equipment and work conditions

The equipment was used as described before [203,204]. The temperature was kept at 25.0 ± 0.1 ºC, atmospheric CO_2 was excluded from the cell during the titrations by passing purified nitrogen across the top of the experimental solution in the reaction cell. The ionic strength of the solutions was kept at 0.10 mol dm^{-3} with KNO_3.

Measurements

The $[H^+]$ of the solutions was determined by the measurement of the electromotive force (emf) of the cell, $E = E^{o\prime} + Q \log [H^+] + E_j$ [***Equation 4.2***]. $E^{o\prime}$, Q, E_j and $K_w = ([H^+][OH^-])$ were obtained as described previously [203,204]. The value of K_w was found equal to $10^{-13.80}$ (mol $dm^{-3})^2$. The potentiometric equilibrium measurements were made on 20.00 cm^3 of ≈ 2.00×10^{-3} mol dm^{-3} ligand solutions diluted to a final volume of 30.00 cm^3, in the absence of metal ions and in the presence of each metal ion for which the C_M : C_L ratio was 1:1. A minimum of two replicate measurements was taken. The emf data were taken after additions of 0.050 cm^3 increments of standard KOH solution, and after stabilisation in this direction, equilibrium was then approached from the other direction adding standard nitric acid.

For determination of the stability constants, out-of-cell titrations were performed in the pH region from which the direct and back titrations were not superimposed. In such regions, independent vials each one at different pH were prepared and left to equilibrate in a water bath at 25.0 ºC and the corresponding pH values checked every week till stabilisation of the pH, which occurred generally within 2-4 weeks.

Calculation of equilibrium constants

Overall protonation constants, β_i^H were calculated by fitting the potentiometric data obtained for the free ligand with HYPERQUAD program [179]. Stability constants of the various species formed in solution were obtained from the experimental data

corresponding to the titration of solutions of the different metal ions, each of them with different metal to ligand ratios, also using the HYPERQUAD program. The initial computations were obtained in the form of overall stability constants, $\beta_{M_mH_hL_l}$ values, $\beta_{M_mH_hL_l} = [M_mH_hL_l]/([M]^m \times [H]^h \times [L]^l)$ [***Equation 4.3***]. Differences, in log units, between the values $\beta_{M(HL)}$ (or $\beta_{MLH_{-1},}$) and β_{ML} provide the stepwise reaction constants. The species considered in a particular model were those that could be justified by the principles of co-ordination chemistry. The errors quoted are the standard deviations of the overall stability constants given directly by the program for the input data, which include all the experimental points of all titration curves. The hydrolysis constants of the metal ions were taken from the literature and kept constant for the calculations [236].

NMR Titration

The electrode was calibrated with standard buffer solutions and the final pD was calculated according to the equation *Equation 4.1* [157]. The solutions (≈ 2×10^{-3} M) used for the ^{13}C-NMR titration measurements were made up in D_2O and the pD value was adjusted by adding DCl or freshly prepared CO_2-free KOD. The solutions were allowed to stabilize and the pD values were measured directly in the NMR-tube with a combination microelectrode.

4.8.2. do3aSH

Potentiometric titration

Titrations were carried out in a cell thermostated at 25°C, at an ionic strength 0.1 mM KCl, using a combined glass electrode (LL Biotrode, Metrohm) connected to a Metrohm Titrino 702 automatic burette. The initial volume was 3 mL. An inert atmosphere was ensured by constant passage of N_2 through the solution. For the determination of the ligand protonation constants, the concentration of the ligand was 4 mM and the titration was carried in the presence of extra HCl in the –log[H^+] range 1.7–11.5. For the determination of the complex protonation constants, the concentration of the complex was 1 mM. The complex was pre-prepared as follows: The ligand and the metal solutions were mixed in the titration cell, KOH solution was added stepwise to reach pH ~ 9 and the mixture was stirred. After 2 hours, HCl was added to reach pH ~ 5.

The stability constant is defined according to *Equation 4.3*. The constants (with standard deviations) were calculated with program OPIUM [169]. The program

minimizes the criterion of the generalized least-squares method using the calibration function $E = E_0 + S \times \log[H^+] + j_A \times [H^+] + j_B \times K_w / [H^+]$, where the additive term E_0 contains the standard potentials of the electrodes used and contributions of inert ions to the liquid-junction potential, S corresponds to the Nernstian slope and $j_A \times [H^+]$ and $j_B \times [OH^-]$ terms are contributions of the H^+ and OH^- ions to the liquid-junction potential. It is clear that j_A and j_B cause deviation from a linear dependence between E and $-\log[H^+]$ only in strong acid and strong alkaline solutions. The calibration parameters were determined from titration of standard HCl with standard KOH before any titration of the ligand to give a pair of calibration titrations used for calculations of the constants.

UV-Vis

Measurements were carried out on a PERKIN ELMER Lambda 19 spectrometer in the region 200–350 nm with data steps of 1 nm. A constant temperature of 25°C was maintained by using thermostatisable cells with a 1 cm optical length. The ligand concentrations were ~0.5 mM. The formation kinetics of Ce^{3+} complex was studied at pH 4.7 (50 mM N-methylpiperazine buffer), 6.0 (50 mM urotropine buffer) and 7.6 (50 mM HEPES buffer). The titrations were carried at an ionic strength of 0.1 mM KCl. Each point was prepared in a separate eppendorf tube and equilibrated for 14 days at room temperature. After another 7 days, the measurement was repeated to confirm the thermodynamic equilibrium. The values of the stability constant were calculated with program OPIUM [169] by simultaneous treatment of the data in the range 245-305 nm.

NMR Titration

The electrode was calibrated with standard buffer solutions and the final pD was calculated according to the *Equation 4.1* [157]. 0.034g of *trans*-do2a2p were dissolved in 0.3mL of D_2O. This solution (≈ 2×10^{-3} M) was used for the ^{13}C-NMR titration measurements and the pD value adjusted by adding DCl or freshly prepared CO_2-free KOD. The solutions were allowed to stabilize and the pD values were measured directly in the NMR-tube with a combination microelectrode.

4.8.3. *trans*-do2a2p

Reagents and stock solutions

The stock solution of hydrochloric acid (~0.03 mol dm^{-3}) was prepared from 35% aqueous solution (puriss, Fluka). Comercial NMe_4OH solution (99%, Fluka) was recristallized from boiling i-PrOH and the solid salt was dried over P_2O_5 in vacuum to constant weight (this dried form of the salt is extremely hydroscopic). Carbonate-free NMe_4OH solution (~0.2 mol dm^{-3}) was prepared from NMe_4Cl using ion exchange Dowex 1 in the OH^- form (elution with carbonate-free water, under argon). The hydroxide solution was standadirzed against potassium hydrogen phthalate and the HCl solution against ca. 0.2 M NMe4OH solution. Stock solutions of the individual metal cations were prepared by dissolving hydrates of $LnCl_3$ (99.9%, Strem) or $M(NO_3)_2$ (). The metal content in the solutions was determined by titration with a standard Na_2H_2edta solution. Analytical concentration of a stock solution of the ligand was determined together with refinement of protonation constants using OPIUM software package (see below).

Measurements

Titrations were carried out in a vessel thermostatted at 25.0 ± 0.1 °C, at ionic strength I = 0.1 mol dm^{-3} (NMe_4Cl) and in the presence of extra HCl in the pH range 1.7–11.9 using a PHM 240 pH-meter, a 2 mL ABU 900 automatic piston burette and a GK 2401B combined electrode (all Radiometer, Denmark). The initial volume was 5 mL and the concentration of the ligand was ~0.004 mol dm^{-3}. Five parallel titrations were carried out; each titration consisted of about 40 points. An inert atmosphere was ensured by constant passage of argon saturated with the solvent vapour. Titrations with metal ions were performed at metal-to-ligand molar ratios 1:1 and 2:1. In the case of lanthanides the complexation was too slow for conventional titration and therefore the "out-of-cell" method was used. Each titration consisted of 25 points in the pH range 1.8–6.0 (at least two titrations for each 1:1 and 2:1 metal-to-ligand ratio). Equilibrium was reached after 3 weeks. The constants determined by this technique showed higher standard deviations due to less precise measurements and a smaller number of experimental points.

Calculation of equilibrium constants

The constants (with standard deviations) were calculated with program OPIUM [169]. The program minimizes the criterion of the generalized least-squares method using the calibration function

$$E = E_0 + S \log [H]^+ + j_1[H]^+ + j_2 K_w / [H]^+ \quad [\textbf{\textit{Equation 4.4}}]$$

where the additive term E_0 contains the standard potentials of the electrodes used and contributions of inert ions to the liquid-junction potential, S corresponds to the Nernstian slope, the value of which should be close to the theoretical value and the $j_1[H^+]$ and $j_2[OH^-]$ terms are the contributions of the H+ and OH^- ions to the liquid-junction potential. It is clear that j_1 and j_2 cause deviation from a linear dependence of E on pH only in strongly acidic and strongly alkaline solutions. The calibration parameters were determined from titration of standard HCl with standard NMe_4OH before each ligand or ligand–metal titration to give a pair of calibration/titration, which was used for calculations of the constants. The protonation constants ß*n* are concentration constants, defined by $ß_n = [H_nL]/([H]^n[L])$ [***Equation 4.5***] (they were transformed to dissociation constants as $pK_1 = \log ß_1$ and $pK_n = \log ß_n - \log ß_{n-1}$). The stability constants are defined according to *Equation 4.3*. The water ion product p*K*w (13.81) and stability constants of Ln^{3+}–OH^- systems included into the calculations were taken from refs [237].

NMR titrations

The $^{31}P\{^1H\}$ NMR titration experiment for determination of the highest protonation constant (pH range 12.5–13.6, about 30 points) was carried out under the conditions close to the potentiometric titrations (0.1 M $NMe_4(Cl,OH)$; no control of ionic strength, 25.0 °C, ligand concentration ~0.004 mol dm^{-3}). A coaxial capillary tube with D_2O was used for the lock. Protonation contants were calculated with OPIUM from δP of the phosphonate group.

NMR titrations over the whole pD region were performed at 25.0 °C in D_2O at ligand concentration 0.05 mol dm^{-3}. Solution pD (1–14) was adjusted with freshly prepared KOD or DCl solutions and measured with a pH-meter calibrated with standard buffers. The final pD was calculated according to the *Equation 4.1* [157].

4.9. EPR studies

EPR spectroscopic measurements of the copper complex were recorded with a Bruker ESP 380 spectrometer equipped with continuous-flow cryostats for liquid nitrogen, operating at X-band. The Cu-bz2ac complexes (≈ 2×10^{-3} mol dm^{-3} in 1:1 DMSO:H_2O solution) were prepared at pH 3.51, 6.37 and 10.26 and the results were recorded at 96 K. The EPR spectrum of a 1:1 DMSO/ H_2O solution of **C1** (at pH 3.23) was also recorded.

The Cu^{2+}/do1SH complexes (≈ 1.6×10^{-3} mol dm^{-3} in 40% DMSO/H_2O solution) were prepared at pH 5, 8 and 12 and were recorded at 104 K. The EPR spectra of Cu^{2+}/cyclen complexes were recorded at the same pH values and using the same experimental conditions, for comparison.

4.10. Synthesis of $^{64/67}$Cu complexes

General method for the synthesis of $^{64/67}$Cu-complexes

An aqueous solution of $^{64}Cu(OAc)_2$ (50µL, 5MBq) was added to 10µL of solutions of ligand in 90µL of buffer solution (pH 5.5 to 8). The reaction mixtures were stirred for 30min and checked by TLC or HPLC.

The labelling reactions of bz2ac and do3aSH were followed by TLC, using the conditions presented in table 4.1.

Table 4.1: TLC systems for the follow-up of the $^{64/67}$Cu reactions (RP-18, Methanol / NH_4OAc 10% (50:50))

Ligand	Rf_{ligand}	Rf_{Cu}	$Rf_{Cu\ complex}$	$Rf_{64\text{-}Cu\ complex}$
bz2ac	0.70	0	0.79	0.8
do3aSH	0.40	0	0.65	0.2 0.8

For bz2ac-Lys-Fmoc and bz2ac-$(Lys\text{-}Fmoc)_2$ we have used HPLC. The conditions found for each ligand are shown in table 4.2.

Table 4.2: HPLC systems for the follow-up of the ^{64}Cu reactions (column III, method 5)

Ligand	"Cold" complexes (UV-Vis detector)			"Hot" complexes (γ detector)	
	Rt_{ligand}	Rt_{Cu}	$Rt_{Cu\ complex}$	Rt_{Cu}	$Rt_{Cu\ complex}$
bz2ac-Lys-Fmoc	18.10	2.5	11.91	3.17	14.93
Bz2ac-$(Lys\text{-}Fmoc)_2$	19.96	2.0	13.78		18.40 18.93

pH Dependence

100 μL of an aqueous solution of ligand (final concentration: 10^{-4} M) in different buffer solutions, with pH values between 5.5 and 8, were added to 50 μL of $^{64}Cu(OAc)_2$ and the mixture stirred at room temperature. An aliquot of the mixtures was analyzed by TLC or HPLC to determine the degree of complexation after 30 min.

Kinetic Studies

100 μL of an aqueous solution of ligand (10^{-4} M in HEPES buffer pH 7) and 50 μL of $^{64}Cu(OAc)_2$ were added and the mixture stirred. Aliquots of the mixtures were analyzed by TLC or HPLC to determine the degree of complexation. Samples were taken after 1, 5, 10, 30, 60 and 240 min.

Concentration Dependence

To 100 μL aqueous solution of ligand (10^{-3} M, 10^{-4} M, and 10^{-5} M in HEPES buffer pH 7), 50 μL of $^{64}Cu(OAc)_2$ was added and the mixture stirred. The mixtures were shaken for 20 min and then analyzed by TLC or HPLC.

Challenge Studies in the Presence of a Competing Ligand: cyclam or teta

A solution containing 100 kBq $^{64}CuCl_2$ was added to 500 μg of ligand dissolved in 100 μL of 0.1 M NH_4OAc. After 10 min, full complexation of the ligand was checked by TLC. Cyclam (40 mg, more than 100-fold excess) dissolved in 1 mL of 0.1 M NH_4OAc was then added to the complex solution, which was stirred for 24h. Aliquots of the mixtures were assayed by TLC or HPLC to determine the degree of decomposition.

***In Vitro* Stability**

The *in vitro* stability of the ^{64}Cu-complexes was analyzed using rat arterial blood samples at different time points (0.5, 2 and 24h). The samples were incubated at 37ºC. An aliquot of 300 μL was taken after 2 and 24h, cold ethanol was added and the solution was centrifuged to precipitate the blood cells. The supernatant was taken and the procedure was repeated twice. The total supernatant was collected and concentrated. The residue was taken in CH_3CN/H_2O and was analysed by TLC or HPLC.

4.11. Synthesis of ^{153}Sm and ^{166}Ho Complexes and in Vitro Assays

Synthesis of ^{153}Sm/^{166}Ho-do3aSH ^{153}Sm-do3a, ^{153}Sm/^{166}Ho-do2a2p, ^{153}Sm/^{166}Ho-do3ap, ^{153}Sm/^{166}Ho-do3ap^{Pr} and ^{153}Sm/^{166}Ho-do3ap^{ABn}

Radiolabelling of the macrocyclic ligand was performed by dissolving 5mg of the ligand in 0.4mL double-distilled water followed by the addition of an adequate amount of ^{153}Sm or ^{166}Ho solutions to achieve a 2:1 ligand-to-metal molar ratio. The pH was adjusted to the desired value with a freshly prepared 1.0 M NaOH solution. The labelling was optimized by changing the pH (from 5 to 10), the temperature and the time of reaction.

Labelling efficiency, chelation kinetics and stability of the radiolanthanide complexes were followed by ascending silica gel ITLC developed with the mobile phase MeOH:H_2O:NH_4OH (2:4:0.2). In this system all the ^{153}Sm/^{166}Ho complexes migrate with R_f = 1.0, except ^{153}Sm-do3a which has R_f = 0.8. $^{153}Sm(NO_3)_3$ and $^{166}Ho(NO_3)_3$ remain at the origin. The colloidal radioactive forms, if present, also remain at the origin. These species can be assessed by ascending instant thin layer chromatography using silica gel ITLC strips developed with saline. In this system both, the radiolanthanide complexes and ^{153}Sm/$^{166}Ho(NO_3)_3$ migrate with R_f = 1.0.

Table 4.3: Labelling conditions for radiolanthanide complexes.

	^{153}Sm-macrocyclic complexes		^{166}Ho-macrocyclic complexes	
Ligand	**Labelling conditions**	**Labelling Efficiency**	**Labelling conditions**	**Labelling efficiency**
do2a2p	30 min RT, pH 6-9	> 98%	30 min RT, pH 6-9	> 98%
do3ap	15 min RT, pH 6-9	> 98%	15 min RT, pH 6-9	> 98%
doa3p^{Pr}	15 min RT, pH 7-9	> 98%	15 min RT, pH 7-9	> 98%
do3ap^{ABn}	15 min RT, pH 7	> 98%	15 min RT, pH 7	> 98%
do3a	5 min RT, pH 6-8	> 98%	-----	
do3aSH	5 min RT, pH 6	> 98%	5 min RT, pH 6	> 98%

Kinetic Studies

Aliquots of the reaction mixtures (1 μL) were analyzed by ITLC, using the eluent systems referred above, to determine the degree of complexation. Samples were taken after 1, 5, 15, 30, 60, 120 and 240 min.

In vitro studies

In vitro stability studies

The *in vitro* stability of the complexes was evaluated in saline, 0.1 M phosphate buffer (pH 7.4), 0.1 M Tris-HCl buffer (pH 7.4), 0.1 M glycine-HCl solution (pH 4.0) and human serum, at 37 ºC at various time points (1, 2, 3, 4 and 5 days). Typically, 50 μL of each ^{153}Sm- or ^{166}Ho-complexes were added to 100 μL of the different solutions and stored at 37ºC. Daily, an aliquot of each mixture was taken and evaluated by ITLC analysis, as described above. The percentage of the radiochemical impurities was then calculated.

Lipophilicity

Lipophilicity was assessed by determination of the partition coefficient (*P*) *n*-octanol/ saline and expressed as *log P*. A "shake-flask" method was used: 100 μL of each radiolanthanide complex was added to a solution containing 1 mL of saline (pH 7.4) (previously saturated with *n*-octanol solution) and 1 mL of *n*-octanol. The resulting solutions were vortexed and centrifuged at 3000 rpm for 10 min. Three aliquots of 100 μL were removed from the *n*-octanol phase and from the water phase and the activity measured in a gamma counter. The lipophilicity was calculated as the average $logP_{O/W}$, being $P_{O/W}$ as defined in Equation 4.6:

$$P_{O/W} = \frac{A_O}{A_W} \qquad \textbf{[Equation 4.6]}$$

A_O = activity of the organic fraction

A_w = activity of the aqueous fraction

Protein binding

Plasmatic protein binding was determined by a trichloroacetic acid (TCA) precipitation method: 50 μL of a complex solution was incubated with 500 μL of human blood plasma for 1h at 37ºC. An aliquot of this solution (100 μL) was added to 1 mL of TCA. This mixture was centrifuged and the supernatant separated. The precipitation procedure was repeated twice and the supernatant solution and the precipitated were measured in a gamma-counter. The percentage of protein binding is given by the ratio between the activity of the precipitate (A_{pp}) and the total activity used for the assay (A_{total}):

$$\%\ protein\,binding = \frac{A_{pp}}{A_{total}} \qquad \textbf{[Equation 4.7]}$$

Challenge Studies in the Presence of Cysteine and Glutathione

100 μL of the radiocomplex were incubated at 37ºC, in the presence of 500 μL of different concentrations of cysteine (0.5 and 2 mM) and glutathione (1 and 10 mM). Aliquots of these solutions were taken after 0.3, 2 and 24h and their stability was analysed by ITLC.

Hydroxyapatite Adsorption Studies.

Adsorption of the $^{153}Sm/^{166}Ho$-do2a2p, $^{153}Sm/^{166}Ho$-do3ap, $^{153}Sm/^{166}Ho$-do3ap^{Pr} and $^{153}Sm/^{166}Ho$-do3ap^{ABn} complexes onto hydroxyapatite (HA) was determined by incubation of those complexes with different amounts of HA. Briefly, 50 μL of the complex (3-5 MBq/50 μL) was incubated for 1 h at room temperature with 5, 10, 25, 50, 100 and 150 mg of HA in 2 mL of 0.1 M Tris-HCl buffer (pH 7.4). Immediately after incubation, the mixture was centrifuged and the liquid phase separated. The solid phase was washed twice with 2.5 mL of 0.1 M Tris-HCl buffer (pH 7.4). Washing buffer was pooled with liquid phase. The radioactivity in the liquid and solid phases was measured in a dose calibrator. The HA adsorption is determined by the ratio between the activity of the liquid phase and the total activity of both phases:

$$\%\,HA binding = \frac{A_{liquid\ phase}}{A_{total}} \quad being \quad A_{total} = A_{liquid\ phase} + A_{solid\ phase} \qquad \textbf{[Equation 4.8]}$$

4.12. *In vivo* Studies

Biodistribution Studies

The *in vivo* behaviour of the radioactive complexes was evaluated in groups of 4-5 female CD-1 mice (randomly bred, from Charles River Laboratories, Spain) weighing approximately 20-22 g. Animals were intravenously (i.v.) injected through tail vein with 100 μL (10-15 MBq/100 μL) of the radiolanthanide complex, were maintained on normal diet *ad libitum* and were sacrificed by cervical dislocation at 30 minutes, 2 h and 24 h post injection, according to a previously described method [203]. Results were expressed as percentage of injected dose per gram of organ (% I.D./g organ $\pm$ SD). Whole body excretion of the radioactivity was assumed to be the difference between the measured radioactivity in the injected and sacrificed animal and was expressed as percentage of injected dose (% I.D.).

The *in vivo* stability of the complexes was assessed by urine and blood ITLC analysis, using the above referred experimental conditions for the radiochemical purity evaluation.

Animal experiments were carried out in accordance with the guidelines on the use of living animal in scientific investigation, and followed the principles of laboratory animal care.

Biodistribution results

The biodistribution results obtained in CD-1 mice with the radiolanthanide complexes studied are presented in the following tables.

Table 4.4: Biodistribution results of ^{153}Sm-do3aSH (%I.D./g organ ± SD) in mice (n = 4).

Organ	^{153}Sm –do3aSH	
	30 min	2 h
Blood	2.8 ± 0.5	0.5 ± 0.2
Liver	1.6 ± 0.2	0.9 ± 0.1
Intestine	0.6 ± 0.2	0.5 ± 0.1
Spleen	0.15 ± 0.02	0.21 ± 0.07
Heart	0.8 ± 0.1	0.20 ± 0.05
Lung	1.6 ± 0.4	0.7 ± 0.3
Kidney	4.1 ± 0.5	1.7 ± 0.1
Muscle	0.4 ± 0.3	0.19 ± 0.09
Bone	1.1 ± 0.3	0.8 ± 0.2
Stomach	0.8 ± 0.3	0.3 ± 0.1
Carcass (%I.D.)	31.5 ± 5.1	12.8 ± 7.7
Excretion (%I.D.)	49.2 ± 8.9	79.7 ± 3.9

Table 4.5: Biodistribution results of ^{153}Sm-do3a (%I.D./g organ ± SD) in mice (n = 4).

Organ	^{153}Sm –do3a	
	30 min	2 h
Blood	0.87 ± 0.05	0.09 ± 0.04
Liver	0.78 ± 0.08	0.3 ± 0.1
Intestine	0.2 ± 0.1	0.4 ± 0.2
Spleen	0.29 ± 0.09	0.06 ± 0.01
Heart	0.3 ± 0.1	0.03 ± 0.01
Lung	0.7 ± 0.1	0.18 ± 0.05
Kidney	6.0 ± 2.0	6.0 ± 2.5
Muscle	0.24 ± 0.08	0.02 ± 0.01
Bone	0.5 ± 0.2	0.10 ± 0.04
Stomach	0.3 ± 0.2	0.4 ± 0.3
Carcass (%I.D.)	11.7 ± 0.1	2.5 ± 0.4
Excretion (%I.D.)	81.2 ± 0.1	90.3 ± 2.2

Table 4.6: Biodistribution results of ^{153}Sm/^{166}Ho-do2a2p (%I.D./g organ ± SD) in mice (n = 4).

Organ	^{153}Sm –do2a2p		^{166}Ho-do2a2p	
	30 min	2 h	30 min	2 h
Blood	2.4 ± 0.9	0.09 ± 0.03	0.5 ± 0.2	0.06 ± 0.02
Liver	0.9 ± 0.2	0.05 ± 0.01	0.6 ± 0.1	< 0.02
Intestine	1.0 ± 0.4	0.6 ± 0.2	0.56 ± 0.01	0.26 ± 0.07
Spleen	0.15 ± 0.02	0.04 ± 0.02	0.10 ± 0.01	0.03 ± 0.01
Heart	0.10 ± 0.03	< 0.01	0.08 ± 0.01	< 0.01
Lung	0.31 ± 0.03	0.02 ± 0.01	0.22 ± 0.03	0.010 ± 0.005
Kidney	4.0 ± 0.6	0.35 ± 0.07	3.3 ± 0.5	0.18 ± 0.02
Muscle	0.5 ± 0.1	0.06 ± 0.01	0.08 ± 0.02	0.02 ± 0.01
Bone	1.6 ± 0.2	0.18 ± 0.05	2.2 ± 1.4	0.23 ± 0.03
Stomach	1.20 ± 0.04	0.07 ± 0.01	0.11 ± 0.03	0.06 ± 0.01
Carcass (%I.D.)	34.5 ± 16.5	2.6 ± 0.2	18.6 ± 3.5	3.8 ± 0.3
Excretion (%I.D.)	57.0 ± 15.1	95.3 ± 1.8	71.2 ± 2.8	93.1 ± 0.9

Table 4.7: Biodistribution results of $^{153}Sm/^{166}Ho$-do3ap (%I.D./g organ ± SD) in mice (n = 4).

Organ	^{153}Sm –do3ap		^{166}Ho-do3ap	
	30 min	2 h	30 min	2 h
Blood	1.1 ± 0.3	0.04 ± 0.01	3.0 ± 0.9	0.05 ± 0.02
Liver	0.5 ± 0.2	0.07 ± 0.01	0.4 ± 0.1	0.19 ± 0.02
Intestine	1.4 ± 1.0	0.4 ± 0.2	0.4 ± 0.1	0.20 ± 0.03
Spleen	0.4 ± 0.2	0.09 ± 0.04	0.6 ± 0.3	0.16 ± 0.06
Heart	0.4 ± 0.1	0.02 ± 0.01	0.7 ± 0.2	0.04 ± 0.01
Lung	0.9 ± 0.4	0.05 ± 0.02	1.1 ± 0.7	0.08 ± 0.01
Kidney	2.6 ± 0.4	0.8 ± 0.1	3.0 ± 0.8	2.44 ± 0.02
Muscle	0.4 ± 0.2	0.02 ± 0.01	0.7 ± 0.3	0.06 ± 0.01
Bone	0.7 ± 0.4	0.14 ± 0.05	1.4 ± 0.4	0.30 ± 0.02
Stomach	0.8 ± 0.4	0.53 ± 0.04	0.5 ± 0.1	0.14 ± 0.02
Carcass (%I.D.)	16.0 ± 6.3	1.4 ± 0.2	11.3 ± 3.6	1.4 ± 0.3
Excretion (%I.D.)	71.5 ± 9.6	94.5 ± 1.4	83.6 ± 4.5	96.7 ± 1.0

Table 4.8: Biodistribution results of $^{153}Sm/^{166}Ho$-do3ap^{PrA} (%I.D./g organ ± SD) in mice (n = 4).

Organ	^{153}Sm –do3ap^{PrA}		^{166}Ho-do3ap^{PrA}	
	30 min	2 h	30 min	2 h
Blood	1.4 ± 0.2	0.02 ± 0.01	4.0 ±0.5	0.03 ± 0.01
Liver	0.9 ± 0.1	0.08 ± 0.01	0.47 ± 0.05	0.10 ± 0.02
Intestine	0.25 ± 0.04	0.3 ± 0.1	0.6 ± 0.2	0.15 ± 0.06
Spleen	0.4 ± 0.1	0.04 ± 0.03	1.2 ± 0.6	0.05 ± 0.02
Heart	0.28 ± 0.06	0.02 ± 0.01	1.0 ± 0.1	0.02 ± 0.01
Lung	0.8 ± 0.1	0.05 ± 0.01	2.2 ± 0.3	0.04 ± 0.01
Kidney	4.4 ± 1.5	1.1 ± 0.2	2.6 ± 0.8	0.9 ± 0.1
Muscle	0.4 ± 0.2	0.02 ± 0.01	0.6 ± 0.2	0.02 ± 0.01
Bone	0.40 ± 0.09	0.03 ± 0.01	1.1 ± 0.3	0.04 ± 0.01
Stomach	0.29 ± 0.02	0.3 ± 0.1	0.9 ± 0.2	0.4 ± 0.1
Carcass (%I.D.)	14.5 ± 2.3	1.9 ± 0.7	11.2 ± 3.1	0.56 ± 0.04
Excretion (%I.D.)	75.0 ± 6.7	94.9 ± 1.5	81.9 ± 3.8	98.2 ± 0.6

Table 4.9: Biodistribution results of $^{153}Sm/^{166}Ho$-do3ap^{ABn} (%I.D./g organ ± SD) in mice (n = 4).

Organ	^{153}Sm –do3ap^{ABn}		^{166}Ho- do3ap^{ABn}	
	30 min	2 h	30 min	2 h
Blood	1.5 ± 0.3	0.03 ± 0.01	1.0 ± 0.2	0.05 ± 0.01
Liver	1.1 ± 0.1	0.34 ± 0.06	1.5 ± 0.2	1.2 ± 0.1
Intestine	0.8 ± 0.2	0.35 ± 0.06	0.22 ± 0.06	0.3 ± 0.2
Spleen	0.5 ± 0.2	0.04 ± 0.01	0.4 ± 0.1	0.6 ± 0.1
Heart	0.5 ± 0.2	0.03 ± 0.02	0.27 ± 0.01	0.04 ± 0.01
Lung	1.0 ± 0.3	0.04 ± 0.02	2.4 ± 1.0	0.44 ± 0.06
Kidney	5.1 ± 1.1	1.2 ± 0.1	3.1± 0.7	2.0 ± 0.3
Muscle	0.3 ± 0.1	0.02 ± 0.01	0.26 ± 0.05	0.03 ± 0.01
Bone	0.4 ± 0.2	0.04 ± 0.01	0.26 ± 0.04	0.14 ± 0.01
Stomach	0.8 ± 0.3	0.07 ± 0.03	0.19 ± 0.04	0.13 ± 0.01
Carcass (%I.D.)	16.6 ± 4.3	3.1 ± 1.5	9.4 ± 2.7	-
Excretion (%I.D.)	67.4 ± 11.1	92.8 ± 1.5	78.9 ± 3.9	92.5 ± 0.1

REFERENCES

1. P. Blower, "Towards molecular imaging and treatment of disease with radionuclides: the role of inorganic chemistry", *Dalton Trans.*, **2006**, 1705–1711.

2. "Radioisotopes in medicine" in http://world-nuclear.org/info/inf55.html, January **2008**.

3. R. Weissleder, U. Mahmood, "Molecular Imaging", *Radiology*, **2001**, *219*, 316-333.

4. S. Liu, "The role of coordination chemistry in the development of target-specific Radiopharmaceuticals", *Chem. Soc. Rev.*, **2004**, *33*, 445-461.

5. S. Liu, "Bifunctional coupling agents for radiolabeling of biomolecules and target-specific delivery of metallic radionuclides", *Advanced Drug Delivery Reviews*, **2008**, *60*, 1347-1370.

6. G.B. Saha, "Fundamentals of Nuclear Pharmacy", 5th Ed, Springer-Verlag, New York, **2004**.

7. R.J. Kowalsky and S.W. Falen, "Radiopharmaceuticals in Nuclear Pharmacy and Nuclear Medicine", vol. 1-3, 2nd Edition, American Pharmacists Association, Washington, **2004**.

8. J.F.W. Nijsen, G.C. Krijger and A.D. Van het Schip, "The Bright Future of Radionuclides for Cancer Therapy", *Anti-Cancer Agents in Medicinal Chemistry*, **2007**, *7*, 271-290.

9. (a) A.R. Kherlopian, T. Song, Q. Duan, M.A. Neimark, M.J. Po, J.K. Gohagan and A.F. Laine, "A review of imaging techniques for systems biology", *BMC Systems Biology,* **2008**, *2*, 74; (b) T.F. Massoud, S.S. Gambhir, "Molecular imaging in living subjects: seeing fundamental biological processes in a new light", *Genes Dev.*, **2003**, *17*, 545-580.

10. R. Weissleder and M. J. Pittet, "Imaging in the era of molecular oncology", *Nature*, **2008**, *452*, 580-589.

11. T.J. Wadas, E.H. Wong, G.R. Weisman and C.J. Anderson, "Copper Chelation Chemistry and its Role in Copper Radiopharmaceuticals", *Current Pharmaceutical Design*, **2007**, *13*, 3-16.

12. P.A. Salvadori, "Radiopharmaceuticals, Drug Development and Pharmaceutical Regulations in Europe", *Current Radiopharmaceuticals*, **2008**, *1*, 7-11.

13. D.E. Reichert, J.S. Lewis and C.J. Anderson, "Metal complexes as diagnostic tools", *Coord. Chem. Rev.*, **1999**, *184*, 3-66.

14. D.M. Taylor and D.R. Williams, "Trace element Medicine and Chelation Therapy", The Royal Society of Chemistry Paperbacks, Cambridge, **1995**.

15. L. Giovagnini, S. Sitran, M. Montopoli, L. Caparrotta, M. Corsini, C. Rosani, P. Zanello, Q.P. Dou and D. Fregona, "Chemical and Biological Profiles of Novel Copper(II) Complexes Containing S-Donor Ligands for the Treatment of Cancer", *Inorg. Chem.*, **2008**, *47*, 6336-6343.

16. G.J. Brewer, "Copper in medicine", *Current Opinion in Chemical Biology*, **2003**, *7*, 207–212.

17. P.J. Blower, J.S. Lewis and J. Zweit, "Copper Radionuclides and Radiopharmaceuticals in Nuclear Medicine", *Nucl Med Biol.*, **1996**, *23*, 957-980.

18. C.J. Anderson, M.A. Green and Y.F. Yashi, "*Chemistry of copper radionuclides and radiopharmaceutical products*", in: M.J. Welch, C.S. Redvanly (Eds.), "Handbook of

Radiopharmaceuticals: Radiochemistry and Applications", John Wiley & Sons, New York, **2003**, pp. 402–422.

19. S.V. Smith, "Molecular imaging with copper-64", *J. Inorg. Biochem.*, **2004**, *98*, 1874-1901.

20. M.A. Green, "The potential for generator-based PET perfusion tracers", *J. Nucl. Med.*, **1993**, *31*, 1641–1645.

21. K.H. Thompson and C. Orvig, "Metal complexes in medicinal chemistry: new vistas and challenges in drug design", *Dalton Trans.*, **2006**, 761-764.

22. C.J. Anderson and M.J. Welch, "Radiometal labeled agents (non-technetium) for diagnostic imaging", *Chem. Rev.* **1999**, *99*, 2219–2234.

23. S. Liu, "The role of coordination chemistry in development of target-specific radiopharmaceuticals", *Chem. Soc. Rev*. **2004**, *33*, 1–18.

24. J.R. Morphy, D. Parker, R. Alexander, A. Bains, A.F. Carne, M.A.W. Eaton, A. Harrison, A. Millican, A. Phipps, S.K. Rhind, R. Titmas and D. Weatherby, "Antibody labeling with functionalized cyclam macrocycles", *J. Chem. Soc., Chem. Commun.*, **1988**, 156–158.

25. D. Parker, R. Morphy, K. Jankowski and J. Cox, "Implementation of macrocycle conjugated antibodies for tumor targeting", *Pure Appl. Chem.*, **1989**, *61*, 1637–1641.

26. W.P. Li, L.A. Meyer and C.J. Anderson, "Radiopharmaceuticals for positron emission tomography imaging of somatostatin receptor positive tumors", *Top. Curr. Chem.* **2005**, *252*, 179–192.

27. (a) L.J. Ackerman, D.X. West, C.J. Mathias and M.A. Green, "Synthesis and Evaluation of Copper Radiopharmaceuticals with Mixed Bis(thiosemicarbazone) Ligands" *Nucl. Med. Biol*. **1999**, *26*, 551-554; (b) N.G. Haynes, J.L. Lacy, N. Nayak, C.S. Martin, D. Dai, C.J. Mathias and M.A. Green, "Performance of a ^{62}Zn/^{62}Cu generator in clinical trials of the perfusion agent ^{62}Cu-PTSM."; *J Nucl Med.,* **2000**, *41*, 309–314.

28. P.J. Blower, J.S. Lewis and J. Zweit, "Copper Radionuclides and Radiopharmaceuticals in Nuclear Medicine", *Nucl. Med. Biol.*, **1996**, *23*, 957-980.

29. P.J. Blower, T.C. Castle, A.R. Cowley, J.R. Dilworth, P.S. Donnelly, E. Labisbal, F.E. Sowrey, S.J. Teat and M.J. Went, "Structural trends in copper(II) bis(thiosemicarbazone) Radiopharmaceuticals", *Dalton Trans.*, **2003**, 4416–4425.

30. J.S. Lewis, T.L. Sharp, R. Laforest, Y. Fujibayahsi and M.J. Welch, **"**Tumor Uptake of Copper-Diacetyl-Bis(N^4-Methylthiosemicarbazone): Effect of Changes in Tissue Oxygenation**",** *J. Nucl. Med.*, **2001**, *42*, 655-661.

31. M.A. Green, C.J. Mathias, L.R. Willis, R.K. Handa, J.L. Lacy, M.A. Miller and G.D. Hutchins, "Assessment of Cu-ETS as a PET radiopharmaceutical for evaluation of regional renal perfusion", *Nucl. Med. Biol.*, **2007**, *34*, 247–255.

32. M. Kodama, T. Yatsunami and E. Kimura, "Displacement kinetics of copper(II) macrocyclic triamines with EDTA and CyDTA", *Inorg. Chem.*, **1980**, *19*, 1600-1602.

33. G. Anderegg, F. Arnaud-Neu, R. Delgado, J. Felcman and K. Popov, "Critical Evaluation of Stability Constants of Metal Complexes of Complexones for Biomedical and Environmental Applications"**,** *Pure Appl.Chem.*, **2005**, *77*, 1445-1495.

34. M. Meyer, V. Dahaoui-Gindrey, C. Lecomte and R. Guilard, "Conformations and coordination schemes of carboxylate and carbamoyl derivatives of the tetraazamacrocycles cyclen and cyclam, and the relation to their protonation states", *Coord. Chem. Rev.*, **1998**, *178–180*, 1313–1405.

35. R. Delgado, V. Félix, L.M.P. Lima and D.W. Price, "Metal complexes of cyclen and cyclam derivatives useful for medical applications: a discussion based on thermodynamic stability constants and structural data", *Dalton Trans.*, **2007**, 2734–2745.

36. (a) T.M. Jones-Wilson, K.A. Deal, C.J. Anderson, D.W. McCarthy, Z. Kovacs, R.J. Motekaitis, A.D. Sherry, A.E. Martell and M.J. Welch, "The *In Vivo* Behavior of Copper-64-Labeled Azamacrocyclic Complexes", *Nucl. Med. Biol.*, **1998**, *25*, 523–530; (b) K. Kumar, M.F. Tweedle, M.F. Malley and J.Z. Gougoutasi, "Synthesis, Stability, and Crystal Structure Studies of Some Ca^{2+}, Cu^{2+}, and Zn^{2+} Complexes of Macrocyclic Polyamino Carboxylates", *Inorg. Chem.*, **1995**, *34*, 6472-6480; (c) R. Yang and L.J. Zompa, "Metal Complexes of Cyclic Triamines. 1. Complexes of 1,4,7-Triazacyclononane ([9]aneN3) with Nickel(II), Copper(II), and Zinc(II)", *Inorg. Chem.*, **1976**, *15*, 1499-1502; (d) K.S. Woodin, K.J. Heroux, C.A. Boswell, E.H. Wong, G.R. Weisman, W. Niu, S.A. Tomellini, C.J. Anderson, L.N. Zakharov and A.L. Rheingold, "Kinetic Inertness and Electrochemical Behavior of Copper(II) Tetraazamacrocyclic Complexes: Possible Implications for in Vivo Stability", *Eur. J. Inorg. Chem.*, **2005**, *23*, 4829-4833.

37. M.C. Styka, R.C. Smierciak, E.L. Blinn, R.E. Desimone and J.V. Passariello, "Copper(II) complexes containing 12-membered", *Inorg. Chem.*, **1978**, 17, 82-86.

38. R.L. Webb, M.L. Mino, E.L. Blinn and A.A. Pinkertod, "Comparison of Copper(II) Complexes Containing Various Saturated 12-Membered Macrocycles", *Inorg. Chem.*, **1993**, *32*, 1396-1402.

39. P. Chaudhuri, K. Oder, K. Wieghardt, J. Weiss, J. Reedijk, W. Hinrichs, J. Wood, A. 0zarowski, H. Stratemaier and D. Reinen, "Variable-Temperature Single-Crystal Electron Spin Resonance Study and Crystal Structure of $[Cu(C_6H_{15}N_3)_2][Cu(CN)_3].2H_2O$ at 110 and 293 K. Static and Dynamic Jahn-Teller Distortions in the CuN_6 Polyhedron", *Inorg. Chem.*, **1986**, *25*, 2951-2958.

40. K. Wieghardt, U. Bossek, P. Chaudhuri, W. Herrmann, B.C. Menke and J. Weiss, "1,4,7-Triazacyclononane-N,N',N"-triacetate (TCTA), a Hexadentate Ligand for Divalent and Trivalent Metal Ions. Crystal Structures of $[Cr^{III}(TCTA)]$, $[Fe^{III}(TCTA)]$, and $Na[Cu^{II}(TCTA)].2NaBr.8H_2O$", *Inorg. Chem.*, **1982**, *21*, 4308-4314.

41. M.J. Van Der Merwe, J.C.A. Boeyens and R.D. Hancock, "Crystallographic and Thermodynamic Study of Metal Ion Size Selectivity in the Ligand 1,4,7-Triazacyclononane-N ,N',N"-triacetate", *Inorg. Chem.*, **1985,** *24*, 1208-1213.

42. P.V. Bernhardt, R. Bramley, L.M. Engelhardt, J.M. Harrowfield, D.C.R. Hockless, B.R. Korybut-Daszkiewicz, E.R. Krausz, T. Morgan, A.M. Sargeson, B.W. Skelton and A.H. White; "Copper(II) Complexes of Substituted Macrobicyclic Hexaamines: Combined Trigonal and Tetragonal Distortions", *Inorg. Chem.*, **1995**, *34*, 3589–3599.

43. S. Liu and D.S. Edwards, "Bifunctional Chelators for Therapeutic Lanthanide Radiopharmaceuticals", *Bioconjugate Chem.*, **2001**, *12*, 7-34.

44. J. Fichna and A. Janecka, "Synthesis of Target-Specific Radiolabeled Peptides for Diagnostic Imaging", *Bioconjugate Chem.* **2003**, *14,* 3-17.

45. L.M. De León-Rodríguez and Z. Kovacs, "The Synthesis and Chelation Chemistry of DOTA–Peptide Conjugates", *Bioconjugate Chem.,* **2008**, *19*, 391-402.

46. M. Nahrendorf, H. Zhang, S. Hembrador, P. Panizzi, D.E. Sosnovik, E. Aikawa, P. Libby, F.K. Swirski and R. Weissleder, "Nanoparticle PET-CT Imaging of Macrophages in Inflammatory Atherosclerosis", *Circulation*, **2008**, *117*, 379-387.

47. A.R. Cowley, J.R. Dilworth, P.S. Donnelly, J.M. Heslop and S.J. Ratcliffe, "Bifunctional chelators for copper radiopharmaceuticals: the synthesis of [Cu(ATSM)–amino acid] and [Cu(ATSM)–octreotide] conjugates", *Dalton Trans.* **2007**, 209-217.

48. C.F. Meares, "Chelating agents for the binding of metal ions to antibodies", *Nucl. Med. Biol.* **1986**, *13*, 311–318.

49. G.L. DeNardo, S.J. DeNardo, C.F. Meares, D. Kukis, H. Diril, J.J. McCall, G.P. Adams, L.F. Mausner, D.C. Moody and S.V. Deshpande, "Pharmacokinetics of copper-67 conjugated Lym-1, a potential therapeutic radioimmonuconjugate, in mice and in patients with lymphoma.", *Antibod. Iimmunoconj. Radiopharm.*, **1991**, *4*, 777-785.

50. X. Chen, S. Liu, Y. Hou, M. Tohme, R. Park, J.R. Bading and P.S. Conti, "MicroPET imaging of breast cancer αv-integrin expression with ^{64}Cu-labeled dimeric RGD peptides", *Mol. Imag. Biol.*, **2004**, *6*, 350–359.

51. Y. Wu, X. Zhang, Z. Xiong, Z. Cheng, D.R. Fisher, S. Liu, S.S. Gambhir and X. Chen, "MicroPET imaging of glioma $\alpha v\beta 3$ integrin expression using ^{64}Cu-labeled tetrameric RGD peptide", *J. Nucl. Med.*, **2005**, *46*, 1707–1718.

52. X. Chen, R. Park, M. Tohme, A.H. Shahinian, J.R. Bading and P.S. Conti, "MicroPET and autoradiographic imaging of breast cancer αv-integrin expression using ^{18}F- and ^{64}Cu-labeled RGD peptide", *Bioconjugate Chem.*, **2004**, *15*, 41–49.

53. X. Chen, "Multimodality imaging of tumor integrin $\alpha v\beta 3$ expression", *Mini-Rev. Med. Chem.*, **2006**, *6*, 227–234.

54. C.J. Anderson, T.S. Pajeau, E.B. Edwards, E.L.C. Sherman, B.E. Rogers and M.J. Welch, "*In vitro* and *in vivo* evaluation of copper-64-octreotide conjugates", *J. Nucl. Med.*, **1995**, *36*, 2315–2325.

55. C.J. Anderson, L.A. Jones, L.A. Bass, E.L.C. Sherman, D.W. McCarthy, P.D. Cutler, M.V. Lanahan, M.E. Cristel, J.S. Lewis and S.W. Schwarz, "Radiotherapy, toxicity and dosimetry of *in vitro* and *in vivo* evaluation of copper-64 TETA-octrotide in tumor bearing rats", *J. Nucl. Med.*, **1998**, *39*, 1944–1951.

56. J.S. Lewis, A. Srinivasan, M.A. Schmidt and C.J. Anderson, "*In vitro* and *in vivo* evaluation of ^{64}Cu-TETA-Tyr3-octreotate. A new somatostatin analog with improved target tissue uptake", *Nucl. Med. Biol.*, **1999**, *26*, 267–273.

57. J.S. Lewis, M.R. Lewis, P.D. Cutler, A. Srinivasan, M.A. Schmidt, S.W. Schwarz, M.M. Morris, J.P. Miller and C.J. Anderson, "Radiotherapy and dosimetry of ^{64}Cu-TETA-Tyr3-octreotate in a

somatostatin receptor-positive, tumor-bearing rat model", *Clin. Cancer Res.*, **1999**, *5*, 3608–3616.

58. M.K. Moi, C.F. Meares, M.J. McCall, W.C. Cole and S.J. DeNardo, "Copper chelates as probes of biological systems: stable copper complexes with macrocyclic bifunctional chelating agent", *Anal. Chem.*, **1985**, *148*, 249–253.

59. W.P. Li, J.S. Lewis, J. Kim, J.E. Bugaj, M.A. Johnson, J.L. Erion and C.J. Anderson, "DOTA-DTyr1- Octreotate: a somatostatin analogue for labeling with metal and halogen radionuclides for cancer imaging and therapy", *Bioconjugate Chem.*, **2002**, *13*, 721–728.

60. P. McQuade, Y. Miao, J. Yoo, T.P. Quinn, M.J. Welch and J.S. Lewis, "Imaging of melanoma using ^{64}Cu- and ^{86}Y-DOTA-ReCCMSH(Arg11), a cyclized peptide analogue of α-MSH", *J. Med. Chem.*, **2005**, *48*, 2985–2992.

61. G.B. Biddlecombe, B.E. Rogers, M. de Visser, J.J. Parry, M. de Jong, J.L. Erion and J.S. Lewis, "Molecular imaging of gastrin-releasing peptide receptor-positive tumors in mice using ^{64}Cu- and ^{86}Y-DOTA-(Pro1, Tyr4)-Bombesin(1–14)", *Bioconjugate Chem.*, **2007**, *18*, 724–730.

62. J.J. Parry, R. Andrews and B.E. Rogers, "MicroPET imaging of breast cancer using radiolabeled bombesin analogs targeting the gastrin-releasing peptide receptor", *Breast Cancer Res. Treat.*, **2007**, *101*, 175–183.

63. J.J. Parry, T.S. Kelly, R. Andrews and B.E. Rogers, "*In vitro* and *in vivo* evaluation of ^{64}Cu-labeled DOTA-Linker-Bombesin(7–14) analogues containing different amino acid linker moiety", *Bioconjugate Chem.*, **2007**, *18*, 1110–1117.

64. J.E. Sprague, H. Kitaura, W. Zou, Y. Ye, S. Achilefu, K.N.Weilbaecher, S.L. Taitebaum and C.J. Anderson, "Noninvasive imaging of osteoclasts in pyrathyroid hormoneinduced osteolysis using a ^{64}Cu-labeled RGD peptide", *J. Nucl. Med.*, **2007**, *48*, 311–318.

65. C.J. Anderson, "Metabolism of radiometal labeled proteins and peptides: what are the real radiopharmaceuticals *in vivo*?", Cancer Biother. Radiopharm., **2001**, *16*, 451–455.

66. Y-S. Yang, X. Zhang, Z. Xiong and X. Chen, "Comparative in vitro and in vivo evaluation of two ^{64}Cu-labeled bombesin analogs in a mouse model of human prostate adenocarcinoma", *Nucl. Med. Biol.*, **2006**, *33*, 371–380.

67. W. Cai, Y. Wu, K. Chen, Q. Cao, D.A. Tice and X. Chen, "*In vitro* and *In vivo* Characterization of ^{64}Cu-Labeled Abegrin^{TM}, a Humanized Monoclonal Antibody against Integrin $\alpha\nu\beta3$", *Cancer Res,* **2006**, 66, 9673-9681.

68. K. Tanaka and K. Fukase, "PET (positron emission tomography) imaging of biomolecules using metal–DOTA complexes: a new collaborative challenge by chemists, biologists, and physicians for future diagnostics and exploration of *in vivo* dynamics", *Org. Biomol. Chem.*, **2008**, *6*, 815–828.

69. J.D. Silversides, C.C. Allan and S.J. Archibald, "Copper(II) cyclam-based complexes for radiopharmaceutical applications: synthesis and structural analysis", *Dalton Trans.*, **2007**, 971–978.

70. K.J. Heroux, K.S. Woodin, D.J. Tranchemontagne, P.C.B. Widger, E. Southwick, E.H. Wong, G.R. Weisman, S.A. Tomellini, T.J. Wadas, C.J. Anderson, S. Kassel, J.A. Golen and A.L. Rheingold,

"The long and short of it: the influence of *N*-carboxyethyl *versus N*-carboxymethyl pendant arms on *in vitro* and *in vivo* behavior of copper complexes of cross-bridged tetraamine macrocycles", *Dalton Trans.*, **2007**, 2150–2162.

71. S.V. Deshpande, S.J. DeNardo, C.F. Meares, M.J. McCall, G.P. Adams, M.K. Moi and G.L. DeNardo, "Copper-67-labeled monoclonal antibody Lym-1, a potential radiopharmaceutical for cancer therapy: Labeling and biodistribution in RAJI tumored mice", *J. Nucl. Med.*, **1988**, *29*, 217–225.

72. L.A. Bass, M. Wang, M.J. Welch and C.J. Anderson, "*In Vivo* Transchelation of Copper-64 from TETA-Octreotide to Superoxide Dismutase in Rat Liver", *Bioconjugate Chem.* **2000**, *11*, 527-532.

73. C.A. Boswell, P. McQuade, G.R. Weisman, E.H. Wong and C.J. Anderson, "Optimization of labeling and metabolite analysis of copper-64-labeled azamacrocyclic chelators by radio-LC-MS", *Nucl. Med. Biol.*, **2005**, *32*, 29–38.

74. C.A. Boswell, X. Sun, W. Niu, G.R. Weisman, E.H. Wong, A.L. Rheingold and C.J. Anderson, "Comparative *in vivo* stability of copper-64-labeled cross-bridged and conventional tetraazamacrocyclic complexes", *J. Med. Chem.*, **2004**, *47*, 1465–1474.

75. X. Chen, Y. Hou, M. Tohme, R. Park, V. Khankaldyyan, I. Gonzales-Gomez, J.R. Bading, W.E. Laug and P.S. Conti; "Pegylated Arg-Gly-Asp Peptide: ^{64}Cu Labeling and PET Imaging of Brain Tumor $\alpha_v\beta_3$-Integrin Expression", *J. Nucl. Med.*, **2004**, *45*, 1776–1783.

76. A.F. Prasanphanich, P.K. Nanda, T.L. Rold, L. Ma, M.J. Lewis, J.C. Garrison, T.J. Hoffman, G.L. Sieckman, S.D. Figueroa and C.J. Smith, "[^{64}Cu-NOTA-8-Aoc-BBN(7-14)NH_2] targeting vector for positron-emission tomography imaging of gastrin releasing peptide receptor-expressing tissues", PNAS, **2007**, *104*, 12462–12467.

77. G. Gasser, L. Tjioe, B. Graham, M.J. Belousoff, S. Juran, M. Walther, J-U. Künstler, R. Bergmann, H. Stephan and L. Spiccia, "Synthesis, Copper(II) Complexation, ^{64}Cu-Labeling, and Bioconjugation of a New Bis(2-pyridylmethyl) Derivative of 1,4,7-Triazacyclononane", *Bioconjugate Chem.*, **2008**, *19*, 719–730.

78. L. Li, J. Bading, P.J. Yazaki, A.H. Ahuja, D. Crow, D. Colcher, L.E. Williams, J.Y.C. Wong, A. Raubitschek and J.E. Shively, "A Versatile Bifunctional Chelate for Radiolabeling Humanized Anti-CEA Antibody with In-111 and Cu-64 at Either Thiol or Amino Groups: PET Imaging Of CEA-Positive Tumors with Whole Antibodies", *Bioconjugate Chem.*, **2008**, *19*, 89-96.

79. N. Di Bartolo, A.M. Sargeson, T.M. Donlevy and S.V. Smith, **"**Synthesis of a new cage ligand, SarAr, and its complexation with selected transition metal ions for potential use in radioimaging", *J. Chem. Soc. Dalton Trans.*, **2001**, 2303–2309.

80. N. Di Bartolo, A.M. Sargeson and S.V. Smith, "New ^{64}Cu PET imaging agents for personalised medicine and drug development using the hexa-aza cage, SarAr", *Org. Biomol. Chem.*, **2006**, *4*, 3350–3357.

81. K. Wang, R.C. Li, Y. Cheng and B. Zhu, "Lanthanides - the future drugs?", *Coord. Chem. Rev.*, **1999**, *192*, 297-308.

82. S.P. Fricker, "The therapeutic application of lanthanides", *Chem. Soc. Rev.*, **2006**, *35*, 524–533.

83. W.A. Volkert and T.J. Hoffman, "Therapeutic Radiopharmaceuticals", *Chem. Rev*. **1999**, *99*, 2269-2292.

84. F. Rösch and E.F. Aronsson, "Radiolanthanides in Nuclear Medicine." In: *Metal Ions in Biological Systems*: "Metal Complexes in Tumour Diagnosis and as Anticancer Agents", A. Siegel and H. Siegel, eds, Marcel Decker, Inc., New York.: **2004**, *42*, 77-108.

85. L. Thunus and R. Lejeune, "Overview of transition metal and lanthanide complexes as diagnostic tools", *Coord. Chem. Rev.*, **1999**, *184*, 125–155.

86. A. Ando, I. Ando, T. Hiraki and K. Hisda, "Relation between the location of elements in the periodic table and various organ-uptake rates", *Nucl. Med. Biol.*, **1989**, *16*, 57–80.

87. P. Hermann, J. Kotek, V. Kubíčcek and I. Lukeš, "Gadolinium(III) complexes as MRI contrast agents: ligand design and properties of the complexes", *Dalton Trans.*, **2008**, 3027–3047.

88. G. De Witt, P. May, J. Webb and G. Hefter, "Biospeciation, by potentiometry and computer simulation, of Sm-EDTMP, a bone tumor palliative agent", *BioMetals*, **1996**, *9*, 351-361.

89. K.P. Wainwright, "Synthetic and structural aspects of the chemistry of saturated polyaza macrocyclic ligands bearing pendant coordinating groups attached to nitrogen", *Coord. Chem. Rev.,* **1997**, *166*, 35-90.

90. G. Ferro-Flores, O. Hernández-Oviedo, C. Arteaga de Murphy, J.I. Tendilla, F. Monroy-Guzmán, M. Pedraza-López, K. Aldama-Alvarado, "[^{166}Dy]Dy/^{166}Ho hydroxide macroaggregates: an in vivo generator system for radiation synovectomy", *Appl. Radiat. Isot.* **2004**, *61*, 1227-1233.

91. M. Fani, S. Vranjes, S.C. Archimandritis, S. Potamianos, S. Xanthopoulos, P. Bouziotis, A.D. Varvarigou, "Labeling of monoclonal antibodies with ^{153}Sm for potential use in radioimmunotherapy", *Appl. Radiat. Isot.* **2002**, *57*, 665-674.

92. F. Hu, C.S. Cutler, T. Hoffman, G. Sieckman, W.A. Volkert and S.S. Jurisson, "Pm-149 DOTA bombesin analogs for potential radiotherapy: *in vivo* comparison with Sm-153 and Lu-177 labeled DO3A-amide-βAla-BBN(7–14)NH_2", *Nucl. Med. Biol.* **2002**, *29*, 423-430.

93. W.P. Li, C.J. Smith, C.S. Cutler, T.J. Hoffman, A.R. Ketring and S.S. Jurisson, "Aminocarboxylate complexes and octreotide complexes with no carrier added ^{177}Lu, ^{166}Ho and ^{149}Pm", *Nucl. Med. Biol.,* **2003**, *30*, 241-251.

94. V. Lungu, D. Niculae, M. Panait and D. Chiper, "177Lu-DOTA-Tyr3-TATE radiotherapy experiments using animal models. Flow cytometric analysis in evaluation of therapeutic effect", *J. Label Compd. Radiopharm.* **2007**, *50*, 489-491.

95. S. Froidevaux and A.N. Eberle, "Somatostatin analogs and radiopeptides in cancer therapy", *Biopolymers*, **2002**, *66*, 161-183.

96. R.E. Weiner and M.L. Thakur, "Radiolabeled peptides in the diagnosis and therapy of oncological diseases", *Appl. Radiat. Isot.* **2002**, *57*, 749-763.

97. C.J. Smith, W.A. Volkert and T.J. Hoffman, "Gastrin releasing peptide (GRP) receptor targeted radiopharmaceuticals: A concise update", *Nucl. Med. Biol.* **2003**, *30*, 861-868.

98. J.E. Bugaj, J.L. Erion, M.A. Johnson, M.A. Schmidt and A. Srinivasan, "Radiotherapeutic efficacy of ^{153}Sm-CMDTPA-Tyr^3-octreotate in tumor-bearing rats", *Nucl. Med. Biol.* **2001**, *28*, 327-334.

99. W.A. Breeman, M. Jong, T.J. Visser, J.L. Erion and E.P. Krenning, "Optimising conditions for radiolabelling of DOTA-peptides with ^{90}Y, ^{111}In and ^{177}Lu at high specific activities", *Eur. J. Nucl. Med. Mol. Imaging*, **2003**, *30*, 917-920.

100. C.J. Smith, H. Gali, G.L. Sieckman, D.L. Hayes, N.K. Owen, D.G. Mazuru, W.A. Volkert and T.J. Hoffman, "Radiochemical investigations of ^{177}Lu-DOTA-8-Aoc-BBN[7-14]NH_2: an *in vitro/in vivo* assessment of the targeting ability of this new radiopharmaceutical for PC-3 human prostate cancer cells", *Nucl. Med. Biol.* **2003**, *30*, 101-109.

101. S. Banerjee, T. Das, S. Chakraborty, G. Samuel, A. Korde, S. Srivastava, M. Venkatesh and M.R.A. Pillai, "^{177}Lu-DOTA-lanreotide: a novel tracer as a targeted agent for tumor therapy", *Nucl. Med. Biol.* **2004**, *31*, 753-759.

102. H. Zhang, J. Chen, C. Waldherr, K. Hinni, B. Waser, J.C. Reubi and H.R. Maecke, "Synthesis and Evaluation of Bombesin Derivatives on the Basis of Pan-Bombesin Peptides Labeled with Indium-111, Lutetium-177, and Yttrium-90 for Targeting Bombesin Receptor-Expressing Tumors", *Cancer Res.*, **2004**, 64, 6707-6715.

103. H. Zangh, J. Schuhmacher, B. Waser, D. Wild, M. Eisenhut, J.C. Reubi and H.R. Maecke, "DOTA-PESIN, a DOTA-conjugated bombesin derivative designed for the imaging and targeted radionuclide treatment of bombesin receptor-positive tumours", *Eur. J. Nucl. Med. Mol. Imaging*, **2007**, *34*, 1198-1208.

104. D.J. Kwekkeboom, W.W. de Herder, B.L. Kam, C.H. van Eijck, M. van Essen, P.P. Kooij, R.A. Feelders, M.O. van Aken, and E.P. Krenning, "Treatment With the Radiolabeled Somatostatin Analog [^{177}Lu-DOTA^0,Tyr^3]Octreotate: Toxicity, Efficacy, and Survival", *J. Clin. Oncol.*, **2008**, *26*, 2124-2130.

105. J.J.M. Teunissen, D.J. Kwekkeboom and E.P. Krenning, "Staging and treatment of differentiated thyroid carcinoma with radiolabeled somatostatin analogs", *Trends Endocrinol. Metab.*, **2006**, *17*, 19-25.

106. N.H. Bander, M.I. Milowsky, D.M. Nanus, L. Kostakoglu, S. Vallabhajosula and S.J. Goldsmith, "Phase I Trial of ^{177}Lutetium-Labeled J591, a Monoclonal Antibody to Prostate-Specific Membrane Antigen, in Patients With Androgen-Independent Prostate Cancer", *J. Clin. Oncol.*, **2005**, *23*, 4591-4601.

107. LE. Lantry, E. Cappelletti, ME. Maddalena, JS. Fox, W. Feng, J. Chen, R. Thomas, SM. Eaton, NJ. Bogdan, T. Arunachalam, JC. Reubi, N. Raju, EC. Metcalfe, L. Lattuada, KE. Linder, RE. Swenson, MF. Tweedle and AD. Nunn, "^{177}Lu-AMBA: Synthesis and Characterization of a Selective ^{177}Lu-Labeled GRP-R Agonist for Systemic Radiotherapy of Prostate Cancer", *J Nucl Med.*, **2006**, *47*, 1144–1152.

108. DJ. Kwekkeboom, JJ. Teunissen, WH. Bakker, PP. Kooij, WW. de Herder, RA. Feelders, CH. van Eijck, J-P. Esser, BL. Kam and EP. Krenning, "Radiolabeled Somatostatin Analog [^{177}Lu-DOTA^0,Tyr^3]Octreotate in Patients With Endocrine Gastroenteropancreatic Tumors", *J. Clin. Oncol.*, **2005**, *23*, 2754-2762.

109. H. Mohsin, J. Fitzsimmons, T. Shelton, TJ. Hoffman, CS. Cutler, MR. Lewis, PS. Athey, G. Gulyas, GE. Kiefer, RK. Frank, J. Simon, SZ. Lever and SS. Jurisson, "Preparation and

biological evaluation of ^{111}In-, ^{177}Lu- and ^{90}Y-labeled DOTA analogues conjugated to B72.3", *Nucl. Med.Biol.*, **2007**, *34*, 493–502.

110. M-A. Fortin, A. Orlova, P-U. Malmstrom and V. Tolmachev, "Labelling chemistry and characterization of [^{90}Y/^{177}Lu]-DOTA-ZHER2:342-3 Affibody molecule, a candidate agent for locoregional treatment of urinary bladder carcinoma", *Int. J. Mol. Med.*, **2007**, *19*, 285-291.

111. J.E. Bayouth, D.J. Macey, L.P. Kasi, J.R. Garlich, K. Mcmillan, M.A. Dimopoulos and R.E. Champlin, "Pharmacokinetics, Dosimetry and Toxicity of Holmium-166-DOTMP for Bone Marrow Ablation in Multiple Myeloma", *J. Nucl. Med.*, **1995**, *36*, 730-737.

112. W.F. Goeckeler, B. Edwards, W.A. Volkert, R.A. Holmes, J. Simon and D. Wilson, "Skeletal Localization of Samarium-153 Chelates: Potential Therapeutic Bone Agents", *J. Nucl. Med.*, **1987**, *28*, 495-504.

113. H. Breitz, R. Wendt, M. Stabin, L. Bouchet and B. Wessels, "Dosimetry of High Dose Skeletal Targeted Radiotherapy (STR) with ^{166}Ho-DOTMP", *Cancer Biother. Radiopharm.*, **2003**, *18*, 225-230.

114. F.C. Alves, P. Donato, A.D. Sherry, A. Zaheer, S. Zhang, A.J.M. Lubag, M.E. Merritt, R.E. Lenkinski, J.V. Frangioni, M. Neves, M.I.M. Prata, A.C. Santos, J.J.P. de Lima, C.F.G.C. Geraldes, "Silencing of Phosphonate-Gadolinium Magnetic Resonance Imaging Contrast by Hydroxyapatite Binding.", *Invest. Radiol*. **2003**, *38*, 750-760.

115. S. Chakraborty, T. Das, S. Banerjee, P.R. Chaudhari, H.D. Sarma, M. Venkatesh and M.R.A. Pillai, "Preparation and biological evaluation of 153Sm-DOTMP as a potential agent for bone pain palliation", *Nucl. Med. Commun.*, **2004**, *25*, 1169-1176.

116. H.B. Breitz, R.E. Wendt, M.S. Stabin, S. Shen, W.D. Erwin, J.G. Rajendran, J.F. Eary, L. Durack, E. Delpassand, W. Martin and R.F. Meredith, "^{166}Ho-DOTMP Radiation-Absorbed Dose Estimation for Skeletal Targeted Radiotherapy", *J. Nucl. Med.*, **2006**, *47*, 534–542.

117. T. Das, S. Chakraborty, H.D. Sarma and S. Banerjee, "^{177}Lu-DOTMP: A viable agent for palliative radiotherapy of painful bone metastasis", *Radiochim. Acta*, **2008**, *96*, 55–61.

118. A. El-Mabhouh, C. Angelov, A. McEwan, G. Jia and J. Mercer, "Preclinical Investigations of Drug and Radionuclide Conjugates of Bisphosphonates for the Treatment of Metastatic Bone Cancer", *Cancer Biother. Radiopharm.*, **2004**, *19*, 627-640.

119. J. Rudovský, J. Kotek, P. Hermann, I. Lukeš, V. Mainero and S. Aime, "Synthesis of a Bifunctional Monophosphinic Acid DOTA Analogue Ligand and Its Lanthanide(III) Complexes. A Gadolinium(III) Complex Endowed with an Optimal Water Exchange Rate for MRI Applications", *Org. Biomol. Chem.*, **2005**, *3*, 112-117.

120. J. Rudovský, P. Cígler, J. Kotek, P. Hermann, P. Vojtíšek, I. Lukeš, J.A. Peters, L.V. Elst and R.N. Muller, "Lanthanide(III) Complexes of a Mono(methylphosphonate) Analogue of H_4dota: The Influence of Protonation of the Phosphonate Moiety on the TSAP/SAP Isomer Ratio and the Water Exchange Rate", *Chem. Eur. J.*, **2005**, *11*, 2373-2384.

121. J. Rudovský, P. Hermann, M. Botta, S. Aime and I. Lukeš, "Dendrimeric Gd(III) Complex of a Monophosphinated DOTA Analogue: Optimizing Relaxivity by Reducing Internal Motion", *Chem. Commun.*, **2005**, 2390-2392.

122. G. Nancollas, R. Tang, R. Phipps, Z. Henneman, S. Gulde, W. Wu, A. Mangood, R. Russell and F. Ebetino, "Novel insights into actions of bisphosphonates on bone: Differences in interactions with hydroxyapatite", *Bone*, **2006**, *38*, 617-627.

123. V. Kubíček, J. Rudovský, J. Kotek, P. Hermann, L. Vander Elst, R. N. Muller, Z. I. Kolar, H. Th. Wolterbeek, J. A. Peters and I. Lukeš: "A Bisphosphonate Monoamide Analogue of DOTA: A Potential Agent for Bone Targeting", *J. Am. Chem. Soc.*, **2005**, 16477–16485.

124. J. Rudovský, M. Botta, P. Hermann, K.I. Hardcastle, I. Lukeš and S. Aime, "PAMAM Dendrimeric Conjugates with a Gd-DOTA Phosphinate Derivative and Their Adducts with Polyaminoacids: The Interplay of Global Motion, Internal Rotation, and Fast Water Exchange", *Bioconjugate Chem.* **2006**, *17*, 975-987.

125. M. Försterová, I. Svobodová, P. Lubal, P. Táborský, J. Kotek, P. Hermann and I. Lukeš, "Thermodynamic Study of Lanthanide(III) Complexes with Bifunctional Monophosphinic Acid Analogues of H_4dota and Comparative Kinetic Study of Yttrium(III) Complexes", *Dalton Trans.*, **2007**, 535-549.

126. M.P. Campello, F. Marques, L. Gano, S. Lacerda and I. Santos, "Radiochemichal and biological evaluation of ^{153}Sm and ^{166}Ho complexes anchored by a novel bis(methylphosphonate) tetraazamacrocycles", *Radiochimica Acta*, **2007**, *95*, 329-334.

127. F. Marques, M.P. Campello, L. Gano, S. Lacerda and I. Santos, "Biological evaluation of ^{153}Sm and ^{166}Ho complexes with tetraazamacrocycles containing methylcarboxylate and/or methylphosphonate pendant arms", *Radiochimica Acta*, **2007**, *95*, 335-342.

128. L. Gano, F. Marques, M.P. Campillo, M. Balbina, S. Lacerda and I. Santos, "Radiolanthanide complexes with tetraazamacrocycles bearing methylphosphonate pendant arms as bone seeking agents", *Q. J. Nucl. Med. Mol. Imaging*, **2007**, *51*, 6-15.

129. P. Řezanka, V. Kubíček, P. Hermann and I. Lukeš, "Synthesis of a Bifunctional Monophosphinate DOTA Derivative Having a Free Carboxylate Group in the Phosphorus Side Chain", *Synthesis*, **2008**, 1431–1435.

130. T. Vitha, V. Kubícek, P. Hermann, L.V. Elst, R.N. Muller, Z.I. Kolar, H.T. Wolterbeek, W.A.P. Breeman, I. Lukeš and J.A. Peters, "Lanthanide(III) Complexes of Bis(phosphonate) Monoamide Analogues of DOTA: Bone-Seeking Agents for Imaging and Therapy", *J. Med. Chem.*, **2008**, *51*, 677-683.

131. T. Vitha, V. Kubíček, P. Hermann, Z. I. Kolar, H. Th. Wolterbeek, J. A. Peters and I. Lukeš, "Complexes of DOTA-Bisphosphonate Conjugates: Probes for Determination of Adsorption Capacity and Affinity Constants of Hydroxyapatite", *Langmuir,* **2008**, *24*, 1952–1958.

132. M. Försterová, Z. Jandurová, F. Marques, L. Gano, P. Lubal, J. Vaněk, P. Hermann and I. Santos, "Chemical and Biological Evaluation of ^{153}Sm and ^{166}Ho Complexes of 1,4,7,10-tetraazacyclododecane-1,4,7,10-tetrakis(methylphosphonic acid monoethylester) (H_4dotp^{OEt})", *J. Inorg. Biochem.,* **2008**, *102*, 1531–1540.

133. W. Goeckeler, D. Troutner, W. Volkert, B. Edwards, J. Simon and D. Wilson, "153-Sm radiotherapeutic bone agents", *Nucl. Med. Biol.*, **1986**, *13*, 479–482.

134. C.S. Cutler, M. Wuest, C.J. Anderson, D.E. Reichert, Y. Sun, A.E. Martell and M.J. Welch, "Labeling and in vivo evaluation of novel copper(II) dioxotetraazamacrocyclic complexes.", *Nucl. Med. Biol.*, **2000**, *27*, 375-380.

135. J. Yoo, D.E. Reichert, and M.J. Welch, "Regioselective N-substitution of cyclen with two different alkyl groups: synthesis of all possible isomers", *Chem. Commun.*, **2003**, 766-767.

136. J. Yoo, D.E. Reichert, and M.J. Welch, "Comparative in vivo behavior studies of cyclen-based copper-64 complexes: regioselective synthesis, X-ray structure, radiochemistry, log P, and biodistribution", *J. Med. Chem.*, **2004**, *47*, 6625-6637.

137. X. Sun, J. Kim, A.E. Martell, M.J. Welch and C.J. Anderson, "*In vivo* evaluation of copper-64-labeled monooxotetraazamacrocyclic ligands", *Nucl. Med. Biol.*, **2004**, *31*, 1051-1059.

138. A. Lewin, J. P. Hill, R. Boetzel, T. Georgiou, R. James, C. Kleanthous and G. R. Moore, "Site-specific labeling of proteins with cyclen-bound transition metal ions", *Inorg. Chim. Acta*, **2002**, *331*, 123-130.

139. (a) D. Tschudin, A. Basak and T.A. Kaden, "Metal Complexes with Macrocyclic Ligands. Part XXVI. Synthesis and spectral properties of Cu^{2+} complexes with mono-*N*-functionalized 1,4,8-trimethyl-1,4,8,11-tetraazacyclotetradecanes", *Helv. Chim. Acta*, **1988**, *71*, 100-106; (b) R. Ma, M.J. Welch, J. Reibenspies and A.E. Martell, "Stability of metal ion complexes of 1,4,7-tris(2-mercaptoethyl)-1,4,7-triazacylclonane (TACN-TM) and molecular structure of In($C_{12}H_{24}N_3S_3$)", *Inorg. Chim. Acta*, **1995**, *236*, 75-82; (c) R.P. Houser, J.A. Halfen, V.G. Young, Jr., N.J. Blackburn and W.B. Tolman, "Structural Characterization of the First Example of a Bis(.mu.-thiolato)dicopper(II) Complex. Relevance to Proposals for the Electron Transfer Sites in Cytochrome c Oxidase and Nitrous Oxide Reductase", *J. Am. Chem. Soc.*, **1995**, *117*, 10745-10746; (d) T. Gyr, H.R. Mäcke and M. Herming, "A Highly Stable Silver(I) Complex of a Macrocycle Derived from Tetraazatetrathiacyclen", *Angew. Chem., Int. Ed. Engl.*, **1997**, *36*, 2786-2788.

140. L. Li, S-W. Tsai, A-L. Anderson, D.A. Keire, A.A. Raubitschek, J.E. Shively, "Vinyl Sulfone Bifunctional Derivatives of DOTA Allow Sulfhydryl- or Amino-Directed Coupling to Antibodies. Conjugates Retain Immunoreactivity and Have Similar Biodistributions", *Bioconjugate Chem.* **2002**, *13*, 110-115.

141. M.R. Lewis, and J.E. Shively, "Maleimidocysteineamido-DOTA Derivatives: New Reagents for Radiometal Chelate Conjugation to Antibody Sulfhydryl Groups Undergo pH-Dependent Cleavage Reactions", *Bioconjugate Chem.* **1998**, *9*, 72-86.

142. B. Yoo, M.D. Pagel, "A facile synthesis of α-amino-DOTA as a versatile molecular imaging probe" , *Tetrahedron Letters* **2006**, *47*, 7327-7330.

143. (a) C. Wängler, B. Wängler, M. Eisenhut, U. Haberkorn and W. Mier, "Improved syntheses and applicability of different DOTA building blocks for multiply derivatized scaffolds", *Bioorg. Med. Chem.*, **2008**, *16*, 2606-2616; (b) Z. Miao, M.R. McCoy, D.D. Singh, B. Barrios, O.L. Hsu, S.M. Cheal and C.F. Meares, "Cysteinylated Protein as Reactive Disulfide: An Alternative Route to Affinity Labeling", *Bioconjugate Chem.* **2008**, *19*, 15-19.

144. N. Raghunand, B. Jagadish, T.P. Trouard, J-P. Galons, R.J. Gillies, E.A. Mash, "Redox-sensitive contrast agents for MRI based on reversible binding of thiols to serum albumin", *Magn. Res. Med.* **2006**, *55*, 1272-1280.

145. C. Carrera, G. Digilio, S. Baroni, D. Burgio, S. Consol, F. Fedeli, D. Longo, A. Mortillaro and S. Aime, "Synthesis and characterization of a Gd(III) based contrast agent responsive to thiol containing compounds**"**, *Dalton Trans.*, **2007**, 4980–4987.

146. D. Thonon, V. Jacques and J.F. Desreux, "A gadolinium triacetic monoamide DOTA derivative with a methanethiosulfonate anchor group. Relaxivity properties and conjugation with albumin and thiolated particles", *Contrast Media Mol. Imaging* **2007**, *2*, 24–34.

147. (a) T.J. Lotz and T.A. Kaden, "pH-Induced co-ordination geometry change in a macrocyclic nickel(II) complex", *J. Chem. Soc., Chem. Commun.*, **1977**, 15-16; (b) T.J. Lotz and T.A. Kaden, "Metal Complexes with Macrocyclic Ligands. IX. Synthesis and properties of a new class of branched N_4-macrocycles with an additional ligating group in the side chain", *Helv. Chim. Acta*, **1978**, *61*, 1376-1387; (c) N.W. Alcock, H.A. Omar, P. Moore and C. Pierpoint, **"**Preparation of 11-(2'-dimethylaminoethyl)-1,4,7-trimethyl-1,4,7,11-tetra-azacyclotetradecane, and characterisation of its nickel(II), copper(II), and zinc(II) complexes", *J. Chem. Soc., Dalton Trans.*, **1985**, 219-221.

148. Z. Kovacs and A.D. Sherry, "pH-Controlled Selective Protection of Polyaza Macrocycles", *Synthesis*, **1997**, 759-763.

149. (a) K. Malesse and A. Loos, "Transesterification of Phosphodiester by a Zinc-Containing Cyclen Derivative: Identification of the Active Species", *Liebigs Ann.*, **1996**, 935-939; (b) M. Woods, G.E. Kiefer, S. Bott, A. Castillo-Muzquiz, C. Eshelbrenner, L. Michaudet, K. McMillan, S.D.K. Mudigunda, D. Ogrin, G. Tircsó, S. Zang, P. Zhao and A.D. Sherry, "Synthesis, Relaxometric and Photophysical Properties of a New pH-Responsive MRI Contrast Agent: The Effect of Other Ligating Groups on Dissociation of a *p*-Nitrophenolic Pendant Arm", *J. Am. Chem. Soc.*, **2004**, *126*, 9248-9256; (c) G. Hervé, H. Bernard, N. Le Bris, M. Le Baccon, J-J. Yaouanc and H. Handel, "Condensation of glyoxal with triethylenetetraamine. Stereochemistry, cyclization and deprotection, *Tetrahedron Letters*, **1999**, *40*, 2517-2520; (d) J. Rohovec, R. Gyepes, I. Císařová, J. Rudovský and I. Lukeš, "Nucleophilic reactivity of perhydro-3,6,9,12-tetraazacyclopenteno[1,3-*f,g*]acenaphthylene. A unified approach to *N*-monosubstituted and *N,N″*-disubstituted cyclene derivatives", *Tetrahedron Letters*, **2000**, *41*, 1249-1253.

150. M. Studer and T.A. Kaden, "Nucleophilic reactivity of perhydro-3,6,9,12-tetraazacyclopenteno[1,3-*f,g*]acenaphthylene. A unified approach to *N*-monosubstituted and *N,N″*-disubstituted cyclene derivatives", *Helv. Chim. Acta*, **1986**, *69*, 2081-2086.

151. P.J. Davies and K.P. Wainwright, "3-Hydroxypropylation of tetraazamacrocycles and its effect on the stability of divalent metal complexes", *Inorg. Chim. Acta*, **1999**, *294*, 103-108.

152. (a) K. Stolarczyk, R. Bilewicz, L. Siegfried and T. Kaden, "The dual role of self-assembled monolayers of a tetraazamacrocyclic copper(II) complex in ascorbate oxidation catalysis", *Inorg. Chim. Acta*, **2003**, *348*, 129-134; (b) T. Kaden, "Labelling monoclonal antibodies with macrocyclic radiometal complexes. A challenge for coordination chemists", *Dalton Trans.*, **2006**, 3617-3623.

153. S. Meegalla, K. Plossl, M-P. Kung, S. Chumpradit, D.A. Stevenson, D. Frederick, H.F. Kung, "Tc-99m-Labeled Tropanes as Dopamine Transporter Imaging Agents", *Bioconjugate Chem.*, **1996**, *7*, 421-429.

154. (a) W. Clegg, P.B. Iveson and J.C. Lockhart, "Macrocyclic ligands with pendant phosphonic acid groups**"**, *J. Chem. Soc. Dalton Trans.*, **1992**, 3291-3298 and references therein; (b) E. Kimura, H. Kitamura, T. Koike and M. Shiro, "Facile and Selective Electrostatic Stabilization of Uracil N(1)$^-$ Anion by a Proximate Protonated Amine: A Chemical Implication for Why Uracil

N(1) Is Chosen for Glycosylation Site", *J. Am. Chem. Soc.*, **1997**, *119*, 10909-10919; (c) C. Bazzicalupi, A. Bencini, E. Berni, A. Bianchi, S. Ciattini, C. Giorgi, S. Maoggi, P. Paoletti and B. Valtancoli, "Synthesis of New Tren-Based Tris-Macrocycles. Anion Cluster Assembling Inside the Cavity Generated by a Bowl-Shaped Receptor", *J. Org. Chem.*, **2002**, *67*, 9107-9110.

155. (a) A.P. Leugger, L. Hertli and T.A. Kaden, "Metal Complexes with Macrocyclic Ligands. XI. Ring size effect on the complexation rates with transition metal ions", *Helv. Chim. Acta*, **1978**, *61*, 2296-2306; (b) M. Kodama and E. Kimura, "Reaction of cobalt(II) macrocyclic tetraamine complexes with dioxygen", *J. Chem. Soc., Dalton Trans.*, **1980**, 327-333; (c) T. Koike, S. Kajitani, I. Nakamura and E. Kimura, "The catalytic carboxyester hydrolysis by a new zinc(II) complex with an alcohol-pendant cyclen (1-(2-hydroxyethyl)-1,4,7,10-tetraazacyclododecane): A novel model for indirect activation of the serine nucleophile by zinc(II) in zinc enzymes", *J. Am. Chem. Soc.*, **1995**, *117*, 1210-1219; (d) E. Kimura, T. Gotoh, S. Aoki and M. Shiro, "Study of pH-Dependent Zinc(II)-Carboxamide Interactions by Zinc(II)-Carboxamide-Appended Cyclen Complexes (Cyclen = 1,4,7,10-Tetraazacyclododecane)", *Inorg. Chem.* **2002**, *41*, 3239-3248.

156. C. Frassineti, L. Alderighi, P. Gans, A. Sabatini, A. Vacca and S. Ghelli, "Determination of protonation constants of some fluorinated polyamines by means of ^{13}C NMR data processed by the new computer program HypNMR2000. Protonation sequence in polyamines", *Anal. Bioanal. Chem.*, **2003**, *376*, 1041-1052.

157. R. Delgado, J.J.R.F. DaSilva, M.T.S. Amorim, M.F. Cabral, S. Chaves and J. Costa, "Dissociation constants of Brönsted acids in D_2O and H_2O: studies on polyaza and polyoxa-polyaza macrocycles and a general correlation", *Anal. Chim. Acta*, **1991**, *245*, 271-282.

158. (a) Ryszard Nazarski, "Assignment of pH-dependent NMR spectra of the scorpiand macrocycle: an application of titration profiles and spectral linewidths", *Magn. Reson. Chem.*, **2003**, *41*, 70-74, and references cited therein; (b) R. Clay, S. Corr, M. Micheloni and P. Paoletti, "Non-cyclic reference ligands for tetraaza macrocycles. Synthesis and thermodynamic properties of a series of .alpha.,.omega.-di-N-methylated tetraaza ligands and their copper(II) complexes", *Inorg. Chem.*, **1985**, *24*, 3330-3336; (c) A. Bianchi, B. Escuder, E. Garcia-España, S.V. Luis, V. Marcelino, J.F. Miravet and J.A. Ramírez, "Protonation tendencies of azaparacyclophanes. A thermodynamic and NMR study", *J. Chem. Soc. Perkin Trans. 2*, **1994**, 1253-1259; (d) J.E. Sarneski, H.L. Surprenant, F.K. Molen and C.N. Reilley, "Chemical shifts and protonation shifts in carbon-13 nuclear magnetic resonance studies of aqueous amines", *Anal. Chem.*, **1975**, *47*, 2116-2124; (e) M. Ciampolini, M. Micheloni, N. Nardi, P. Paoletti, P. Dapporto and F. Zanobini, "Synthesis and characterisation of 1,7-dimethyl-1,4,7,10-tetra-azacyclododecane: crystal structure of the nickel(II) bromide monohydrate complex of this macrocycle; thermodynamic studies of protonation and metal complex formation", *J. Chem. Soc., Dalton Trans.*, **1984**, 1357-1362.

159. V.J. Thöm, G.D. Hosken and R.D. Hancock, "Anomalous metal ion size selectivity of tetraaza macrocycles", *Inorg. Chem.*, **1985**, *24*, 3378-3381.

160. L. Alderighi, P. Gans, A. Ienco, D. Peters, A. Sabatini, A. Vacca, "Hyperquad simulation and speciation (HySS): a utility program for the investigation of equilibria involving soluble and partially soluble species", *Coord. Chem. Rev.*, **1999**, *184*, 311-318.

161. K. Miyoshi, H. Tanaka, E. Kimura, S. Tsuboyama, S. Murata, H. Shimizu and K. Ishizu, "Electrochemical and spectroscopic studies on copper(II) complexes of macrocyclic ligands as models for square-pyramidal metal active sites of copper(II) complexes of bleomycin and glutathione, *Inorg. Chim. Acta*, **1983**, *78*, 23-30.

162. E.I. Solomon, K.W. Penfield and D.E. Wilcox, "Active sites in copper proteins an electronic structure overview", *Structure and Bonding*, **1983**, *53*, 1-57.

163. F. Neese, Diploma Thesis, University of Konstanz, Germany, **1993**.

164. A.W. Addison, M. Carpenter, L.K-M. Lau, M. Wicholas, "Coordination sphere flexibility at copper: chemistry of a unipositive copper(II) macrocycle, [Cu(cyclops)]+", *Inorg. Chem.*, **1978**, *17*, 1545-1552.

165. M.J. Maroney and N.J. Rose, "Coordination chemistry of copper macrocyclic complexes: synthesis and characterization of copper complexes of TIM", *Inorg. Chem.*, **1984**, *23*, 2252-2261.

166. P.W. Lau and W.C. Lin, "Electron spin resonance and electronic structure of some metalloporphyrins", *J. Inorg. Nucl. Chem.*, **1975**, *37*, 2389-2398.

167. P.A. Tasker and L. Sklar, "Crystal and molecular structure of di(perchlorato)(1,4,8,11-tetraazacyclotetradecane)copper (II). Cu(cyclam) $(ClO_4)_2$", *J. Cryst. Mol. Struct.*, **1975**, *5*, 329-344 and J.C.A. Boeyens and S.M. Dobson, in *Stereochemical and Stereophysical Behaviour of Macrocycles*, ed. Ivan Bernal, Elsevier, Amsterdam, **1987**, vol. 2, pp. 1–102.

168. S. Lacerda, M.P. Campello, I.C. Santos, I. Santos and R. Delgado, "Study of the cyclen derivative 2-[1,4,7,10-tetraazacyclododecan-1-yl]-ethanethiol and its complexation behaviour towards d-transition metal ions", *Polyhedron* **2007**, *26*, 3763-3773.

169. M. Kývala and I. Lukeš, *International Conference, Chemomotrics '95*, p. 63. Pardubice, Czech Republic, 1995; full version of *"OPIUM"* is available on http://www.natur.cuni.cz/~kyvala/opium.html.

170. C. Frassineti, S. Ghelli, P. Gans, A. Sabatini, M.S. Moruzzi and A. Vacca, "Nuclear Magnetic Resonance as a Tool for Determining Protonation Constants of Natural Polyprotic Bases in Solution", *Anal. Biochem.*, **1995**, *231*, 374-382.

171. K. Kumar, C.A. Chang, L.C. Francesconi, D.D. Dischino, M.F. Malley, J.Z. Gougoutas and M.F. Tweedle, "Synthesis, Stability, and Structure of Gadolinium(III) and Yttrium(III) Macrocyclic Poly(amino carboxylates)", *Inorg. Chem.*, **1994**, *33*, 3567-3575.

172. A. Bianchi, L. Calabi, C. Giorgi, P. Losi, P. Mariani, P. Paoli, P. Rossi, B. Valtancoli and M. Virtuani, "Thermodynamic and structural properties of Gd^{3+} complexes with functionalized macrocyclic ligands based upon 1,4,7,10-tetraazacyclododecane", *J. Chem. Soc., Dalton Trans.*, **2000**, 697–705.

173. H-Z. Cai and T.A. Kaden, "Metal complexes with macrocyclic ligands. Part XXXVI. Thermodynamic and kinetic studies of bivalent and trivalent metal ions with 1,4,7,10-tetraazacyclododecane-1,4,7-triacetic acid", *Helv. Chim. Acta*, **1994**, *77*, 383-398.

174. J.F. Desreux, E. Merciny, and M.F. Loncin, "Nuclear magnetic resonance and potentiometric studies of the protonation scheme of two tetraaza tetraacetic macrocycles", *Inorg. Chem.*, **1981**, *20*, 987-991.

175. (a) P. Antunes, M.P. Campello R. Delgado, M.G.B. Drew, V. Félix, and I. Santos, "Metal complexes of a tetraazacyclophane: solution and molecular modelling studies", *J. Chem. Soc. Dalton Trans.* **2003**, 1852-1860; (b) R. Fossheim, J.H. Dugstad and S.G. Dahlf, "Structure-

stability relationships of gadolinium(III) ion complexes for magnetic resonance imaging", *J. Med. Chem.* **1991**, *34*, 819-826; (c) R.S. Rauganathan, R.K. Pillai, N. Raju, H. Fan, H. Nguyen, M.F. Tweedle, J.F. Desreux and V. Jacques, "Polymethylated DOTA Ligands. 1. Synthesis of Rigidified Ligands and Studies on the Effects of Alkyl Substitution on Acid−Base Properties and Conformational Mobility", *Inorg. Chem.* **2002**, *41*, 6846-6855; (d) T.J. McMurry, C.G. Pippin, C. Wu, K.A. Deal, M.W. Brechbiel, S. Mirzadeh and O.A. Gansow, "Physical Parameters and Biological Stability of Yttrium(III) Diethylenetriaminepentaacetic Acid Derivative Conjugates", *J. Med. Chem.* **1998**, *41*, 3546-3549; (e) H.S. Chong, K. Garmestani, L.H. Bryant and M.W. Brechbiel, "Synthesis of DTPA Analogues Derived from Piperidine and Azepane: Potential Contrast Enhancement Agents for Magnetic Resonance Imaging", *J.Org. Chem.* **2001**, *66*, 7745-7750.

176. O. Reany, T. Gunnlaugsson and D. Parker, "A model system using modulation of lanthanide luminescence to signal Zn^{2+} in competitive aqueous media", *J. Chem. Soc. Perkin Trans.2* **2000**, 1819-1831.

177. B. Cathala, C. Picard, L. Cazaux, P. Tisnès and M. Momtchev, "Macrocyclic dilactams with pendant acidic functions as discriminating agents for lanthanide ions", *Tetrahedron*, **1995**, *51*, 1245-1252.

178. M.B. Inoue, L. Machi, I.C. Muñoz, S. Rojas-Rivas, M. Inoue and Q. Fernando, "Metal–ligand interactions in benzodioxotetraaza-macrocyclic metal chelates", *Inorg. Chim. Acta*, **2001**, *324*, 73-80.

179. P. Gans, A. Sabatini and A. Vacca, "Investigation of equilibria in solution. Determination of equilibrium constants with the HYPERQUAD suite of programs", *Talanta*, **1996**, *43*, 1739-1753.

180. M.B. Inoue, P. Oram, G. Andreu-de-Riquer, M. Inoue, P. Borbat, A. Raitsimring and Q. Fernando, "Transition Metal Complexes of 12- and 13-Membered Functionalized Macrocycles, Dioxotetraazacycloalkanediacetates", *Inorg. Chem.*, **1995**, *34*, 3528-3535.

181. M.B. Inoue, P. Oram, M. Inoue and Q. Fernando, "Solution ^{1}H NMR and X-ray crystal structures of Ca^{2+}, Zn^{2+} and Cd^{2+} complexes with 12− and 13-membered macrocycles, dioxotetraazacycloalkanediacetic acids", *Inorg. Chim. Acta*, **1996**, *246*, 401-412.

182. P. Antunes, R. Delgado, M.G.B. Drew, V. Félix and H. Maecke, "Copper Complexes of New Benzodioxotetraaza Macrocycles with Potential Applications in Nuclear Medicine", *Inorg. Chem.*, **2007**, *46*, 3144-3153.

183. R. Delgado, M.F. Cabral, R. Castanheira, A. Zhang, R. Herrmann, "Metal complexes of edta-derived macrocyclic ether bis(lactones). Hydrolysis of the macrocycles and the metal catalysis effect", *Polyhedron*, **2002**, *21*, 2265-2276.

184. (a) M.B. Inoue, I.C. Muñoz, L. Machi, M. Inoue and Q. Fernando, "Structural and spectroscopic studies of binuclear Cu^{2+} and Co^{2+} complexes with an amide-based naphthalenophane", *Inorg. Chim. Acta*, **2000**, *311*, 50-56; (b) M.B. Inoue, E.F. Velazquez, F. Medrano, K.L. Ochoa, J.C. Galvez, M. Inoue and Q. Fernando, "Binuclear Copper(II) Chelates of Amide-Based Cyclophanes", *Inorg. Chem.*, **1998**, *37*, 4070-4075.

185. H. Irving and R.J.P. Williams, "The stability of transition-metal complexes", *J. Chem. Soc.*, **1953**, 3192-3210.

186. (a) R. Yang and L.J. Zompa, "Metal complexes of cyclic triamines. 1. Complexes of 1,4,7-triazacyclononane ([9]aneN3) with nickel(II), copper(II), and zinc(II)", *Inorg. Chem.*, **1976**, *15*, 1499-1502; (b) L.J. Zompa, "Metal complexes of cyclic triamines. 2. Stability and electronic spectra of nickel(II), copper(II), and zinc(II) complexes containing nine- through twelve-membered cyclic triamine ligands", *Inorg. Chem.*, **1978**, *17*, 2531-2536; (c) R.D. Hancock, V.J. Thöm, "Macrocyclic effect in transition metal ion complexes of a mixed (nitrogen, oxygen) donor macrocycle", *J. Am. Chem. Soc.*, **1982**, *104*, 291-292; (d) V.J. Thöm, J.C.A. Boeyens, G.J. McDougall, R.D. Hancock, "Origin of the high ligand field strength and macrocyclic enthalpy in complexes of nitrogen-donor macrocycles", *J. Am. Chem. Soc.*, **1984**, *106*, 3198-3207; (e) D-Y. Kong and Y-Y. Xie, "Synthesis, structural characterization and potentiometric studies of divalent metal complexes with an octadentate tetraazamacrocyclic ligand and their DNA cleavage ability", *Polyhedron*, **2000**, *19*, 1527-1537; (f) M. Sandow, B.L. May, C.J. Easton and S.F. Lincoln, "Binary and Ternary Metallo-ß-cyclodextrins of 6^A-[Bis(carboxylatomethyl)amino]-6^A-deoxy-ß-cyclodextrin", *Aust. J. Chem.*, **2000**, *53*, 149-152; (g) A.V. Bordunov, J.S. Bradshaw, X. Zhang, N.K. Dalley, X. Kou and R.M. Izatt, "Synthesis and Properties of 5-Chloro-8-hydroxyquinoline-Substituted Azacrown Ethers: A New Family of Highly Metal Ion-Selective Lariat Ethers", *Inorg. Chem.*, **1996**, *35*, 7229-7240; (h) S.E. Livingstone and E.A. Sullivan, "Thio derivatives of ß-diketones and their metal chelates. XI. Stability constants of nicke(II), copper(II). zinc(II), cadniium(II), and lead(II) chelates of two monothio-ß-diketones", *Aust. J. Chem.*, **1969**, *22*, 1363-1379; (i) S. Murakam, "Semi-xylenol orange complexes with bivalent metal ions", *J. Inorg. Nucl. Chem.*, **1981**, *43*, 335-343.

187. S. Chaves, A. Cerva and R. Delgado, "13-Membered macrocycles and their complexometric properties: study of 7,11-bis(carboxymethyl)-1,4-dioxa-7,11-diazacyclotridecane", *Polyhedron*, **1998**, *17*, 93-104.

188. J. Peisach and W.E. Blumberg, "Structural implications derived from the analysis of electron paramagnetic resonance spectra of natural and artificial copper proteins", *Arch. Biochem. Biophys.*, **1974**, *165*, 691-708.

189. H.R. Gersmann, J.D. Swalen, "Electron Paramagnetic Resonance Spectra of Copper Complexes", *J. Chem. Phys.*, **1962**, *36*, 3221-3233.

190. (a) L. Burai, J. Ren, Z. Kovacs, E. Brucher and A.D. Sherry, "Synthesis, Potentiometry, and NMR Studies of Two New 1,7-Disubstituted Tetraazacyclododecanes and Their Complexes Formed with Lanthanide, Alkaline Earth Metal, Mn^{2+}, and Zn^{2+} Ions", *Inorg. Chem.*, **1998**, *37*, 69–75; (b) R. Delgado, J.J.R. Frausto da Silva, "Metal complexes of cyclic tetra-azatetra-acetic acids", *Talanta*, **1982**, *29*, 815–822; (c) H. Stetter and W. Frank, "Complex Formation with Tetraazacycloalkane-*N,N*',*N*'',*N*'''-tetraacetic Acids as a Function of Ring Size", *Angew Chem. Int. Ed. Engl.*, **1976**, *15*, 686.

191. J. Schlesinger, I. Koezle, R. Bergmann, S. Tamburini, C. Bolzati, F. Tisato, B. Noll, S. Klussmann, S. Vonhoff, F. Wuest, H-J. Pietzsch and J. Steinbach, "An ^{86}Y-Labeled Mirror-Image Oligonucleotide: Influence of Y-DOTA Isomers on the Biodistribution in Rats", *Bioconjugate Chem.*, **2008**, *19*, 928-939.

192. (a) G.A. McLachlan, G.D. Fallon, R.L. Martin and L. Spiccia, "Synthesis, Structure and Properties of Five-Coordinate Copper(II) Complexes of Pentadentate Ligands with Pyridyl Pendant Arms", *Inorg. Chem.*, **1995**, *34*, 254-261; (b) A.W. Addison, T.N. Rao, J. Reedijk, J. van Rijn, G.C. Verschoor, "Synthesis, structure, and spectroscopic properties of copper(II) compounds containing nitrogen–sulphur donor ligands; the crystal and molecular structure of aqua[1,7-bis(*N*-methylbenzimidazol-2'-yl)-2,6-dithiaheptane]copper(II) perchlorate", *J. Chem. Soc., Dalton Trans.*, **1984**, 1349-1356.

193. S-G. Kang, K. Ryu and J. Kim, "Synthesis of Copper(Ⅱ) Complexes of Pentaamine Ligands Containing One 1,3-Diazacyclohexane Ring", *Bull. Korean Chem. Soc.*, **1998**, *19*, 1005-1008.

194. M. Gupta, P. Mathur and R.J. Butcher, "Synthesis, Crystal Structure, Spectral Studies, and Catechol Oxidase Activity of Trigonal Bipyramidal Cu(II) Complexes Derived from a Tetradentate Diamide Bisbenzimidazole Ligand", *Inorg. Chem.*, **2001**, *40*, 878-885.

195. (a) B.S. Nakani, J.J.B. Welsh and R.D. Hancock, "Formation constants of some complexes of tetramethylcyclam", *Inorg. Chem.*, **1983**, *22*, 2956-2958; (b) R.D. Hancock, "Polar and steric effects in the stability of silver complexes of primary amines", *J. Chem. Soc., Dalton Trans.*, **1980**, 416-418.

196. R.D. Hancock, B.S. Nakani and F. Marsicano, "Relationship between Lewis acid-base behavior in the gas phase and in aqueous solution. 1. Role of inductive, polarizability, and steric effects in amine ligands", *Inorg. Chem.*, **1983**, *22*, 2531-2535.

197. R.J. Motekaitis, B.E. Rogers, D.E. Reichert, A.E. Martell and M.J. Welch, "Stability and Structure of Activated Macrocycles. Ligands with Biological Applications", *Inorg. Chem.*, **1996**, *35,* 3821-3827.

198. (a) C.A. Hoefnagel, "Radionuclide Cancer Therapy", *Ann. Nucl. Med.* **1998**, *12*, 61-70; (b) J. Carlsson, E.F. Aronsson, S-O. Hietala, T. Stigbrand and J. Tennvall, "Tumour therapy with radionuclides: assessment of progress and problems", *Radiotherapy and Oncology* **2003**, *66*, 107-117.

199. S. Meyer, B. Andrioletti, J.L. Sessler, V. Lynch, "Synthesis and Structural Characterization of the First Schiff-Base Macrocycles Containing Terpyrrole Subunits", *J. Org. Chem.,***1998**, *63*, 6752-6756.

200. A.K. Mishra, P. Panwar, M. Hosono, K. Chuttani, P. Mishra, R.K. Sharma and J.F. Chatal, "A New Bifunctional Chelating Agent Conjugated with Monoclonal Antibody and Labelled with Technetium-99m for Targeted Scintigraphy: 6-(4-isothiocyanatobenzyl)-5,7-dioxo-1,11-(carboxymethyl)-1,4,8,11-tetraazacyclotridecane", *J. Drug Target,* **2004**, *12*, 559-567.

201. (a) K. Kumar, C.A. Chang and M.F. Tweedle, "Equilibrium and kinetic studies of lanthanide complexes of macrocyclic polyamino carboxylates", *Inorg. Chem.*, **1993**, *32*, 587-593; (b) S.L. Wu, , *Anal. Chem.*, **1996**, *68*, 394-401; (c) C.A. Chang, L.C. Francesconi, M.F. Malley, K. Kumar, J.Z. Gougoutas, M.F. Tweedle, D.W. Lee and L.J. Wilson, "Synthesis, characterization, and crystal structures of M(DO3A) (M = iron, gadolinium) and Na[M(DOTA)] (M = Fe, yttrium, Gd)", *Inorg. Chem.*, **1993**, *32*, 3501-3508; (d) H-Z. Cai and T.A. Kaden, *Helv. Chim. Acta*, **1994**, *77*, 383-398; (e) S.J.A. Pope, , *Dalton Trans.*, **2006**, 2907-2912; (f) L. Cong, Y-X. Li, G-L. Law, K. Man, W-T. Wong and H. Lei, "Fast Water-Exchange Gd^{3+}-(DO3A-like) Complex Functionalized with Aza-15-Crown-5 Showing Prolonged Residence Lifetime in Vivo", *Bioconjugate Chem.*, **2006**, *17*, 571-574; (g) A. Mishra, J. Pfeuffer, R. Mishra, J. Engelmann, A.K. Mishra, K. Ugurbil and N.K. Logothetis, "A New Class of Gd-Based DO3A-Ethylamine-Derived Targeted Contrast Agents for MR and Optical Imaging", *Bioconjugate Chem.*, **2006**, *17*, 773-780.

202. (a) W.P. Cacheris, S.K. Nickle and A.D. Sherry, "Thermodynamic study of lanthanide complexes of 1,4,7-triazacyclononane-N,N',N''-triacetic acid and 1,4,7,10-tetraazacyclododecane-N,N',N'',N'''-tetraacetic acid", *Inorg. Chem.*, **1987**, *26*, 958-960; (b) E. Toth and E. Brücher, "Stability constants of the lanthanide(III)-1,4,7,10-

tetraazacyclododecane-*N*,*N*′,*N*″,*N*‴-tetraacetate complexes", *Inorg. Chimica Acta*, **1994**, *221*, 165-167.

203. F. Marques, K.P. Guerra, L. Gano, J. Costa, M.P. Campello, L.M.P. Lima, R. Delgado and I. Santos, "^{153}Sm and ^{166}Ho complexes with tetraaza macrocycles containing pyridine and methylcarboxylate or methylphosphonate pendant arms", *J. Biol. Inorg. Chem.*, **2004**, *9*, 859-872.

204. F. Marques, L. Gano, M.P. Campello, S. Lacerda, I. Santos, L.M.P. Lima, J. Costa, P. Antunes abd R. Delgado, "13- and 14-membered macrocyclic ligands containing methylcarboxylate or methylphosphonate pendant arms: Chemical and biological evaluation of their ^{153}Sm and ^{166}Ho complexes as potential agents for therapy or bone pain palliation", *J. Inorg. Biochem.*, **2006**, 100, 270-280.

205. A.K. Mishra and J-F. Chatal, "Synthesis of macrocyclic bifunctional chelating agents: 1,4,7-tris(carboxymethyl)-10-(2-aminoethyl)-1,4,7,10-tetraazacyclododecane and 1,4,8-tris(carboxymethyl)-11-(2-aminoethyl)-1,4,8,11-tetraazacyclotetradecane", *New J. Chem.*, **2001**, *25*, 336-339.

206. W.A. Kleinman and J.P. Jr. Richie, "Status of glutathione and other thiols and disulfides in human plasma", *Biochem. Pharmacology*, **2000**, *60*, 19-29.

207. (a) J.H. Reibenspies, "Structure of 1,4,7,10-tetraazacyclododecane trihydrate", *Acta Crystallogr. C*, **1992,** *48*, 1717-1718; (b) J.H. Reibenspies and O.P. Anderson, "Structure of 1,4,7,10-tetraazacyclododecane tetrahydrochloride", *Acta Crystallogr. C* **1990**, 46, 163-165; (c) C. Nave, M.R. Truter, "Crystal structure of the dihydroperchlorate of 1,4,8,11-tetra-azacyclotetradecane (cyclam)", *J. Chem. Soc., Dalton Trans.*, **1974**, 2351-2354; (d) J. Xu, S. Ni and Y. Lin, "Syntheses and characterization of 5,5,7,12,12,14-hexamethyl-1,4,8,11-tetraazacyclotetradecane-N-acetic acid (HL1) and its transition-metal complexes: crystal structures of HL1.cntdot.2HBr.cntdot.H2O, [NiL1(H2O)]Br, and [NiL1(NCS)]H2O", *Inorg. Chem.*, **1988,** *27*, 4651-4657; (e) M.R. Maurya, E.J. Zaluzec, S.F. Pavkovic and A.W. Herlinger, "Alkaline-earth-metal complexes of 1,4,8,11-tetraazacyclotetradecane-1,4,8,11-tetraacetic acid, H4TETA, and crystal and molecular structure of H4TETA.cntdot.6H2O and [Mg(H2TETA)(H2O)4].cntdot.4H2O", *Inorg. Chem.*, **1991**, *30*, 3657-3662; (f) M.R. Spirlet, J. Rebizan, P.P. Barthélemy and J.F. Desreux, *J. Chem. Soc., Dalton Trans.*, **1991**, 2477-2481; (g) V. Dahaoui-Gindrey, C. Lecomte, H. Chollet, A.K. Mishra, C. Mehadji and R. Guilard, "Synthesis, Characterization, and X-ray Crystal-structures of Cyclam derivatives .2. Heptahydrate Tetraprotonated 1,4,8,11-(Tetra-2-Carboxyethyl)-1,4,8,11-tetraazacyclotetradecane H(4)tetp-center-dot-7H(2)0, the perchlorate pentaprotonated form (H(5)tetp)(+)CL0(4), and the tetrachloride dihydrate octaprotonated form (H(8)tetp)(4+),4CL(-)center-dot-2H(2)0", *New J. Chem*. **1995**, 19, 839-850; (h) V. Dahaoui-Gindrey, S. Dahaoui, C. Lecomte, F. Barbette and R. Guilard, "Disodium hexadecahydrate diprotonated form of 1,4,8,11-tetra(2-carboxy)ethyl-1 ,4,8,11-tetraazacyclotetradecane (H2TETP)(2-) at 110 K", *Acta Crystallogr. C*, **1997**, *53*, 1797-1799; (i) V. Dahaoui-Gindrey, C. Lecomte, C. Gros, A.K. Mishra and R. Guilard, "Synthesis, characterization and X-ray crystal-structures of Cyclam derivatives .1. 1,4,8,11-(Tetra-2-Carbamoylethyl)-1,4,8,11-tetraazacyclotetradecane tetpa-center-dot-2H(2)O and its Bis-protonated form (H(2)tetpa)(2+),2NO(3)(-)center-dot-2H(2)O", *New J. Chem*. **1995**, *19*, 831-838.

208. I. Lázár, C.H. Duane, W. Kim, C.E. Kiefer and A.D. Sherry, "Optimized synthesis, structure, and solution dynamics of 1,4,7,10-tetraazacyclododecane-1,4,7,10-tetrakis(methylenephosphonic acid) (H8DOTP)", *Inorg. Chem.*, **1992**, *31*, 4422-4424.

209. P. Táborský, P. Lubal, J. Havel, J. Kotek, P. Hermann and I. Lukeš, "Thermodynamic and Kinetic Studies of Lanthanide(III) Complexes with H_5do3ap (1,4,7,10-tetraazacyclododecane-1,4,7-triacetic-10-(methylphosphonic acid)), a monophosphonate Analogue of H_4dota", *Collect. Czech Chem. Commun.* **2005**, *70*, 1909-1942.

210. A.D. Sherry, C.F.G.C. Geraldes and W.P. Cacheris, "^{31}P and ^{23}Na NMR lanthanide induced shifts in axially symmetric macrocyclic phosphonate complexes", *Inorg. Chim. Acta* **1987**, *139*, 137-139.

211. F.K. Kálmán, Z. Baranyai, I. Tóth, I. Bányai, R. Király, E. Brücher, S. Aime, X. Sun, A.D. Sherry and Z. Kovács, "Synthesis, Potentiometric, Kinetic, and NMR Studies of 1,4,7,10-Tetraazacyclododecane-1,7-bis(acetic acid)-4,10-bis(methylenephosphonic acid) (DO2A2P) and its Complexes with Ca(II), Cu(II), Zn(II) and Lanthanide(III) Ions", *Inorg. Chem.*, **2008**, *47*, 3851-3862.

212. I. Lukeš, J. Kotek, P. Vojtíšek and P. Hermann, "Complexes of tetraazacycles bearing methylphosphinic/phosphonic acid pendant arms with copper(II), zinc(II) and lanthanides(III). A comparison with their acetic acid analogues", *Coord. Chem. Rev*. **2001**, *216–217*, 287

213. J. Moreau, E. Guillon, J.-C. Pierrard, J. Rimbault, M. Port and M. Aplincourt**,** "Complexing Mechanism of the Lanthanide Cations Eu^{3+}, Gd^{3+}, and Tb^{3+} with 1,4,7,10-Tetrakis(carboxymethyl)-1,4,7,10-tetraazacyclododecane (dota) - Characterization of Three Successive Complexing Phases: Study of the Thermodynamic and Structural Properties of the Complexes by Potentiometry, Luminescence Spectroscopy, and EXAFS", *Chem. Eur. J.* **2004**, *10*, 5218-5232.

214. M. Koudelková, H. Vinsová and V. Jedináková-Krízová, "Isotachophoretic determination of stability constants of Ho and Y complexes with diethylenetriaminepentaacetic acid and 1,4,7,10-tetraazadodecane-N,N′,N″,N‴-tetraacetic acid", *J. Chromatogr., A*, **2003**, *990*, 311-316.

215. R. Delgado, J. Costa, K.P. Guerra and L.M.P. Lima, "Lanthanide complexes of macrocyclic derivatives useful for medical applications", *Pure Appl. Chem.*, **2005**, 77, 569-579.

216. A.E. Martell and R.M. Smith, *Critical Stability Constants*, Vols. 1–6. Plenum Press, New York **1974–1989**.

217. M.I. Kabachnik, T.Y. Medved, F.I. Bel'skii, S.A. Pisareva, "Synthesis and Acid-Base and Complex-Forming Properties of 1,4,7,10-Tetrakis(Dihydroxyphosphorylmethyl)-1,4,7,10-Tetraazacyclododecane", *Iz*V*. Akad. Nauk SSSR, Ser. Khim.*, **1984**, 844-849.

218. (a) F. Avecilla, J.A. Peters and C.F.G.C. Geraldes, "X-ray Crystal Structure of a Sodium Salt of $[Gd(DOTP)]^{5-}$: Implications for Its Second-Sphere Relaxivity and the ^{23}Na NMR Hyperfine Shift Effects of $[Tm(DOTP)]^{5-}$", *Eur. J. Inorg. Chem.* **2003**, *23*, 4179-4186; (b) F. Benetollo, G. Bombieri, L. Calabi, S. Aime and M. Botta, "Structural Variations Across the Lanthanide Series of Macrocyclic DOTA Complexes: Insights into the Design of Contrast Agents for Magnetic Resonance Imaging", *Inorg. Chem.*, **2003**, *42*, 148-157; (c) P. Vojtıšek, P. Cígler, J. Kotek, J. Rudovský, P. Hermann and I. Lukeš, "Crystal Structures of Lanthanide(III) Complexes with Cyclen Derivative Bearing Three Acetate and One Methylphosphonate Pendants", *Inorg. Chem.* **2005**, *44*, 5591-5599; (d) L. Burai, I. Fábián, R. Király, E. Szilágyi and E. Brücher, "Equilibrium and kinetic studies on the formation of the lanthanide(III) complexes, $[Ce(dota)]^-$ and $[Yb(dota)]^-$ (H_4dota = 1,4,7,10-tetraazacyclododecane-1,4,7,10-tetraacetic acid)", *J. Chem.Soc., Dalton Trans.* **1998**, 243-248; (e) T. Sakurai, K. Kobayashi, K. Tsuboyama and S.

Tsuboyama, "The crystal and molecular structure of (2*R*,5*R*,8*R*,11*R*)-2,5,8,11-tetraethyl-1,4,7,10-tetraazacyclododecane", *Acta Cryst. B*, **1978**, 34, 1144-1148.

219. J. Kotek, J. Rudovský, P. Hermann, and I. Lukes, "Three in One: TSA, TSA', and SA Units in One Crystal Structure of a Yttrium(III) Complex with a Monophosphinated H_4dota Analogue", *Inorg. Chem.*, **2006**, *45*, 3097-3102.

220. (a) S. Aime, M. Botta and G. Ermondi, "NMR study of solution structures and dynamics of lanthanide(III) complexes of DOTA", *Inorg. Chem.*, **1992**, *31*, 4291-4299; (b) C.F.G.C. Geraldes, A.D. Sherry and G.E. Kiefer, "The solution structure of Ln $(DOTP)^{5-}$ complexxes. A comparison of lanthanide-induced paramagnetic shifts with the MMX energy-minimized structure", *J. Magn. Reson.*, **1992**, *97*, 290-304.

221. (a) S. Zhang, G. Gangal and H. Uluda, ""Magic Bullets" for bone diseases: progress in rational design of bone-seeking medicinal agents", *Chem. Soc. Rev.*, **2007**, *36*, 507-531; (b) N. Pandit-Taskar, M. Batraki and C. Digvi, "Radiopharmaceutical Therapy for Palliation of Bone Pain from Osseous Metastases", *J. Nucl. Med.*, **2004**, *45*, 1358-1365.

222. (a) W.R. Harris and Y. Chen, "Difference ultraviolet spectroscopic studies on the binding of lanthanides to human serum transferring", *Inorg. Chem.*, **1992**, *31*, 5001–5006; (b) Y. Chen and W.R. Harris, "UV difference spectra study on the binding of europium ion with apotransferrin", *Acta Chim. Sinica*, **1999**, *57*, 503–509.

223. A.C.T. North, D.C. Phillips, F.S. Mathews, "A semi-empirical method of absorption correction", *Acta Crystallogr., Sect. A 24*, **1968**, 351-359.

224. A. Altomare, M.C. Burla, M. Camalli, G.L. Cascarano, C. Giacovazzo, A. Guagliardi, A.G.G. Moliterni, G. Polidori, R. Spagna, "*SIR*97: a new tool for crystal structure determination and refinement", *J. Appl. Crystallogr.*, **1999**, *32*, 115-119.

225. G.M. Scheldrick, Programs for Crystal Structure Analysis (Release 97-2), Institüt für Anorganische Chemie der Universität, Tammanstrasse 4, D-3400 Göttingen, Germany, **1998**.

226. L.J. Farrugia, "*WinGX* suite for small-molecule single-crystal crystallography", *J. Appl. Crystallogr.*, **1999**, *32*, 837-838.

227. L.J. Farrugia, "*ORTEP*-3 for Windows - a version of *ORTEP*-III with a Graphical User Interface (GUI)", *J. Appl. Crystallogr.*, **1997**, *30*, 565.

228. G.M. Sheldrick, SADABS, Bruker AXS Inc., Madison, WI, USA, **2004**.

229. Bruker, SMART and SAINT, Bruker AXS Inc., Madison, WI, USA, **2004**.

230. (a) Z. Otwinowski and W. Minor, *HKL Denzo and Scalepack Program Package*, Nonius BV, Delft, Netherlands, **1997**; (b) Z. Otwinowski and W. Minor, "Processing of X-ray diffraction data collected in oscillation mode", *Methods Enzymol.*, **1997**, *276*, 307-326.

231. A. Altomare, G. Cascarano, C. Giacovazzo, A. Guagliardi, M. C. Burla, G. Polidori and M. Camalli, "SIR92—A Program for Automatic Solution of Crystal Structures by Direct Methods", *J. Appl. Crystallogr.*, **1994**, *27*, 435.

232. G.M. Sheldrick and T.R. Schneider, "SHELXL: High Resolution Refinement", *Methods Enzymol.*, **1997**, *277*, 319-343.

233. (a) F. Szelecsényi, G. Blessing and S.M. Qaim, "Excitation functions of proton induced nuclear reactions on enriched ^{62}Ni and ^{64}Ni: Possibility of production of no-carrier added ^{62}Cu and ^{64}Cu at a small cyclotron", *Appl. Radiat. Isot.*, **1993**, *44*, 575–580; (b) D.W. McCarthy, R.E. Shefer, R.E. Klinkowstein, L.A. Bass, W.H. Margeneau, C.S. Cutler, C.J. Anderson and W.J., W. "Efficient production of high specific activity ^{64}Cu using a biomedical cyclotron." *Nucl. Med. Biol.*, **1997**, *24*, 35–43.

234. G. Shwardzenbach and W. Flaschka, "Complexometric Titrations", Methuen & Co, London, **1969**.

235. G. Shwardzenbach and W. Biedermann, "Komplexone VII. Titration von Metallen mit Nitrilotriessigsäure H_3X. Endpunktsindikation durch p_H-Effekte", *Helv. Chim. Acta*, **1948**, *31*, 331-340.

236. NIST Standard Reference Database 46. NIST Critically Selected Stability Constants of Metal Complexes Database. Version 5.0. Data collected and selected by R.M. Smith and A.E. Martell, US Department of Commerce, National Institute of Standards and Technology, Washington, DC, **1998**.

237. (a) A.E. Martell and R.M. Smith: *Critical Stability Constants*, Vols 1–6. Plenum Press, New York **1974–1989**; (b) *NIST Standard Reference Database 46* (*Critically Selected Stability Constants of Metal Complexes*), Version 7.0, **2003**; (c) Baes C. F., Jr., Mesmer R. E.: *The Hydrolysis of Cations*. Wiley, New York, **1976**.